ABSTRACT

Title of Dissertation: STUDIES ON THE STEP-GROWTH POLYMERIZATION OF AROMATIC POLYCARBONATES

Yuesheng Ye, Doctor of Philosophy, 2007

Directed by: Professor Kyu Yong Choi
Department of Chemical and Biomolecular Engineering

Bisphenol A polycarbonate (BAPC) is a versatile engineering polymer that has a broad spectrum of applications. In this dissertation, theoretical and experimental studies of step-growth polymerization of BAPC are presented to gain better understandings in both solid-state polymerization (SSP) and melt copolymerization systems.

The reactive end group mole ratio in the prepolymer is one of the most important parameters in the AA-BB type polycondensation system. However, it often deviates from the stoichiometric ratio due to the loss of diphenyl carbonate during the melt transesterification process, limiting the molecular weight increase in a subsequent SSP process. In this work, a new back calculation method has been developed to estimate the initial mole ratio of reactive end groups for the melt transesterification using the data of prepolymer's molecular weight and end group mole ratio. An end group model and a

molecular species model have been developed to describe the reaction kinetics of SSP in a single polymer particle. A single particle model is combined with a dynamic moving packed bed reactor model to investigate the steady-state and dynamic behaviors of a continuous polymerization reactor process. The model simulations show that any temperature nonuniformity in the reactor caused by poor heat transfer from the purge gas or the reactor walls leads to a slow increase in the polymer molecular weight averages and molecular weight distribution. A new method has been developed to calculate the sequence length distributions for condensation terpolymers and applied to calculating the time evolution of sequence length distributions for a semibatch melt copolymerization process. Finally, the crystalline structures of BAPC have been investigated using scanning electron microscopy. We observed that BAPC crystallization occurs readily by solvent-induced crystallization technique when the polymer is deposited as a thin film onto a substrate surface. When acetone is used as a swelling agent, the polycarbonate crystals grow to three dimensionally structured spherulites that have been rarely reported in the literature.

STUDIES ON THE STEP-GROWTH POLYMERIZATION OF AROMATIC POLYCARBONATES

by

Yuesheng Ye

Dissertation submitted to the Faculty of the Graduate School of the
University of Maryland, College Park, in partial fulfillment
of the requirements for the degree of
Doctor of Philosophy
2007

Advisory Committee:

Professor Kyu Yong Choi, Chair
Professor F. Joseph Schork
Professor Robert M. Briber
Professor Sheryl Ehrman
Professor Sang Bok Lee

Dedication

To my lovely wife Hong Liu and daughter Pricilla S. Ye.

Acknowledgements

I would like to express my sincere gratitude and appreciation to my advisor Professor Kyu Yong Choi, for his mentorship, guidance and support throughout the study, also thank LG Chem. Company for the financial support throughout the research work. Many thanks go to my lab mates, Seung Young Park, Hyung Woo Lee, Joong Jin Han, Yun Ju Jung and visiting scholars, Su Yeon Na, Yong Jeon Kim, Sung Won Kim and Kyu Hwang Lee. Thank Brent Machado for his help with experiments for the startup of this project.

I am truly thankful to those friends who helped and supported me in many ways: Jingtao Wang, Jing Chen, Jianfeng Du, Jun Li, Yechun Wang, Ta-I Yang, Xin Fang, Xiaolong, Luo, Quanzeng Wang. My special thanks go to Juchen Guo and Yonghui Zhang for the friendship, equipment help, and useful discussion. I also would like to thank Professor Lawrence R. Sita, Professor Sang Bok Lee and Professor Bongtae Han for allowing me to use DSC, SEM and a spinning coater.

The deepest heart-felt gratitude goes to my lovely wife Hong Liu, for her support, encouragement and thoughtfulness. Thank my lovely daughter, Yaoyao, for bringing my family such joyful time. Thank my parents, Yabin Ye and Chunyuan Ye, and mother-in-law, Lin Jin, for the support and care as always.

Let all the thankfulness go to GOD!

Table of Contents

List of Tables

List of Figures

Chapter 1

Introduction

Polycarbonates, as important engineering thermoplastics, have been widely used in a large variety of applications, ranging from optical recording data media, water bottles, electrical components, safety goggles to automotive interiors and exteriors due to their special properties such as high transparency, excellent toughness, thermal and chemical stabilities. The resins of polycarbonates are available not only in general purpose molding and extrusion grades but also in several special grades that provide specific properties or processing characteristics. Clear, transparent grades are popular for optical devices such as safety gaggles, green house windows. Opaque and highly colored grades are common for electronic parts such as LCD display diffusers and sporting goods. Currently, polycarbonates are produced by more than a dozen of companies in the world with global output 2.7 million tons annually.[1] The vast majority of polycarbonate products are based on bisphenol A (BPA), and sold under commercial trade names such as Lexan® (GE, U.S.), Makrolon® (Bayer, Germany), Caliber® (LG-Dow, Korea-U.S.), Panlite® (Teijin, Japan) and Iupilon® (Mitsubishi, Japan) (Brunelle and Korn, 2005).[2]

1.1 Overview of Aromatic Polycarbonates

The definition of aromatic polycarbonates refers to polyesters of carbonic acid derived from dihydroxyl compounds in which the hydroxyl groups are directly attached to an aromatic ring.[3] The discovery of polycarbonates dates back to 1898.

Einhorn[3] reported the first aromatic polycarbonate via the reaction of phosgene with resorcinol and hydroquinone in pyridine. A few years later, in 1902 the same polycarbonate was synthesized by Bischoff and Hedenström[3] via transesterification of diols with diphenyl carbonate (DPC). However, the development of aromatic polycarbonates had not been advanced further for the next 50 years due to many factors such as commercially unavailable of suitable monomers and the absence of processing techniques to fabricate useful products. In 1953, reinvestigations of aromatic polycarbonate chemistry carried out by Schnell at Bayer (a phosgenation process) and by Fox at GE (a melt transesterification process) led to independent discoveries of bisphenol A polycarbonate (BAPC) preparation.[2] Currently, both the interfacial polymerization process and the melt polymerization process are still used in a large scale production of BAPC, whereas other techniques are commonly utilized in a small scale for specialty materials.

1.1.1 Bisphenol A Polycarbonates

The most important hydroxyl component for aromatic polycarbonates today is 4,4′-dihydroxy-diphenyl-2,2-propane or 2,2-bis(4-hydroxyphenyl)propane, which is also called as bisphenol A (BPA) with the following structure formula.

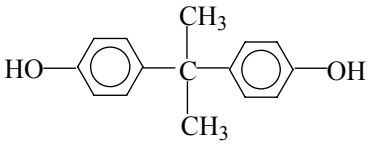

The condensation polymer of BPA with DPC is known as BAPC with the following general chain structure.

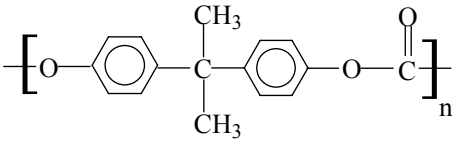

BAPC has a high glass transition temperature (T_g=145ºC) [4], which is relatively high compared to other thermoplastics such as polystyrene (T_g=100°C), poly(ethylene terephthalate) (T_g=61ºC), nylon-6,6 (T_g=45ºC), or polyethylene (T_g=-125ºC).[5] Crystallized BAPC has a high melting range (T_m=220-230ºC).[3] The high value of T_g is important for the application of BAPC in many fields because T_g, as the point which marks the significant difference of molecular mobility, determines many properties such as dimensional stability, resistance to creep, modulus. Together with other excellent properties such as optical clarity, exceptional impact resistance and ductility, BAPC polymer has gained great commercial interest. Compared with BAPC, no other polycarbonates have commercially gained such great success. BAPC has become the foundation of the polycarbonate engineering thermoplastic resin industry today.

The preparation of BAPC, in general, can be classified as the following processes.

1) Phosgenation Process

Aromatic polycarbonates cannot be prepared by the direct phosgenation of aromatic dihydroxy compounds.[3] But it is possible to couple bisphenols with phosgene in the presence of pyridine, which is one of the earliest solvent techniques for the synthesis of polycarbonate. The advantage of this process is that the polycondensation reaction is carried out in a homogenous liquid phase at low reaction

temperatures. But due to difficulties in the separation and purification of BAPC from pyridine and the hydrochloride, this method is not very commercially attractive.

Anther phosgenation process, interfacial polymerization method, became one of the most common commercial routes to synthesize polycarbonates after this process was commercialized by Bayer in 1958 and by G.E. in 1960, respectively.[6] By the 1970s, the majority of commercial BPA-PC was produced via the interfacial technology.[7] Nowadays most BAPC is still produced by this interfacial polymerization method, and it plays an important role in the polycarbonate industry.

Generally speaking, a typical interfacial polymerization process involves two steps: the phosgenation of BPA and the polycondensation to prepare BAPC in a heterogeneous reaction system.[1] In the first step, to an agitated two-phase liquid system: methylene chloride and aqueous alkaline solution of salt, gaseous phosgene (bp 4°C) is added. The phosgenation step of BPA mainly produces chloroformates of BPA. In the second step, the polycondensation of chloroformates is carried out to produce BAPC with a proper catalyst such as tertiary amines or quaternary ammonium salts. In this process, it is important to provide effective mixing for the following four phases: solid BPA, gaseous phosgene, methylene chloride, and the aqueous phase.[2]

A two-stage reaction scheme can be briefly described as follows.[8]

Phosgenation:

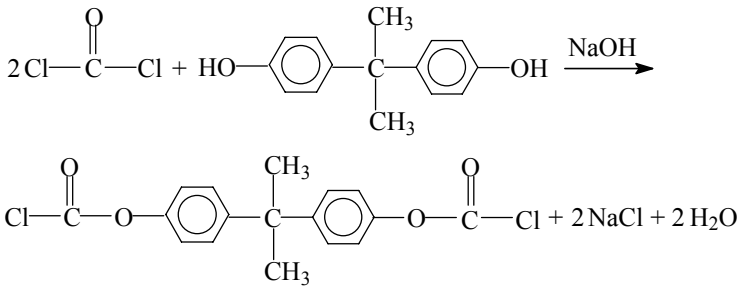

(1.1)

Polycondensation:

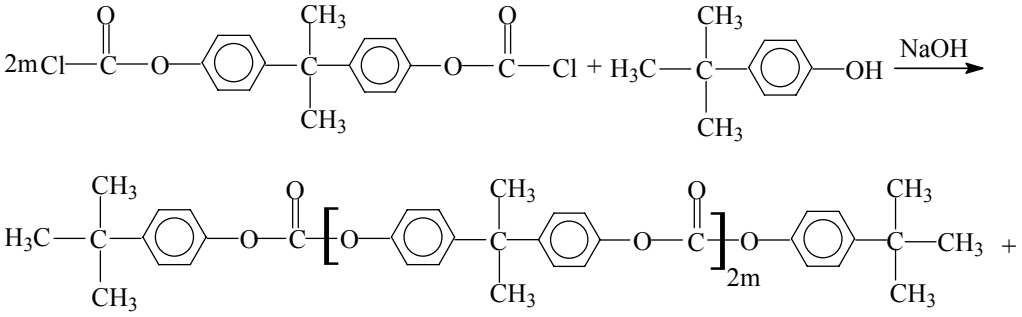

$4m\,NaCl + (2m\text{-}1)\,Na_2CO_3 + 4m\,H_2O$

(1.2)

A number of variations of this basic interfacial polymerization process have been patented, including continuous or semi-continuous processes. The attractive features of the interfacial polymerization process are: 1) low reaction temperature, 2) only one organic solvent involved, and 3) high molecular weight, up to 200 000.[2] On the other hand, this method carries some drawbacks such as: 1) environmental problems and safety concerns involved in utilizing a large amount of highly toxic phosgene as a reagent, 2) corrosive chlorine-containing by-products such as hydrogen chloride and sodium chloride[9], and 3) impurities such as sodium chloride and methylene chloride could cause the deterioration of the properties because they are hard to remove.[1]

2) Melt Polymerization

Like the interfacial process, the melt polymerization process for the preparation of BAPC dates back over 100 years. However, in the early time, the effect of catalysts and discoloration caused by side reactions such as thermal oxidation were not well understood. Therefore, this process was supplanted by the interfacial polymerization process.[2] Decades later, when the technology for processing came out and suitable catalysts became available, the melt polymerization process received renewed interest due to the feature of environmental friendliness. In 1964, GE was the first to commercialize this phosgene-free process.[10]

The melt polymerization process is a reversible reaction with phenol produced as a condensate. To facilitate the forward reaction, either vacuum[11] or a sweep gas[12] can be used. This process is first carried out at low reaction temperatures between 180 and 250ºC at a medium reduced pressure between 20 and 100 mmHg. After the majority of phenol is removed, the reaction temperature is gradually raised up to 280-300ºC and the pressure is reduced down to 1 mmHg or less.[8] In the early stage of melt polymerization, it is not difficult to obtain the degree of polymerization less than 10 because of relatively low viscosity and high phenol removal rate. But at late stages, the melt viscosity increases dramatically, which greatly increases the operational difficulties. A relative low diffusivity and long diffusion path of phenol limit the further increase of molecular weight. In order to effectively remove phenol condensate and achieve high molecular weight, a special reactor design may be required. For example, a gravity-driven polymerization reactor developed by Komiya

et al.[13] at Asahi has no moving parts but provides an effective surface renewal and mixing as polymer melt flows downward through the guiders inside of the reactor.

The general reaction scheme for the melt transesterification is shown as follows.[3]

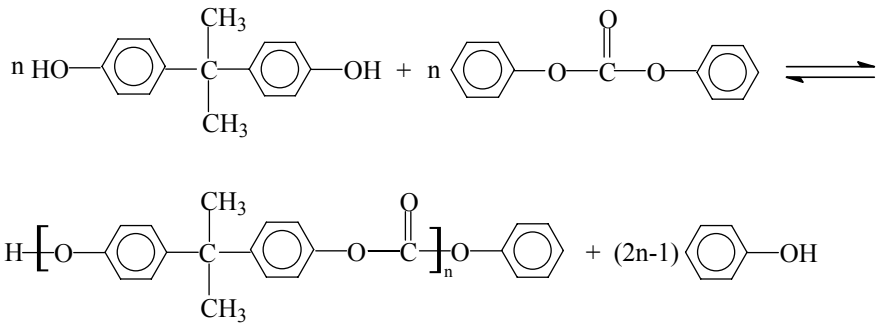

(1.3)

Theoretically, to reach high conversion and obtain high molecular weight, the preparation of BAPC by means of melt transesterification requires equimolar quantities of BPA and DPC as shown in eq 1.3. However, in practice, a slight excess of DPC is often used to compensate its loss during the course of transesterification process, which has been known since the early 1960s.[2,14]

As compared with the interfacial polymerization process, the melt polymerization process offers an alternative way to prepare BAPC without any additional solvent, drying steps and phosgene. Once the process is appropriately designed and operated, the quality of final resin is directly related with the quality of the starting monomers, which makes the quality of final product much more controllable. However, the disadvantages of this process lie in the discoloration problem caused by high reaction temperatures and the mechanical difficulties due to the high melt viscosity, which greatly limits phenol removal rate, reaction rate and the maximum molecular weight obtainable.[3]

3) Solid-State Polymerization

Solid-state polymerization (SSP) is a widely practiced polymerization technique to obtain high molecular weight condensation polymers such as poly(ethylene terephthalate) (PET) and polyamides.[15] In 1978, an early attempt to prepare aromatic polycarbonates via SSP was made for those polycarbonates derived from aromatic dicarboxylic acid or aromatic oxycarboxylic acid having both an aromatic ester bond and an aromatic carbonate bond because the resulting products at the end of melt process are crystalline polymers and no further crystallization is required.[16] Thus, it was thought that BAPC would not be feasible for SSP.[17] The molten state occurs before reaching a high temperature for polymerization because BAPC is hard to crystallize under thermal treatment only. In 1987, Fukuoka et al.[1] at Asahi (Japan) first patented the SSP of BAPC, and disclosed the technology in other countries as well. Fukuoka et al.[17] reported that BAPC oligomer obtained from melt polymerization could first crystallize under acetone treatment, and then undergo chain extension in the solid state to get substantially high molecular weight polymers. Later, chloroform treatment was employed to crystallize BAPC oligomer.[18,19] As supercritical carbon dioxide (CO_2) is utilized to crystallize BAPC polymer,[20] tremendous effort has been devoted to developing this new process of SSP.[21-23]

In a SSP process, the reaction is usually carried out at a temperature well above the polymer's glass transition temperature, T_g, to provide enough mobility for end functional groups, but below its melting point, T_m, to prevent sticking of particles. Fusion of particles should be prevented in that it significantly reduces the reaction rate and hence the molecular weight increase. Like a melt transesterification process,

the SSP of BAPC is a reversible reaction. To facilitate the forward reaction and obtain high molecular weight, either vacuum[19] or an inert purge gas such as nitrogen[24,25] or supercritical carbon dioxide[21-23] is often used.

In a typical SSP process, the first step is to prepare low molecular weight oligomer by a melt transesterification process using an appropriate catalyst such as lithium hydroxide monohydrate ($LiOH \cdot H_2O$). Then amorphous oligomer of BAPC obtained from the melt polymerization is partially crystallized by using a proper method. In practice, a number of methods have been reported to promote the crystallization of BAPC.[26] The partially crystallized BAPC particles with an initial crystallinity ranging from 20% to 30% are subjected to vacuum or an purge gas at elevated temperatures but below its melting point. After many hours, BAPC with desired molecular weight is obtained after SSP.

On the one hand, the SSP process of BAPC offers some advantages. First, it provides a way to reduce diffusion path and effectively remove phenol condensate compared to the melt process. Second, it dissolves the discoloration problem because it is carried out at a temperature lower than T_m. And finally, it involves no phosgene in the process. On the other hand, it usually requires the crystallization step to prepare partially crystallized prepolymer before the SSP, and it takes long reaction time to get final high molecular weight.

The purpose of SSP is to further increase molecular weight that cannot be obtainable from the melt polymerization. The highest molecular weight obtained from SSP is clamed to be 200 000 described in the patent of Fukawa et al.[9]. However, a detailed example has not been given. A relatively high value, $\bar{M}_w$ = 117 600, appears

in the recent patent.[25] Although attempts have been made to increase molecular weight, there is no effective method to prepare BAPC whose molecular weight is beyond the above values. Therefore, to further increase molecular weight via the method of SSP, it is important to reinvestigate reaction conditions that potentially lead to high molecular weight (e.g. particle size, end group mole ratio, reaction temperature, and purge gas rate or vacuum level).

4) Other Polymerization Methods

Ring-opening polymerization (ROP) is an appealing concept to prepare high molecular weight polycarbonates. In a ROP, the essential step is to prepare the building block of cyclic monomers. In 1962, Schnell and Botttenbruch[27] reported the preparation, purification and polymerization of the cyclic tetrameric carbonate of BPA. In 1991, Brunelle and Shannon[28] found that it is not necessary to prepare cyclic oligomers with a specific monomer unit length, and reported the selective preparation of mixtures of cyclic oligomers in high yields, ranging from 2 to 26 monomer units in length. It is believed that ROP is a thermodynamically driven process, which is similar with the melt polymerization process. But it leads to a much higher reaction rate and molecular weight because of the perfect stoichiometric ratio of functional groups and free of phenol removal. However, ROP has not been studied extensively because the preparation of cyclic oligomers is tedious and multiple purification steps are required. Although this technology currently leads to the highest molecular weight polycarbonates achievable by any process, it is far beyond the stage of commercialization.

The oxidative carbonylation of BPA was considered as one of the promising methods because it achieves direct synthesis of BAPC from BPA, carbon monoxide and oxygen without involving phosgene. Over two decades ago, Chalk[29] and Hallgren[30] at GE disclosed their first attempts. It was demonstrated that with a palladium catalyst, carbon monoxide and oxygen could be directly introduced into BPA group by the oxidative carbonylation of BPA with the byproduct of water accompanied. However, the following drawbacks make this process difficult to be commercialized: 1) expensive catalyst and very complex co-catalyst, 2) difficult to obtain high quality products, and 3) low selectivity and yield.[1]

1.1.2 Aromatic Polycarbonate Copolymers

During the early stage in the development of polycarbonates, many other diols were extensively investigated for potentially applications. However, no other polycarbonate homopolymers were as successful as BAPC in the polycarbonate industry. Polycarbonate copolymers based on BPA, on the other hand, have been quite successful. Over the past decades, a variety of aromatic polycarbonate copolymers based on BPA have been prepared and evaluated. The properties of BAPC can be significantly improved by adding a third monomer or oligomer to meet a variety of special applications, which renews the interest in BAPC homopolymer. An excellent review of many types of polycarbonate copolymers has recently appeared.[31] Some monomer or oligomers used to modify the properties of BAPC are listed in Table 1.1. They are: 1) α,ω-dichloropoly(dimethylsiloxane); 2) 3,3′,5,5′-tetrabromobisphenol A; 3) 3,3′,5,5′-tetramethylbisphenol A; 4) 6,6'-dihdyroxy-

3,3,3',3'-tetramethyl-1,1'-spiro(bis)indane; 5) dodecanedioic acid; 6) bis(4-hydoxyphenyl)dimethylsilane 7) 4,4′-dihydroxydiphenyl; 8)1,1′-bis(4-hydroxyphenyl)-3,3,5-trimethylcyclohexane.

Table 1.1 Third Component used for polycarbonate copolymers

no.	chemical structure	properties	ref
1	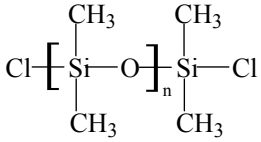	Mechanical toughness	32
2	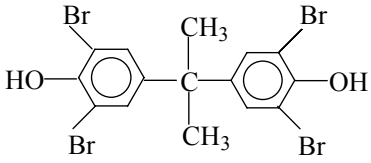	Flame retardancy	33
3	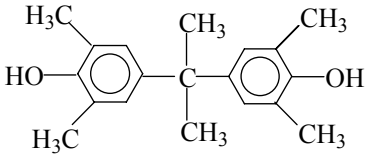	High gas permeability	34
4	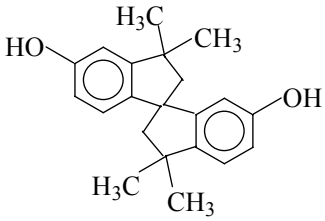	Low birefringence	35
5	$HOOC(CH_2)_{10}COOH$	High melt flow	36
6	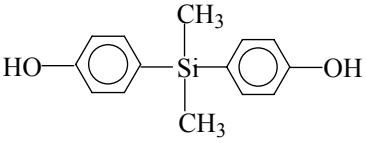	Better weatherability	37
7	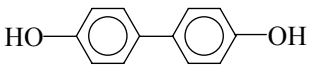	Impact resistance	38
8	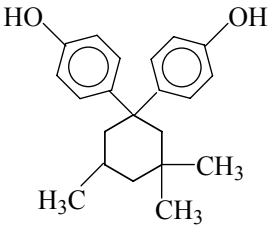	Heat resistance	39

1.2 Modeling of Solid-state Polymerization and Chain Length Distribution

In principal, the nature of SSP is not an independent process of, but rather an extension to, the melt transesterification process. However, the SSP process becomes much more complicated because crystallization, concentration gradients, and crystalline morphology as well as other factors are involved. The general aspects of SSP have been reviewed by many researchers including Pilati[40], Gantillon et al.[41] and Vouyiouka et al.[42]. The modeling study of SSP, as an alternative to the experimental approach, has been carried out for several decades. It has gained good insights into reaction mechanisms, kinetics and reaction behaviors of SSP. In the following, the review on the modeling of solid-state polymerization will be divided into two categories: 1) particle modeling and 2) reactor modeling.

1.2.1 Solid-State Polymerization in a Single Particle

The SSP in a single polymer particle is a very complex process. In the model simulation, some researchers[43,44] described it as having the following steps: 1) the diffusion of functional end groups in the particle, 2) the forward and backward reactions, 3) the diffusion of condensate inside of polymer particle (internal diffusion), and 4) the diffusion of condensate from the particle surface to the inert gas phase (external diffusion), while others[45-47] lumped the first and the second steps as one single reaction step. Each one of chemical and physical steps is important for the SSP process and the overall reaction rate is controlled by one or more of these steps depending on a number of factors such as reaction chemistry, physical shape of particles, diffusion rate of condensate, and operating conditions, etc. Thus, a SSP

process could be controlled by the reaction rate[48-51], or by the diffusion rate of condensates[46,52], meaning that the rate-controlling step is subjected to change depending on reaction conditions[45,53]. As a result, for a SSP process, it is difficult to come up with a universal model which could cover all the SSP processes in a single polymer particle.

According to the reaction kinetics and mechanisms assumed, models developed for a single polymer particle may be classified as the following three categories: 1) the reaction model, 2) the diffusion model, and 3) the comprehensive model. The reaction model assumes that chemical reaction is the rate-controlling step, which holds at low reaction temperature or for a polymer particle with a very small size.[48,49] Under these conditions, the diffusion of byproducts, as compared to the reaction of SSP, is negligible, and the reaction tends to be irreversible because of fast phenol removal. The concentrations of end groups may be described as a set of ordinary equations (ODEs),[24,48,49] which is different from the diffusion model and the comprehensive mode that involve a set of partial differential equations (PDEs). An empirical model is one of the simplest models that have been used to describe SSP kinetics. In the empirical model, chemical reaction kinetics is usually expressed as a power-law model with different orders: 2^{nd} order for BAPC[24], 2^{nd} order for PET[49,50,54], -0.49^{th} order for nylon-6,6[55]. Obviously, there is no universal agreement on the relevant chemical kinetic expressions, and the empirical determination of the power order is based on experimental data fitting. Generally, these models only simulate the change of number average molecular weight, and fail to capture an observed SSP kinetic characteristic of broadening molecular weight distribution.

The diffusion model considers the diffusion of byproducts is the rate-controlling step. Usually, a SSP is carried out under low pressure or at an effective flow rate of purge gas. Thus the external diffusion of byproducts from particle surface to the inert gas phase has much higher rate than that inside of a particle. Therefore, a diffusion model, in general, refers that the reaction rate is controlled by the internal byproduct diffusion. Other than a reaction model, diffusion models usually can be used to describe the reaction behaviors in relative big particles. If particle size is small enough, a diffusion model (PDEs) may be simplified as a reaction model (ODEs). Most models[23,56-61] developed for SSP processes can be put into this category. With a diffusion model, the effect of particle size has been extensively studied[57,60], and the broadening of molecular weight distribution can be explained[57]. Some researchers[23,62] even further developed equilibrium models where it is assumed to reach reaction equilibrium so fast that chemical reaction can be ignored in a diffusion model. Since equilibrium models assume reaction equilibrium is built in each layer of a particle, they provide an upper bound on the polymerization kinetics, and capture the overall reaction behavior. However, an equilibrium model may not truly reflect local reaction behavior such as a place near the surface where the diffusion rate of byproducts could be much faster than the reaction rate due to the short diffusion path.

Comprehensive models consider chemical reactions, together with the diffusion of byproducts, but also with the diffusion of end groups in the model simulation.[43,44,63,64] Kumar and Saksena[63] adopted the idea of segmental diffusion of end groups from the model developed by Chiu et al.[65] that was used to account for the Trommsdorff effect (or gel effect) in the free radical polymerization. This approach

assumes that chemical reaction does not occur until two kinds of functional end groups diffuse into a certain reaction range. Thus, the effect of end group diffusion can be incorporated into model equations that may be able to describe both the diffusion control of end groups at low reaction temperature and the diffusion control of byproducts at higher reaction temperature. A comprehensive model places an emphasis on the molecular basis, which is more fundamental and general than other types of models, and provides a whole picture of the process of SSP. However, it is impossible to experimentally determine the range of reaction zone that only has a theoretical basis. Moreover, the kinetic parameters, such as frequency factors, activation energies, may not be suitable for adopting from the melt polymerization because of the effect of end group diffusion[43]. The diffusion of end groups and reaction usually occur simultaneously. It is difficult to determine diffusivities of end groups experimentally. Furthermore, it is quite troublesome to fit so many unknown parameters with experimental data for a comprehensive model.

Crystallization is a major factor that differentiates the SSP from the melt polymerization process. It certainly has a significant effect on SSP. In a semicrystalline prepolymer particle, the crystalline portion in prepolymers is important and serves as a molecular "scaffold" to maintain dimensional and thermal stability. During the crystallization, the polymer chains fold into the lattice of lamellae and form spherulites. Li et al.[66] directly observed the growth of lamella and spherulites in a semicrystalline polymer by using AFM. Generally, it is believed that functional end groups are expelled from crystalline region and oriented in the amorphous phase where reaction occurs.[56,67,68] The crystallinity has double-sided

effects on the SSP reaction rate. On the one hand, the concentrations of end groups and catalyst in the amorphous phase are increased due to crystallization, which accelerates the reaction rate.[47,56] On the other hand, the mobility of polymer chains is greatly limited due to crystalline phase, which also hinders the by-product removal rate.[69] Crystallization during SSP is often considered as a secondary crystallization, and the crystallization behavior may be described by the Avrami equation and the crystallization rate is proportional to the fraction of amorphous phase.[56] Some researchers, on the contrary, used a constant crystallinity in model simulation for simplicity.[44,57] This simple treatment, however, cannot study the effect of crystallinity change and its effect on SSP. Furthermore, Gross et al.[70] indicated there is a crystallinity gradient inside of particle and the shell of particles has the highest crystallinity during the SSP of BAPC, which is also observed by Lu et al.[71]. According to the experimental results from Lu et al.[71], a gradient of crystallinity may be developed along the radial direction in a crystalline polymer particle, and the gradient of crystallinity after SSP process is even greater than that in prepolymer samples. However, quantitative equations to describe these crystallinity gradients in a polymer are still not available. Thus, it is common to assume a uniform distribution before and after SSP in the model simulation.[56,60] Moreover, the complexity is not only from the effect of crystallinity, but also from the crystalline morphology of prepolymer because the diffusion rate of byproducts also depends on the surface morphology of crystalline structure.[72] However, there are a few studies available on the morphological effect on the SSP.

Although the SSP in a single particle has been studied extensively, there are several problems remain unsolved. For example, it is well known that the stoichiometric balance of end group ratio is of great importance. However, few studies are available on the effect of prepolymer end group ratio because it is hard to characterize end group concentrations in a prepolymer. Moreover, the molecular species model has been developed to describe the process of SSP.[57] But the method proposed to calculate the initial conditions of moments should be improved. It is still worthwhile to investigate the SSP in a single polymer particle and provide a throughout picture of SSP behaviors.

1.2.2 Solid-State Polymerization in Continuous Reactors

In industry, several different types of reactors that are used for the SSP processes include tumbler reactors[73,74], fixed bed reactors[75], moving packed bed reactors[76,77], fluidized bed reactors[78] and stirred bed reactors[79]. The advantage of batch mode reactors is that all the polymer particles experience a same residence time and there is no residence distribution. Polymer particles would have the same molecular weight if particle size stays the same. However, to produce BAPC on a massive scale, a continuous reactor is preferable to a batch reactor. For a continuous fluidized bed reactor, it is impossible to have a uniform residence time for each particle. A gravity-driven moving packed bed reactor[76], on the other hand, can greatly reduce the non-uniformity of residence time and it is currently the most common reactor design for an industrial SSP process.[80]

To understand more detailed features of alternative reactor designs, a fundamental reactor modeling study is very helpful. In the reactor modeling studies of SSP, however, the number of publication is much less than that for modeling a single polymer particle probably due to the following reasons: 1) It is costly to construct and run a continuous SSP reactor even in pilot scale. 2) The reaction behavior of SSP operated in batch-mode reactors may be described by a SSP process in a single particle. 3) It is very hard to consider the nonuniformity in particle scale together with the nonuniformity in reactor scale.

In reactor modeling studies, most work focused on a moving packed reactor[80-86], while little work available for continuous stirred tank reactors in series (CSTRs)[87]. Mallon and Ray[80] studied a moving packed bed reactor using a CSTRs-in-series model and studied the effects of operating conditions such as gas flow rate, gas phase temperature and condensate concentrations in gas phase, and predicted dynamic behaviors in response to several operating variables such as particle feed rate, feed molecular weight, and gas phase temperature. Yao et al. did a series of reactor modeling work on the SSP of polyester[81-84] starting with POLYRED simulation package[81] and then developed a combined 1-D dispersion reactor model and 1-D particle model[82,83]. At the end, Yao et al. [84] simplified the combined 1-D reactor model and 1-D particle model by performing a lumped heat and mass transfer analysis. Algeri et al.[85] adopted the frame work developed by Yao et al.[82] and applied it to the SSP of PET process with the crystallization effect considered. Based on this improved reactor model, a predictive control scheme has been developed to control the quality of product at the reactor outlet. In recent work of Lucas et al.[87], an entire

SSP process of PET from precrystallizers, crystallizers, SSP reactors to product dryers has been studied. A CSTRs-in-series model was used to model the SSP reactor.

In the past studies, the radial nonuniformities such as temperature and molecular weight in reactor scale, however, were assumed to be absent. For a relative large scale moving packed bed, it is possible to have radial nonuniformities such as temperature and molecular weight. Therefore, it is necessary to understand the nonuniformities in reactor radial direction and how they would affect the reactor performance.

1.3 Modeling of Chain Sequence Length

The interest of chain sequence length distribution arises when it comes to a polycarbonate copolymer. To modify or improve the properties of BAPC, a third monomer or oligomer is often added to copolymerize into a condensation terpolymer. It is well known that not only the composition of third component, but also chain length distribution plays an important role in the physical properties[88]. With the current experimental techniques, it is not easy to obtain the accurate characterization of chain sequence length distributions. However, modeling of chain length distribution provides an alternative to the experimental measurement. It is essential to develop quantitative formulas to understand the evolution of chain microstructures.

Unlike a free radical polymerization, a statistical method is often involved to simulate a step-growth polymerization process. Statistical approach begins with the pioneering work from Flory[89] and Stockmayer[90]. Case[91] applied Flory's statistical

approach to a number of complicated systems, including the system with AR_1A, BR_2B, and BR_3B monomers where only A reacts with B. The equations of overall molecular weight distribution and chain length distribution have been given, but the chain sequence remained unstudied. Later on, the recursive method developed by Lopez-Serrano[92] and the Monte Carlo method developed by Johnson and O'Driscoll[93] were capable of calculating sequence length averages. In recent work, Beers[94] developed a general model framework to calculate monomer sequence length distributions for polymer melt blending. However, this method is complicated and not straightforward. It is still necessary to develop a simple method to obtain sequence length distributions.

1.4 Research Objectives and Chapter Overview

1.4.1 Research Objectives

This dissertation is devoted to studying fundamental problems in the step-growth polymerization of aromatic polycarbonates. The purpose is to address unsolved problems in the step-growth polymerization processes in the solid state and in the molten state, to provide deeper insights on the reaction mechanism and reaction kinetics of SSP. This in turn will allow us to develop new processes to prepare high molecular weight polycarbonates and other specialty polycarbonates, and to help design and scale up new rectors, optimize operating conditions and improve product qualities.

1.4.2 Chapter Overview

In Chapter 2, an end group model is developed to describe the kinetics of the SSP of BAPC. This model allows us to calculate polymer chain length distributions in a polymer particle at different radial positions with reaction time, and to reveal strong intraparticle nonuniformities in large particles. Through the model simulation, it is found that the end group ratio has a significant effect on the molecular weight increase, and that the reaction kinetics of SSP is not dependent on the prepolymer molecular weight *per se*, but it depends strongly on the end group mole ratio in the starting prepolymer.

Chapter 3 presents a new method to calculate initial moments in a prepolymer for the molecular species model. Based on the theory of the most probable chain length distribution, it is shown that the back calculation method is capable of not only determining the end group concentrations and conversions, but also calculating initial moments of molecular species for both stoichiometric balanced and imbalanced cases. With the molecular species model, the methods to increase reaction rate such as adjusting end group mole ratio by blending with another prepolymer and remelting particles have been discussed through model simulation.

In Chapter 4, a new dynamic process model has been developed for the continuous SSP of BAPC in a moving packed bed reactor. The process model consists of a macroscopic reactor model and a single particle model to calculate the reactor temperature profiles and the polymer properties. This process model allows us to design a moving packed bed reactor, to study the effects of operation parameters

on the performance, and to study the reactor radial nonuniformities of the SSP in a moving packed reactor.

In Chapter 5, a statistical model is developed to calculate the chain length distributions and averages for condensation random terpolymers. This model has been incorporated into a semibatch melt process to show the evolution of chain sequence length distributions and the change of average chain sequence lengths. Important parameters that affect chain microstructures such as end group ratio and reactivity ratio have been investigated. With the relationship between physical properties and chain sequence length distributions available, it also allows us to design and optimize the chain microstructures for the condensation terpolymers.

Chapter 6 presents a new morphology of BAPC in the study of thin-film crystallization: multi-layer stacked three-dimensional spherulites. It is found that the film thickness is a major factor that affects the resulting morphology of the BAPC polymer. SEM and DSC are used to characterize these spherulites.

Chapter 7 draws conclusions and presents recommendations for future work.

Chapter 2

Modeling of Solid-State Polymerization of Bisphenol A Polycarbonate in a Single Particle: I. End Group Model

This chapter has been reproduced in part with permission from the paper:[60]
Ye, Y.; Machado, B.; Choi, K. Y.; Kim, J. H.; Woo, B. G. Modeling of Solid-State Polymerization of Bisphenol A Polycarbonate. *Ind. Eng. Chem. Res.* **2005**, *44*, 2494-2505.

2.1 Introduction

Bisphenol A polycarbonate (BAPC) is an important engineering thermoplastic that has high heat resistance, impact resistance, and excellent optical clarity. Polycarbonate is used in many applications including data storage media (CD, DVD), structural materials for electrical and electronic parts, automobiles, etc. Polycarbonate is manufactured industrially by either an interfacial phosgenation process or by a melt transesterification process with the latter being considered as environmentally more benign than the former. In a melt transesterification process, bisphenol A polycarbonate is manufactured by first reacting diphenyl carbonate and bisphenol A (4,4-dihydroxydiphenyl 2,2-propane) at 180-250°C in the presence of a catalyst such as $LiOH \cdot H_2O$ to form a relatively low molecular weight prepolymer at reduced pressure using a stirred-tank type reactor. The polymerization is a reversible reaction with phenol produced as a byproduct or condensate. The condensate must be removed continuously from the reactor to shift the equilibrium toward chain growth reaction. In a typical melt polycondensation process, it is difficult to obtain high molecular weight polycarbonate in a single stirred tank reactor because increasing melt viscosity makes the removal of phenol from the reaction mass very difficult, limiting the

increase in conversion and molecular weight. Similar problems occur in other melt polycondensation processes to manufacture high molecular weight polyesters such as poly(ethylene terephthalate) (PET) and poly(butylene terephthalate) (PBT). In general, a relatively low molecular weight prepolymer is further polymerized to a high molecular weight final product in a continuous finishing stage polymerization reactor such as rotating disk reactors and screw reactors that provide large mass transfer surface areas for the removal of condensates. Either high vacuum (1-3 mmHg) or inert gas sweeping technique is used to reduce the partial pressures of condensates.[12]

Solid-state polymerization (SSP) is a postmelt polycondensation process that is widely used in PET, PBT, and nylon polymerization processes to obtain high molecular weight not obtainable by melt polycondensation. Either low or moderately high molecular weight polymers produced in the melt polymerization can be used as the feed material for solid-state polymerization.

Solid-state polymerization of a semicrystalline polymer is carried out at a temperature above the glass transition temperature (T_g) to provide the mobility of reactive end groups but below the polymer's melting point (T_m) to prevent the sticking of polymers. One of the primary process design objectives is to develop a technique to obtain high molecular weight final product in the shortest possible reaction time.

In solid-state polymerization, the diffusion of polymer end groups and condensates may affect the reaction rates. However, solid-state polymerization is usually carried out at a temperature close to the melting point, and the mobility of reactive end groups is not a rate-controlling factor.[56,57] Therefore, the diffusion rate of

condensates from the particle interior to the surrounding gas phase will have the strongest effect on the rate of solid-state polymerization and polymer molecular weight. Indeed, many researchers investigated the kinetics of solid-state polymerization of polyesters, nylons, and polycarbonates using diffusion-reaction models and confirmed that the diffusion of condensation byproducts is the rate-controlling process. In the solid-state polymerization of bisphenol A polycarbonate, a stiff concentration gradient can be established in large polymer particles (e.g., 1.4 mm in diameter) to cause a slow increase in molecular weight and the broadening of molecular weight distribution (e.g., $\bar{M}_w / \bar{M}_n = 2.0 - 2.4$).[57] There can also be a mass-transfer resistance at the solid-gas interface of a polymer particle. For the removal of phenol in solid-state polymerization of polycarbonate, either vacuum or nitrogen gas purging is used. The inert purge gas lowers the partial pressure of phenol in the gas phase and enhances the mass transfer of phenol from the polymer particle to the gas phase. Shi et al.[95] reported that supercritical carbon dioxide can also be used as a sweeping fluid to remove phenol in solid-state polymerization of polycarbonate at 90-135ºC and at CO_2 pressure of 138-345 bar.

The performance of solid-state polycondensation of polycarbonate is also affected by other factors such as temperature, degree of crystallinity, catalyst concentration, and prepolymer molecular weight. In solid-state polymerization of polyesters and polycarbonate, it is believed that polymerization occurs in the amorphous phase where reactive end groups are present and mobile. Polycarbonate prefers the amorphous state to the crystalline state when being cooled from the melt.[26] Although it is improbable that the polycondensation occurs in the crystalline phase,

the solid-state polymerization of bisphenol A polycarbonate does not occur if the polymer is completely amorphous. When amorphous polycarbonate pellets or particles are heated above the glass transition temperature under vacuum or inert gas stream, they stick to each other and eventually fuse together before any polycondensation reaction proceeds. Therefore, polycarbonate prepolymer must be crystallized prior to solid-state polymerization by annealing at elevated temperatures, by solvent treatment, or by using nucleating agents. The crystalline portion of the polymer serves as a molecular "scaffold" to maintain dimensional stability of a polymer particle. During the crystallization, the polymer chains fold into the lattice of lamellae and form spherulites. Then, the end groups are expelled and oriented at the amorphous areas among the lamellae of spherulite.[69] The catalyst is also expelled from the crystalline region into the amorphous phase. Higher catalyst concentration is favorable in obtaining high molecular weight polymer at high reaction rate but high concentration of catalyst residue can have adverse effects on the quality of polycarbonate in some end-use applications.

The mathematical modeling of solid-state polymerization of polyesters, nylons, and polycarbonates has been studied by many workers in the past. A recent work by Mallon and Ray[56] provides the most comprehensive modeling framework for the solid-state polycondensation of semicrystalline polymers such as PET and Nylon 66. For example, the PET solid-state polymerization model incorporates a time-varying crystallization model and various reactions including chain degradation reactions. In Nylon 66 modeling, they showed that polymer particle pretreatment can have a great influence on the solid-state polymerization kinetics.

Although there are many reports on the modeling of solid-state polymerization of PET and nylons, not much has been reported on the solid-state polymerization of aromatic polycarbonates. The feasibility of solid-state polymerization to increase the molecular weight of poly(aryl carbonates) was first reported by Iyer et al.[96] They showed that when poly(aryl carbonate) is partially crystallized, the solid-state polymerization temperature can be raised gradually from 220 to 250°C without melting of the polymer particles to obtain high molecular weight polymers. Recently, experimental and modeling studies of solid-state polymerization of bisphenol A polycarbonate have been reported in the literature.[24,57,62,95,97] With the equilibrium model in which instantaneous local reaction equilibrium is assumed, Goodner and co-workers[62] calculated an upper bound on molecular weight and its rate of increase with reaction time in solid-state polymerization of PET and polycarbonate. Goodner et al.[57] presented an interesting modeling work in which a molecular species model of Kim and Choi[11] and a solid-state polymerization model framework by Mallon and Ray[56] were combined. In their solid-state polymerization experiments, the reaction temperature was gradually increased from 180 to 240ºC during the period of 12 h and maximum molecular weight ($\bar{M}_w$) obtained was 15 000 (~6 times the initial molecular weight). They investigated the effects of various reaction parameters including polymer particle size, phenol diffusivity, and stoichiometric excess. For a polymer particle of size 3.6 mm (diameter), they measured the molecular averages in the particle core, middle, and shell regions and found that the spatial difference in the molecular weights can be quite large. For example, the molecular weight ($\bar{M}_w$) in the center region is ~7000 whereas it is ~17 000 in the outer shell region. Another

interesting and important result from the work of Goodner and co-workers[57] is that stoichiometric excess has a large effect on the performance of solid-state polymerization.

In this chapter, we develop a functional group model to develop a new and more quantitative understanding of the kinetics of solid-state polymerization of bisphenol A polycarbonate. Since some important aspects of solid-state polymerization have been examined by other researchers in the past, we focus our research on elucidating how the polymer chain length distribution is influenced by particle size, prepolymer molecular weight, end group mole ratios in prepolymers and initial transesterification mixture, and polymer crystallinity. In particular, we present a detailed analysis of the prepolymer molecular weight effect on the solid-state polymerization.

2.2 Experimental

Bisphenol A polycarbonate prepolymer was prepared by melt polycondensation (transesterification) of diphenyl carbonate with bisphenol A with $LiOH \cdot H_2O$ catalyst in a stirred semibatch reactor using the polymerization procedure reported in the literature.[11,98] The prepolymer was crystallized to fine powders of ~0.1 mm in diameter by precipitating the prepolymer solution in acetone. The solid-state polymerization of dry prepolymer particles was carried out using a small stirred glass reactor at constant reaction temperature (200°C). No melting or sticking of polymer particles occurred during the polymerization. The concentrations of end group in prepolymer samples were determined by ^{13}C NMR analysis,[99] and the degree of

crystallinity was measured using differential scanning calorimeter (DSC, TA Instrument). The DSC thermograms were obtained with increasing temperature from 50 to 300ºC for 25 min under nitrogen atmosphere. The polymer molecular weight was measured by gel permeation chromatography using methylene chloride as a solvent.

2.3 Modeling of Solid State Polymerization of Polycarbonate

To develop a solid-state polymerization model for a single polymer particle, we consider a partially crystalline spherical polycarbonate prepolymer particle at a temperature above the glass transition temperature (T_g) but below the melting point (T_m). The actual solid-state polymerization temperature is close to the polymer's melting point. We assume that following polycondensation reaction occurs in the amorphous phase without any side reactions:

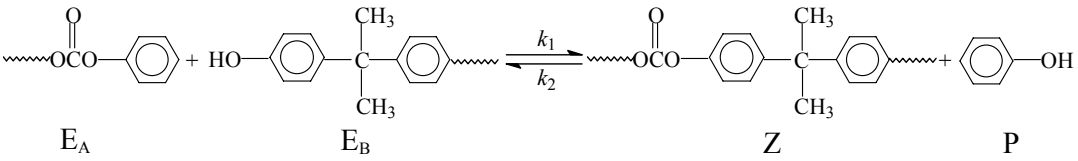

where E_A = phenyl carbonate group, E_B = hydroxyl group, Z = polymer repeat unit, and P = phenol. The above stoichiometric equation shows that phenol (P) must be removed from the reaction phase to shift the equilibrium toward the forward reaction (chain growth reaction). The rate expressions for the functional end groups, polymer linkage (Z), and phenol are represented as

$$r_{E_A} = -k_1[E_A][E_B] + k_2[Z][P] \tag{2.1}$$

$$r_{E_B} = r_{E_A} = -r_Z = -r_P \tag{2.2}$$

From the reaction stoichiometry, the following equations are obtained:

$$[E_B] = [E_B]_0 + [E_A] - [E_A]_0 \tag{2.3}$$

$$[Z] = [Z]_0 + [E_A]_0 - [E_A] \tag{2.4}$$

Here, we make the following assumptions that are similar to those employed by Mallon and Ray[56] for the modeling of solid-state polymerization of PET and nylons: (i) Reactive end groups and catalyst are present only in the amorphous phase. They are expelled from the crystalline phase and oriented at the amorphous phase among the lamellae of a spherulite. (ii) Polymerization occurs only in the amorphous phase and polymer particle is spherical. (iii) The reaction chemistry in the amorphous phase follows that of the melt polycondensation because the solid-state polymerization temperature is much closer to the polymer's melting point than the glass transition temperature of the polymer.[24,56] (iv) The initial concentration of phenol in the prepolymer is zero. (v) The particle volume is constant during the solid-state polymerization. (vi) The particle density is uniform. (vii) The particle temperature is unform and constant. (viii) The degree of crystallinity is defined as: $x_c = V_c/V$, where V is the total particle volume and V_c is the crystalline phase volume. (ix) End group reactivities are independent of polymer chain length. (x) All the mass-transfer resistance for phenol resides in the interior of the polymer particle.

Using the above assumptions, we can derive the solid-state polymerization model for a single spherical particle. The mass balance equation for phenol takes the following form:

$$\frac{\partial[P]}{\partial t} = \frac{k_1}{1-x_c}\left[[E_A]\left([E_A]-[E_A]_0+[E_B]_0\right)-\frac{[P]}{K}\left([E_A]_0-[E_A]+[Z]_0\right)\right] + D_p\left(\frac{1}{r^2}\frac{\partial}{\partial r}\left(r^2\frac{\partial[P]}{\partial r}\right)\right) \tag{2.5}$$

where D_p is the diffusivity of phenol in the polymer phase and K is the equilibrium reaction rate constant. The concentrations of phenol and reactive end groups are based on the total particle volume. The initial and boundary conditions are

I.C. @ t = 0, [P] = 0 (2.6)

B.C. @ $r = 0$, $\frac{\partial[P]}{\partial r} = 0$ (2.7.1)

@ $r = R$, $[P] = 0$ (2.7.2)

or $-D_p\left.\frac{\partial[P]}{\partial r}\right|_{r=R} = k_g\left([P]_{r=R}-[P^*]\right)$ (2.7.3)

$[P^*]$ is the phenol concentration in the bulk gas phase. For the phenyl carbonate end group, the mass balance equation is given as

$$\frac{\partial[E_A]}{\partial t} = \frac{k_1}{1-x_c}\left[\frac{[P]}{K}\left([E_A]_0-[E_A]+[Z]_0\right)-[E_A]\left([E_A]-[E_A]_0+[E_B]_0\right)\right] \tag{2.8}$$

I.C. @ t = 0, $[E_A] = [E_A]_0$ (2.9)

In deriving eq 2.8, the diffusion of phenyl carbonate end group in the polymer particle is assumed to be negligible. By solving eqs 2.5 and 2.8, we can calculate the solid-state polymerization rate, polymer molecular weight, and chain length distributions.

Since solid-state polymerization is assumed to occur only in the amorphous phase, the effect of crystallinity or crystallization kinetics needs to be incorporated into the solid-state polymerization model. According to Mallon and Ray[56], the Avrami equation ($x_c = 1-\exp(-kt^n)$) is inadequate to describe the entire stage of

crystallization in solid-state polymerization of PET because the transition from primary to secondary crystallization occurs very rapidly whereas typical solid-state polymerization takes several hours. We employed the following equation to describe the rate of change in the polymer crystallinity:[56]

$$\frac{dx_c}{dt} = k_c \left(x_{\max} - x_c \right) \tag{2.10}$$

Eq 2.10 indicates that the crystallization rate is proportional to the crystallizable amorphous fraction and that the crystallization rate is not directly related to polymer molecular weight. For bisphenol A polycarbonate, the maximum degree of crystallinity (x_{max}) is 0.62.[100] We determined the crystallization kinetic constant k_c from our experimental data. With the two prepolymers of different molecular weight, we measured the degree of crystallinity at different reaction times during the solid-state polymerization and Figure 2.1a shows the measured crystallinity data. Here, the molecular weight of prepolymer B (scaled molecular weight, 2.4) is 3 times larger than prepolymer A (scaled molecular weight, 0.82). Note that the increase in the crystallinity for 15 h of reaction time is quite significant. Figure 2.1b is the plot of the integrated eq 2.10 for these prepolymers. Notice that experimentally measured polymer crystallinity data are reasonably well fitted by eq 2.10. Although eq 2.10 does not explicitly show the effect of polymer molecular weight on the crystallization rate, the crystallization rate constant values obtained from Figure 2.1 are different for the two samples of different molecular weight: $k_c = 6.27\times10^{-4}$ min^{-1} for prepolymer A (low molecular weight sample) and $k_c = 1.50\times10^{-3}$ min^{-1} for prepolymer B (high molecular weight sample). These crystallization rate constants suggest that the rate of crystallization is higher for larger molecular weight polymers. It should be pointed

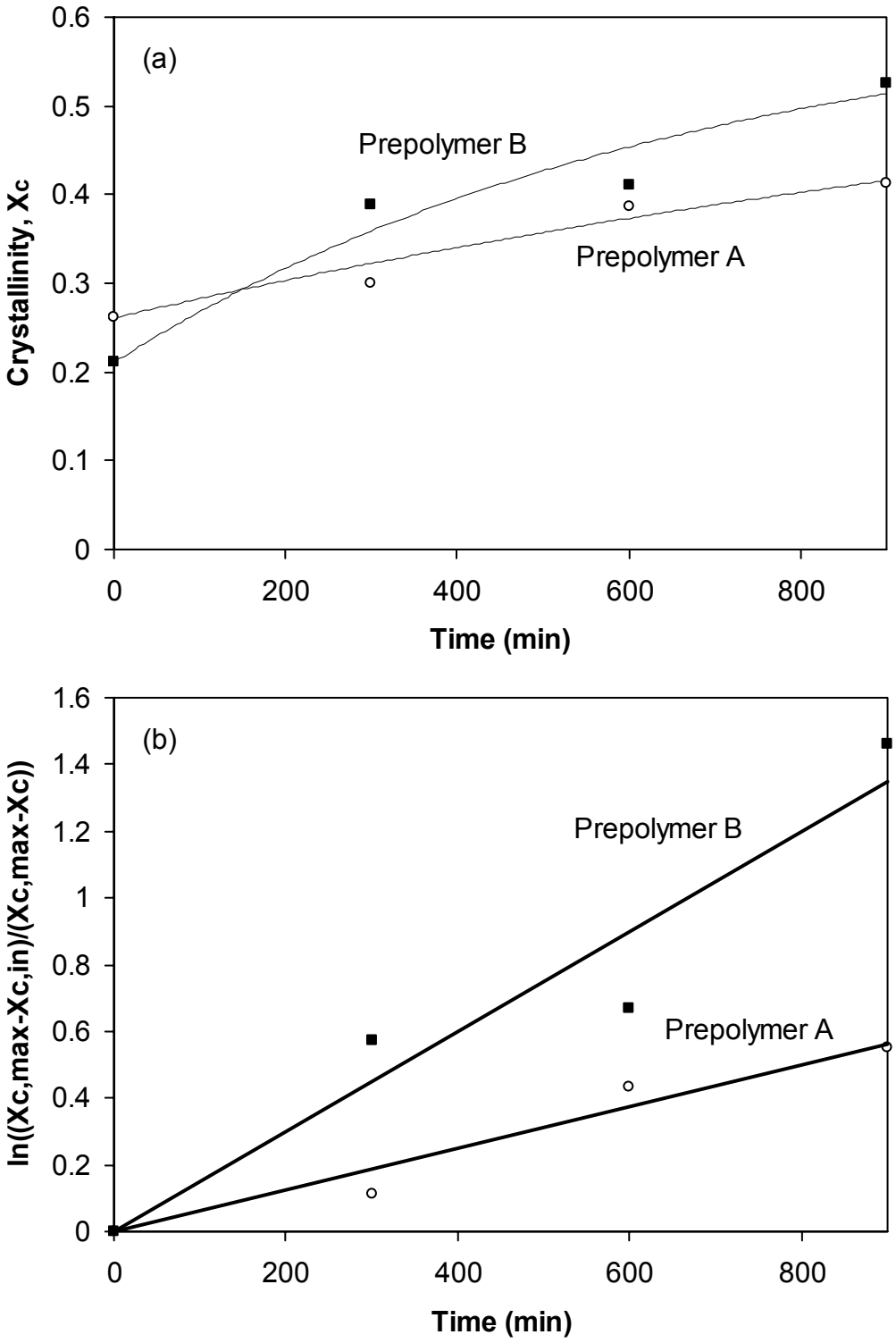

Figure 2.1 (a) Measured crystallinity of polycarbonates, (b) Test of polymer crystallization eq 2.10 with two prepolymers of different molecular weight.

out that the crystallinity values were measured from the samples taken during the solid-state polymerization experiments where the degree of crystallinity increased with an increase in polymer molecular weight.

In the presence of intraparticle diffusion resistance for the removal of phenol, the end group concentrations and the polymer molecular weight vary along the particle radius. If the concentrations of end groups and carbonate linkages are known, the number-average molecular weight can be calculated using the following equation:

$$\bar{M}_n = \frac{w_m}{2}\left(1 + \frac{2[Z]}{[E_A]+[E_B]}\right) \tag{2.11}$$

If the mole ratio of the two functional end groups is defined as r_a (= $[E_A]_i/[E_B]_i$) at the beginning of melt prepolymerization, eq 2.11 can also be expressed as

$$\bar{M}_n = \frac{w_m}{2}\frac{1+r_a}{1-r_a+2r_a(1-p)} \tag{2.12}$$

where w_m is the formula weight of a repeating unit of bisphenol A polycarbonate (w_m = 254.3) and p is the conversion of E_A. The weight-average molecular weight can be calculated using the Flory distribution derived for the system with a nonstoichiometric end group mole ratio. In the numerical solution of the solid-state polymerization model, the average molecular weights in a particle are calculated by the following equations:

$$\bar{M}_n = R^3\left(3\int_0^R \frac{r^2}{\bar{M}_n(r)}dr\right)^{-1} \tag{2.13}$$

$$\bar{M}_w = \frac{1}{R^3}\left(3\int_0^R r^2\bar{M}_w(r)dr\right) \tag{2.14}$$

Here, r is the radial position in the particle of radius R.

In most of the solid-state polymerization modeling work in the literature, complete polymer chain length distributions were not calculated. If a functional group model is used, only the molecular weight averages can be calculated. The polymerization of bisphenol A polycarbonate is classified as A-R-A/B-R'-B type polycondensation when diphenyl carbonate (A-R-A) and bisphenol A (B-R'-B) are used as two starting monomers. In this type of polycondensation, a repeating unit is formed by the coupling of two monomers or functional end groups. To obtain high polymer molecular weight in this type of polycondensation reaction, it is important to keep the mole ratio of the reactive end groups constant as closely as possible to the stoichiometric ratio of 1.0. Polycarbonate prepolymer is typically produced in a semibatch stirred reactor at 150-230ºC and at reduced pressure with a reflux condenser.[11] At 150ºC, the vapor pressure of diphenyl carbonate is 6.97 mmHg but it increases to 114.7 mmHg at 230ºC.[98] Although the bulk amount of vaporized diphenyl carbonate is refluxed back to the reactor, a small amount of diphenyl carbonate is often lost from the reactor together with phenol. Then, the actual reactive end group mole ratio becomes different from the value calculated by the initial charged amounts of monomers. Hence, to keep the mole ratio of the two reactive end groups close to the stoichiometric ratio (i.e., $r_a = 1.0$), a slight excess of diphenyl carbonate is charged to a melt transesterification reactor.[11,98] However, knowing the exact initial mole ratio of the two reactive end groups in the melt transesterification (prepolymerization) is not an easy task. Therefore, there is always an uncertainty concerning the initial mole ratio of the functional end groups. As discussed in what

follows, the performance of the prepolymerization process has a great influence on the performance of subsequent solid-state polymerization.

If we ignore any side reactions, the bisphenol A polycarbonates produced by melt polycondensation can be identified as follows by the type of end groups:

A_n:

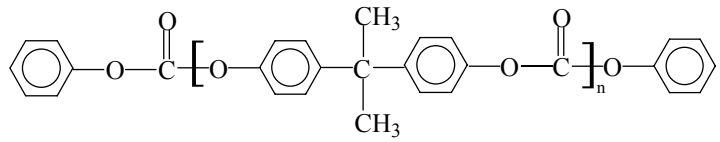

B_n:

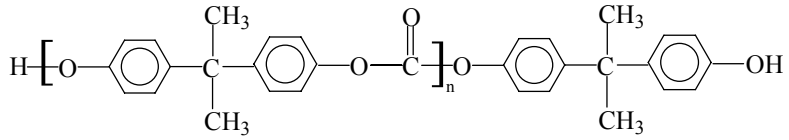

C_n:

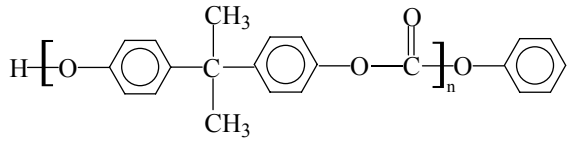

where n is the number of repeating units. Let diphenyl carbonate = A-R-A (A = phenyl carbonate end group), bisphenol A = B-R'-B (B = hydroxyl end group), and x = total number of reactant molecules combined in the polymer molecule. Then, the polymerization reactions leading to the above three species can be represented as follows (condensation byproduct not shown):[101]

(i) If x is an even integer ($n = x/2$, $x \;\; x \geq 2$; even-C; C_n);

$$\frac{x}{2}A-R-A+\frac{x}{2}B-R'-B \rightarrow A-R-A\left[B-R'-BA-R-A\right]_{\frac{x-2}{2}}B-R'-B \qquad (2.14)$$

(ii) If x is odd, either ($n = (x\text{-}1)/2$, $x \geq 3$; odd-A; A_n);

$$\left(\frac{x+1}{2}\right)A-R-A+\left(\frac{x-1}{2}\right)B-R'-B \rightarrow A-R-A[B-R'-BA-R-A]_{\frac{x-3}{2}}B-R'-BA-R-A \qquad (2.15.1)$$

or (odd-B; B_n)

$$\left(\frac{x-1}{2}\right)A-R-A+\left(\frac{x+1}{2}\right)B-R'-B \rightarrow$$
$$B-R'-BA-R-A[B-R'-BA-R-A]_{\frac{x-3}{2}}B-R'-B \tag{2.15.2}$$

The *x*-mer of odd-A is the molecule with an odd number of segments and terminal A functional groups. The *x*-mer of even-C is the molecule with an even number of segments capped by A and B groups. Also, if we let *n* be the number of repeating units, then, for odd-A and odd-B, $n = (x - 1)/2$, and for even C, $n = x/2$.

For the polymers prepared from nonequal amounts of the reactants (i.e., diphenyl carbonate and bisphenol A), the mole fraction of odd-A, odd-B, and even-C can be calculated as

$$P_{n,(odd-A)} = p^{2n} r_a^{\,n} \frac{(1-p)^2}{1+\frac{1}{r_a}-2p} \text{ (mole fraction of } A_n\text{)} \tag{2.16}$$

$$P_{n,(odd-B)} = p^{2n} r_a^{\,n-1} \frac{(1-r_a p)^2}{1+\frac{1}{r_a}-2p} \text{ (mole fraction of } B_n\text{)} \tag{2.17}$$

$$P_{n,(even-C)} = p^{2n-1} r_a^{\,n} \frac{2(1-p)(1-r_a p)}{1+r_a-2r_a p} \text{ (mole fraction of } C_n\text{)} \tag{2.18}$$

where r_a is the molar ratio of the functional end groups at zero conversion in the beginning of prepolymerization ($r_a = [E_A]_i/[E_B]_i < 1$) and *p* is the conversion of the limiting species (E_A).

Then, the number chain length distribution can be represented by the mole fraction of the polymer that has *n* repeating units:

$$P_n = P_{n,(odd-A)} + P_{n,(odd-B)} + P_{n,(even-C)} \tag{2.19}$$

The weight fraction of polymers with n-repeating units is expressed as

$$W_n = W_{n,(odd-A)} + W_{n,(odd-B)} + W_{n,(even-C)} \tag{2.20}$$

where the weight fractions of three different types of molecular species are given by the following equations:

$$W_{n,(odd-A)} = \frac{w_{An} P_{n,(odd-A)}}{\sum_{n=1}^{\infty} \left(w_{An} P_{n,(odd-A)} + w_{Bn} P_{n,(odd-B)} + w_{Cn} P_{n,(even-C)} \right)} \tag{2.21.1}$$

$$W_{n,(odd-B)} = \frac{w_{Bn} P_{n,(odd-B)}}{\sum_{n=1}^{\infty} \left(w_{An} P_{n,(odd-A)} + w_{Bn} P_{n,(odd-B)} + w_{Cn} P_{n,(even-C)} \right)} \tag{2.21.2}$$

$$W_{n,(even-C)} = \frac{w_{Cn} P_{n,(even-C)}}{\sum_{n=1}^{\infty} \left(w_{An} P_{n,(odd-A)} + w_{Bn} P_{n,(odd-B)} + w_{Cn} P_{n,(even-C)} \right)} \tag{2.21.3}$$

where

$$w_{An} = 254.3n + 228.3$$

$$w_{Bn} = 254.3n + 214.2 \tag{2.22}$$

$$w_{Cn} = 254.3n + 94.1$$

Here, the effect of end unit weight decreases with an increase of n (e.g., n up to ~20).

The number and weight chain length distributions can be approximated as

$$P_n = \left(1 - r_a^{1/2} p\right) \left[\left(r_a^{1/2} p \right)^{2n-1} + \left(r_a^{1/2} p \right)^{2n} \right] \tag{2.23.1}$$

$$W_n = \left(1 - r_a^{1/2} p\right)^2 \left[2n \left(r_a^{1/2} p \right)^{2n-1} + (2n+1) \left(r_a^{1/2} p \right)^{2n} \right] \tag{2.23.2}$$

For the A-R-A/B-R'-B type linear polycondensation as considered in this work, the polymer chain length distribution is strongly dependent on the stoichiometric imbalance of the functional end groups. Figure 2.2 illustrates the effect

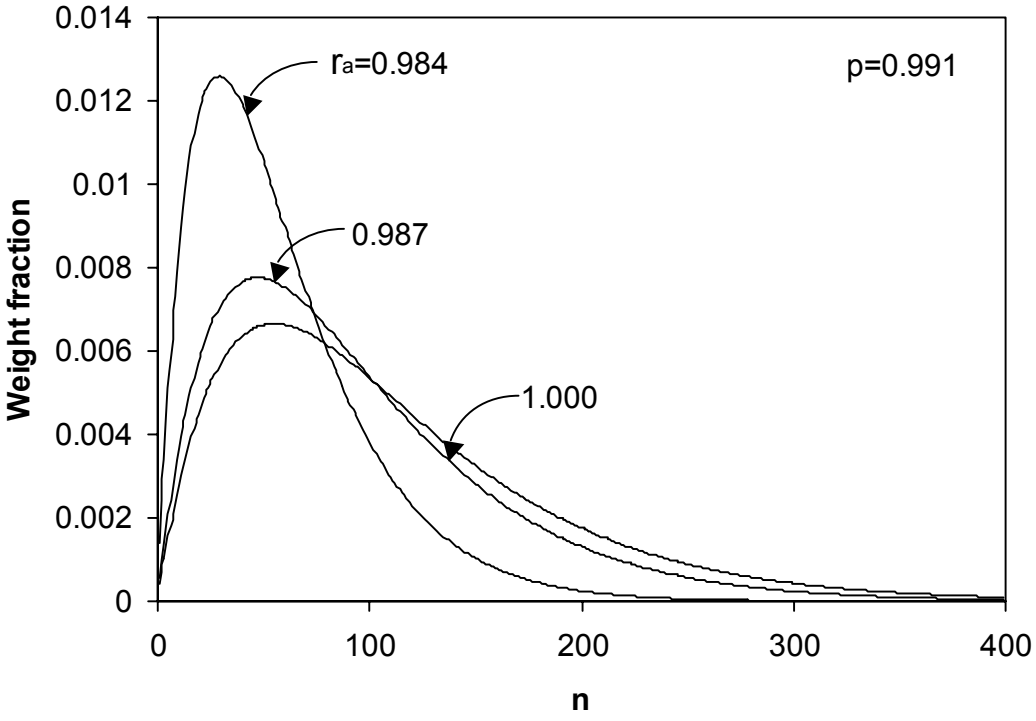

Figure 2.2 Effect of initial stoichiometric imbalance on polymer weight chain length distribution.

of initial end group mole ratio (r_a) at a given conversion of phenyl carbonate group. As the end group mole ratio deviates from the stoichiometric ratio of 1.0, the weight fractions of high molecular weight polymer chains decrease quite significantly. Thus, the weight chain length distribution (WCLD) provides additional insights into the detailed molecular structure of polycarbonate beyond molecular weight averages and polydispersity.

To simulate a solid-state polymerization model (eqs 2.5-2.10), we need to know the initial concentrations of functional end groups and catalyst concentration. The catalyst concentration used in the prepolymerization ($[C^*] = 1.7\times10^{-4}$ mol/L) is used as the initial catalyst concentration in the solid-state polymerization. If the polycondensation (melt prepolymerization) is started with a nonstoichiometric ratio of the reactive end groups, the number-average molecular weight is given by eq 2.12. As mentioned earlier, the exact value of r_a in the prepolymerization process is rather difficult to know because the amount of diphenyl carbonate lost from the reactor is difficult to measure or calculate. In general, the end group mole ratio or the end group concentrations in a prepolymer can be measured by, for example, ^{13}C NMR spectroscopy.[99] To calculate the number and weight chain length distributions using eqs 2.23.1 and 2.23.2, the original end group mole ratio (r_a) needs to be estimated for a given prepolymer sample. In the modeling work by Goodner et al.[57], who used a molecular species model, the initial molecular weight moment values in the beginning of solid-state polymerization were calculated by simulating the model for the prepolymerization stage. If the initial molecular weight averages of a prepolymer ($\bar{M}_{n,0}$) and the mole ratio of the end groups in the prepolymer ($r_a' = [E_A]_0/[E_B]_0 < 1$)

are known, we can calculate the initial end group mole ratio (r_a) at the beginning of melt transesterification and the conversion of phenyl carbonate group (functional end group A) at the end of the transesterification (i.e., in a prepolymer):

$$r_a = \frac{1 - r_a' - (1 + r_a')\left(2\bar{M}_{n,0} / w_m\right)}{r_a' - 1 - (1 + r_a')\left(2\bar{M}_{n,0} / w_m\right)} \tag{2.24}$$

$$p = 1 - \frac{1 + r_a - (1 - r_a)\left(2\bar{M}_{n,0} / w_m\right)}{2r_a\left(2\bar{M}_{n,0} / w_m\right)} \tag{2.25}$$

When these equations are applied to the prepolymer samples used in our experimental and model simulation study (Table 2.1), we find the following:

Prepolymer A: r_a = 0.984 (r_a' = 0.585)

Prepolymer B: r_a = 0.997 (r_a' = 0.728)

Notice that the end group mole ratio decreases quite dramatically during the prepolymerization stage. The difference in r_a values in the beginning of prepolymerization for the two prepolymer samples looks very small, but at the end of prepolymerization, the difference in the mole ratio of the end groups (r_a') is very large, suggesting that the solid-state polymerization behavior of these prepolymers will be quite different. Moreover, these mole ratio values are far away from the ideal value of 1.0. In other words, the solid-state polymerization for each of these two prepolymer samples will start with a significant departure from the stoichiometrically balanced reaction conditions.

Table 2.1 Model parameters

parameter	unit	ref
$k_1 = k_u + k_c[C^*]$		
$k_u = (3.108 \pm 0.102) \times 10^7 \exp(-25290 \pm 1010 / RT)$	$L \cdot mol^{-1} \cdot min^{-1}$	98
$k_c = 9.62 \times 10^8 \exp(-13900 / RT)$	$L^2 \cdot mol^{-2} \cdot min^{-1}$	
$\ln K = \frac{-\Delta H}{RT} + \frac{\Delta S}{R}$		103
$\Delta H = -6.8 \pm 1.2$	$kcal \cdot mol^{-1}$	
$\Delta S = -13.6 \pm 2.7$	$cal \cdot mol^{-1} \cdot K$	
diffusivity of phenol: $D_p = 3 \times 10^{-8}$	$cm^2 \cdot sec^{-1}$	this work
particle diameter = 0.1	mm	
prepolymer A		
$\bar{M}_{w,0} = 0.82$ (scaled)		
end group mole ratio in prepolymer, 0.585		
crystallinity, 25.3 %		
prepolymer B		
$\bar{M}_{w,0} = 2.4$ (scaled)		
end group mole ratio in prepolymer, 0.728		
crystallinity, 18.3 %		

2.4 Results and Discussion

The partial differential equations in the solid-state polymerization model were solved using the parabolic PDE solver in MATLAB. The solid-state polymerization model was first tested on the two experimental solid-state polymerization data and the results are shown in Figure 2.3. With the kinetic constants and the transport parameters listed in Table 2.1, the model provides a reasonable fit of the experimentally measured polymer molecular weight data (note: The actual molecular weight values of the prepolymers are proprietary and scaled with a constant reference value. The actual number-average molecular weight of prepolymer B is much larger than 10 000.) Figure 2.3 shows that the model predicted values of $\bar{M}_w$ are slightly larger than the experimentally measured for prepolymer A (low molecular weight prepolymer), but the qualitative trend is quite accurate. The model predictions of $\bar{M}_w$ for prepolymer B (high molecular weight prepolymer) are much better. Also, it is interesting to observe that while the molecular weight of lower molecular weight prepolymer practically stops after ~400 min of reaction, the molecular weight of higher molecular weight prepolymer B continues to rise. The solid-state polymerization model provides the correct picture of these behaviors. Thus, we conclude that the solid-state polymerization model is quite acceptable, and we develop more insights into the solid-state polymerization in a single particle through model simulations.

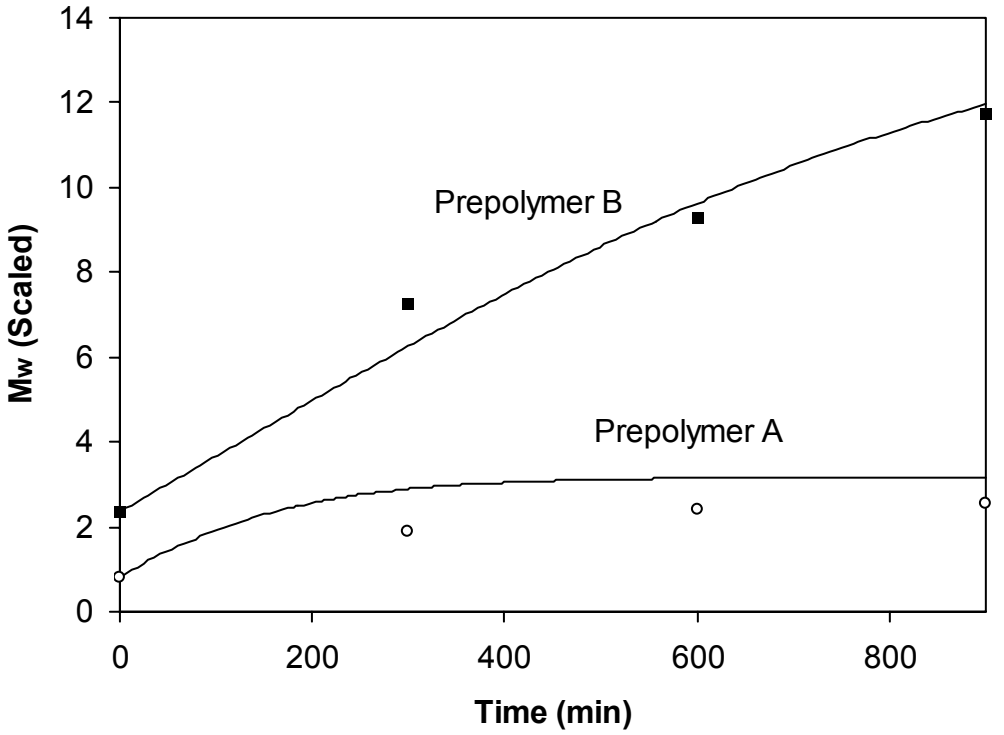

Figure 2.3 Weight-average molecular weights of two SSP samples: symbols, experimental data; lines, model simulations.

2.4.1 Effect of Polymer Particle Size

One of the most important factors that affect the rate of solid-state polymerization is polymer particle size. Regardless of the method used to prepare prepolymer particles, a prepolymer mixture will be a mixture of particles of different sizes. Therefore, understanding the effect of individual polymer particle size on the polymerization rate and polymer molecular weight is important for the design of a solid-state polymerization reactor system where a heterogeneity in polymer particle size will definitely be present. In general, we can easily expect that small polymer particles will show very little intraparticle mass-transfer effects, and therefore, high molecular weight polymer can be obtained in shorter reaction time than with larger polymer particles. Goodner et al.[57] showed in their simulation work that diffusional limitation becomes quite significant for the polycarbonate particles larger than 1 mm in diameter. Their model simulations show that intraparticle diffusional limitation leads to the broadening of molecular weight distribution (e.g., polydispersity as large as 2.4) because of steep concentration gradients in the particle. However, it is not well known whether such MWD broadening is an important factor in polycarbonate's end use properties.

The effect of polymer particle size on the molecular weight in solid-state polymerization is shown in Figure 2.4 (simulations). The average particle size of prepolymer A and prepolymer B used in our experiments is 0.1 mm. Figure 2.4 shows the $\bar{M}_w$ values of the prepolymers of same initial molecular weight but with different particle sizes. Here the lines are the model simulations and the symbols are the experimental data. It is seen that raising the molecular weight by solid-state

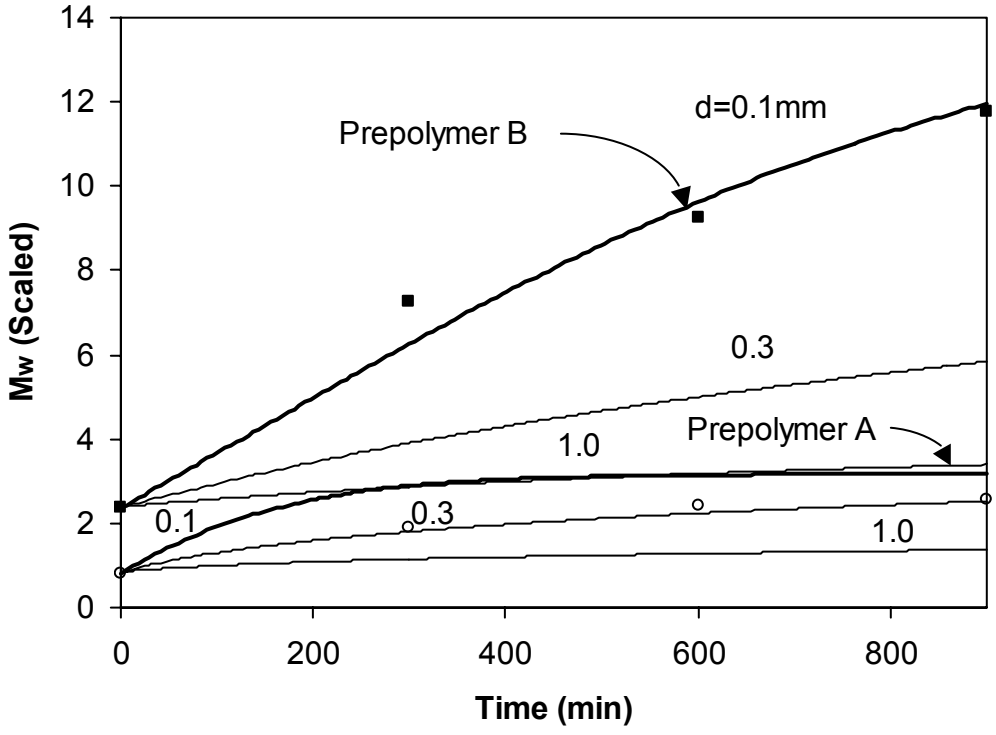

Figure 2.4 Effect of particle size on weight-average molecular weight.

polymerization is very difficult for large prepolymer particles (e.g., $d > 1.0$ mm). The effect of prepolymer particle size can be quite significant. For example, to raise the molecular weight of prepolymer B (scaled $\bar{M}_w$ =2.4) to $\bar{M}_w$ = 5 (scaled), it takes ~200 min in a 0.1-mm particle whereas it takes ~500 min in a 0.3-mm particle of the same initial molecular weight. Also, Figure 2.4 shows that it is practically impossible to obtain a high molecular weight polymer if the prepolymer particle size is larger than 1.0 mm for both low molecular weight prepolymer A and high molecular weight prepolymer B.

In addition to molecular weight averages ($\bar{M}_n$, $\bar{M}_w$), a complete polymer chain length distribution is an important characteristic of a polymer's molecular structure. Using the polymer chain length distribution functions presented in eqs 2.16-2.23, we calculated the WCLD for different polymer particle sizes as illustrated in Figures 2.5 and 2.6 for prepolymer A (low molecular weight sample) and prepolymer B (high molecular weight sample). The WCLD curves of the prepolymer and the polymers at different radial positions (center, middle, particle surface) are shown. The overall average WCDL is also shown. For a small prepolymer particle (d = 0.1 mm), WCLD is almost uniform in the polymer particle (Figure 2.5a, Figure 2.6a). However, for a larger prepolymer particle (d = 1.0 mm), WCLD varies significantly with the radial position (Figure 2.5b, Figure 2.6b). Figures 2.5b and 2.6b indicate that the WCLD at r = 0-0.5R (particle center-middle point) are almost the same as that of prepolymer whereas only the WCLD near the particle surface advances to high molecular weight region. In other words, a quite significant degree of heterogeneity in WCLD is present in large polymer particles regardless of the initial prepolymer

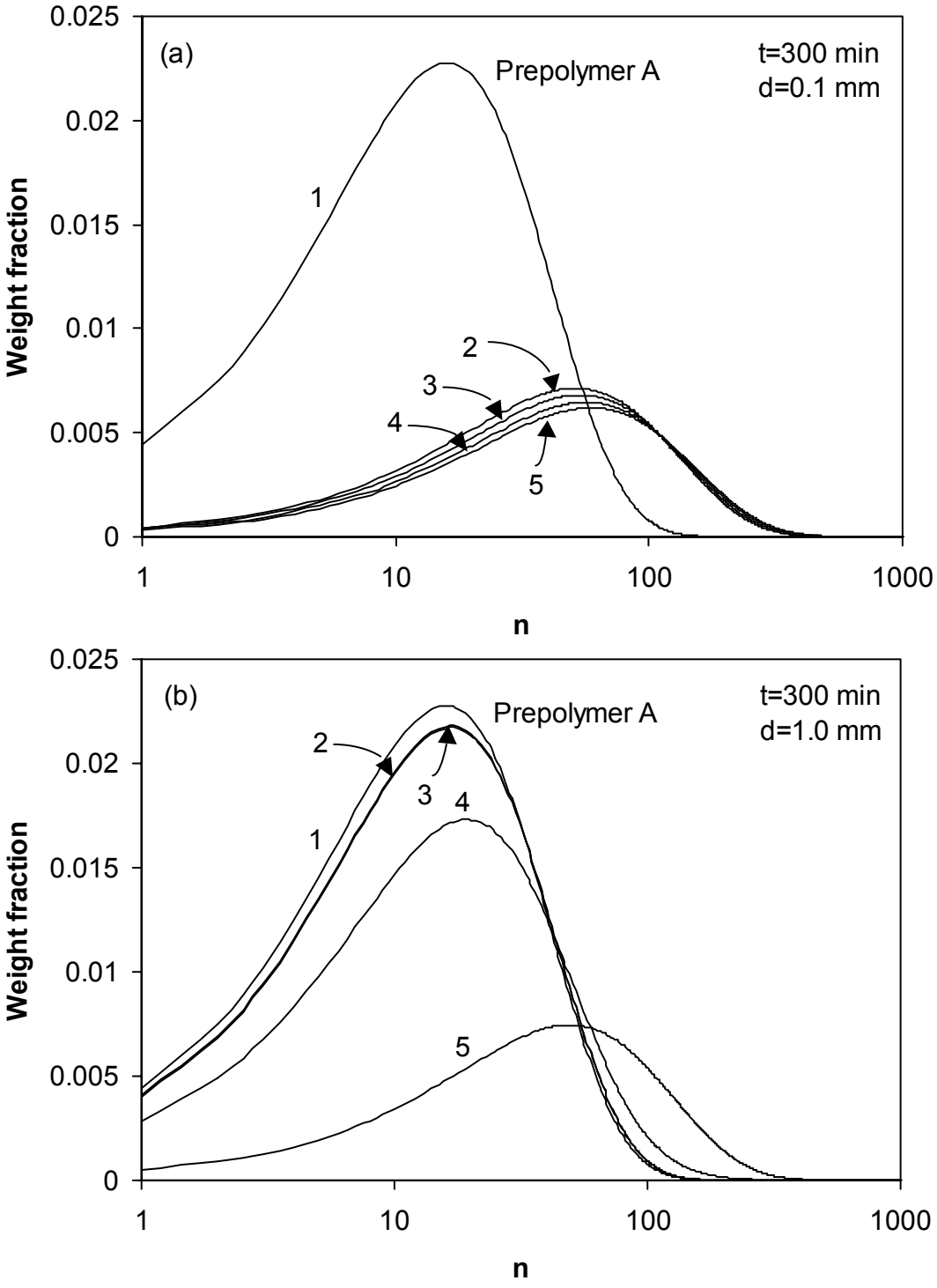

Figure 2.5 Weight chain length distributions during solid-state polymerization for two different size polymer particles of prepolymer A: 1, prepolymer; 2, center; 3, middle; 4, average; 5: surface.

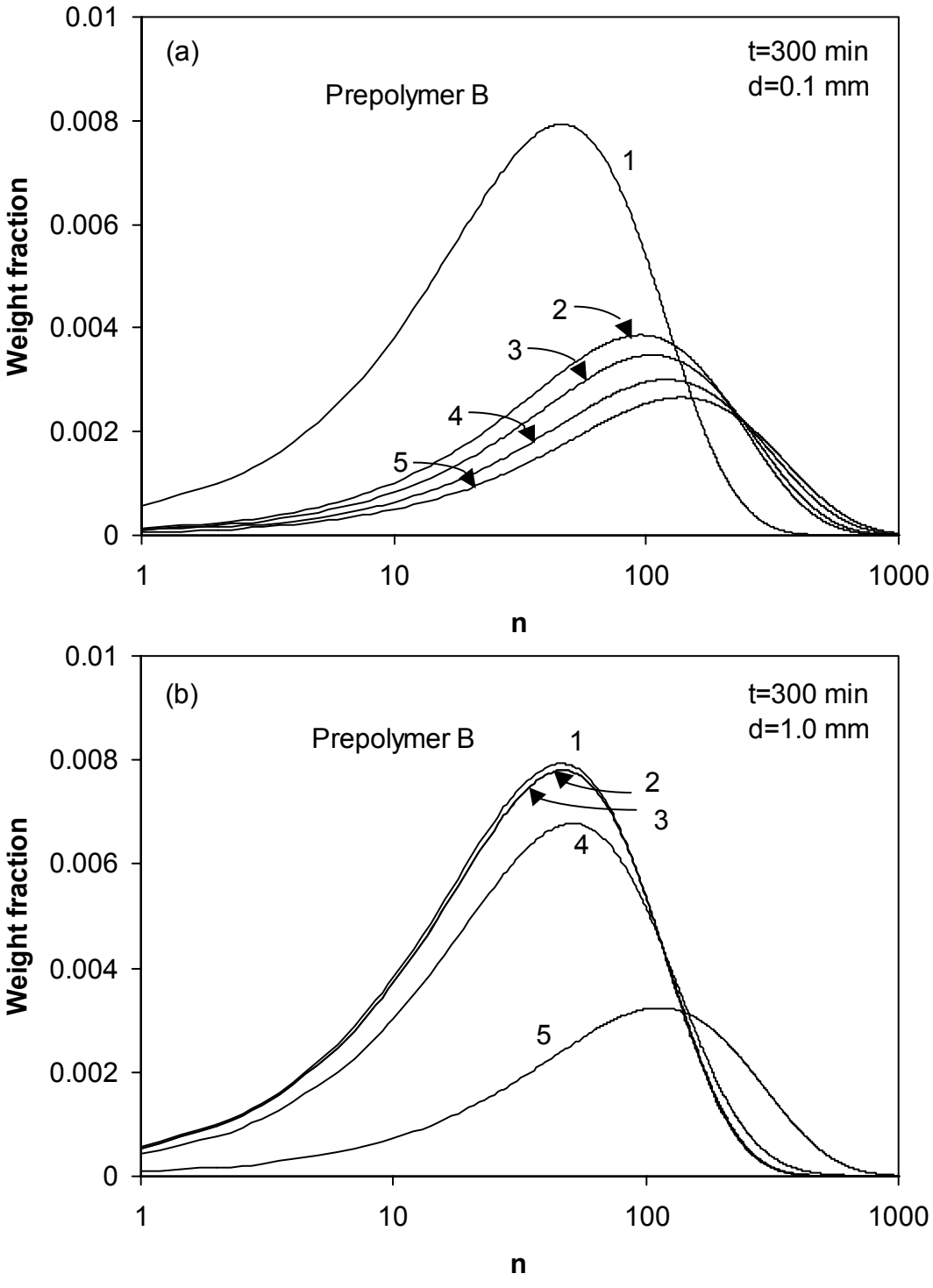

Figure 2.6 Weight chain length distributions during solid-state polymerization for two different size polymer particles of prepolymer B: 1, prepolymer; 2, center; 3, middle; 4, average; 5, surface.

molecular weight and the overall increase in polymer molecular weight becomes quite small. As noted earlier, Goodner et al.[57] showed experimentally that the molecular weight averages vary quite significantly from the particle core to the outer shell region of a polymer particle. It is also very interesting to observe that the maximum chain length of some polymer chains can be very large: e.g., for prepolymer B, some polymers have chain lengths as large as 1000 (MW = 254 000), which is several times larger than the average chain length of the prepolymers used in our experimental study. (Note: In our solid-state polymerization experiments, we observed that there was a small fraction of polycarbonate that did not dissolve in methylene chloride used as a solvent for gel permeation chromatographic analysis of the polymer. It is possible that these undissolved polymer molecules might have extremely large molecular weight as predicted by the model.) Also, Figures 2.5 and 2.6 show that, even after many hours of solid-state polymerization, a large fraction of polycarbonate molecules have chain lengths smaller than 10. It is worth noting that the amount of polycarbonate with only one repeating unit (n = 1) is not negligible, especially in large polymer particles. The presence of short-chain polymers can be practically important. For example, if a bisphenol A polycarbonate of high molecular weight average is used as a bottle for high temperature fluid, such low molecular weight polymers may diffuse out from the polymer matrix to the fluid phase, if the contact time is very long. Therefore, it will be important to use small polymer particles to reduce the amount of short-chain polycarbonates. The simulation results shown in Figures 2.5 and 2.6 clearly illustrate that knowing the complete polymer

chain length distribution is very important to understand the quality of polymers and the performance of solid-state polymerization.

The reason polymer molecular weight is affected by the particle size is because nonuniform radial concentration distribution is present. Figure 2.7 shows the effect of polymer particle size on the concentration profiles of phenol. Recall that the prepolymer particle is free of phenol at the beginning of solid-state polymerization. In a small particle (d = 0.1 mm), phenol concentration quickly rises as solid-state polymerization begins, but it drops quickly to very low concentration because the resistance to the diffusion of phenol in the polymer particle is very small, and hence, it can be easily removed from the particle to the bulk gas phase. In a larger particle (d = 1.0 mm), phenol concentration also rises quickly in the beginning, but even after 900 min of reaction, the phenol concentration at the particle center is still quite high because of low diffusion rate. As a result, polymer molecular weight does not increase as shown in Figure 2.4. Figure 2.8 illustrates the three-dimensional portraits of the phenol concentration profiles in two different size polymer particles. The concentration profiles of phenyl carbonate end group A ($[E_A]$) are shown in Figure 2.9. The overall qualitative effect of polymer particle size is quite similar to that of phenol.

2.4.2 Effect End Group Mole Ratio

Another important factor that affects the performance of solid-state polymerization is the mole ratio of the functional end groups in prepolymers. As mentioned earlier, conducting the melt polymerization of bisphenol A carbonate with

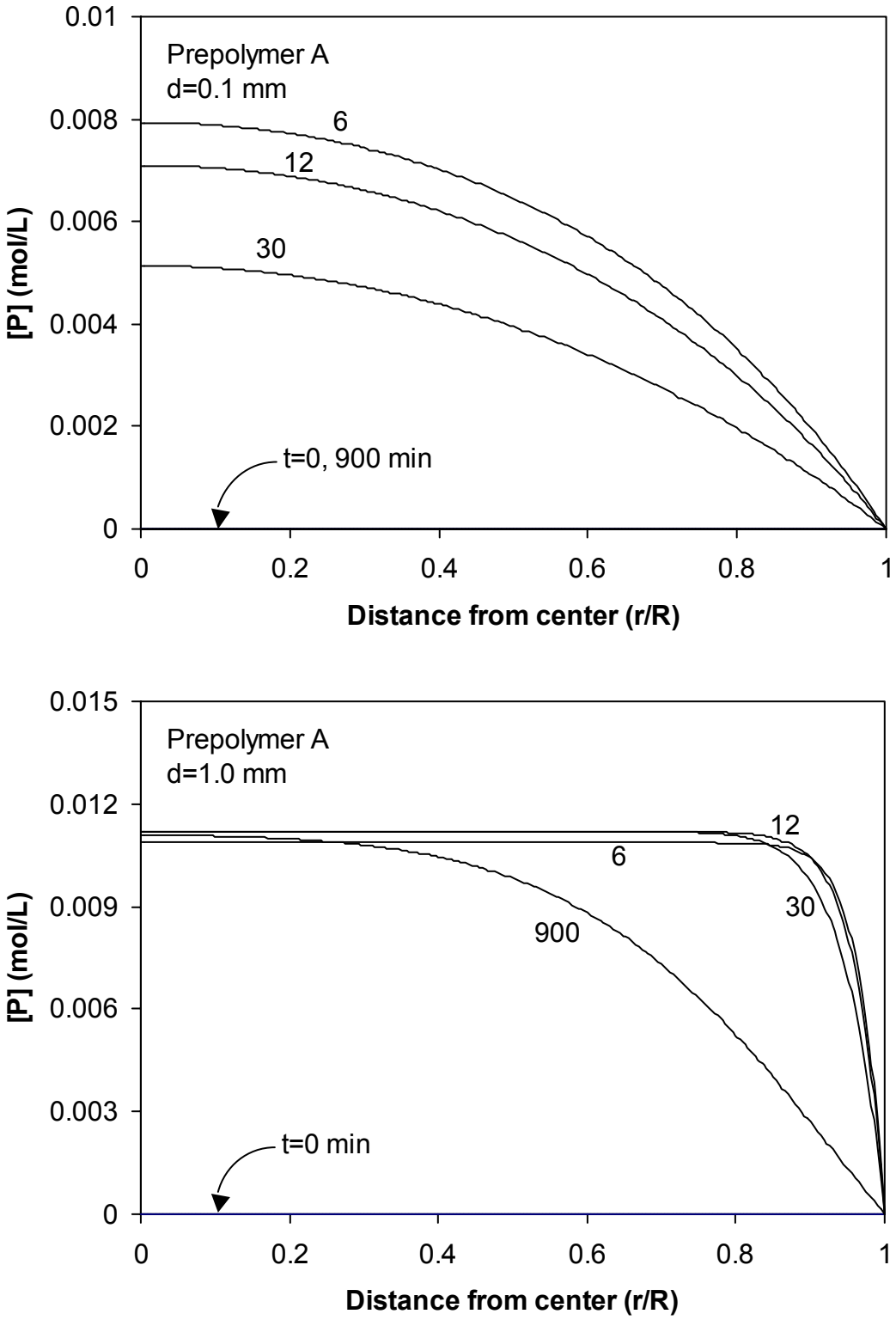

Figure 2.7 Effect of polymer particle size on phenol concentration profiles (prepolymer A).

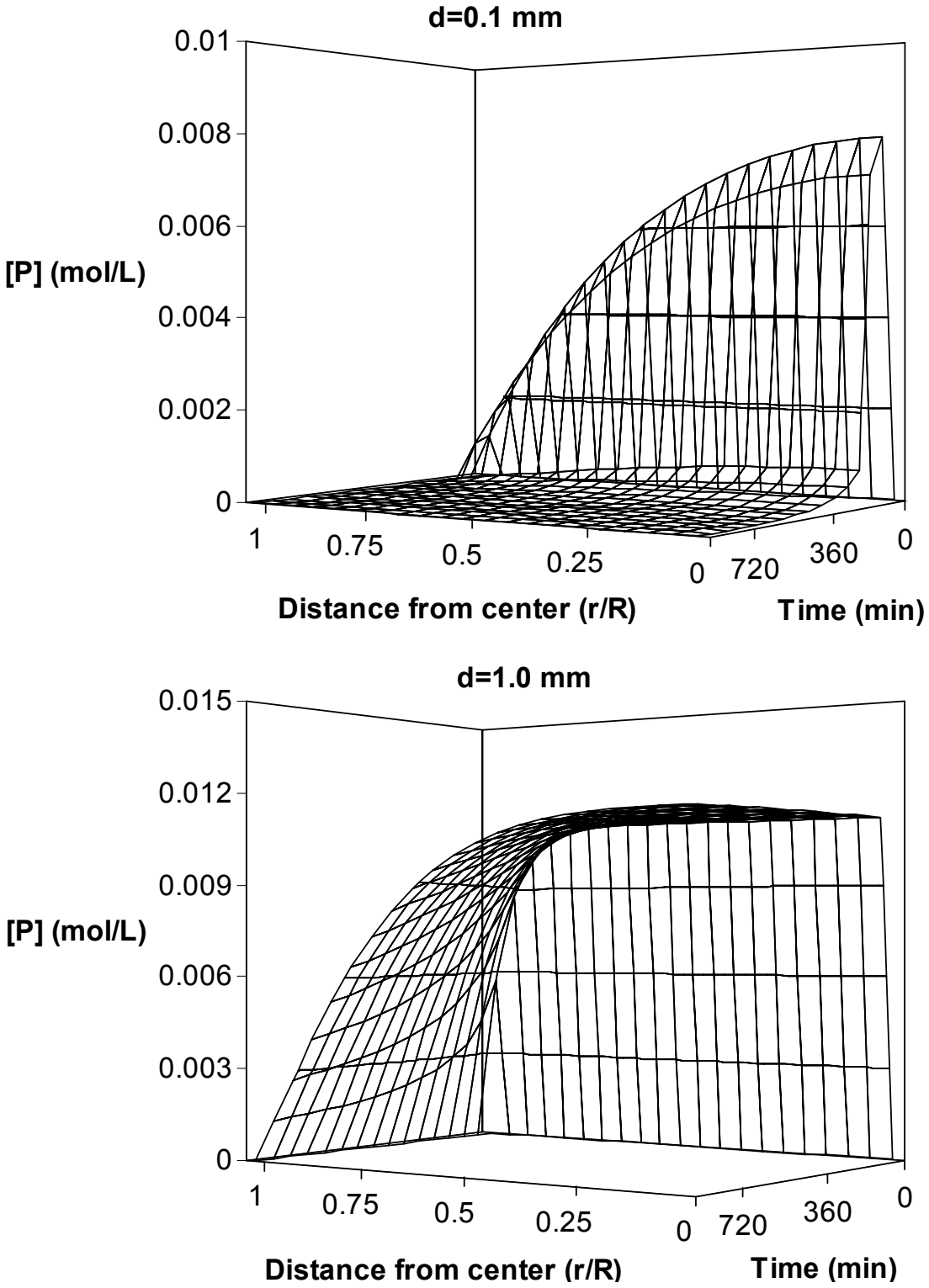

Figure 2.8 3-D plots of phenol concentration profies in solid-state polymerization for small and large polymer particles.

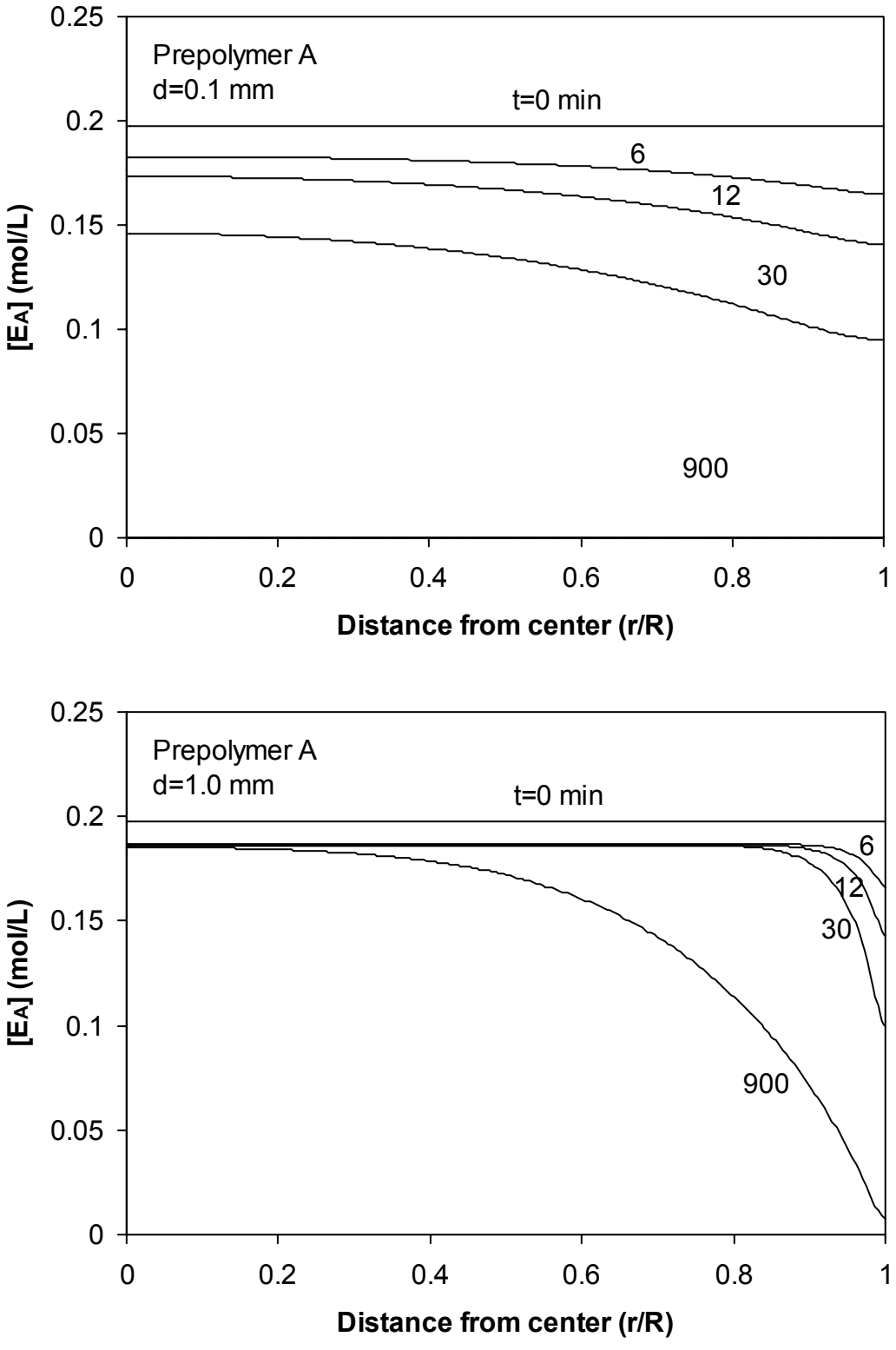

Figure 2.9 Effect of polymer particle size on the concentration profiles of phenyl carbonate end groups (prepolymer A).

the mole ratio of phenyl carbonate groups to hydroxyl groups ($[E_A]_i/[E_B]_i$) close to unity is a very important objective in operating a semibatch prepolymerization reactor. Since the vapor pressure of diphenyl carbonate is not negligibly small compared to that of phenol, the reactor is equipped with a reflux condenser that must be operated in such a way that the loss of diphenyl carbonate is minimized. But in practice, some loss of diphenyl carbonate is unavoidable. A slight excess of diphenyl carbonate is often used at the beginning of polymerization to precompensate for the loss of diphenyl carbonate, but the exact mole ratio is generally difficult to know because the amount of diphenyl carbonate lost in the reflux condenser is hard to measure or calculate. Such uncertainties in the initial end group mole ratio may result in inconsistent product quality (e.g., batch-to-batch variations). In our prepolymer samples, we found that the concentration of phenyl carbonate groups was lower than the concentration of hydroxyl groups, indicating that indeed some loss of diphenyl carbonate might have occurred in the melt transesterification stage to synthesize the prepolymers. Furthermore, these mole ratios of the end groups in the two prepolymers are far from 1.0 (e.g., $r_a' = 0.585$ for prepolymer A and $r_a' = 0.728$ for prepolymer B).

To see the effect of end group mole ratio in solid-state polymerization, we consider the polycarbonate prepolymers whose molecular weight values are same but the end group mole ratios are different. Figure 2.10 illustrates the model-calculated effects of end group mole ratio on $\bar{M}_w$ in solid-state polymerization for such prepolymers. The scaled prepolymer molecular weights are 0.82 in Figure 2.10a and 2.4 in Figure 2.10b. Figure 2.10 clearly shows that it is not the molecular weight itself

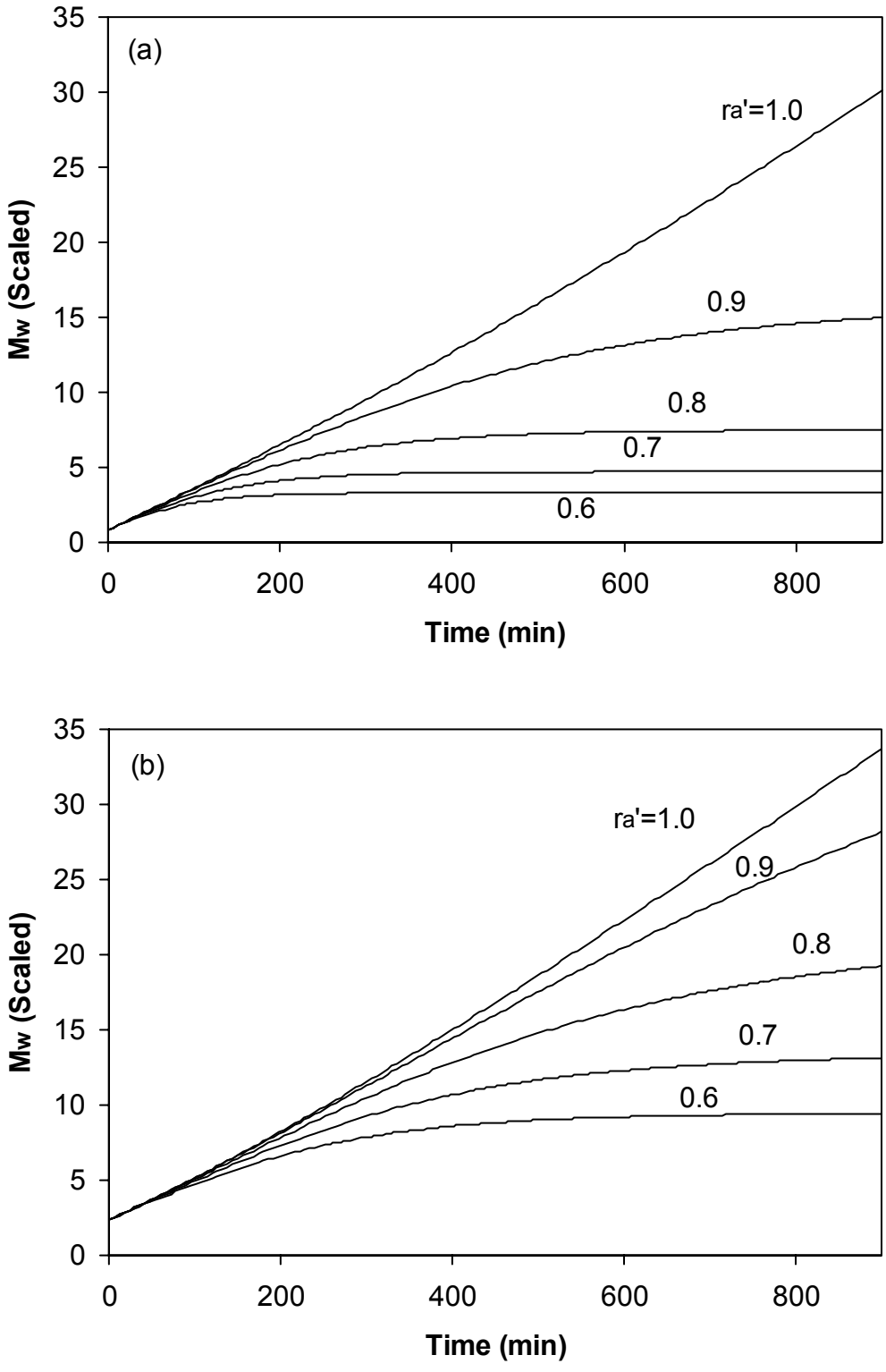

Figure 2.10 Effect of end group mole ratio on solid-state polymerization: (a) initial molecular weight 0.8 (scaled); (b) initial molecular weight 2.4 (scaled).

but the end group mole ratio that influences the polymer molecular weight in solid-state polymerization.

It is also interesting to observe in Figure 2.10 that if the mole ratio in the prepolymer is far from the stoichiometric ratio, the maximum obtainable molecular weight is severely limited. For example, for a prepolymer of scaled molecular weight of 0.82 with $r_a' = 0.6$, the maximum polymer molecular weight (scaled) obtainable after 900 min is ~3.5. However, for a higher molecular weight prepolymer (scaled $\bar{M}_{w,0} = 2.4$) with same $r_a' = 0.6$, the polymer molecular weight can be reached to ~9.5 (scaled) after 900 min of reaction. In other words, to obtain high molecular weight polymer by solid-state polymerization, the prepolymer molecular weight must be high also. Table 2.2 shows more information about the effect of end group mole ratio on the molecular weight for the simulation data shown in Figure 2.10. Note that the original mole ratio (r_a) values employed in the beginning of melt transesterification are quite close to unity and the conversion values of phenyl carbonate groups (p) are also very high at the end of prepolymerization stage. But the data in Table 2.2 show that a small difference in the original end group mole ratio at the beginning of melt transesterification (prepolymerization stage) (r_a) results in a huge difference in the end group mole ratio at the end of prepolymerization (r_a').

The simulation results shown in Figure 2.10 indicate that the performance of solid-state polymerization is not dependent on the prepolymer molecular weight per se, but it depends strongly on the end group mole ratio in the starting prepolymer. There are some reports on the effect of prepolymer molecular weight in solid-state polymerization of PET and nylon 6. Gaymans et al.[102] reported that, the higher the

Table 2.2 Effect of end group mole ratios

	$\bar{M}_{w,0}$ (scaled)	r_a	r_a'	p	$[E_A]_0$* (mol/L)	$\bar{M}_{w,max}$ (scaled)
		0.985	0.6	0.977	0.201	3.35
		0.989	0.7	0.975	0.220	4.58
Figure 9a	0.82	0.993	0.8	0.973	0.238	7.22
		0.997	0.9	0.971	0.254	16.90
		1.000	1.0	0.969	0.268	∞
		0.995	0.6	0.992	0.0706	10.12
		0.996	0.7	0.991	0.0775	12.66
Figure 9b	2.4	0.998	0.8	0.9905	0.0836	25.36
		0.999	0.9	0.9898	0.0891	50.76
		1.000	1.0	0.9893	0.0941	∞

* In prepolymer

starting molecular weight of the nylon prepolymer, the faster the rate of solid-state polymerization. They proposed that such behavior is due to a concentration distribution or end group-to-end group distribution in a particle. Similar solid-state polymerization behavior is observed in our study. The simulation results shown in Figure 2.10 indicate that, for the polymers of same end group mole ratio, the higher the prepolymer molecular weight, the faster the molecular weight increases in solid-state polymerization. But the end group mole ratio at the beginning of solid-state polymerization is the key factor for such behavior.

To obtain high molecular weight polymers in solid-state polymerization, we can use either low molecular weight prepolymers or high molecular weight prepolymers. If high molecular weight prepolymers are used, the solid-state polymerization time can be reduced. But to prepare such prepolymers, longer prepolymerization time would be needed in the prepolymerization stage. Therefore, to optimize the entire polymerization process, it will be necessary to consider both melt transesterfication (prepolymerization) and solid-state polymerization together.

2.4.3 Effect of Crystallinity

In our model simulations, we assumed that solid-state polymerization occurs only in the amorphous phase. With an increase of crystallinity during the solid-state polymerization, the effective volumetric concentrations of end groups and catalyst increase as the amorphous-phase volume decreases. Thus, the polymerization rate is expected to increase in part by this volume effect. For the case of stoichiometric end group mole ratio, Figure 2.11 shows the model-calculated polymer molecular weight

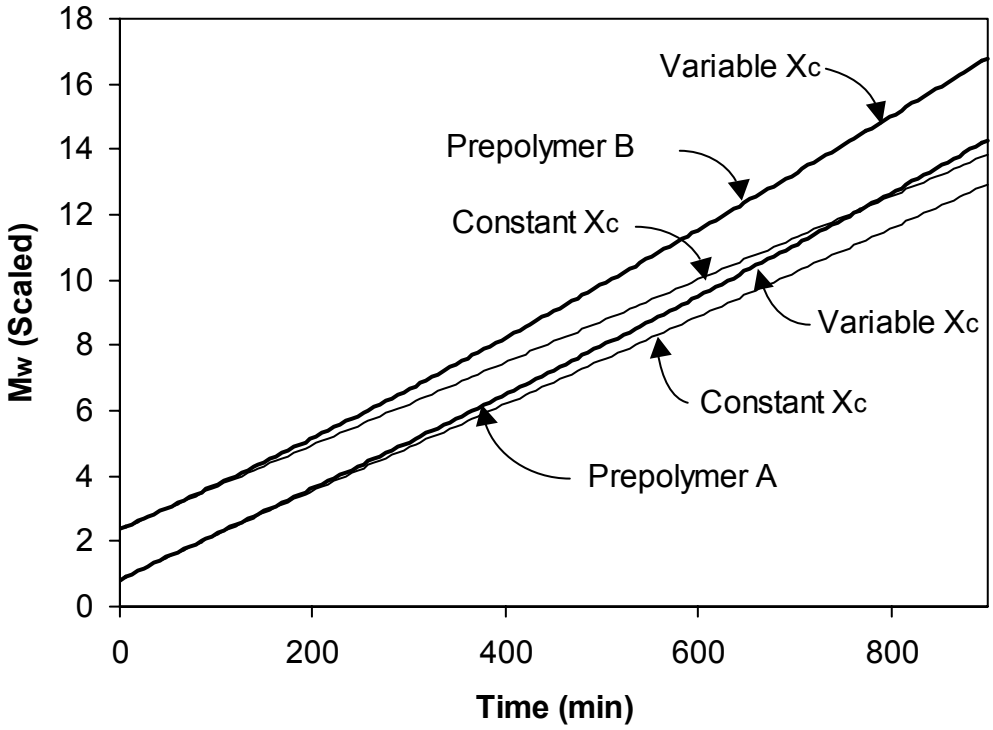

Figure 2.11 Effect of crystallinity on polymer molecular weight.

profiles with time-varying crystallinity and constant crystallinity. The effect of time-varying crystallinity is rather small in the first few hours of reaction but eventually, higher molecular weight is reached faster as polymer crystallinity increases with time.

2.5 Conclusions

In this work, we developed a diffusion-reaction model for the solid-state polymerization of partially crystalline polycarbonate in a spherical particle. The model was validated on the experimental solid-state polymerization data. The major findings from our model simulations are as follows: (1) The polymer particle size has a significant impact on the performance of solid-state polymerization. If the particle size is larger than 1.0 mm in diameter, the intraparticle phenol diffusion resistance is too large to effectively increase the polymer molecular weight. In some extreme cases, it becomes practically impossible to increase the polymer molecular weight in large particles. (2) The weight chain length distributions have been calculated for stoichiometrically imbalanced polymerization using the Flory's molecular species model combined with a functional group model. Even in a polymer with very large molecular weight average, the amounts of short-chain polycarbonates and very long chain polycarbonates are not small. The model simulations suggest that the polymer chain length distribution provides additional insights into the molecular structure of polycarbonate in solid-state polymerization. (3) In large particles, the chain length distribution inside the particle remains practically unchanged. (4) The end group mole ratio in the beginning of melt prepolymerization has a dominant effect on the efficiency of solid-state polymerization. It is not the prepolymer molecular weight

itself but the end group mole ratio that influences the rate of solid-state polymerization and final molecular weight. (5) The polymer crystallinity also affects the solid-state polymerization. As the polymer crystallinity increases during the solid-state polymerization, the effective concentrations of catalyst and reactive end groups increase in the amorphous phase and polymer molecular weight increases faster than the constant crystallinity case.

2.6 Notation

d = particle diameter, mm

D_p = diffusivity of phenol, $cm^2 \cdot s^{-1}$

$[E_A]$ = concentration of phenyl carbonate group at time t, $mol \cdot L^{-1}$

$[E_A]_i$ = initial concentration of phenyl carbonate group for prepolymerization, $mol \cdot L^{-1}$

$[E_A]_0$ = initial concentration of phenyl carbonate group for SSP, $mol \cdot L^{-1}$

$[E_B]$ = concentration of hydroxyl group at time t, $mol \cdot L^{-1}$

$[E_B]_i$ = initial concentration of hydroxyl group for prepolymerization, $mol \cdot L^{-1}$

$[E_B]_0$ = initial concentration of hydroxyl group for SSP, $mol \cdot L^{-1}$

K = equilibrium constant

k_1 = forward reaction rate, $L \cdot mol^{-1} \cdot min^{-1}$

k_2 = backward reaction rate, $L \cdot mol^{-1} \cdot min^{-1}$

k_c = crystallization rate constant, min^{-1}

$\bar{M}_n$ = number-average molecular weight

$\bar{M}_{n,0}$ = number-average molecular weight of prepolymer

$\bar{M}_w$ = weight-average molecular weight

$\bar{M}_{w,0}$ = weight-average molecular weight of prepolymer

n = number of repeating unit

p = conversation of phenyl carbonate group

$[P]$ = concentration of phenol at time t, $mol \cdot L^{-1}$

$[P]_0$ = initial concentration of phenol for SSP, $mol \cdot L^{-1}$

$[P^*]$ = concentration of phenol at the bulk phase, $mol \cdot L^{-1}$

P_n = mole fraction of n-mer

r = distance from particle center, cm

r_a = mole ratio of end group at the beginning of melt prepolymerization, $[E_A]_i/[E_B]_i$

r_a' = mole ratio of end group in the prepolymer, $[E_A]_0/[E_B]_0$

R = particle radius, cm

t = reaction time, min

V_c = amorphous-phase volume, cm^3

V = particle volume, cm^3

w_m = molecular weight of repeating unit

W_n = weight fraction of n-mer

x = total number of reactants combined in the polymer molecule

x_c = crystallinity at time t

[Z] = concentration of polymer linage at time t, $mol \cdot L^{-1}$

$[Z]_0$ = initial concentration of polymer linage for SSP, $mol \cdot L^{-1}$

Chapter 3

Modeling of Solid-State Polymerization of Bisphenol A Polycarbonate in a Single Particle: II. Molecular Species Model

3.1 Introduction

To have a good understanding of reaction mechanism, reaction kinetics and the effects of parameters such as reaction temperature, particle size, and end group ratio, extensive modeling studies have been carried out. Two types of models are available to simulate the transesterification reaction of polycondensation of bisphenol A polycarbonate (BAPC): 1) end group model[12] and 2) molecular species model[98]. The end group model does not differentiate the difference of molecular species, and only focuses two functional end groups: hydroxyl group and phenyl carbonate group. With the end group model, the overall conversion and end group concentrations can be easily calculated. For the molecular species model, however, it is more convenient to track each one of moments in the reaction system. It is also straightforward to obtain monomer concentrations, which is necessary for the calculation of vapor-liquid equilibrium if the evaporation of diphenyl carbonate (DPC) is taken into consideration.[98] Furthermore, it is capable of calculating the weight-average molecular weight even for polymer chains not following the most probable distribution as long as the initial conditions of moments are known.

Originally, a molecular species model was developed to describe the mass balance of monomers in the melt polymerization of bisphenol A (BPA) and DPC. In

1990, Hersh and Choi[104] developed a moment model to describe mass balance of molecular species in the melt polymerization of BPA and DPC at relatively low reaction temperature (150-180°C). Kim and Choi[105] extended their work into higher temperature region (180-250°C), and improved the molecular species model by experimental justification and provided a more detailed experimental analysis in the reaction kinetics of melt transesterification. To accurately account for the loss of DPC during the melt polymerization in a semibatch reactor, Woo and Choi[98] incorporated the vapor-liquid equilibrium equations of the binary system of phenol and DPC to improve the empirical method used by Kim and Choi[105]. Thus, the simulation results became more accurate by keeping tracking the loss of DPC and updating the system volume. The effect of DPC loss on the kinetics of the semibatch melt process was investigated through experimental verification.

For a SSP, Goodner et al.[57] adopted the molecular species model developed by Kim and Choi[105] and successfully applied to the SSP of BAPC. The reaction conditions such as polymer particle size, phenol diffusivity have been extensively investigated. One interesting and important result from their work is that the stoichiometric excess of an end group has a large effect on the performance of SSP. It is well known that during the melt polymerization, some loss of DPC is unavoidable.[98,105] In practice, a slight excess of DPC is often used at the beginning of melt polymerization to pre-compensate for the loss of DPC. Therefore, the exact end group mole ratio is different from what is initially charged in the beginning of melt polymerization. However, in order to use the molecular species model for SSP, initial conditions such as the values of moments have to be determined. For the end group

concentrations, although the initial conditions of hydroxyl end group concentrations may be obtained either from experimental measurement such as titration[48,61], FTIR[58] or from a back calculation method[60], it is impossible to determine initial moments experimentally without any calculation. The determination of initial conditions is not straightforward and a calculation method has to be developed in order to use molecular species model. Goodner et al.[57] developed different methods to calculate the initial moments for the cases with and without perfect end group ratio, respectively. For the case with perfect end group ratio, the conservation equation of monomer moieties was used, i.e. the total number of monomer units stays same before and after the melt polymerization. The idea is correct. However, the conservation should be held through the mass of monomer unit moieties instead of the concentration due to the significant difference of density before and after melt polymerization. In other words, the total concentrations of monomer moieties initially charged for the melt polymerization is different from those concentrations of monomer moieties in the prepolymer after the melt polymerization. But it is true if the effect of volume change is taken into account. For the case without perfect end group ratio, very often a molecular species model may be applied to the stage of melt polymerization with excess one monomer to obtain final results as initial conditions for the further modeling of SSP.[57,106] However, this method does not consider the significant volume change in melt polymerization either. In this chapter, we have developed a new method to determine the initial conditions for SSP based on the most probable distribution with back-calculated initial end group ratio and the conversion

of monomers. This method is valid for both stoichiometric balanced and imbalanced cases.

For the modeling of SSP, parametric effects have been widely studied in previous work[56,57,60]. In chapter 2, it was mentioned that the end group mole ratio and particle size are the major factors controlling the molecular weight further increase during SSP. In this chapter, we have proposed a way to modify the end group ratio by adding another prepolymer with the excess of the opposite end group. For example, prepolymer A is in excess of hydroxyl end group. Prepolymer B with excess of phenyl carbonate group may be dissolved together with prepolymer A and then crystallized as a new prepolymer. The effect of adding another monomer has been studied through model simulation. For relatively large particles, the concentration gradient of phenol may be significant, which could seriously hamper molecular weight increase. Remelting was proposed to further increase molecular weight during the second SSP[43,102,106]. To further increase molecular weight for such big particles after SSP, remelting can help to redistribute end groups and potentially further increase molecular weight by migrating end groups from particle center to surface. However, only number-average molecular weight has been investigated in the past. With the molecular species model, we have studied the change of weight-average molecular weight after remelting and its effect on the further SSP. Simulation results show that there is a drop of weight-average molecular weight, which has never been reported before.

3.2 Model Development

A SSP is carried out at a temperature much higher than polymer's glass transition temperature (T_g) but below its melting point (T_m). At reaction temperatures, the transesterification reaction occurs between the hydroxyl end group and the phenyl carbonate end group in the presence of a catalyst. The reaction scheme of molecular species model can be presented as follows.[104]

$$A_n + B_m \rightleftharpoons C_{n+m+1} + P \quad (n, m \geq 0) \tag{3.1.1}$$

$$A_n + C_m \rightleftharpoons A_{n+m} + P \quad (n \geq 0, m \geq 1) \tag{3.1.2}$$

$$B_n + C_m \rightleftharpoons B_{n+m} + P \quad (n \geq 0, m \geq 1) \tag{3.1.3}$$

$$C_n + C_m \rightleftharpoons C_{n+m} + P \quad (n, m \geq 1) \tag{3.1.4}$$

where P is phenol and three kinds of polymeric molecular species, A_n, B_n, C_n, are defined as follows.

A_n:

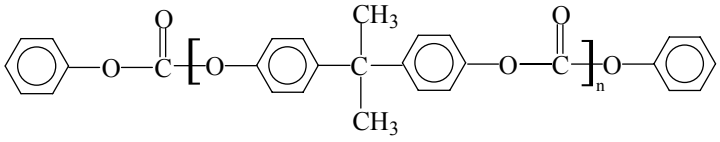

B_n :

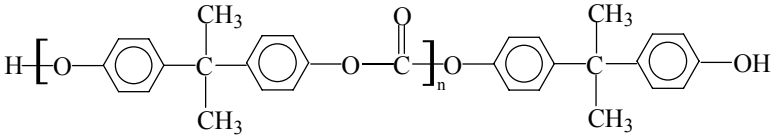

C_n :

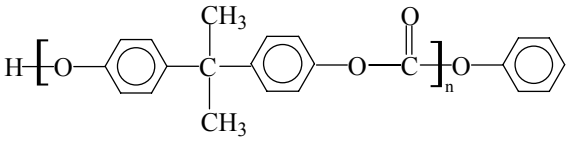

In the SSP of BAPC, the mass balance equations for molecular species moments take the following form.

$$\frac{\partial P}{\partial t}=\frac{k_1}{1-x_c}\begin{bmatrix}4\left(\lambda_{A,0}+A_0\right)\left(\lambda_{B,0}+B_0\right)\\+2\lambda_{C,0}\begin{pmatrix}\lambda_{A,0}+A_0\\+\lambda_{B,0}+B_0\end{pmatrix}+\\\lambda_{C,0}{}^2\end{bmatrix}+\frac{k_2P}{1-x_c}\begin{bmatrix}\lambda_{C,0}-\\2\begin{pmatrix}\lambda_{A,1}+\\\lambda_{B,1}+\\\lambda_{C,1}\end{pmatrix}\end{bmatrix}+D_P\left(\frac{1}{r^2}\frac{\partial}{\partial r}\left(r^2\frac{\partial P}{\partial r}\right)\right) \quad (3.2)$$

$$\frac{\partial A_0}{\partial t}=\frac{-2k_1A_0}{1-x_c}\left[2\left(\lambda_{B,0}+B_0\right)+\lambda_{C,0}\right]+\frac{k_2P}{1-x_c}\left(\lambda_{C,0}+2\lambda_{A,0}\right) \quad (3.3)$$

$$\frac{\partial B_0}{\partial t}=\frac{-2k_1B_0}{1-x_c}\left[2\left(\lambda_{A,0}+A_0\right)+\lambda_{C,0}\right]+\frac{k_2P}{1-x_c}\left(\lambda_{C,0}+2\lambda_{B,0}\right) \quad (3.4)$$

$$\frac{\partial \lambda_{A,0}}{\partial t}=\frac{2k_1}{1-x_c}\left[-2\lambda_{A,0}\left(\lambda_{B,0}+B_0\right)+\lambda_{C,0}A_0\right]+\frac{k_2P}{1-x_c}\left(\lambda_{C,1}-\lambda_{C,0}-2\lambda_{A,0}\right) \quad (3.5)$$

$$\frac{\partial \lambda_{B,0}}{\partial t}=\frac{2k_1}{1-x_c}\left[-2\lambda_{B,0}\left(\lambda_{A,0}+A_0\right)+\lambda_{C,0}B_0\right]+\frac{k_2P}{1-x_c}\left(\lambda_{C,1}-\lambda_{C,0}-2\lambda_{B,0}\right) \quad (3.6)$$

$$\frac{\partial \lambda_{C,0}}{\partial t}=\frac{k_1}{1-x_c}\begin{bmatrix}4\left(\lambda_{A,0}+A_0\right)\left(\lambda_{B,0}+B_0\right)-\\2\lambda_{C,0}\begin{pmatrix}\lambda_{A,0}+A_0\\+\lambda_{B,0}+B_0\end{pmatrix}-\lambda_{C,0}{}^2\end{bmatrix}+\frac{k_2P}{1-x_c}\left[-\lambda_{C,0}+2\left(\lambda_{A,1}+\lambda_{B,1}\right)\right] \quad (3.7)$$

$$\frac{\partial \lambda_{A,1}}{\partial t}=\frac{2k_1}{1-x_c}\begin{bmatrix}-2\lambda_{A,1}\left(\lambda_{B,0}+B_0\right)\\+\lambda_{C,1}\left(\lambda_{A,0}+A_0\right)\end{bmatrix}+\frac{k_2P}{2\left(1-x_c\right)}\left[\lambda_{C,2}-\lambda_{C,1}-2\left(\lambda_{A,2}+\lambda_{A,1}\right)\right] \quad (3.8)$$

$$\frac{\partial \lambda_{B,1}}{\partial t}=\frac{2k_1}{1-x_c}\begin{bmatrix}-2\lambda_{B,1}\left(\lambda_{A,0}+A_0\right)\\+\lambda_{C,1}\left(\lambda_{B,0}+B_0\right)\end{bmatrix}+\frac{k_2P}{2\left(1-x_c\right)}\left[\lambda_{C,2}-\lambda_{C,1}-2\left(\lambda_{B,2}+\lambda_{B,1}\right)\right] \quad (3.9)$$

$$\frac{\partial \lambda_{C,1}}{\partial t}=\frac{2k_1}{1-x_c}\begin{bmatrix}2\left(\lambda_{A,1}+\lambda_{A,0}+A_0\right)\\\left(\lambda_{B,1}+\lambda_{B,0}+B_0\right)-\\\lambda_{C,1}\left(\lambda_{A,0}+A_0+\lambda_{B,0}+B_0\right)\\-2\lambda_{A,1}\lambda_{B,1}\end{bmatrix}+\frac{k_2P}{1-x_c}\left(\lambda_{A,2}+\lambda_{A,1}+\lambda_{B,2}+\lambda_{B,1}-\lambda_{C,2}\right) \quad (3.10)$$

$$\frac{\partial \lambda_{A,2}}{\partial t} = \frac{2k_1}{1-x_c}\begin{bmatrix} -2\lambda_{A,2}\left(\lambda_{B,0}+B_0\right) \\ +\lambda_{C,2}\left(\lambda_{A,0}+A_0\right) \\ +2\lambda_{A,1}\lambda_{C,1} \end{bmatrix} + \frac{k_2 P}{6\left(1-x_c\right)}\begin{bmatrix} 2\lambda_{C,3}-3\lambda_{C,2}+ \\ \lambda_{C,1}-8\lambda_{A,3}- \\ 6\lambda_{A,2}+2\lambda_{A,1} \end{bmatrix} \tag{3.11}$$

$$\frac{\partial \lambda_{B,2}}{\partial t} = \frac{2k_1}{1-x_c}\begin{bmatrix} -2\lambda_{B,2}\left(\lambda_{A,0}+A_0\right) \\ +\lambda_{C,2}\left(\lambda_{B,0}+B_0\right) \\ +2\lambda_{B,1}\lambda_{C,1} \end{bmatrix} + \frac{k_2 P}{6\left(1-x_c\right)}\begin{bmatrix} 2\lambda_{C,3}-3\lambda_{C,2}+ \\ \lambda_{C,1}-8\lambda_{B,3}- \\ 6\lambda_{B,2}+2\lambda_{B,1} \end{bmatrix} \tag{3.12}$$

$$\frac{\partial \lambda_{C,2}}{\partial t} = \frac{2k_1}{1-x_c}\begin{bmatrix} 2\begin{pmatrix}\lambda_{A,2}+\lambda_{A,1} \\ +\lambda_{A,0}+A_0\end{pmatrix}\begin{pmatrix}\lambda_{B,2}+\lambda_{B,1} \\ +\lambda_{B,0}+B_0\end{pmatrix} \\ -2\lambda_{A,2}\left(\lambda_{B,1}+\lambda_{B,2}\right)-2\lambda_{B,2} \\ \left(\lambda_{A,1}+\lambda_{A,2}\right)+ \\ 2\lambda_{B,1}\left(\lambda_{A,1}+\lambda_{A,0}+A_0\right) \\ +2\lambda_{A,1}\left(\lambda_{B,1}+\lambda_{B,0}+B_0\right)- \\ 2\lambda_{A,1}\lambda_{B,1}+2\lambda_{A,2}\lambda_{B,2}- \\ \lambda_{C,2}\begin{pmatrix}\lambda_{A,0}+A_0 \\ +\lambda_{B,0}+B_0\end{pmatrix}+{\lambda_{C,1}}^2 \end{bmatrix} + \frac{k_2 P}{3\left(1-x_c\right)}\begin{pmatrix} 2\lambda_{A,3}+ \\ 3\lambda_{A,2}+ \\ \lambda_{A,1}+ \\ 2\lambda_{B,3}+ \\ 3\lambda_{B,2}+ \\ \lambda_{B,1}+ \\ \lambda_{C,1}- \\ 4\lambda_{C,3} \end{pmatrix} \tag{3.13}$$

where P is the phenol condensate, A_0, B_0, are DPC and BPA, and each moment is defined as $\lambda_{A,k} = \sum_{n=1}^{\infty} n^k A_n$, $\lambda_{B,k} = \sum_{n=1}^{\infty} n^k B_n$, $\lambda_{C,k} = \sum_{n=1}^{\infty} n^k C_n$; k_1, k_2 are variables, and stand for the forward reaction rate and backward reaction rate, respectively.

The initial condition is

I.C. @ t = 0, S = S_0 (3.14)

where S stands for all the molecular species.

The boundary conditions for phenol condensate are

B.C. @ $r = 0$, $\frac{\partial [P]}{\partial r} = 0$ (3.15.1)

@ $r = R$, $[P] = 0$ (3.15.2)

where eq 3.15.2 indicates that phenol is quickly removed from the particle surface to the surrounding environment due to effective phenol removal. The number- and weight-average molecular weight for each thin layer inside of a particle can be calculated by,[98]

$$\bar{M}_n = \frac{\sum_{n=1}^{\infty}\left(A_n w_{An} + B_n w_{Bn} + C_n w_{Cn}\right)}{\sum_{n=1}^{\infty}\left(A_n + B_n + C_n\right)} \approx w_m \frac{\lambda_{A,1} + \lambda_{B,1} + \lambda_{C,1}}{\lambda_{A,0} + \lambda_{B,0} + \lambda_{C,0}} \tag{3.16.1}$$

$$\bar{M}_w = \frac{\sum_{n=1}^{\infty}\left(A_n w_{An}^2 + B_n w_{Bn}^2 + C_n w_{Cn}^2\right)}{\sum_{n=1}^{\infty}\left(A_n w_{An} + B_n w_{Bn} + C_n w_{Cn}\right)} \approx w_m \frac{\lambda_{A,2} + \lambda_{B,2} + \lambda_{C,2}}{\lambda_{A,1} + \lambda_{B,1} + \lambda_{C,1}} \tag{3.16.2}$$

where

$$w_{An} = 254.3n + 228.29 \tag{3.17.1}$$

$$w_{Bn} = 254.3n + 214.22 \tag{3.17.2}$$

$$w_{Cn} = 254.3n + 94.11 \tag{3.17.3}$$

$$w_m = 254.3 \tag{3.17.4}$$

For a particle, the number- and weight-average molecular weight can be calculated by,

$$\bar{M}_n = R^3 \left(3\int_0^R \frac{r^2}{\bar{M}_n(r)} dr \right)^{-1} \tag{3.18.1}$$

$$\bar{M}_w = \frac{1}{R^3}\left(3\int_0^R r^2 \bar{M}_n(r) dr \right) \tag{3.18.2}$$

3.3 Initial Conditions

As mentioned before, in order to use the molecular species model, it is essential to obtain initial conditions: the moments of molecular species. In the following, the most probable chain length distribution is used to calculate the initial moments of molecular species for both stoichiometric balanced and imbalanced cases. It is generally accepted that melt polymerized BAPC can be characterized by the most probable distribution.[7,107] Hagenaars, et al.[107] characterized the molecular weight distribution after redistribution reaction in the mixed factions of melt polymerized BAPC and found that it follows the most probable distribution at the end of redistribution reaction. Thus, the relationships between moments of molecular species depend upon the properties of prepolymer, i.e. end group ratio in the beginning of melt polymerization, r_a, and conversion, p. According to the definition of k-th moments of molecular species, we have

$$\lambda_{A,k} = \sum_{n=1}^{\infty} n^k A_n = \left(\sum_{n=1}^{\infty} A_n + \sum_{n=1}^{\infty} B_n + \sum_{n=1}^{\infty} C_n \right) \sum_{n=1}^{\infty} n^k \frac{A_n}{\sum_{n=1}^{\infty} A_n + \sum_{n=1}^{\infty} B_n + \sum_{n=1}^{\infty} C_n} \qquad (3.19.1)$$

$$= \left(\lambda_{A,0} + \lambda_{B,0} + \lambda_{C,0} \right) \sum_{n=1}^{\infty} n^k P_{n,(odd-A)}$$

where $P_{n,\,(odd\text{-}A)}$, the mole fraction of species A_n in the mixture of species A_n, B_n, C_n, was defined in chapter 2 (See eq 2.14 for the meaning of odd A, and the definition for the chain structure of species A_n is given in p78). Similarly,

$$\lambda_{B,k} = \left(\lambda_{A,0} + \lambda_{B,0} + \lambda_{C,0} \right) \sum_{n=1}^{\infty} n^k P_{n,(odd-B)} \qquad (3.19.2)$$

$$\lambda_{C,k} = \left(\lambda_{A,0} + \lambda_{B,0} + \lambda_{C,0} \right) \sum_{n=1}^{\infty} n^k P_{n,(even-C)} \qquad (3.19.3)$$

Eqs 3.19.1-3.19.3 indicate that the *k*-th moments of molecular species can be calculated from 0-th moments of molecular species together with the number distributions of chain length. Moreover, according to the most probable distribution, the mole fractions of molecular species can be expressed as the functions of end group mole ratio, r_a, and conversion, p.

$$P_{n,(odd-A)} = p^{2n} r_a{}^{n} \frac{(1-p)^2}{1+\frac{1}{r_a}-2p} \text{ (mole fraction of } A_n\text{)} \tag{3.20.1}$$

$$P_{n,(odd-B)} = p^{2n} r_a{}^{n-1} \frac{(1-r_a p)^2}{1+\frac{1}{r_a}-2p} \text{ (mole fraction of } B_n\text{)} \tag{3.20.2}$$

$$P_{n,(even-C)} = p^{2n-1} r_a{}^{n} \frac{2(1-p)(1-r_a p)}{1+r_a-2r_a p} \text{ (mole fraction of } C_n\text{)} \tag{3.20.3}$$

Thus, eq 3.16.1 and eq 3.16.2 can be expressed as follows.

$$\bar{M}_n = \sum_{n=1}^{\infty}\left(P_{n,(odd-A)} w_{An} + P_{n,(odd-B)} w_{Bn} + P_{n,(even-C)} w_{Cn}\right) \tag{3.21.1}$$

$$\bar{M}_w = \frac{\sum_{n=1}^{\infty}\left(P_{n,(odd-A)} w_{An}^2 + P_{n,(odd-B)} w_{Bn}^2 + P_{n,(even-C)} w_{Cn}^2\right)}{\sum_{n=1}^{\infty}\left(P_{n,(odd-A)} w_{An} + P_{n,(odd-B)} w_{Bn} + P_{n,(even-C)} w_{Cn}\right)} \tag{3.21.2}$$

With eqs 3.19.1-3.19.3, the mole ratio of end groups in a prepolymer can be expressed as follows.

$$r_a{}' = \frac{2\lambda_{A,0} + \lambda_{C,0}}{2\lambda_{B,0} + \lambda_{C,0}} = \frac{2\sum_{n=1}^{\infty} P_{n,(odd-A)} + \sum_{n=1}^{\infty} P_{n,(even-C)}}{2\sum_{n=1}^{\infty} P_{n,(odd-B)} + \sum_{n=1}^{\infty} P_{n,(even-C)}} \tag{3.22}$$

From eq 3.21.1 and eq 3.22 or eq 3.21.2 and eq 3.22, r_a and p can be calculated. The measurement of molecular weight and end group ratio in a prepolymer can be done by GPC and ^{13}C-NMR,[99] respectively. However, the determination of r_a and p is not straightforward. According to the back calculation method given in chapter 2 (eq 2.24 and 2.25), r_a and p values can be also determined. These values can be taken as a set of good initial guess. Then, a trail and error method has been used to find out more accurate solutions to r_a and p values for the molecular species model. The comparison of r_a and p values calculated by different methods is given in Table 3.1. To calculate the initial values of moments, the following equation is provided to calculate the total concentration of end groups.

$$\begin{aligned}[E_A]_0 + [E_B]_0 &= 2\left(\lambda_{A,0} + \lambda_{B,0} + \lambda_{C,0}\right) \\ &= \frac{2\times 10^3 \rho_p}{\bar{M}_n} \\ &= \frac{2\times 10^3 \rho_p}{\bar{M}_w / PD}\end{aligned} \tag{3.23}$$

where $[E_A]_0$ and $[E_B]_0$ are the concentrations of phenyl carbonate end group and hydroxyl end group, respectively; $PD = 1 + r_a^{1/2} p$.[101]

Thus, all the zeroth moments of molecular species can be calculated. The moments with higher order can be determined through those relationships shown in eqs 3.19.1-3.19.3. For initial conditions of monomer BPA, monomer DPC and condensate phenol, the concentrations may be negligible at the end of melt polymerization and they may be set up as zero at the beginning of SSP. Therefore, we are able to back track r_a and p, and to calculate the initial conditions of moments of

molecular species for both the stoichiometric balanced case and stoichiometric imbalanced cases.

3.4 Results and Discussion

3.4.1 Model Comparison

In order to calculate the initial conditions, the first step is to determine the values of r_a and p. The calculation of r_a and p requires the information about the molecular weight and end group ratio of prepolymer. For example, the values of r_a and p can be calculated by using eq 3.21.2 and eq 3.22. The calculation of r_a and p can be done either by the equations developed in this work or by those given in chapter 2 (eq 2.24 and eq 2.25). Table 3.1 shows r_a and p values calculated by both methods for the different end group ratios with the molecular weight of a prepolymer fixed ($\bar{M}_w$ = 10 000). It is seen that there is only slight difference in r_a and p values, meaning that considering the molecular weight of end unit and excluding monomers does not carry much difference for the molecular species model. Then, initial conditions of molecular species can be obtained by using eqs 3.19.1-3.19.3, eqs 3.20.1-3.20.3 and eq 3.23. Table 3.1 also gives the comparison of the end group concentrations calculated by both methods. Again, the results are in an excellent agreement.

The partial differential equations in the SSP model are solved using the parabolic PDE solver in MATLAB. Simulation results from the molecular species model are first compared with those calculated by the end group model as shown in Figure 3.1. Assume the reference case for a prepolymer: the weight-average

Table 3.1 Model comparison (back calculation)

	model name	$r_a' = 0.5$	$r_a' = 0.75$	$r_a' = 1$
r_a	molecular species model	0.982978	0.992656	1
	end group model	0.983398	0.992851	1
p	molecular species model	0.983258	0.978453	0.974853
	end group model	0.983118	0.978399	0.974889
$[E_A]_0$	molecular species model	0.146934	0.188891	0.220393
	end group model	0.146934	0.188913	0.220398
$[E_B]_0$	molecular species model	0.293822	0.251884	0.220393
	end group model	0.293869	0.251884	0.220398

Note: the calculation is based on $\bar{M}_w$ = 10 000.

weight is 10 000, and the end group ratio of phenyl carbonate group to hydroxyl group is 0.75, and particle size is 0.1 mm. With the model parameters given in Table 3.2, the simulation results of number- and weight-average molecular weights from the molecular species model are in an excellent agreement with those from the end group model.

3.4.2 Adjusting End Group Ratio

It is known that end group mole ratio in the prepolymer greatly affects the molecular weight increase in the SSP.[57,60] With the molecular species model, the concentrations of three species, A_n, B_n, C_n can be easily obtained. Figure 3.2 shows the effect of prepolymer end group ratio on the number fraction of moments of molecular species, A_n, B_n, C_n. We can see that for the perfect end group ratio (i.e. r_a' = 1), the following relationship holds: $\lambda_{A,0} = \lambda_{B,0} = \frac{1}{2}\lambda_{C,0}$. As the end group ratio decreases from the perfect ratio of 1, the number of molecular species of B_n is on the increase, while the other two is on the decrease. As the end group ratio approaches to 0, the number factions of A_n, C_n are close to 0 and that of B_n approaches to 1, indicating that polymer chains are mainly capped with hydroxyl end groups at this time and further polycondensation is nearly impossible. Interestingly, as shown in Figure 3.3, the back-calculated end group ratio in the beginning of melt polymerization is at least above 0.95. It means that controlling the stoichiometric balance of end groups is the key issue on the final molecular weight not only in a melt polymerization but also in a SSP. Only slight difference in the beginning of melt polymerization could result in a significant difference in the further SSP.

Table 3.2 Model parameters

parameter	unit	ref
$k_1 = k_u + k_x[C^*]$		
$k_u = (3.108 \pm 0.102) \times 10^7 \exp(-25290 \pm 1010 / RT)$	$L \cdot mol^{-1} \cdot min^{-1}$	98
$k_x = 9.62 \times 10^8 \exp(-13900 / RT)$	$L^2 \cdot mol^{-2} \cdot min^{-1}$	
$\ln K = \frac{-\Delta H}{RT} + \frac{\Delta S}{R}$		103
$\Delta H = -6.8 \pm 1.2$	$kcal \cdot mol^{-1}$	
$\Delta S = -13.6 \pm 2.7$	$cal \cdot mol^{-1} \cdot K$	
$D_p = 3 \times 10^{-8}$	$cm^2 \cdot sec^{-1}$	60
$k_c = 6.27 \times 10^{-4}$	min^{-1}	60
$d = 0.01$	cm	
$M_w = 10000$	$g \cdot mol^{-1}$	

$r_a^{'} = 0.75$ (phenyl carbonate group/hydroxyl group in prepolymer)

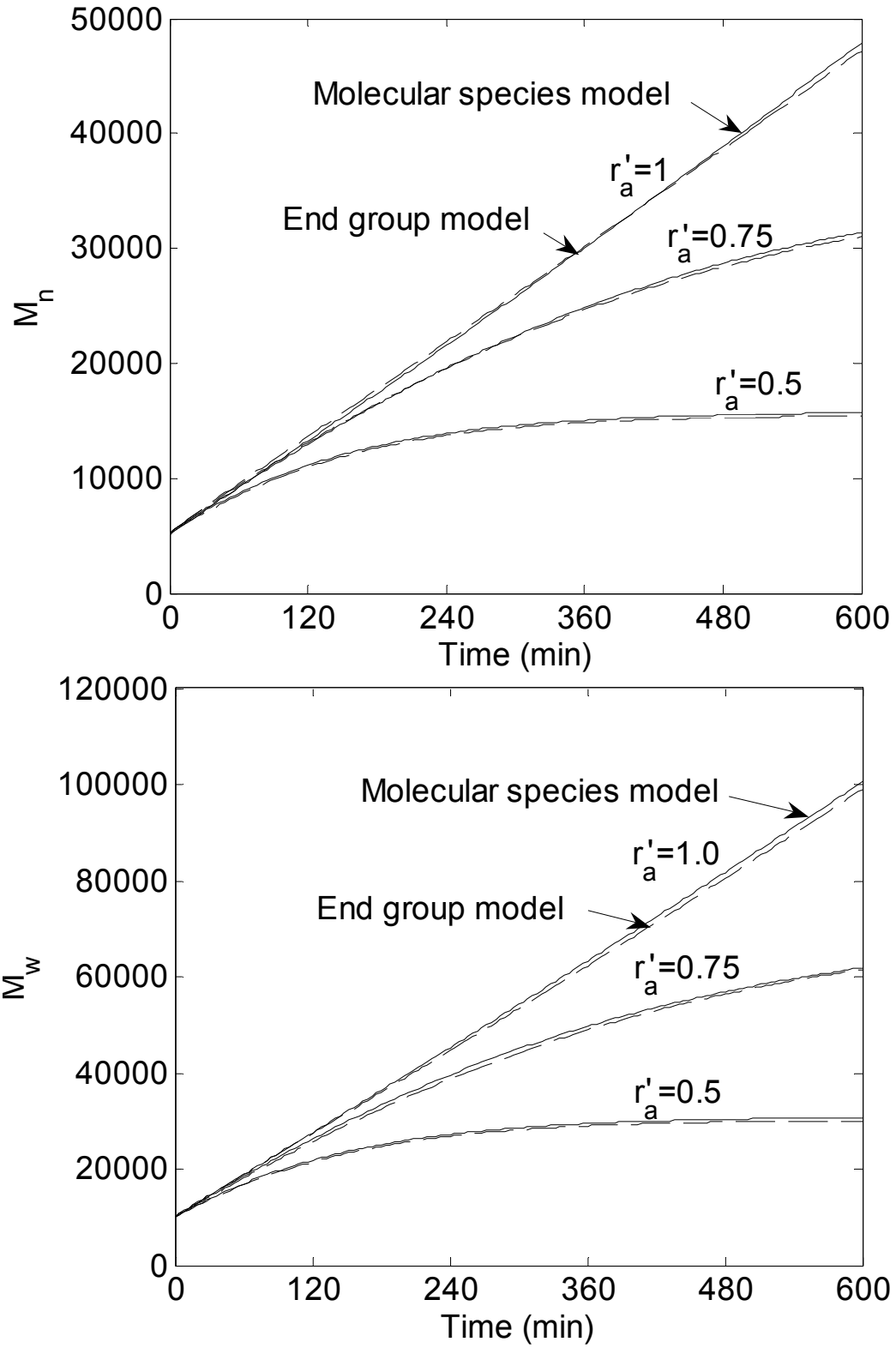

Figure 3.1 Model comparison of number- and weight-average molecular weight calculated by the molecular species model and the end group model.

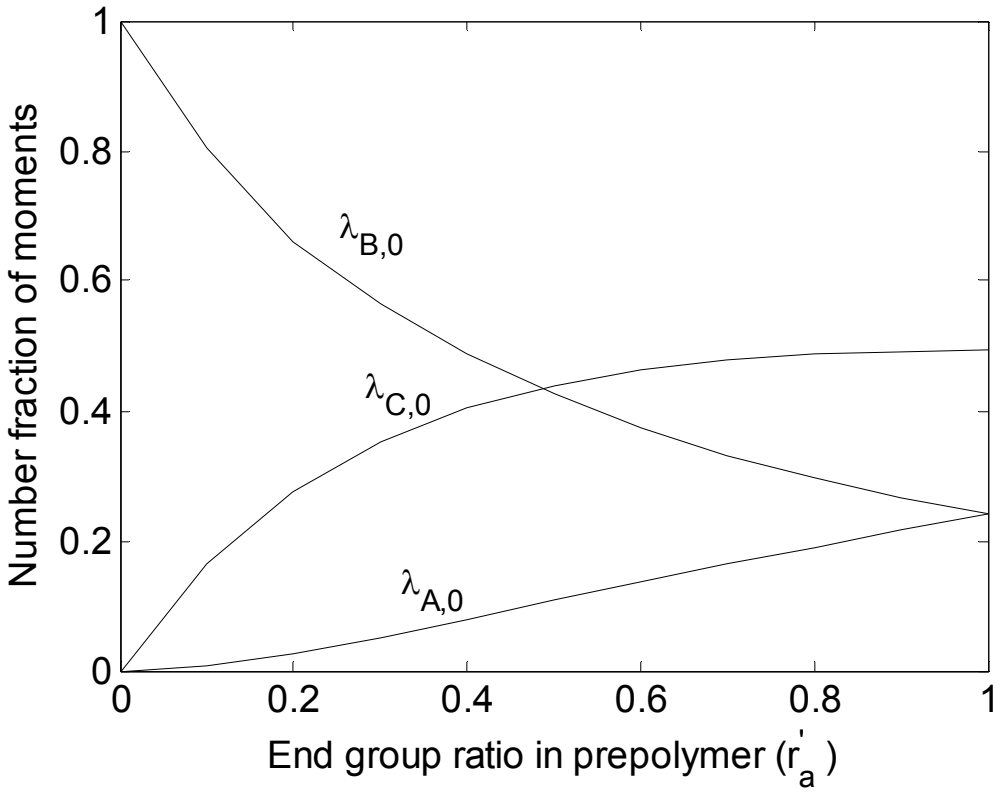

Figure 3.2 Effect of prepolymer end group ratios on the initial concentrations of molecular species.

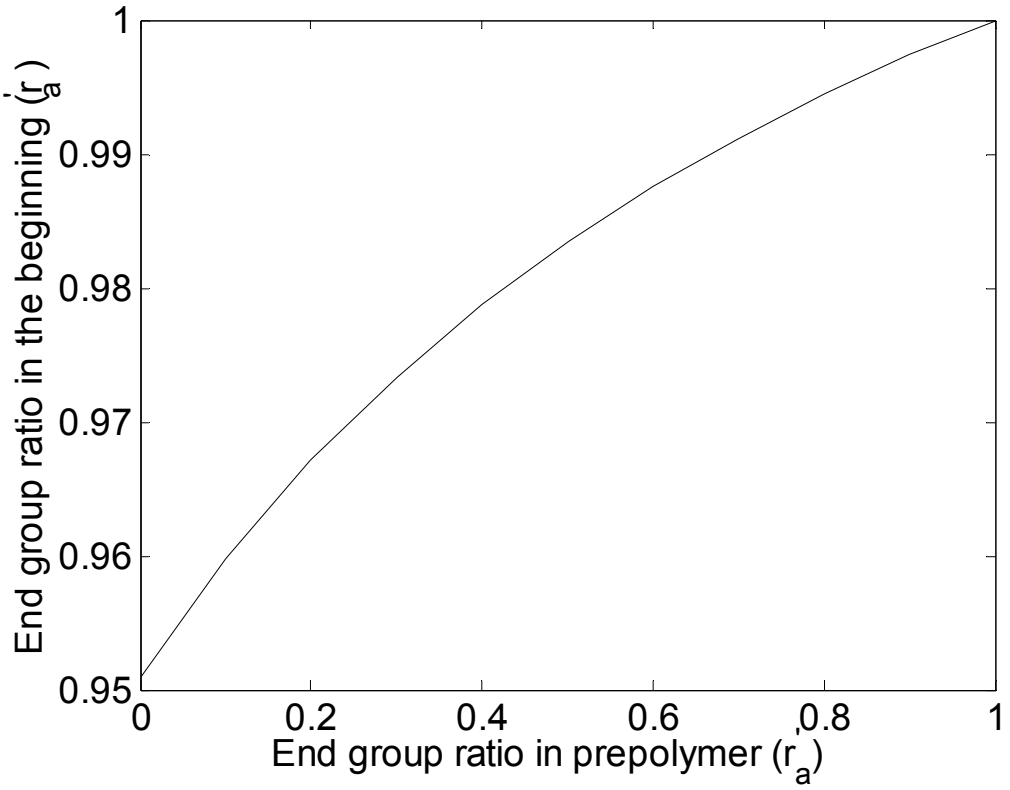

Figure 3.3 Effect of prepolymer end group ratios (r_a') on the initial end group ratios (r_a) for the melt polymerization.

Figure 3.4 shows the concentrations of molecular species of A_n, B_n, C_n at the different reaction times t = 0, 5, and 10 hr in the particle for the reference case (see Table 3.2). We assume that the concentrations of molecular species are uniform along particle radial direction in the prepolymer. From Figure 3.4a, it is seen that and the amount of species B_n is in excess compared with A_n. Figure 3.4b shows the decrease of three molecular species compared with Figure 3.4a. Figure 3.4c shows that the species of A_n is almost depleted after 12 hr's reaction, while the amount of molecular species of B_n is still quite significant. Note that there is still some C_n species left in the particle center compared with that in the surface, and further molecular weight increase is possible. Figure 3.4 indicates that the imbalance of end groups gets more severe after the SSP and that further molecular weight increase is nearly impossible if the phenyl carbonate group is completely consumed.

If the end group ratio can be altered before the SSP, it may be very useful for the highest molecular weight obtainable in the SSP. In practice, due to the loss of DPC during melt polymerization, end group imbalance general usually presents in a prepolymer. With ^{13}C-NMR analysis[99], we are able to determine end group ratios in prepolymers. Hence, a method proposed here is to blend the prepolymer with another prepolymer that has the other end group in excess. To do so, both prepolymers may be dissolved together in chloroform and crystallized in particle form using a non-solvent such as acetone. In prepolymer A, as shown in Table 3.2, it has hydroxyl end group in excess. As an example, we assume that prepolymer B has the end group ratio of 1.33 and weight-average molecular weight is 4 000. We also assume that the end groups uniformly distributed in each particle.

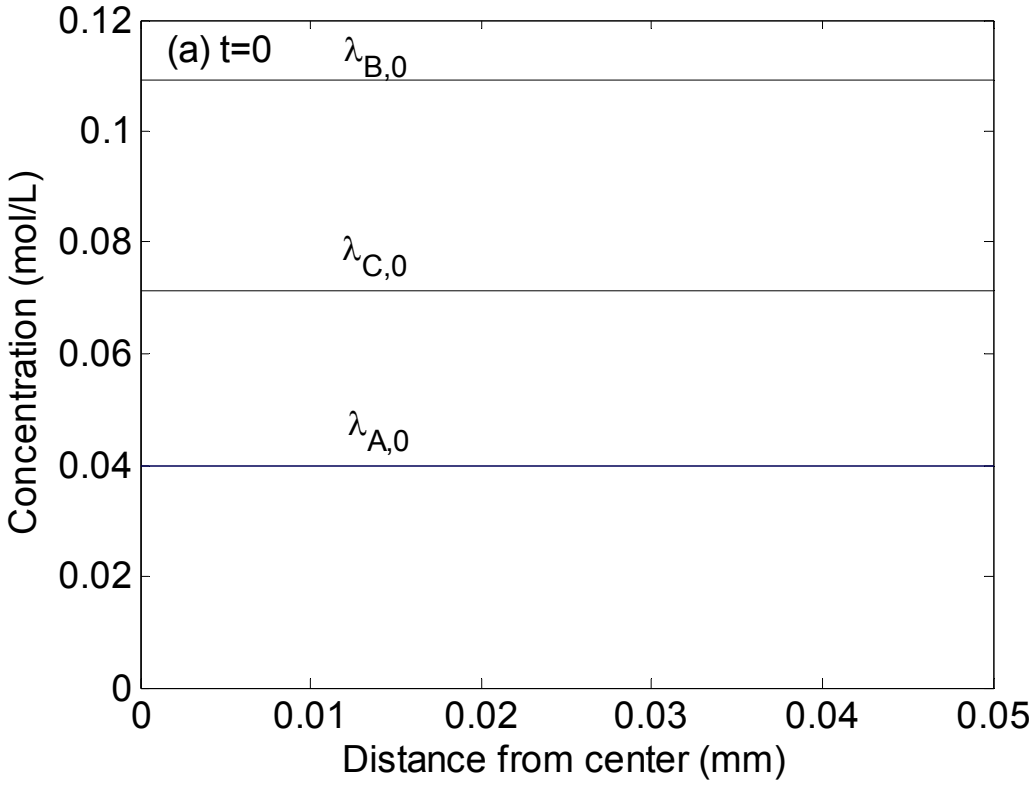
(a) t=0
$\lambda_{B,0}$
$\lambda_{C,0}$
$\lambda_{A,0}$
Concentration (mol/L)
Distance from center (mm)
0.12
0.1
0.08
0.06
0.04
0.02
0
0
0.01
0.02
0.03
0.04
0.05

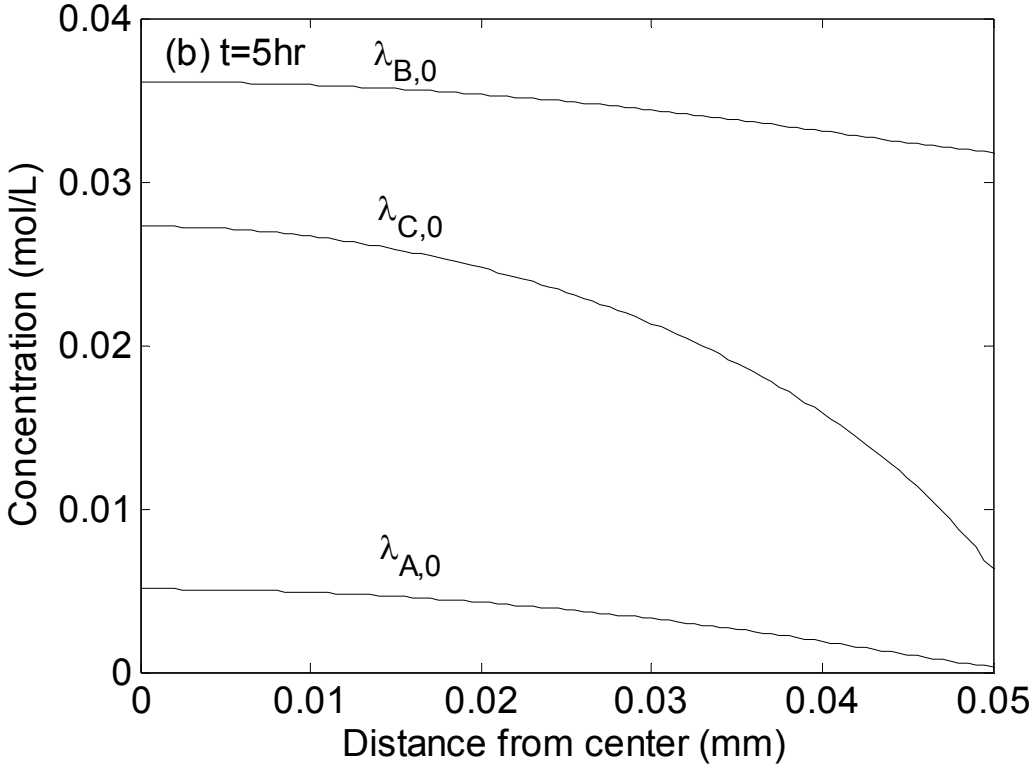
(b) t=5hr
$\lambda_{B,0}$
$\lambda_{C,0}$
$\lambda_{A,0}$
Concentration (mol/L)
Distance from center (mm)
0.04
0.03
0.02
0.01
0
0
0.01
0.02
0.03
0.04
0.05

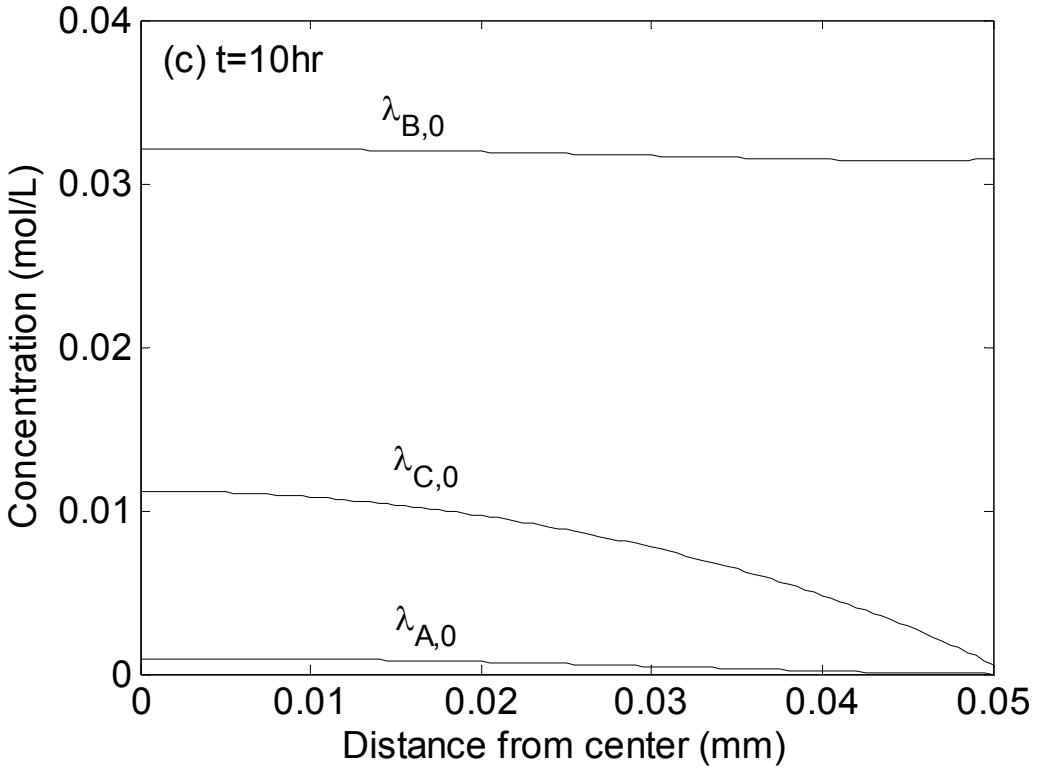

Figure 3.4 Concentration profiles of molecular species at t = 0 (a), 5 (b), 10 hr (c) in a particle.

Figure 3.5 shows chain length distributions of blends. It is seen that the blends with different compositions give broader chain length distributions. The polydispersities of blends are higher than prepolymer A and prepolymer B as shown in Figure 3.6. It also indicates that the 50/50 (w = 0.5) blending gives highest polydispersity and the broadest chain length distribution. In this case, the end group model is not capable of calculating the weight-average molecular weight because the polymer chain distribution of blends does not follow the most probable distribution. But it can be calculated by the summating moments of species from the molecular species model. To calculate the initial conditions for blends, the zeroth moments of molecular species in blends are calculated first, and the first and second moments can be determined from the zeroth moments. Figure 3.7 shows the increase of weight-average molecular weight for the different fractions of prepolymer B added. It is seen that as prepolymer B is added, the molecular weight increases at a higher rate than that of prepolymer A. However, if the end group imbalance is overcompensated (e.g. w = 0.5), the molecular weight increase rate starts to decrease again. Therefore, there is an optimum value for the amount of prepolymer B added. Figure 3.8 shows the end group ratio of blends as a function of the weight fraction of prepolymer B. It is easily found from Figure 3.8 that the end group ratio of a blend nearly reaches the balanced ratio at the point where the weight faction of prepolymer B is about 0.3. The weight faction beyond this point is off the stoichiometric ratio of end groups and will result in the excess of one end group at certain reaction time, which limits the increase of molecular weight finally. Figure 3.9 shows the concentrations of molecular species of A_n, B_n at reaction time t = 12 hr after adjusting the end group ratio. The concentration

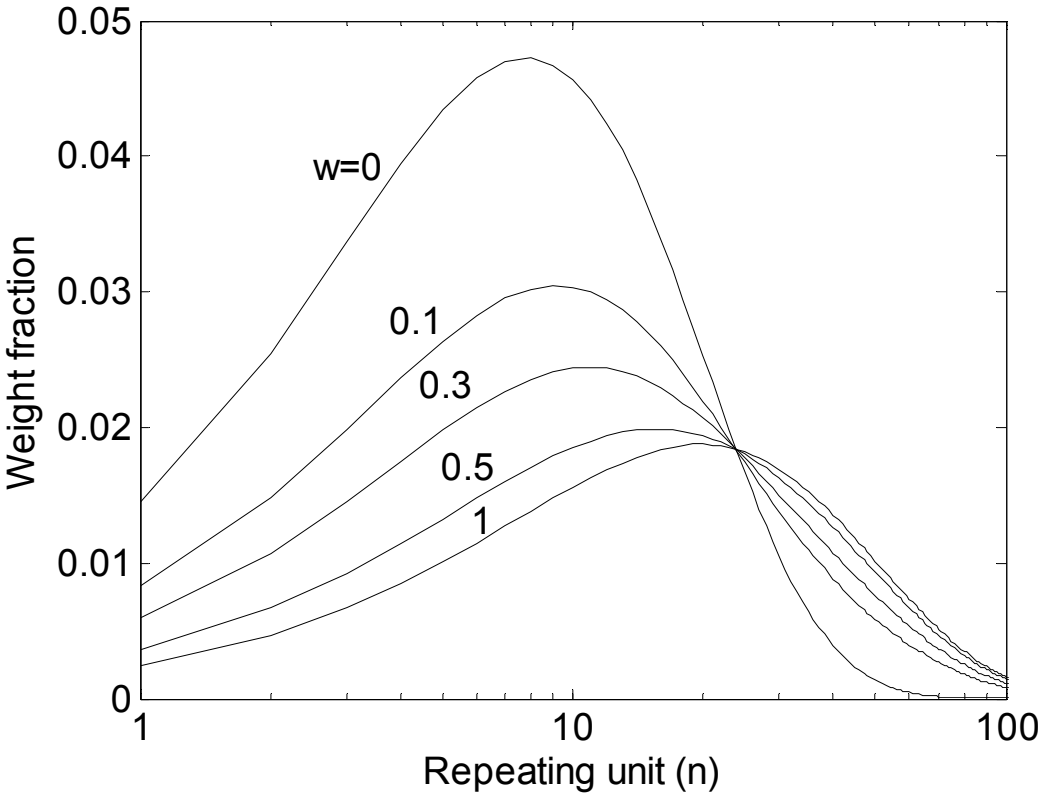

Figure 3.5 Effect of weight fraction of prepolymer B on the chain length distribution of blends.

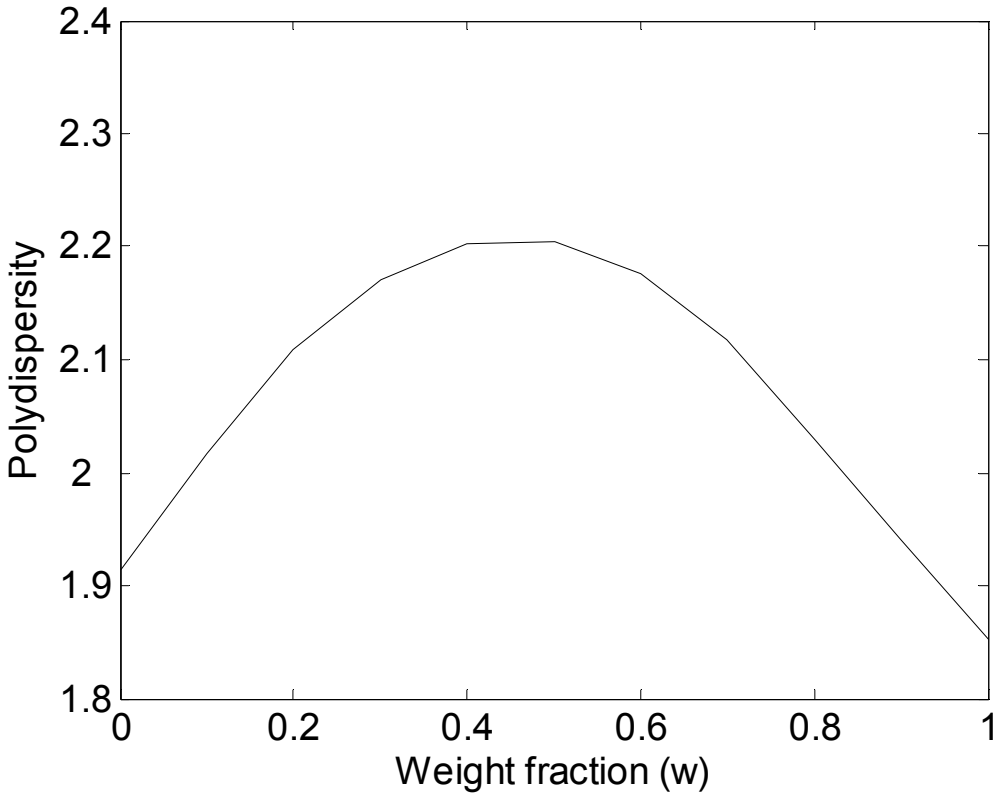

Figure 3.6 Effect of weight fraction of prepolymer B on the polydispersities of blends.

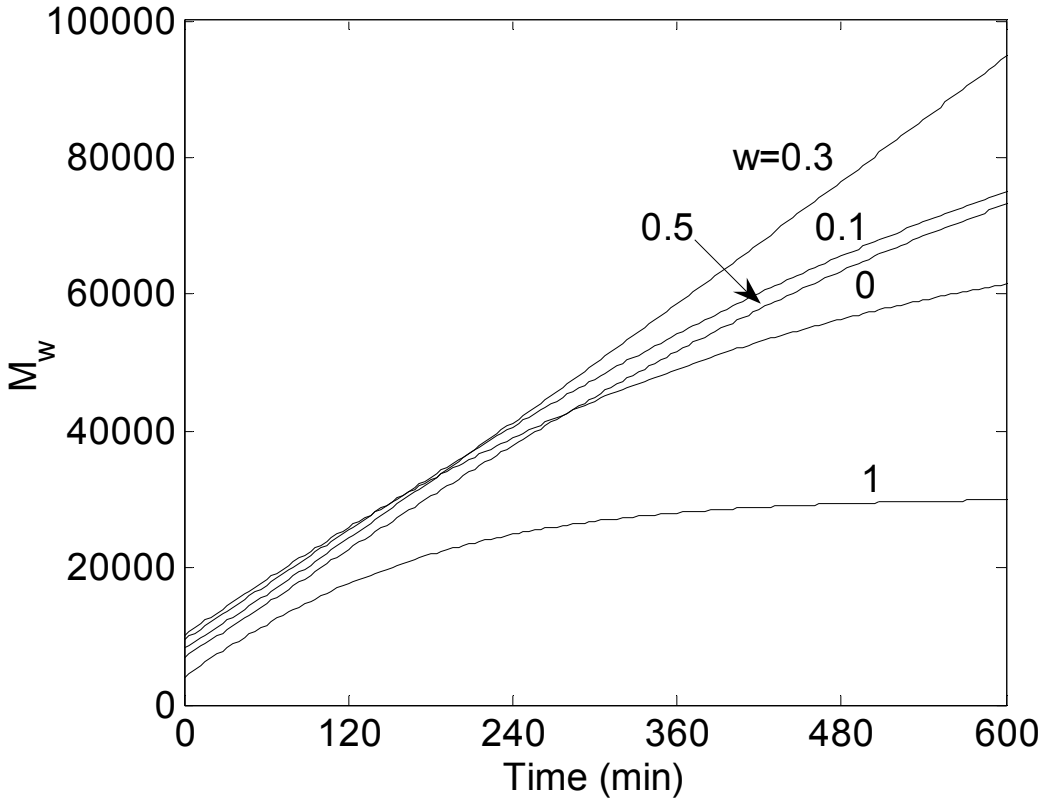

Figure 3.7 Effect of the amount of prepolymer B on the weight-average molecular weight increase (w = weight fraction).

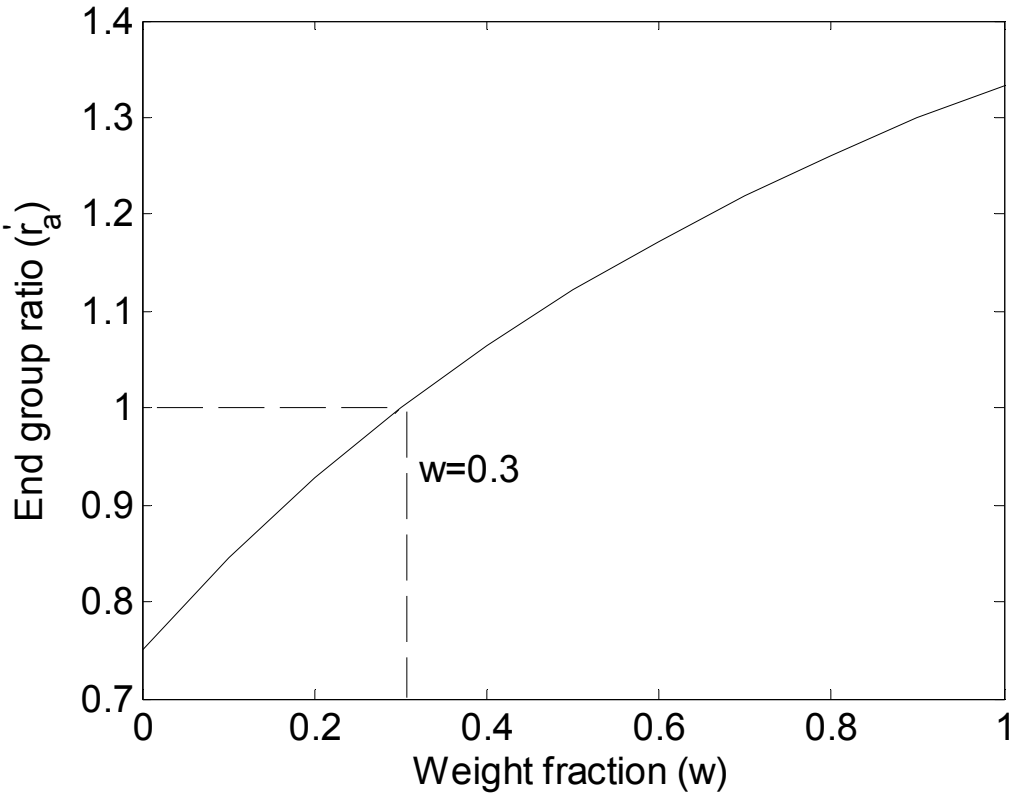

Figure 3.8 Effect of the amount of prepolymer B on the end group ratio after blending (w = weight fraction).

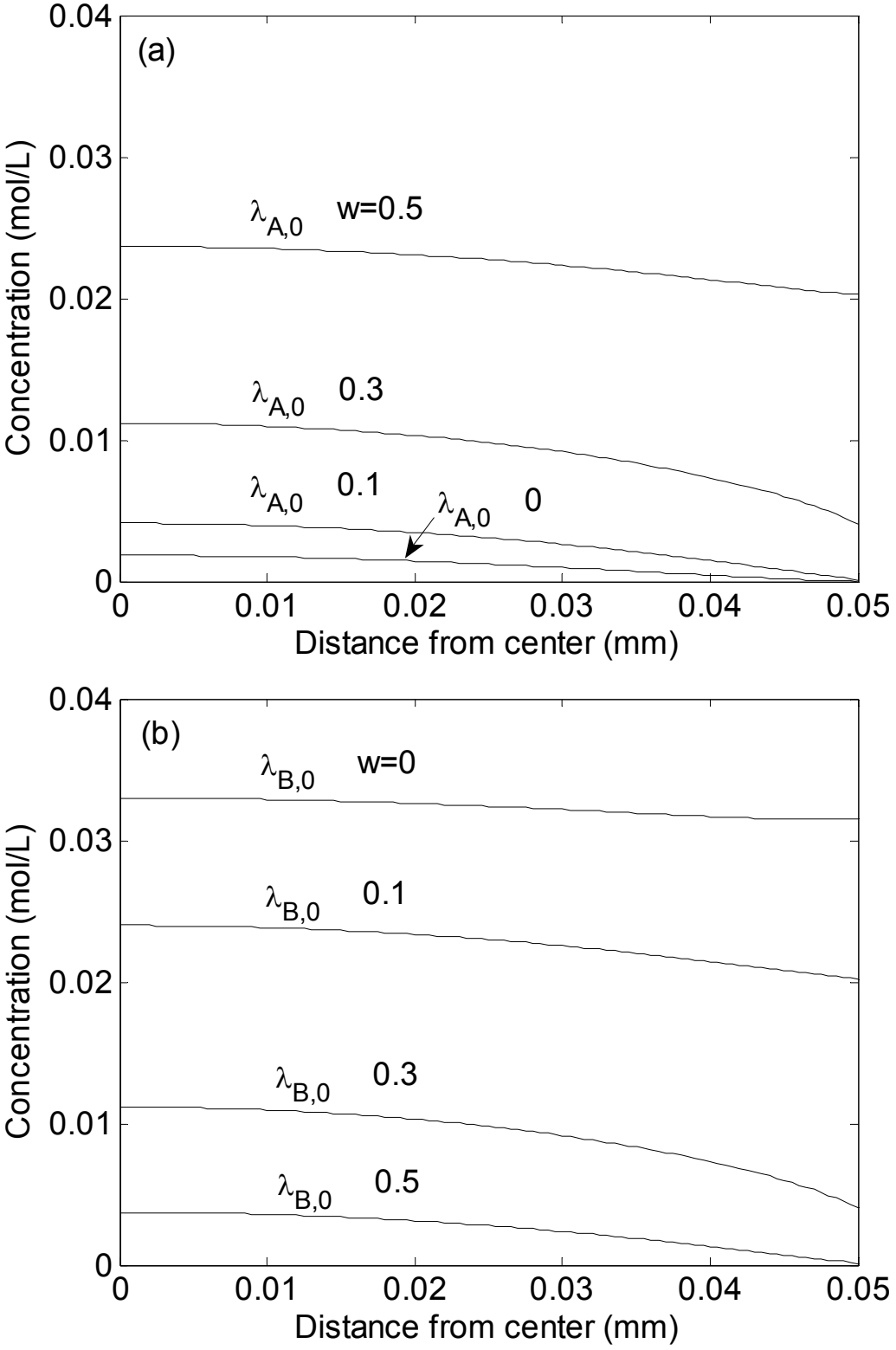

Figure 3.9 Effect of the amount of prepolymer B on the concentrations of molecular species at t = 10 hr in a particle, (a)A_n; (b) B_n (w = weight fraction).

of C_n is not shown here because it is always in balance of end group ratio. It is seen that the concentration of species A_n increases after adding prepolymer B, while that of B_n decreases. At w = 0.3, the concentration profile of A_n is about same as that B_n, meaning that both species have similar concentrations and molecular weight will increase at a high rate even in further SSP.

Certainly, for the same end group ratio, varying the molecular weight of prepolymer B will also affect the adjustment of end group ratio in prepolymer blends. Therefore, to modify the end group ratio, both end group ratio and molecular weight of prepolymer B should be taken into consideration.

3.4.3 Remelting Particles

It is well known that particle size has a significant effect on the reaction rate and hence the increase of molecular weight. Remelting followed by recrystallization is another method to accelerate the rate of molecular weight increase in a further SSP by redistributing end groups.[43,102,106] It is generally accepted that in a relative big particle significant concentration gradients of end groups and phenol present in the particle, which hampers the molecular weight further increase. Remelting redistributes end groups, giving a new fresh start of SSP because the depletion of an end group occurs at the particle surface first, and redistribution helps to deliver the end groups from inside of a particle to surface.

Redistribution processes were first studied by Flory[89] for the interchange reactions of polyester. Although further removal of phenol may not occur during the process redistribution of end groups, it is not only a physical process, but also a

chemical reaction process because each chain undergoes rearrangement through forward and backward condensation reactions during the process of redistribution of end groups. It was indicated that there is no net change in terms of number of unit linkages and the number of molecules stays same.[89] Hagenaars, et al.[107] experimentally investigated the redistribution processes of mixed BAPC fractions obtained from continuous polymer fractionation, and indicated that BAPC made by melt transesterification can further undergo redistribution processes until the Flory most probable distribution is reached.

To compare with the case without remelting, we assume: 1) the particle size is same before and after remelting; 2) no phenol is being removed during the remelting process; 3) after remelting, Flory most probable chain length distribution is reached. Theoretically, if no condensate is removed during the process of redistribution of end groups, there is no mass change in the system. Thus, number-average molecular weight is unaffected, but the molecular weight distribution may be changed because polydispersity has been changed after remelting. Previous modeling studies only investigated number-average molecular weight. However, investigation of weight-average molecular weight may bring additional insights for the remelting process.

To recalculate the initial moments for the secondary SSP, the facts that number average molecular weight and that end group ratio at the end of first SSP do not change in the remelting process can be used by following the same procedure as calculating initial conditions for prepolymers. Figure 3.10 shows the effect of remelting after different reaction times on molecular weight further increase during the secondary SSP (d = 0.1 mm). Figure 3.10a indicates that there is no number-

average molecular weight change in the remelting process, but it changes the further reaction rate and molecular weight increase during the secondary SSP because phenyl carbonate end group, the smaller amount in the reaction system, can be redistributed from particle center to surface. Figure 3.10b shows that the effect of remelting on the weight-average molecular weight. It is noticed that there is no drop in weight-average molecular weight because in such a small particle the polydispersity is close to 2, meaning that the nonuniformity of concentrations is not significant in the particle. Figure 3.11 shows the remelting effect on bigger particles (d = 0.5 mm). It is seen that the time to carry out the secondary SSP is important regarding to the final molecular weight if the total reaction time is fixed. In other words, the best time to carry out remelting is neither close to the beginning of SSP nor near the end of SSP. There is an optimum time to remelt particles that can be found through model simulation. Figure 3.11b shows that weight-average molecular weight drops down first after remelting, but increases a higher rate afterwards, which surpasses the original trend of molecular weight increase. It means that for bigger particles, concentration gradients of end groups become more severe and polydispersity is larger than 2. Remelting brings chain length distribution back to the most probable distribution, and hence reduces the weight-average molecular weight. But it accelerates the rate of molecular weight increase and catches up the original trend afterwards.

For remelting, it may be viewed as a chemically blending process for different layers and redistribute end groups inside of a particle, but the end group imbalance still exits. But by blending with another prepolymer to remake a new prepolymer, the ratio of end groups can be altered and help further molecular weight increase in SSP.

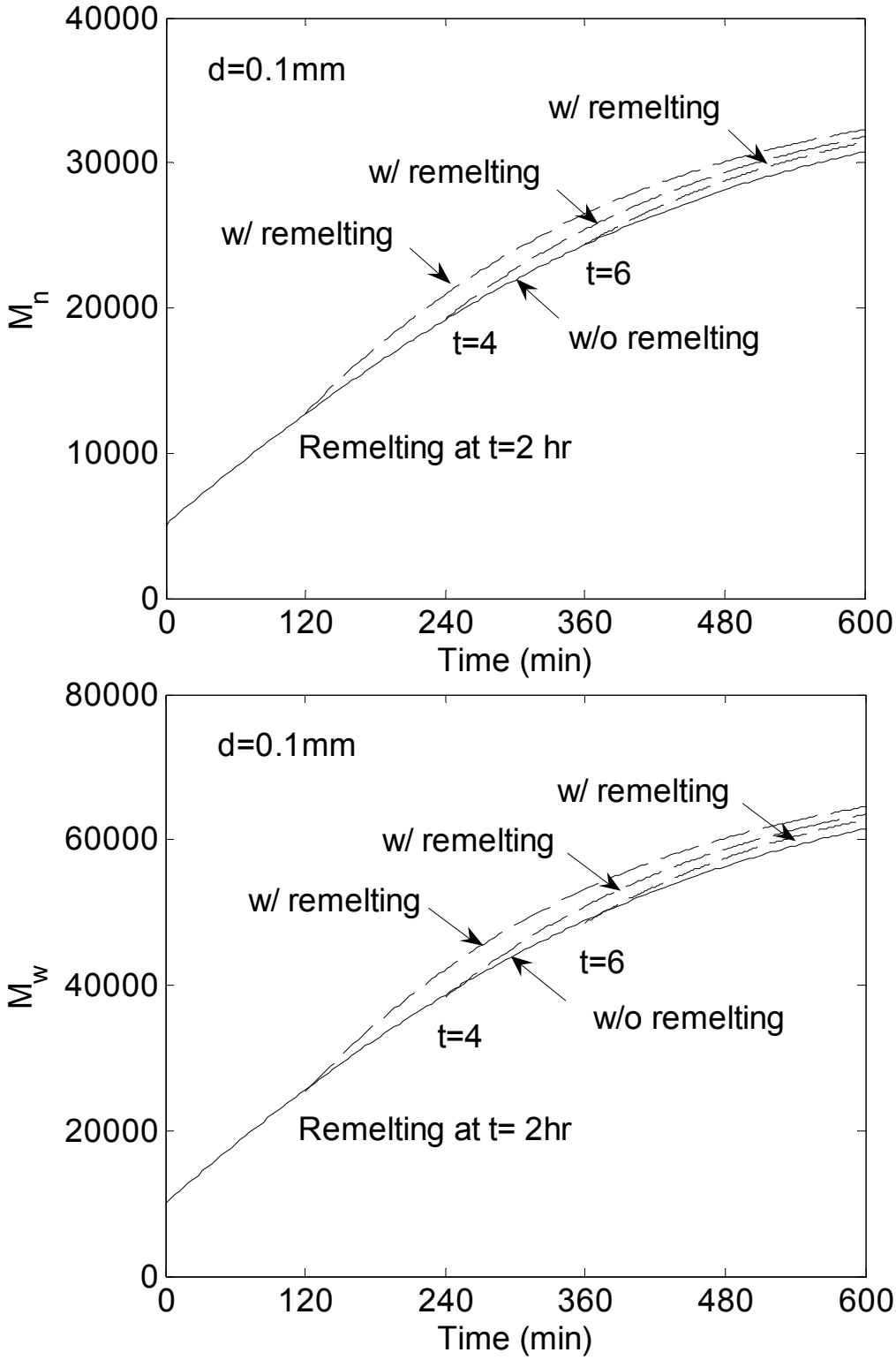

Figure 3.10 Effect of remelting on number- and weight-average molecular weight increase (d = 0.1 mm, "dash line": with remelting, and "solid line": without remelting).

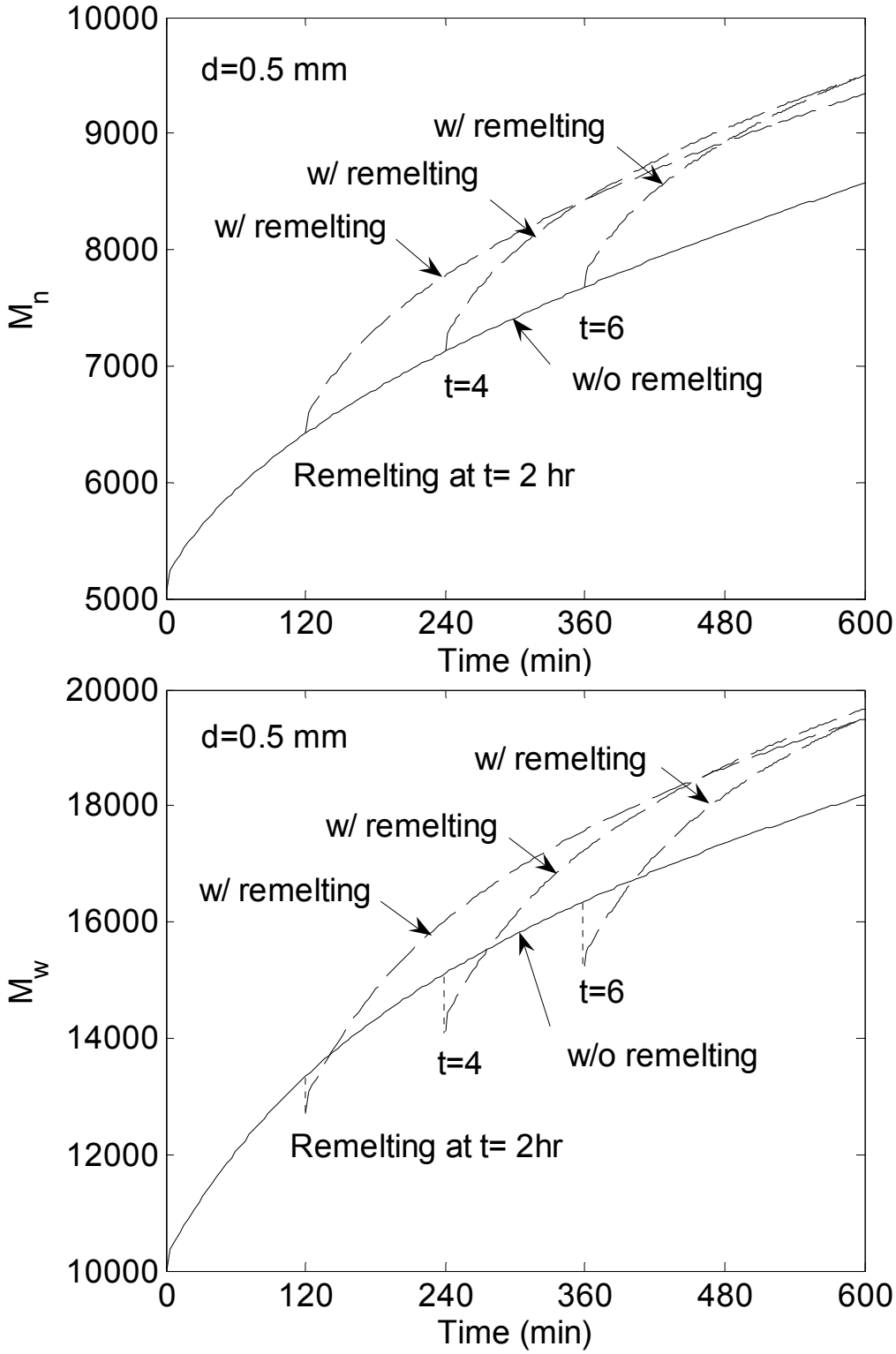

Figure 3.11 Effect of remelting on number- and weight-average molecular weight increase (d = 0.5 mm, "dash line": with remelting, and "solid line": without remelting).

3.5 Conclusions

In this chapter, a back calculation method has been developed to determine initial moments of molecular species for the molecular species model that describes the SSP of BAPC process. The simulation results are in good agreement with the end group model. As compared with the end group model, the molecular species model covers a wider range in calculation of weight-average molecular weight as long as the initial conditions are known. With the molecular species model we developed, the molar concentrations of species can be easily tracked. To accelerate the rate of molecular weight increase, a blending method has been proposed to adjust initial end group ratios in prepolymers. Simulation results show that the overall chain length distribution of blends does not follow the most probable distribution, but the initial conditions can be calculated by the method we developed, and the weight-average molecular weight can be simulated. It is seen that there is an optimum fraction for the second prepolymer B at which the SSP gives the highest reaction rate, and the fraction of prepolymer B is dependant upon the end group ratio and molecular weight of both prepolymers. Remelting is another method used to further increase molecular weight during the SSP. The weight-average molecular weight has been investigated to give a deeper insight of the utilization of remelting. It is noted that after remelting there is a drop of weight-average molecular weight although number-average molecular weight remains same. Simulation results also show that the particle size and the time chosen to remelt affect the effectiveness of remelting.

3.6 Notation

A_0 = diphenyl carbonate

B_0 = bisphenol A

d = particle diameter, cm

D_p = diffusivity of phenol, $cm^2 \cdot s^{-1}$

K = equilibrium constant

k_1 = forward reaction rate, $L \cdot mol^{-1} \cdot min^{-1}$

k_2 = backward reaction rate, $L \cdot mol^{-1} \cdot min^{-1}$

k_c = crystallization rate constant, min^{-1}

$\bar{M}_n$ = number average molecular weight

$\bar{M}_{n,0}$ = number average molecular weight of prepolymer

$\bar{M}_w$ = weight-average molecular weight

$\bar{M}_{w,0}$ = weight-average molecular weight of prepolymer

n = number of repeating unit

OH = hydroxyl end group

p = conversation of phenyl carbonate group

$[P]$ = concentration of phenol at time t, $mol \cdot L^{-1}$

$[P]_0$ = initial concentration of phenol for SSP, $mol \cdot L^{-1}$

$[P^*]$ =concentration of phenol at the bulk phase, $mol \cdot L^{-1}$

P_n = mole fraction of n-mer

Ph = phenyl carbonate end group

r = distance from particle center, cm

r_a = mole ratio of end group at the beginning of melt prepolymerization

$r_a^{'}$ = mole ratio of end group in the prepolymer

t = reaction time, min

x_c = crystallinity at time t

$\lambda_{i,j}$ ($i = A,B,C; j = 0,1,2$) = the moment of molecular species

Chapter 4

Dynamic Modeling of a Moving Packed Bed Reactor for the Solid-State Polymerization of Bisphenol A Polycarbonate

4.1 Introduction

In industry, a variety of reactor designs have been used to carry out the solid-state polymerization (SSP). A rotary drum-type reactor or a stirred bed is a simple reactor design in which all polymer particles have equal residence time.[79] The tendency towards agglomeration can be minimized by continuous agitation in the reactor. An alternative design is a fixed or static bed reactor[109]. However, a drawback is that they are operated only in the batch mode, which greatly limits the productivity. To operate in a continuous mode and increase productivity, a fluidized bed reactor can be used.[108] A fluidized bed reactor offers several advantages over fixed bed reactors. For example, polymer particles can be uniformly spread into the reactor space, which results in the effective removal of condensate and shortening the reaction time. It reduces the sticking tendency of polymer particles because the fluidized particles are not in contact long enough to stick together. However, in a fluidized bed, broad residence time distribution brings a problem, which causes molecular weight at the reactor outlet varying from one particle to another. Recently, to narrow the residence time distribution a multi-stage fluidized reactor has been used.[78] An alternative method to overcome the problem of broad residence time distribution is to operate a fluidized bed in a batch mode instead of continuous mode,

but again the productivity can be greatly reduced. Moreover, the entire process requires relatively large amount of gas and energy for operation, which is very costly.

In a continuous operation process of SSP, a moving packed bed reactor is one of the most common designs at present.[80] It is typically a vertical vessel or column filled with polymer particles that move from the top to the bottom of the reactor by gravity. A heated inert purge gas is supplied to the bottom of the reactor at high flow rate to remove the condensation byproducts. The purge gas velocity should be high enough to effectively remove condensation byproduct but it should also be low enough not to cause any fluidization or entrainment of small prepolymer particles from the reactor. Among several types of SSP reactors, a moving packed bed reactor offers many advantages such as narrow residence time distribution for the solid phase, ease of design and operation, and uniform temperature in the reactor. The uniform distributions of polymer particles and gas stream in the reactor in both radial and axial directions are important to obtain uniform quality products. It is also important to use the polymer particles of certain size range to avoid excessive pressure drop in the reactor. To obtain uniform gas flow across the reactor cross-section, a perforated gas distributor or screen is installed at the bottom of the reactor. Product particles can be withdrawn from the reactor using a discharge device such as a vane-type valve.[76,79,110]

In selecting and designing a moving packed bed reactor, high solid throughput (or short particle residence time), high molecular weight, uniformity of polymer properties, and low energy cost are the major considerations. In general, high polymer throughput can be obtained by employing high reaction temperature but if the SSP

temperature is too close to the polymer's melting point, partial melting and particle sticking may occur. To obtain high molecular weight polymers economically, the purge gas flow rate and temperature should be optimized. To obtain uniform quality polymers, it is desirable to have a narrow residence time distribution and to maintain uniform particle temperature in both the axial and radial directions in the reactor.[78,110]

Hence, understanding the reaction kinetics and reactor performance of SSP processes will be very beneficial in developing an economically competitive industrial process. But compared to the particle modeling work, the studies on the modeling of industrial reactors and continuous processes are very limited. Recently, several researchers have reported the theoretical analysis of moving packed bed reactors for the SSP of nylon and PET.[80,82,83,85] A moving packed reactor can be modeled by a tanks in series model[80] or by an axial dispersion model or a plug-flow model where the polymer particles in the bed are treated as a pseudo-continuum.[82,83,85] Although the solid-state PET and nylon polymerization reactors have been modeled and analyzed in the literature, little has been reported on the modeling of a continuous SSP reactor for the manufacture of BAPC. In the previous SSP reactor modeling of nylon and PET, parametric sensitivity[80,82], dynamic reactor behaviors,[83] and reactor performance under different operating conditions[85] have been investigated but the radial nonuniformities such as temperature and molecular weight in reactor scale were assumed to be absent.

In a large scale moving packed bed reactor, to prevent a heat loss through reactor walls, reactor can be insulated or equipped with a heating jacket in which a heating fluid is circulated.[111,112] For a moving packed bed reactor where the polymer

particles are heated by a high flow rate heated purge gas, however, uneven flow of polymer particles and purge gas, and uneven radial temperature distribution across the reactor may occur and cause the variations in polymer molecular weight in the reactor.[80] Particularly, in the startup period cold prepolymer particles are heated up to a desired SSP temperature as they move downward countercurrently to the gas flow.

In this chapter, we have developed a dynamic reactor model for a continuous SSP of BAPC in a nonisothermal moving packed bed reactor. Since reaction temperature has a large effect on the rate of SSP and polymer molecular weight, our model analysis will focus on the analysis of heat transfer and temperature nonuniformity and their effects on the molecular weight in the SSP reactor. In our model, we assume that the intraparticle temperature gradient is negligibly small and that the solid mass is assumed to behave like a pseudo-continuum in calculating the temperature profiles in the reactor. A separate particle model is also incorporated and solved at each location in the reactor to calculate the polymer properties in presence of intraparticle mass transfer limitation. Through model simulations, we shall investigate and evaluate the performance of the solid-state BAPC polymerization reactor under nonisothermal reactor environment.

4.2 Model Development

In developing a dynamic model for the SSP of polycarbonate in a moving packed bed reactor, we separate the macroscopic reactor model from the particle model. The reactor model consists of energy balances for the solid and gas phases and the particle model consists of mass balance equations for reactive end groups (phenyl

carbonate and hydroxyl groups) and phenol. The following main polycondensation reaction is considered in the particle model:

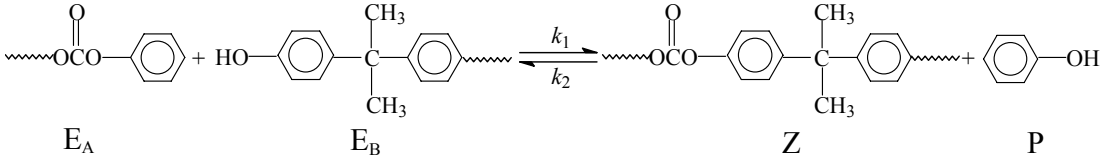

where E_A = phenyl carbonate group, E_B = hydroxyl group, Z = polymer repeat unit, and P = phenol. To obtain a high molecular weight polymer, the reaction equilibrium should be shifted to the right by removing the reaction byproduct (phenol) with an inert purge gas.

In the SSP of BAPC, the apparent reaction heat generation rate is negligibly small. In fact, thermal energy should be supplied to the polymer particles in the reactor to activate reactive end groups for the polymerization. Also, for typical polymer particle sizes (1-3 mm) used in the moving packed bed reactors[113], the intraparticle temperature gradient is negligibly small and hence the particle temperature is nearly uniform (See Figure A.1 in Appendix A).[82,85] Moreover, as very high purge gas flow rate (short gas phase residence time) quickly sweeps the reaction byproduct (phenol), there is a little accumulation of phenol in the gas phase due to the slow reaction rate. Then, we can separate the macroscopic reactor energy balance equations and the microscopic particle mass balance equations to calculate reactor temperature profiles and polymer properties separately. Another issue brought into our attention is the flow patterns, which is important for the modeling of SSP in a moving packed bed reactor. For the countercurrent flows of gas and particles, very often a plug flow model[114] or an axial dispersion model[82] is used. For the particle flow driven by gravity in a moving bed reactor for SSP, a plug flow model may be a good

approximation. For the gas phase, to determine the importance of axial dispersion terms, both Peclet number and the aspect ratio (L/d) should be considered.[115] For the polymer particle size and the purge gas velocity employed in our study, the particle Reynolds number is about 20 and the overall Peclet number[115] ($mPe = (H/d)du/D_a$) is about 2500, indicating that the gas flow can be assumed as plug flow.

The assumptions we make in developing a reactor model are summarized as follows: (i) The reaction heat generation rate during the polymerization is negligible and each polymer particle has no intraparticle temperature gradient; (ii) Both particle flow and gas flow are plug flow; (iii) The amount of phenol in the gas phase is too small to affect the physical properties of a purge gas; (iv) The reactor is a vertical cylindrical reactor.

With the above assumptions, we can derive the energy balance equations for the solid and gas phases as follows:

Solid phase:

$$\frac{\partial \tilde{T}_s}{\partial t} = \frac{k_s}{\rho_s C_{p,s}}\left[\frac{1}{R'^2\tilde{r}}\frac{\partial}{\partial \tilde{r}}\left(\tilde{r}\frac{\partial \tilde{T}_s}{\partial \tilde{r}}\right)+\frac{1}{H^2}\frac{\partial}{\partial \tilde{z}}\left(\frac{\partial \tilde{T}_s}{\partial \tilde{z}}\right)\right]-\frac{6h_{gs}\left(\tilde{T}_s-\tilde{T}_{gas}\right)}{\rho_s C_{p,s} d}-\frac{\dot{m}_s}{(1-\varepsilon)\rho_s SH}\frac{\partial \tilde{T}_s}{\partial \tilde{z}} \tag{4.1}$$

Purge gas phase:

$$\frac{\partial \tilde{T}_{gas}}{\partial t} = \frac{k_g}{\rho_g C_{p,g}}\left[\frac{1}{R^2\tilde{r}}\frac{\partial}{\partial \tilde{r}}\left(\tilde{r}\frac{\partial \tilde{T}_{gas}}{\partial \tilde{r}}\right)+\frac{1}{H^2}\frac{\partial}{\partial \tilde{z}}\left(\frac{\partial \tilde{T}_{gas}}{\partial \tilde{z}}\right)\right]+\frac{6h_{gs}(1-\varepsilon)\left(\tilde{T}_s-\tilde{T}_{gas}\right)}{\rho_p C_{p,p} d_p \varepsilon}+\frac{\dot{m}_g}{\varepsilon\rho_g SH}\frac{\partial \tilde{T}_{gas}}{\partial \tilde{z}} \tag{4.2}$$

where $\tilde{T}_s$, $\tilde{T}_g$, $\tilde{z}$ and $\tilde{r}$ are the scaled values of solid phase temperature, gas phase temperature, bed height and reactor radius, respectively

($\tilde{T}_s = T_s/298\,K$, $\tilde{T}_{gas} = T_{gas}/298\,K$, $\tilde{z} = z/H$, and $\tilde{r} = r'/R'$, R' is the reactor radius).

Other symbols are defined in Notations. The initial and boundary conditions are given in Table 4.1.

It is assumed that polycarbonate prepolymers have been partially crystallized before they are supplied to the SSP reactor. Although, polycarbonate crystallizes slowly by thermal annealing, our previous work shows that the degree of crystallinity increases during the SSP, changing the volume fraction of amorphous reaction phase in a particle.[60] The degree of crystallinity (x_c) is calculated by the following equations:[85]

$$\frac{\partial x_c}{\partial t} = -\frac{\dot{m}_s}{(1-\varepsilon)\rho_s SH}\frac{\partial x_c}{\partial \tilde{z}} + k_c\left(x_{c,max} - x_c\right) \tag{4.3}$$

where k_c is the crystallization rate and $x_{c,max}$ is the maximum degree of crystallinity (0.62).[100]

The pressure drop is calculated using the following equation:[116]

$$\frac{\partial P}{\partial \tilde{z}} = H\left(150\frac{(1-\varepsilon)^2}{\varepsilon^3}\frac{\eta G}{d^2} + 1.75\frac{1-\varepsilon}{\varepsilon^3}\frac{\rho_g G^2}{d}\right) \tag{4.4}$$

The numerical values of the physical parameters are listed in Table 4.2. For the reactor operating conditions used in our model simulations, the pressure drop in the reactor is less than 0.17 atm (See Figure B.1 in Appendix B).

To calculate the phenol and molecular weight in a spherical polymer particle, the end group model shown in chapter 2 is used. The boundary condition for the phenol concentration at particle surface is assumed zero, indicating that once phenol molecules reach a particle surface, they are assumed to be quickly removed by a high flow rate purge gas. Since the residence time for the purge gas is very short (8.2 sec) and the reaction rate of SSP is very slow, the concentration of phenol in the bulk gas

Table 4.1 Initial and boundary conditions for the reactor model

$\tilde{T}_s = \tilde{T}_{s,0} = 1, \quad \tilde{T}_g = \tilde{T}_{g,0} = 1, \quad x_c = x_{c,0} \quad \text{at } t = 0$
$\frac{\partial \tilde{T}_s}{\partial \tilde{z}} = -\frac{\dot{m}_s C_{p,s} H}{k_s (1-\varepsilon) S}\left(\tilde{T}_{s,in} - \tilde{T}_s\right), \quad \frac{\partial \tilde{T}_g}{\partial \tilde{z}} = 0, \; x_c = x_{c,in} \text{ at } \tilde{z} = 0$
$\frac{\partial \tilde{T}_s}{\partial \tilde{z}} = 0 \;\; , \;\; \frac{\partial \tilde{T}_g}{\partial \tilde{z}} = -\frac{\dot{m}_g C_{p,g} H}{k_g \varepsilon S}\left(\tilde{T}_g - \tilde{T}_{g,in}\right) \text{ at } \tilde{z} = 1$
$\frac{\partial \tilde{T}_s}{\partial \tilde{r}} = 0 \;, \;\; \frac{\partial \tilde{T}_g}{\partial \tilde{r}} = 0 \text{ at } \tilde{r} = 0$
$\frac{\partial \tilde{T}_s}{\partial \tilde{r}} = -\frac{h_{sw} R}{k_s}\left(\tilde{T}_s - \tilde{T}_w\right) \;, \; \frac{\partial \tilde{T}_g}{\partial \tilde{r}} = -\frac{h_{gw} R}{k_g}\left(\tilde{T}_g - \tilde{T}_w\right) \text{ at } \tilde{r} = 1$

Table 4.2 Physical parameters

parameter	correlation	ref
$C_{p,g}$	$C_{p,g} = \frac{R}{M}\left(a_0 + a_1 T + a_2 T^2 + a_3 T^3 + a_4 \frac{u^2 \exp(u)}{\left[\exp(u)-1\right]^2} \right)$	117
k_g	$k_g = k_g^0(T) + k_g^r(\tau,\delta)$	118*
	$k_g^0 = N_1 \left[\frac{\eta^0(T)}{1\ \mu Pa \cdot s} \right] + N_2 \tau^{t_2} + N_3 \tau^{t_3}$	
	$k_g^r = \sum_{i=4}^{n} N_i \tau^{t_i} \delta^{d_i} \exp\left(-\gamma_i \delta^{l_i}\right)$	
η	$\eta = \eta^0(T) + \eta^r(\tau,\delta)$	119*
	$\eta^0 = \frac{0.00266958\sqrt{MT}}{\sigma^2 \Omega(T^*)}$ $(\Omega(T^*) = \exp\left(\sum_{i=0}^{4} b_i \left[\ln(T^*) \right]^i \right))$	
	$\eta^r = \sum_{i=1}^{n} N_i \tau^{t_i} \delta^{d_i} \exp\left(-\gamma_i \delta^{l_i}\right)$	
ρ_s	$\rho_s = \rho_a (1-x_c) + \rho_c x_c$	5, 119
	$\rho_c = 1.315,\ \rho_a = \frac{1}{V(0,T)\left[1 - 0.0894 \ln\left(1 + P/B(T)\right)\right]}$	
	$B(T) = 3954 \exp\left(-2.609 \times 10^{-3} T\right),$	
	$V(0,T) = 0.8302 + 2.20 \times 10^{-4} T$	
$C_{p,s}$	$C_{p,s} = (0.559T + 249.17)/254.3$	120
k_s	0.156	121

h_{gs}

$$h_{gs} = \frac{j_H C_{p,g} \dot{m}_g}{S} \left(\frac{\mu_g C_{p,g}}{k_g} \right)_f^{-2/3} \tag{122}$$

$$j_H = \begin{cases} 0.91\,\mathrm{Re}^{-0.51}, & \mathrm{Re} < 50 \\ 0.61\,\mathrm{Re}^{-0.41}, & \mathrm{Re} > 50 \end{cases}, \quad \mathrm{Re} = \frac{\dot{m}_g d_p}{6S\eta(1-\varepsilon)\phi}$$

h_{gw}

$$h_{gw} = \frac{1.1 k_g}{d_p} \mathrm{Pr}^{1/2}\, \mathrm{Re}^{1/2} \tag{123}$$

h_{sw}

$$h_{sw} = \frac{h_{gw} k_g}{k_p} \left[1 + \frac{10\left(k_p / k_g\right)}{\mathrm{Re}\,\mathrm{Pr}} \right] \tag{124}$$

k_c

$$k_c = \begin{cases} 0 & T < T_g \\ 7.82 \times 10^9 \exp\left(-\dfrac{2.8 \times 10^4}{R_g T} \right) & T_g < T < T_{co} \end{cases} \tag{125}$$

$$T_{co} = 213^o C$$

* See the original reference for the values of parameters in the correlations.

phase is negligibly small in the reactor. The number- and weight- average molecular weights for a particle are calculated using eqs 2.13 and 2.14.

At each point in the moving packed bed reactor, the polymer particle model is solved using the end group model and the overall average molecular weight and the chain length distribution in the reactor cross-section are calculated by the following equations:

$$\bar{M}_{n,o} = R'^2 \left(2\int_0^{R'} \frac{r'}{\bar{M}_n(r')} dr' \right)^{-1} \tag{4.5}$$

$$\bar{M}_{w,o} = \frac{1}{R'^2} \left(2\int_0^{R'} r' \bar{M}_w(r') dr' \right) \tag{4.6}$$

$$W_{n,o} = \frac{1}{R'^2} \left(2\int_0^{R'} r' W_n(r') dr' \right) \tag{4.7}$$

where r' is the radial direction in the reactor ($r' = 0$ at the center) and R' is the reactor radius. $\bar{M}_{n,o}$ and $\bar{M}_{w,o}$ are the overall number average and weight average molecular weights across the reactor cross-section, respectively. $W_{n,o}$ is the overall chain length distribution across the reactor cross-section. The kinetic constants and physical parameters are listed in Table 4.3.

Figure 4.1 illustrates how the particle model is solved in conjunction with the reactor model that yields the temperature profiles in the radial and axial directions. The reactor model equations 4.1 and 4.2 are solved first for a given set of initial and boundary conditions. The calculated temperature profiles at the grid points of the mesh network in radial and axial directions in the reactor are stored. Then the temperature value at a particular time at each grid point in the mesh network is

Table 4.3 Transport and kinetic parameters used in the particle model

parameter	correlation	unit	ref
D_p	$D_p = 1.2\times10^{-7}\exp\left(-\frac{32{,}800}{R_g}\left(\frac{1}{T}-\frac{1}{473}\right)\right)$	$cm^2\cdot s^{-1}$	23
k_1	$k_1 = k_u + k_c[C^*]$ $k_u = (3.108\pm0.102)\times10^7\exp(-25290\pm1010/RT)$ $k_u' = (2.028\pm0.226)\times10^{15}\exp(-45030\pm2430/RT)$ $k_c = 9.62\times10^8\exp(-13900/RT)$ $k_c' = 8.04\times10^7\exp(-12090/RT)$	$L\cdot mol^{-1}\cdot min^{-1}$	98
K	$\ln K = \frac{-\Delta H}{R_g T} + \frac{\Delta S}{R_g}$ $\Delta H = -6.8\pm1.2$ $\Delta S = -13.6\pm2.7$		103

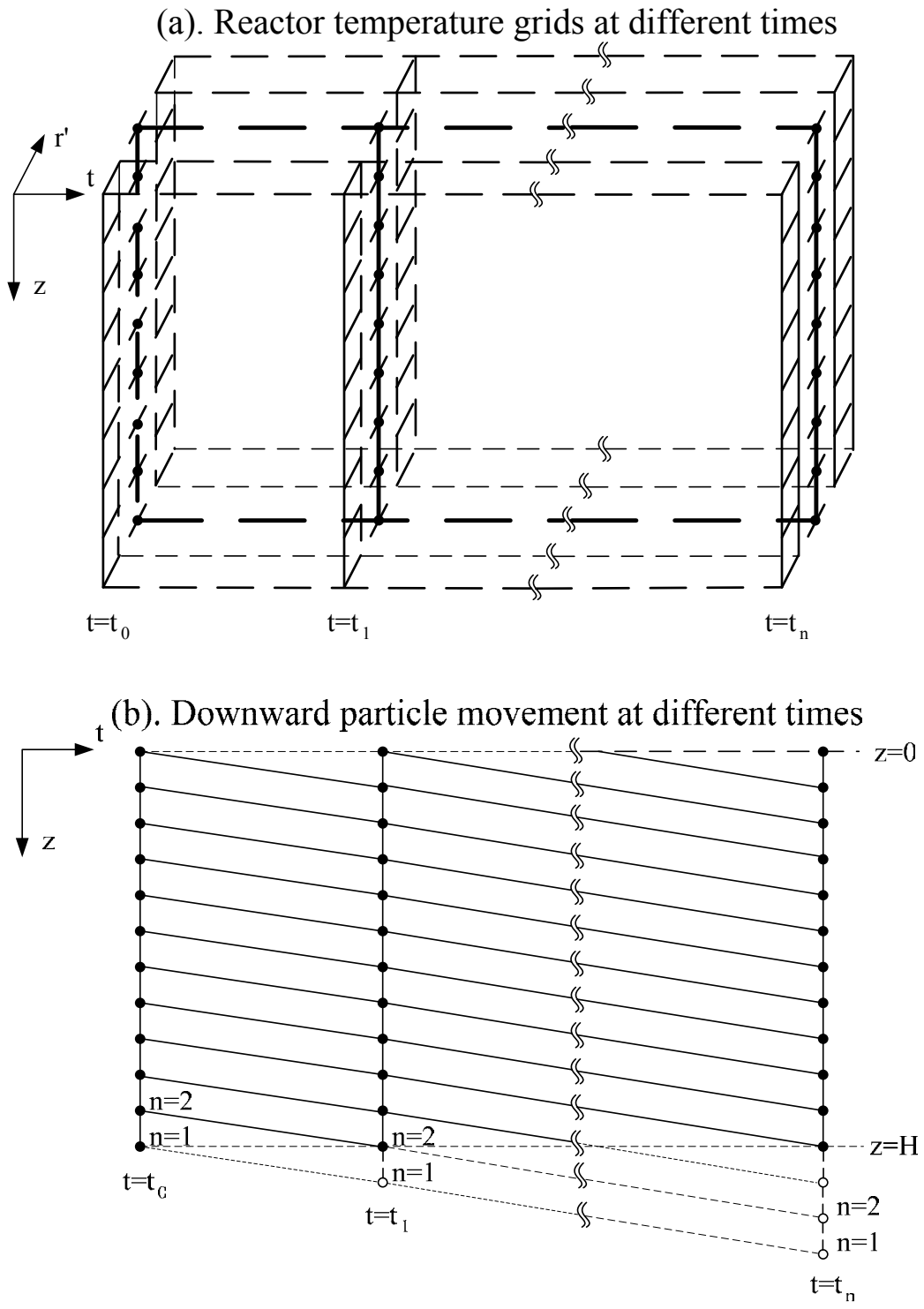

Figure 4.1 Computational mesh network: (a) dynamic reactor mesh points; (b) lines of downward particle movement.

applied to a polymer particle model. To illustrate the computational procedure for a dynamic process simulation, consider a downward movement of the polymer particles along the axial grid line. Here, one line is chosen at a time. Discrete grids in the axial (z) direction are set, and a number is assigned to each particle in the mesh network at $t = t_0$. The initial temperature for each particle is recorded. Then, for a given small time step, a new position of each particle is determined in the z direction accordingly. The temperature of each particle is determined from the dynamic temperature profiles calculated using the reactor model in the solid phase at time $t = t_1$. The number of particles exiting the reactor at the bottom during the time span from t_0 to t_1 is counted. If there are any particles leaving the reactor, then the amount of feed particles is calculated such that the total number or mass of polymer particles in each line is constant. Both time t and temperature of these particles entering and leaving the reactor are recorded. These steps are repeated for a given reactor simulation time. Along the grid line, the particle model is solved at each grid point to calculate polymer molecular weight. Then, another particle line is chosen in the reactor and the foregoing calculation steps are repeated until all the particle lines in the reactor are counted. The average values of polymer properties are calculated for the reactor cross-section using the calculation results obtained for each grid point.

4.3 Results and Discussion

The reactor model and the particle model have been solved separately using the partial differential equation solvers in FEMLAB® and MATLAB®, respectively. To determine the standard or reference model simulation conditions, we reviewed the literature (mostly patents) on the moving packed bed reactors for nylons, polyesters and polycarbonates. As illustrated in Table 4.4, the reactor size and operating conditions vary from patent to patent. In our model simulation work, we use the reactor dimension used by other researchers for the SSP of nylon 6,6 and PET.[76,82,83,85]

The average residence time of 10 hr is taken for the solid phase as a standard value because at a typical solid-state BAPC polymerization temperature (190-220^{o}C), it takes about 5-15 hr to obtain high molecular weight BAPC.[60] Then, for a given reactor dimension and particle residence time, the prepolymer feed rate is calculated. To determine the purge gas velocity, the minimum fluidization velocity (u_{mf}) is calculated for a given particle size and set as the maximum gas flow rate. The purge gas flow rate must be kept below u_{mf}. The minimum fluidization velocity is calculated using the following equation for spherical particles:[129]

$$u_{mf} = \frac{d^2\left(\rho_s - \rho_g\right)g}{150\eta}\frac{\varepsilon_{mf}^3}{1-\varepsilon_{mf}} \quad , \quad \mathrm{Re}_{mf} < 20 \tag{4.8}$$

where d is the particle diameter and ε_{mf} is the bed voidage. For the standard operating conditions, the inlet superficial gas flow rate is 15.7 cm/sec at 1.17atm and 200ºC, and u_{mf} is 68.8 cm/sec.

Table 4.4 Operating conditions and reactor sizes for moving packed bed reactors

SSP of		Nylon 6,6		Nylon 6	BAPC	PET	PET	PET
reactor	diameter(cm)	40.6	152	-	15	50.8	61.0	61
geometry	length (cm)	396	610	-	100	304.8	365.8	350
	particle residence t (hr)	3.5	12	18	10	10	16	12
operating	flow rate ratio *	2.4	4.0	0.05-0.3	5.8	8.1	1.0	-
conditions	inlet gas T (ºC)	190	200	-	210	205	220	226
	inlet particle T (ºC)	25	25	-	210	175	210	180
	ref	76		126	9	127	128	75

Note: Flow rate ratio = mass flow rate of gas/mass flow rate of particles

4.3.1 Simulation of Reactor Startup Operations

The startup operation of a SSP reactor is important because the residence time of polymer particles in the reactor is very long and it is desired to reach a steady state reaction conditions as quickly as possible at minimum utility cost.[82] There are several possible methods of reactor startup operations. For example, a reactor is first fully charged with prepolymer particles and heated up by the preheated purge gas. Until a desired reaction temperature is established in the entire reactor, the SSP is carried out in a batch mode, i.e., no polymer particles are removed from the reactor. Another example of startup operation is to charge the reactor slowly with feed prepolymer particles while a preheated purge gas is supplied to the bottom of the reactor. Since the amount of polymer particles is not large during the particle charging period, it would take less time to bring the particle temperature to its reaction temperature, thereby reducing the total reaction time. In this operation, however, the purge gas flow rate should be carefully controlled to prevent the entrainment of small polymer particles.

In our model simulation, the following startup operation is considered: (i) An empty vertical reactor equipped with a heating jacket is filled with prepolymer particles at room temperature; (ii) The prepolymer particles are heated up by the purge gas supplied to the bottom of the reactor at 200ºC and the reactor jacket temperature is set at 200ºC; (iii) Reactor preheating is continued until the temperature at the reactor top approaches the reaction temperature, 200ºC; (iv) As the reactor temperature reaches 200^{o}C, the reactor operation is switched from a batch fixed bed reactor mode to a continuous moving packed bed reactor mode by starting the

discharge of polymer particles from the reactor bottom. The prepolymer feed particles are also supplied to the top of the reactor to keep the bed weight or height constant during the continuous reactor operation. Table 4.5 shows the standard reactor operating conditions, reactor dimension, and feed prepolymer properties used in our model simulations.

Figure 4.2 shows the temperature profiles of the solid phase during the first 30 hr of reactor operation. Here, the initial particle temperature in the reactor is 25^{o}C. It is observed that the particle heating is a very slow process with a given flow rate of purge gas for a large mass of solid particles in the reactor. Although the heating jacket is used, the radial heat transfer from the reactor walls to the center of reactor is not quite effective. It is clearly seen that heat is predominantly transferred to polymer particles from the heated purge gas. Here, the gas flow rate is 1000 g/min and the residence time for the gas is 8.2 sec. It takes nearly 10 hr for the reactor to reach a uniform temperature of 200^{o}C along the entire bed height. At t =10 hr, the reactor operation is switched from a batch mode to a continuous mode by discharging the product and at the same time feeding prepolymer feed particles to the top of the reactor. Figure 4.2 also shows that these feed particles quickly absorb the heat from the purge gas and a slight temperature nonuniformity is observed only in a very shallow region near the top of the reactor. In other words, once the steady state temperature profile is established during the startup process, the reactor temperature is quite uniform in both the radial and axial directions in the reactor. But it needs to be pointed out that the polymer particles at different locations in the reactor experience different reaction temperature trajectories during the entire startup

Table 4.5 Operating conditions and prepolymer properties

parameter	value
D	reactor diameter, 40 cm
L	total reactor length, 400 cm
H	bed depth, 320 cm
$T_{s,0}$	initial temperature of solid phase, 298 K
$T_{g,0}$	initial temperature of gas phase, 298 K
T_w	reactor wall temperature, 473 K
$T_{s,in}$	inlet temperature of solid phase, 298 K
$T_{g,in}$	inlet temperature of gas phase, 473 K
d	particle diameter, 0.15 cm
$\dot{m}_s$	mass flow rate of particles, 0 g/min (before 600 min) 450 g/min (after 600 min)
$\dot{m}_g$	purge gas flow rate, 1000 g/min
P	outlet pressure, 1 atm
ε	voidage in the reactor, 0.4
$x_{c,0}$	crystallinity of prepolymer feed, 25%
$r_a^{'}$	end group ratio in the prepolymer, 1:1
$\bar{M}_{n,0}$	initial number average molecular weight, 4000
$[C^*]$	catalyst concentration in prepolymer, 1.7×10^{-4} mol/L

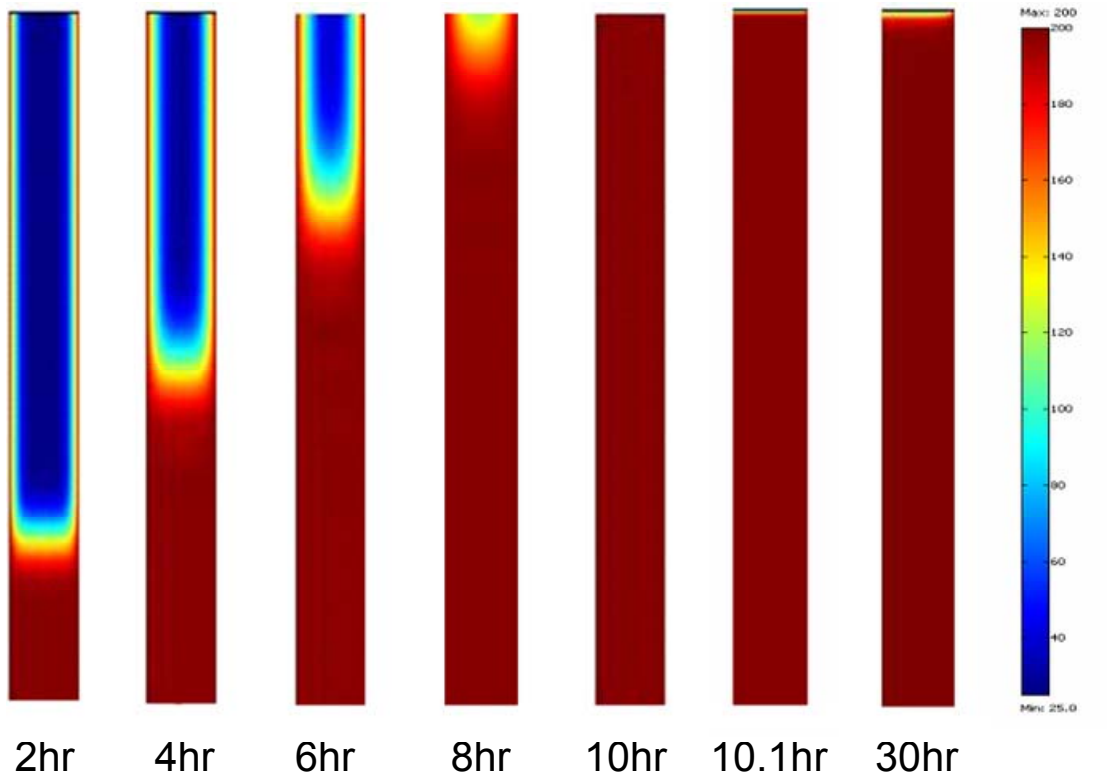

Figure 4.2 Reactor temperature profiles during the startup process; After t = 10 hr, the reactor is operated in a continuous mode.

transient period.

Figure 4.3 shows three dimensional reactor temperature profiles at t = 2 hr and t = 8 hr during the startup process. Notice that the polymer particles near the bottom and the reactor walls reach the reaction temperature quite rapidly whereas the particles in other sections of the reactor remain cold during the transient period.

The polymer molecular weight profiles at the reactor bottom during the start-up and subsequent continuous operation are shown in Figure 4.4. Recall that no polymer particles are removed until t = 10 hr. Polymer molecular weight increases gradually with time during the batch operation (t = 0-10 hr) to a value corresponding to the final reactor temperature of 200^{o}C. Figure 4.4 also shows that the polymer particles trickling down along the reactor walls (r' = 20 cm) have much higher molecular weight than the polymers near the center. This is because particles near the heating jacket are heated up more effectively from the beginning of startup operation and they experience longer time in high temperature zone to polymerize. Figure 4.4 shows that for one solid residence time (10 hr) after the commencement of continuous operation, the molecular weight of the polymers from the reactor wall area continues to rise and then drops sharply as the entire reactor becomes thermally homogeneous at 200^{o}C. However, when these high molecular weight particles are mixed with other particles from other radial positions in the reactor cross-section, they only have a small effect on the overall average molecular weight because the total mass of the high molecular weight polymers near the reactor walls is relatively small.

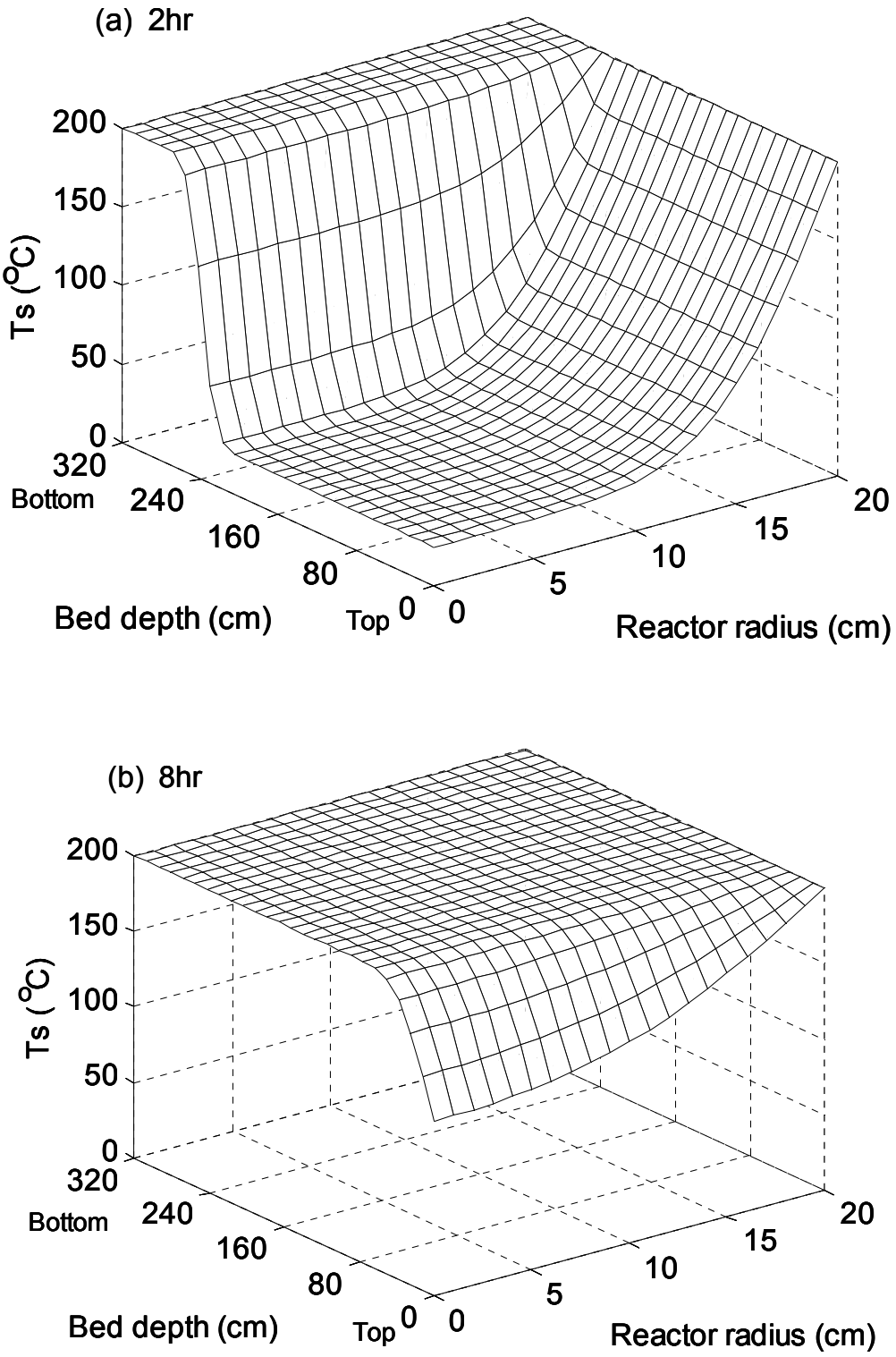

Figure 4.3 Reactor temperature profiles in axial and radial directions during the startup process: (a) 2 hr; (b) 8 hr.

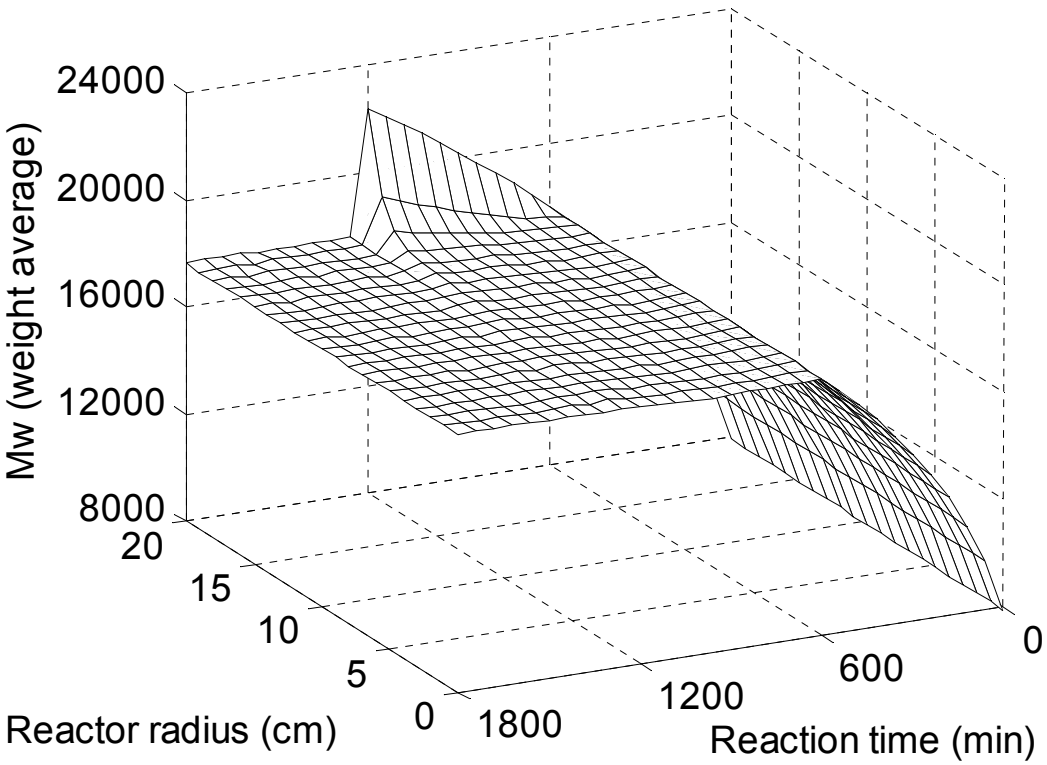

Figure 4.4 Polymer molecular weight profiles at the reactor exit during the reactor startup followed by a continuous operation.

Although each polymer particle in the reactor has no intraparticle temperature gradient, the diffusion resistance for phenol produced by the polymerization is not negligible. The polymer chain length distribution at the centerline of reactor outlet is shown in Figure 4.5. Although it is not shown, the polymer chain length distribution inside of a particle does not change significantly with reaction time. But the molecular weight does increase gradually with time. It is mainly because the portion near the particle surface increases molecular weight. Figures 4.6a and Figure 4.6b illustrate the degree of crystallinity during the startup transient period. Notice that the degree of crystallinity near the bottom and the wall of the reactor reach about 38%.

4.3.2 Effect of Flow Rate Ratio

The ratio of gas and solid phase mass flow rates ($\gamma = \dot{m}_g / \dot{m}_s$) is a very important process parameter that affects the economics of a SSP process. The purge gas has dual functions, i.e., removal of phenol and heating of the solid particles. A major factor in determining the particle phase flow rate is the desired product molecular weight at the bottom of the reactor for a given reactor temperature profile. The purge gas flow rate and temperature are determined to meet these requirements. For process economics, a low purge gas flow rate is desirable but then insufficient thermal energy may be delivered to the solid phase in the reactor. There is also a limit in the maximum feed gas temperature because any partial fusion or melting of the polymer particles must be avoided. If high gas flow rate is used, the packed bed reactor can be heated up more effectively. However, there is an upper limit of the gas velocity to avoid particle fluidization or entrainment. Therefore, it is useful to

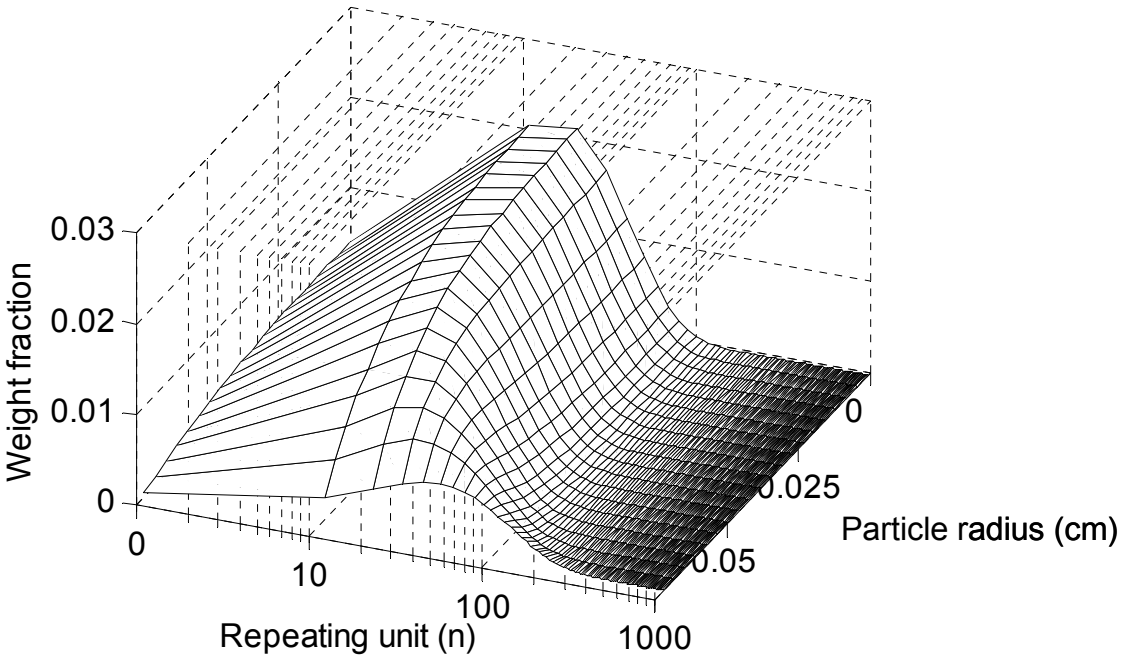

Figure 4.5 Polymer chain length distribution in a particle in the reactor centerline at the outlet (particle diameter = 0.15 cm).

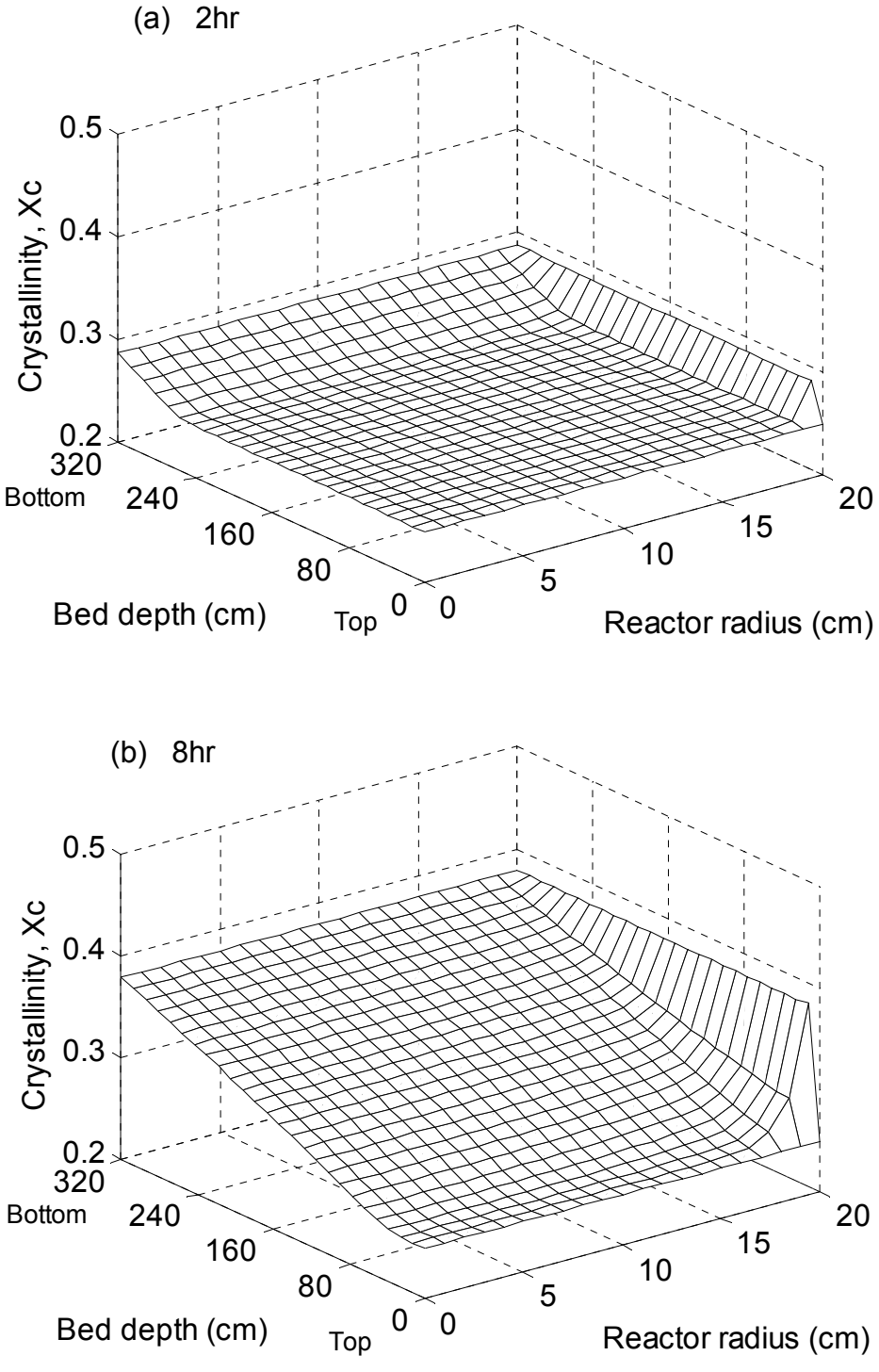

Figure 4.6 Variations in polymer crystallinity during the startup operation: (a) 2 hr; (b) 8hr.

evaluate the effect of gas flow rate through reactor simulations. Table 4.4 illustrates the examples of operating conditions for the SSP of nylon, PET, and polycarbonate. Notice that a broad range of flow rate ratio (e.g., 0.05-8.1) is employed in these processes, although direct comparison of each process may not be possible.

To investigate the effect of flow rate ratio, we keep the particle flow rate (or particle residence time) constant at 450 g/min or γ ($\dot{m}_g / \dot{m}_s$) = 2.2 and vary the purge gas flow rate. Figure 4.7 shows the effect of flow rate ratio on the steady state reactor temperature along the center line of the reactor. It is seen that for the mass flow rate ratio smaller than 2.2, a strong temperature nonuniformity develops in the reactor. When the mass flow rate ratio is 1.5, top 35% of the reactor is below the polymer's glass transition temperature, meaning that no SSP will occur in that region. Figure 4.8 illustrates the molecular weight profiles in the reactor for γ = 1.5. We can observe that near the center and the top regions of the reactor, the polymer molecular weight does not increase much because the temperature in that region is far below the polymer's glass transition temperature. Table 4.6 shows the molecular weight averages and polydispersity values at the exit of the reactor for three different γ values. It is observed that the polydispersity of the polymer deviates from the theoretical value of 2.0 for the homogeneous linear condensation polymerization because of temperature nonuniformity and intraparticle distribution of polymer chain length. Figures 4.7 and 4.8 clearly indicate that the flow rate ratio, or purge gas flow rate for a fixed solid flow rate, is certainly one of the key parameters that affect the performance of SSP.

A dynamic reactor simulation has also been carried out to see how the reactor

Table 4.6 The effect of flow ratio on the average properties at the reactor exit

	prepolymer	γ		
		1.0	1.5	2.2
$\bar{M}_{n,o}$	4000	4824	5801	6891
$\bar{M}_{w,o}$	7873	10685	13967	17418
PD	1.97	2.21	2.41	2.53

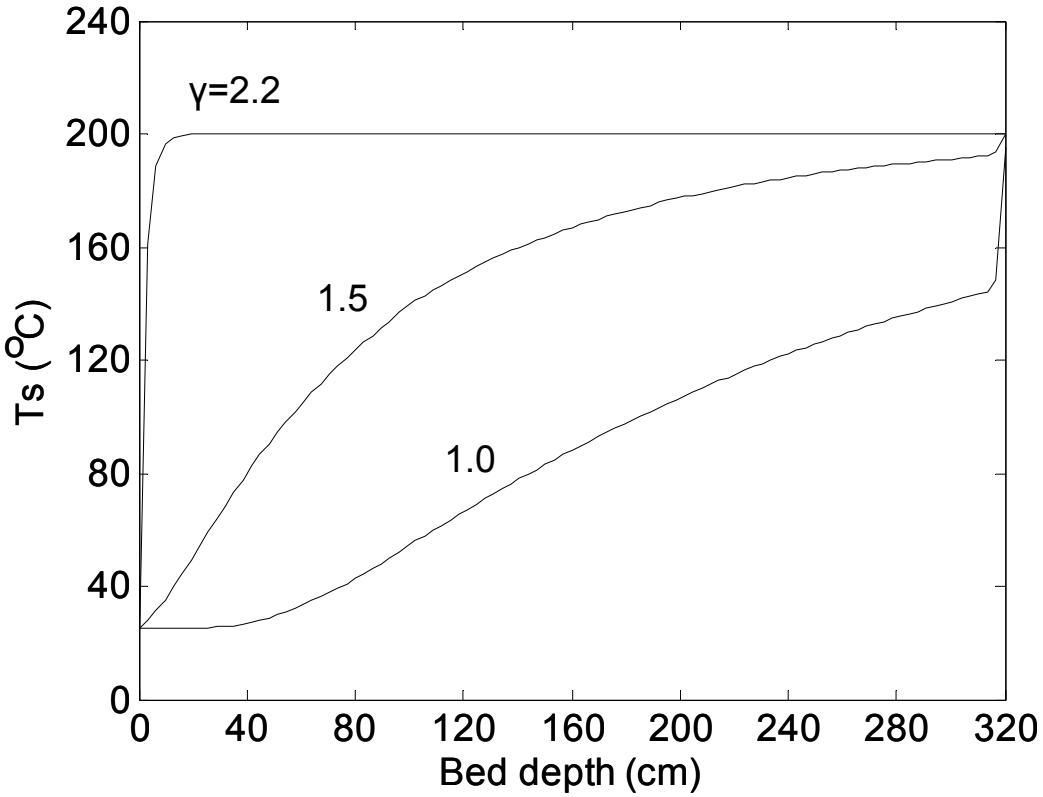

Figure 4.7 Effect of flow rate ratio on reactor temperature profiles at reactor center line (steady state).

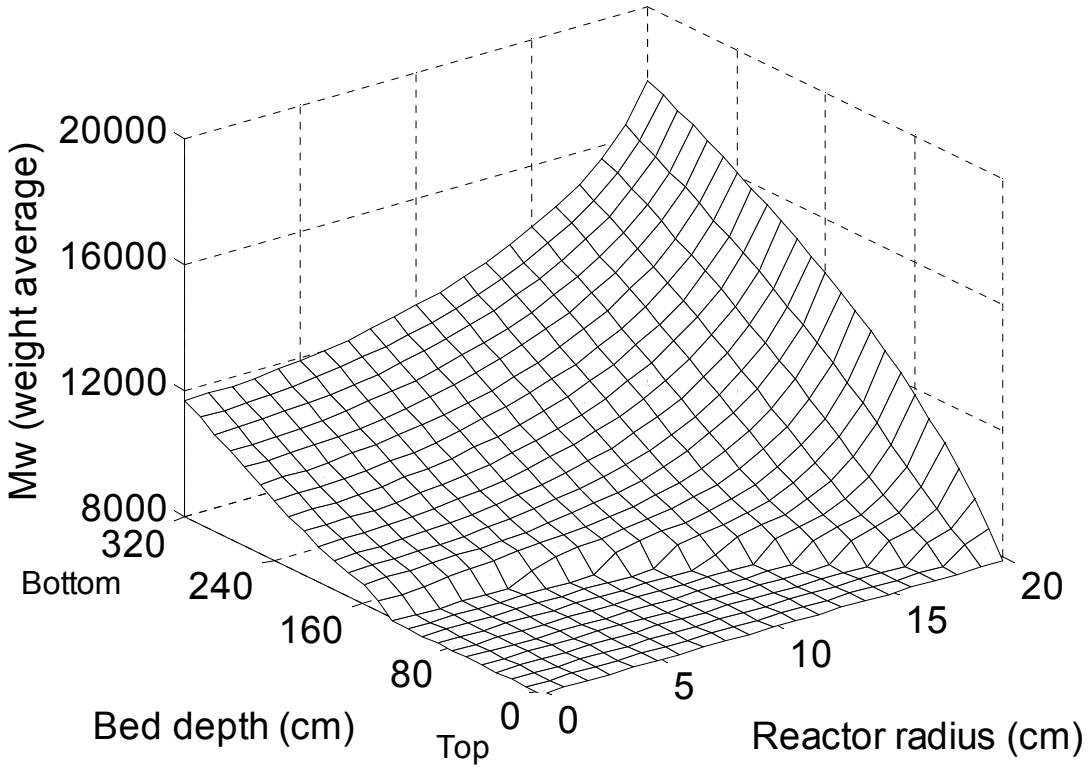

Figure 4.8 Steady state polymer molecular weight profiles at low gas/solid mass flow rate ratio ($\gamma = \dot{m}_g / \dot{m}_s$ =1.5).

temperature profiles change when the purge gas flow rate is decreased by 32% from the standard gas flow rate. Figure 4.9 shows the reactor temperature simulation results. Initially, the reactor is at steady state temperature of 200^{o}C with a continuous flow of solid polymer particles. At t = 0, a step change is made in the purge gas flow rate. Here, a rather large step change is made intentionally to more clearly illustrate the gas flow rate effect. Notice that the reactor temperature reaches a new steady state profiles more than 15 hr after the step change has been made. Also, the upper portion of the reactor is well below the desired SSP temperature. Although the simulation conditions used in Figure 4.9 may not be quite realistic (i.e. 32% decrease in gas flow rate), Figure 4.9 illustrates that with a continuous flow of cold solid particles to the reactor, it takes longer time for the reactor to reach a new steady state than for the initial batch startup process (cf. Figure 4.2).

4.3.3 Effect of Reactor Size

From the model simulation results presented in the previous section, we expect that the reactor size or dimension can also be an important design parameter because heat transfer efficiency is dependent on the reactor dimension. From a practical point of view, sizing the reactor is indeed one of the most important design issues because it will determine the process efficiency and economics. However, the effect of reactor size has not been considered in the previous model simulation work. To illustrate the reactor size effect on the reactor performance, we carry out the model simulations as follows. We keep the solid bed height (H) and the solid phase residence time constant (10 hr) while the reactor diameter and the mass flow rate ratio

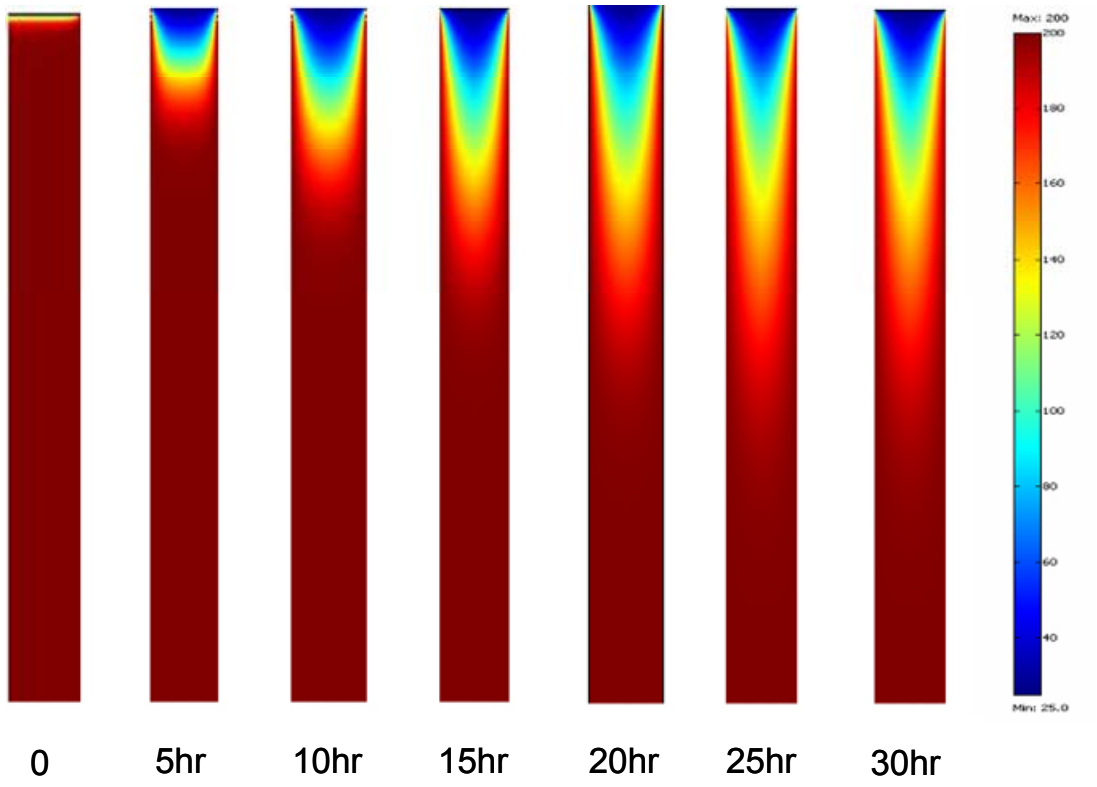

Figure 4.9 Reactor temperature profiles when the purge gas flow rate is reduced from the steady state value by 32% ($\gamma = 2.2 \rightarrow 1.5$).

(γ) are varied. Figure 4.10 shows the steady state temperature profiles along the center line of the reactor. It is seen that for a large value of gas flow rate ($\gamma = 2.2$, standard case), the reactor size effect is negligibly small for steady state operations. However, for a smaller value of gas flow rate ($\gamma = 1.8$), large reactor diameter yields less uniform reactor temperature profiles. Figure 4.11 shows that such temperature nonuniformity results in a marked effect on the polymer molecular weight. Notice that wall temperature is kept constant at 200ºC in both cases. For a small flow rate ratio, the heat transfer between reactor walls and polymer particles results in nonuniformities in radial temperature and molecular weight even at steady states. Figure 4.12 shows the effect of reactor size on the transient temperature profiles when a step change is made in the flow rate ratio from $\gamma = 2.2$ to $\gamma = 1.8$. It is seen that it takes less time for the slim reactor (H/D=10) to reach a new steady state temperature profile. However, a slimmer reactor of small volume may not be economical. One possible design to take advantage of the slim SSP reactor is to use a bundle of slim reactors in parallel housed in a large diameter reactor vessel with a heating fluid running through the reactor bundles.

4.3.4 Effect of Particle Size Distribution

The prepolymer particle size is one of important parameters that affect the efficiency of SSP. If the polymer particles are too small, a purge gas flow may fluidize the particles or cause the entrainment from the reactor. Then, a low gas flow rate needs to be used but the heat transfer efficiency will be poor. On the other hand, if the polymer particles are too large, the diffusion of phenol inside the particle will

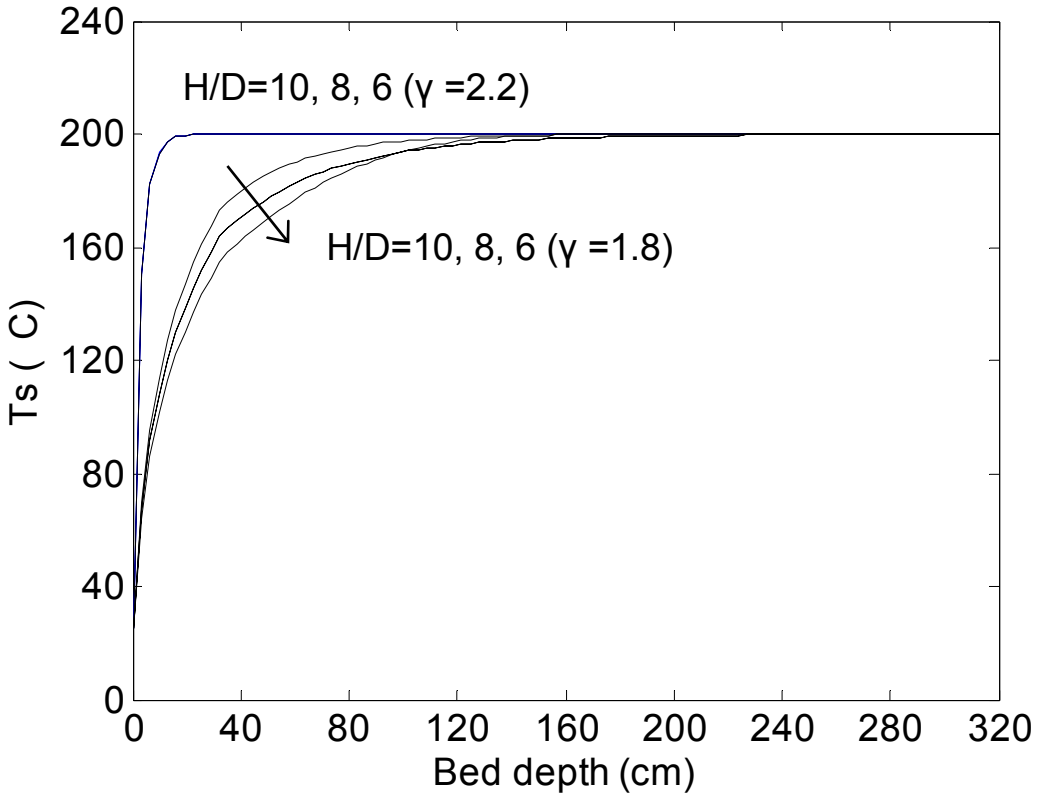

Figure 4.10 Steady state reactor temperature profiles for different reactor diameters and purge gas flow rates in the reactor centerline.

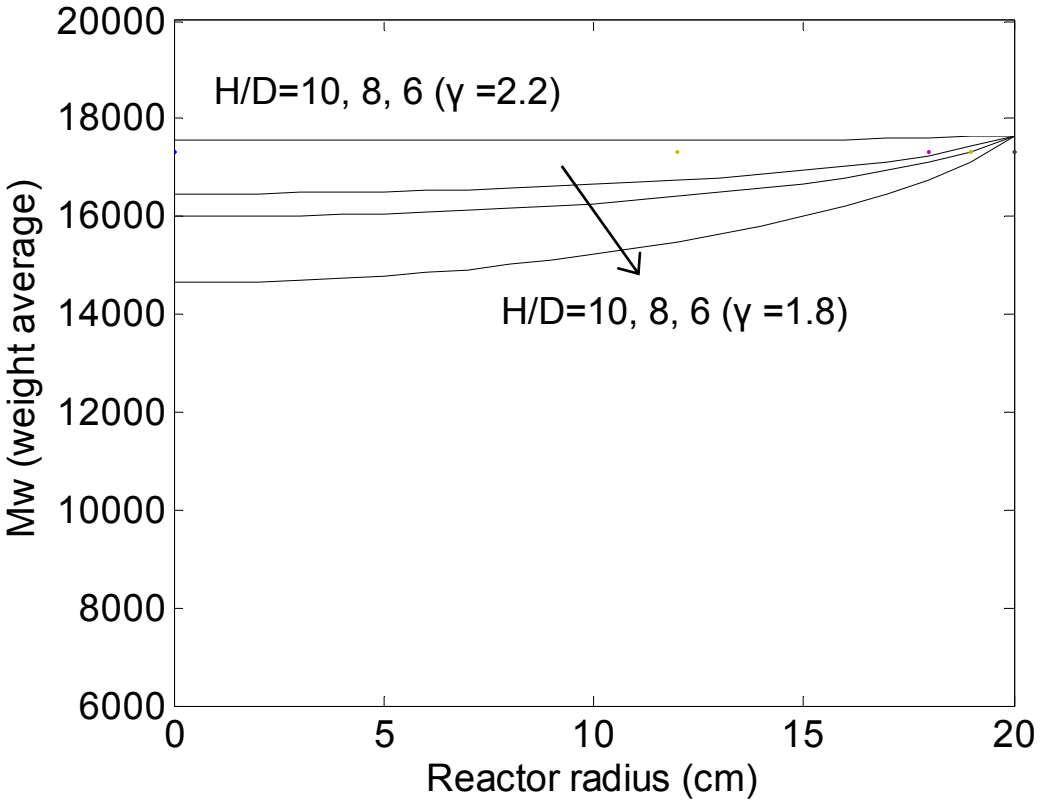

Figure 4.11 Steady state weight-average molecular weight profiles for different reactor diameters and purge gas flow rates at the reactor exit.

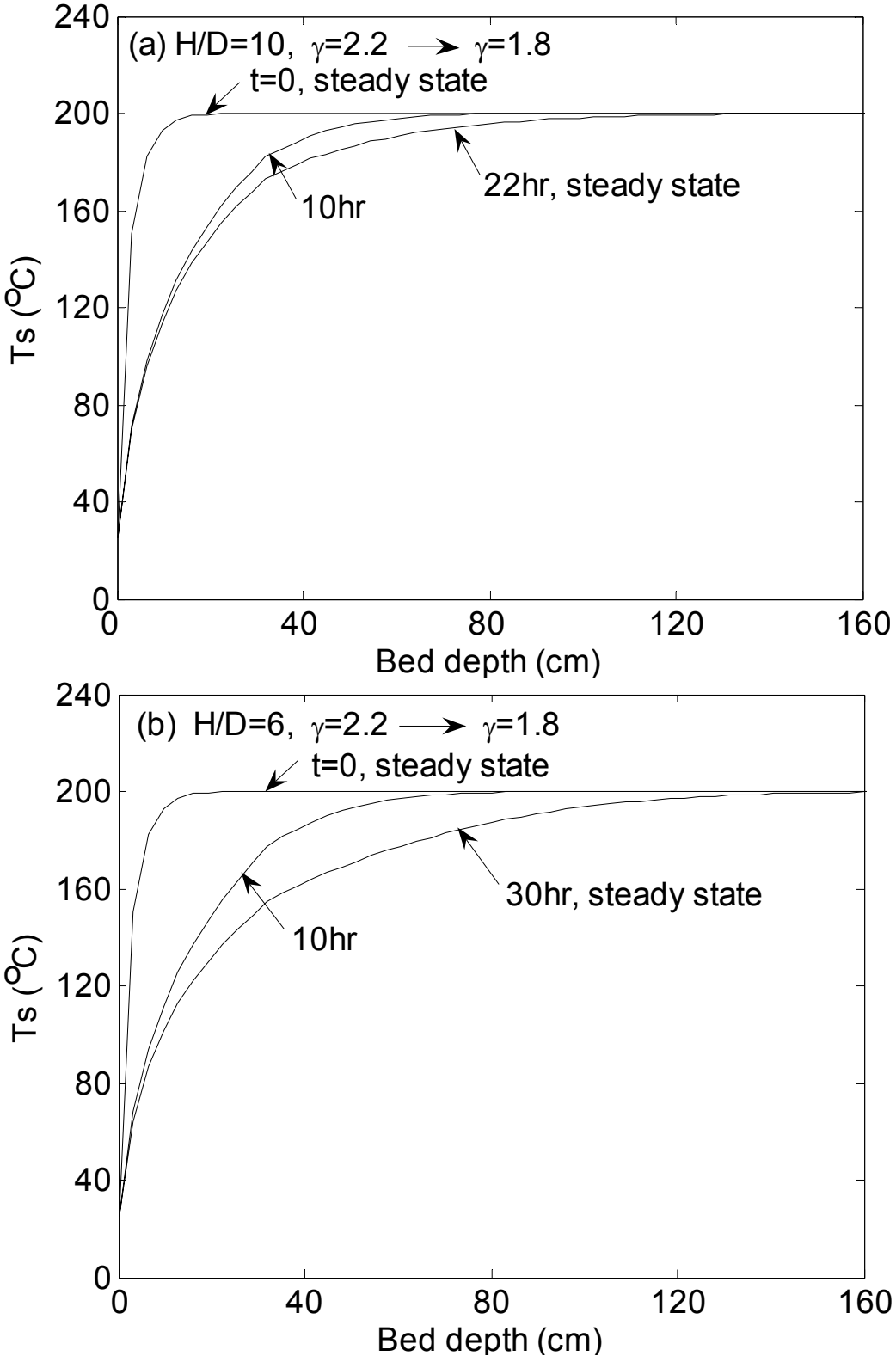

Figure 4.12 Effect of reactor H/D ratio on the reactor temperature transients: (a) H/D = 10; (b) H/D = 6.

be very slow and high molecular weight will be difficult to obtain in short reaction time. As discussed earlier, for typical prepolymer particle sizes (1-3mm) employed in a moving packed bed reactor for SSP, intraparticle temperature gradient is generally negligible but the polymerization rate is strongly affected by the reaction temperature. Hence, both the intraparticle concentration gradient and the axial temperature gradient in the reactor should be taken into consideration in calculating the polymer molecular weight of the product particles at the reactor outlet.

In our previous model simulations, we assumed that the reactor is charged with polymer particles of same size. In practice, the prepolymer particles are expected to have a certain size distribution when they are produced by a crystallization process using, for example, a spray dryer crystallizer.[130-133] Typical particle size of crystallized polycarbonates from a spray dryer is about 80-3000 μm.[130] In this section, we investigate the effect of polymer particle size distribution on the molecular weight in the SSP reactor.

To simulate the particle size effect, the following log-normal distribution function is used to represent the prepolymer particle size distribution[133]:

$$f(d) = \frac{1}{d\sigma\sqrt{2\pi}} \exp\left[-\frac{1}{2}\left(\frac{\ln\left(d/\overline{d}\right)}{\sigma} \right)^2 \right] \tag{4.18}$$

where d is the particle diameter, $\overline{d}$ is the mean particle diameter, and σ is the geometric standard deviation. Figure 4.13 shows the particle size distribution curves used in our simulation study. With the standard operating conditions applied to this case, we calculated the average polymer molecular weight at the reactor outlet and the results are shown in Figure 4.14a and Figure 4.14b. It is seen that particle size greatly

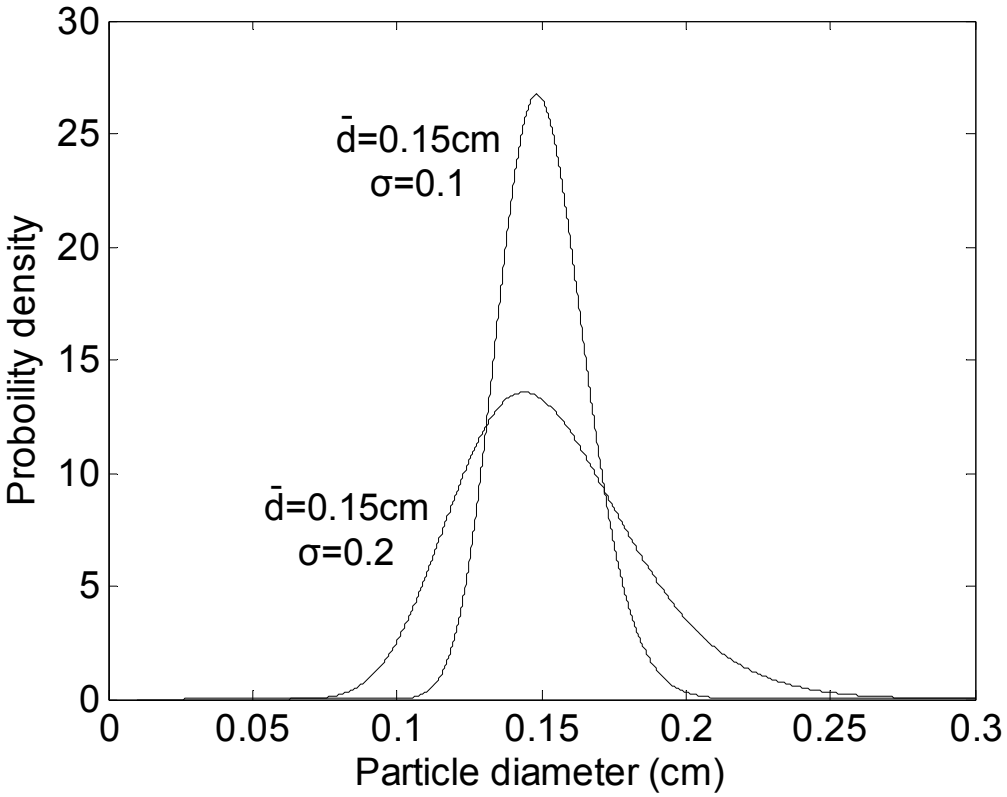

Figure 4.13 Lognormal particle size distributions.

affects the chain length distributions. For a large size particle (d = 0.3 cm), chain length distribution in the interior particle is almost the same as that of prepolymer because the reaction occurred only near the particle surface. For a small particle (d = 0.08 cm), there is less diffusion resistance for phenol and higher molecular weight is obtained than in a large particle. Interestingly, the overall effect of particle size distributions on the average chain length distribution is very small as shown in Figure 4.15. The particle size distribution used in this particular simulation example has a relatively small fraction of large particles and hence, their effect on the overall polymer molecular weight is quite small.

4.4 Conclusions

In this chapter, we have developed a dynamic model of a moving packed bed reactor for the SSP of bisphenol A polycarbonate. The model consists of macroscopic energy balance equations for the reactor and an isothermal polymer particle model. Assuming negligible reaction heat effect and phenol concentration in the high flow rate purge gas stream, we solved the reactor model and the polymer particle model separately to calculate the reactor temperature profiles and polymer properties. We use the reactor model to analyze the effect of various reactor operating conditions on the reactor performance. Through model simulations, it has been illustrated that radial temperature nonuniformity may develop in the reactor as the reactor temperature is raised by the purge gas during the reactor startup operation. The temperature nonuniformity leads to a nonuniform development of polymer molecular weight. The dynamic reactor model has also been used to analyze the effects of purge gas flow

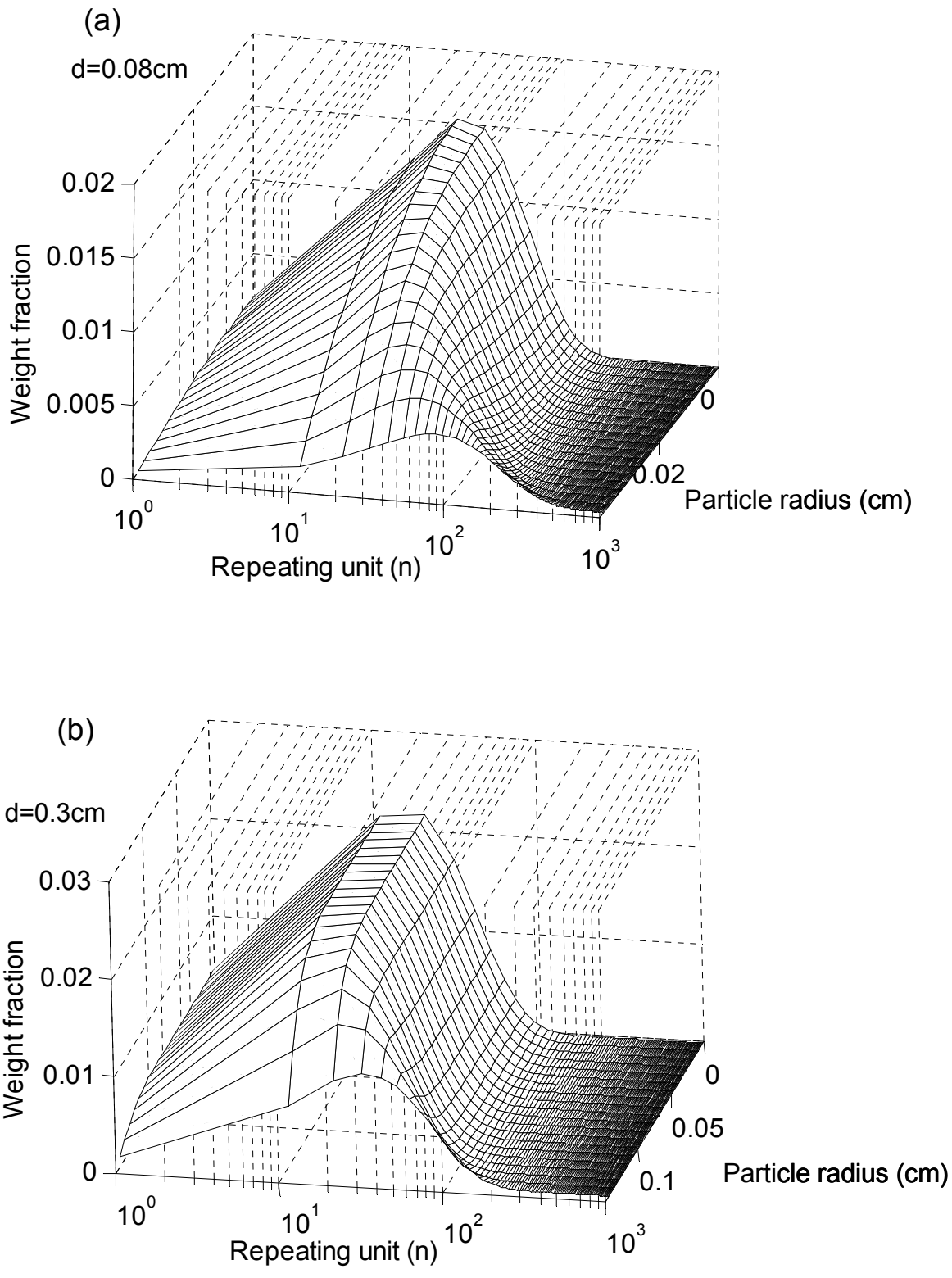

Figure 4.14 Polymer chain length distribution in the centerline at the reactor exit: (a) $d = 0.08$ cm; (b) $d = 0.3$ cm.

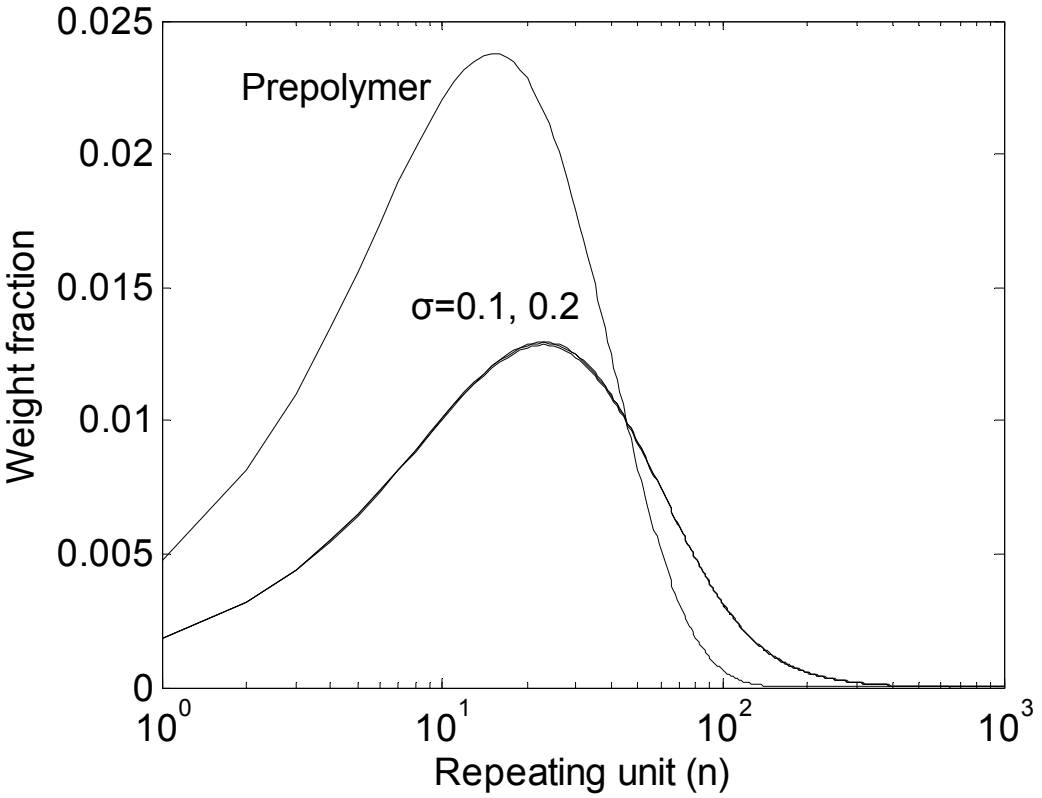

Figure 4.15 Effect of particle size distributions on the chain length distribution.

rate, reactor size, and polymer particle size distribution. The simulation results show that purge gas flow rate is a very important process parameter because when the gas flow rate is sufficiently high, temperature uniformity can be readily established even in a large diameter reactor.

4.5 Notation

C_p = heat capacity, $J \cdot g^{-1} \cdot K^{-1}$

d = particle diameter, cm

$\bar{d}$ = mean particle diameter, cm

D = reactor diameter, cm

D_p =diffusivity of phenol, $cm^2 \cdot s^{-1}$

$[E_A]$ = concentration of phenyl carbonate group, $mol \cdot L^{-1}$

$[E_A]_0$ = initial concentration of phenyl carbonate group, $mol \cdot L^{-1}$

$[E_B]$ = concentration of hydroxyl group, $mol \cdot L^{-1}$

$[E_B]_0$ = initial concentration of hydroxyl group, $mol \cdot L^{-1}$

$G = \rho u$, superficial mass velocity, $g \cdot cm^{-2} \cdot min^{-1}$

h = heat transfer coefficient, $J \cdot cm^{-2} \cdot K^{-1} \cdot min^{-1}$

H = bed height, cm

K = equilibrium constant

k = thermal conductivity of polymer, $J \cdot cm^{-1} \cdot K^{-1} \cdot min^{-1}$

k_1 = forward reaction rate, $L \cdot mol^{-1} \cdot min^{-1}$

k_c = crystallization rate, min^{-1}

L = reactor length, cm

$\dot{m}$ = mass flow rate, $g \cdot min^{-1}$

M_n = number-average molecular weight at the radial position r in a particle

$\bar{M}_n$ = number-average molecular weight for a single particle

$\bar{M}_{n,o}$ = number-average molecular weight in the reactor cross section

M_w = weight-average molecular weight at the radial position r in a particle

$\bar{M}_w$ = weight-average molecular weight for a single particle

$\bar{M}_{w,o}$ = number-average molecular weight in the reactor cross section

n = number of repeating unit

Nu = Nusselt number

p = conversion of phenyl carbonate group

P = pressure in the reactor, atm

$[P]$ = concentration of phenol, mol·L^{-1}

$[P]_0$ = initial concentration of phenol, mol·L^{-1}

r = distance from particle center, cm

r' = distance from reactor center radius, cm

r_a = mole ratio of end group at the beginning of melt prepolymerization

r_a' = mole ratio of end group in the prepolymer, $[E_A]_0/[E_B]_0$

r_p = reaction rate, mol·L^{-1}·min^{-1}

Pr = Prandtl number

R = particle radius, cm

R' = reactor radius, cm

Re = Reynolds number

S = cross sectional area of the reactor, cm^2

t = reaction time, min

T = temperature, K

T_g = glass transition temperature, K

T_m = polymer melting point, K

u = velocity, cm·min^{-1}

w_m = molecular weight of repeating unit, g·mol^{-1}

W_n = weight fraction of n-mer

x_c = degree of crystallinity

$x_{c,\max}$ = the maximum degree of crystallinity

z = axial distance from the top of reactor, cm

$[Z]$ = concentration of polymer linkage, mol·L^{-1}

$[Z]_0$ = initial concentration of polymer linage, mol·L^{-1}

Greek letters

ε = void fraction of moving packed bed

ϕ = sphericity of a particle

η = viscosity, g·cm^{-1}·min^{-1}

ρ = density, g·cm^{-3}

σ = geometric standard deviation

Subscripts

0 = initial condition

a = amorphous

c = crystalline

g = gas

in = inlet

mf = minimum fluidization

o = overall properties across reaction cross section

s = solid

w = reactor wall

Chapter 5

Modeling of Chain Sequence Length for the Melt Copolycondensation Process in a Semibatch Reactor

5.1 Introduction

In a step-growth polymerization process, a small amount of third monomer or component is often added into a linear homopolymer to modify the polymer properties by changing the copolymer composition and chain sequence length distributions. Bisphenol A polycarbonate (BAPC), one of the most important engineering plastics, has been widely used for data storage media (CD, DVD), structural materials for electrical and electronic parts, automobiles, etc. To meet a verity of applications and further improve or modify its properties, a large number of BAPC based terpolymers have been successfully prepared by introducing a third monomer or oligomer via multicomponent copolycondensation. For example, 3,3′,5,5′-tetramethylbisphenol A[134] and 1,1′-bis(4-hydroxyphenyl)-3,3,5-trimethylcyclohexane[39] have been used to improve the heat resistance; aliphatic diols such as 2,2-dimethylpropanediol[135] and aliphatic dicarboxylic diacids such as dodecanedioic acid[36] have been incorporated to get high melt flow and improve processibility; α,ω-dichloropoly(dimethylsiloxane)[32] and 4,4′-dihydroxydiphenyl[38] have been utilized to improve the mechanical strength. As a third component is incorporated into polymer chains, not only chain composition but also chain sequence length of each monomer comes to play an important role in product properties. Chain

sequence length distribution, which differs from molecular weight distribution, provides a deeper insight of chain microstructures. It is generally accepted that chain sequence length distributions affect the physical properties of a copolymer. A good example is polyurethane copolymers that obtained from the copolycondensation of diisocyanate with a short diol (short segment) and a long diol (soft segment).[88] The sequence length distributions of short diol and long diols have a strong impact on the thermal and mechanical properties.[136,137] Therefore, it is useful to develop quantitative formulas to calculate polymer chain sequence length averages and distributions that could provide additional information on the polymer chain microstructures towards understanding polymer properties.

For a free radical polymerization process, the analysis of copolymer composition is well known based on the standard reactivity ratio method.[138] Kinetic methods such as the digital encoding method[139] and a general kinetic model framework[88] have been developed to further calculate chain microstructures: sequence length distributions. However, these methods are not directly applicable to a step-growth copolymerization process. Unlike a free radical polymerization, no polymer chain is dead or inactive in condensation polymerization as long as both reactive end groups are present in the reaction mixture.[94] For modeling of sequence length averages and distributions in step-growth polymerizations, statistical methods are often involved including probabilistic approach[92,140,141], Monte Carlo method[142-145] and linkage moment approach[94]. Peebles[140,141] has shown that under certain conditions, sequence length should follow the most probable distribution and developed a set of differential equations for the calculation of number-average

sequence length. The analysis, however, is limited only in the case of equal reactivity, 100% conversion and exact stoichiometric balance between the sums of two end groups. With a probabilistic approach, an in-out recursive model developed by Lopez-Serrano[92] gives simple expressions to directly obtain number- and weight-average sequence lengths with no assumptions of equal reactivitiy and stoichiometry required. The merit of this method is that with statistical argument the equations to calculate sequence length averages are extremely simple and straightforward. However, detailed sequence length distributions cannot be obtained. Speckhard and Miller[142,143] improved Peebles' work and developed a Monte Carlo model to calculate monomer compositions and sequence length distributions. Generally, for a Monte Carlo model, in order to obtain accurate simulation results, a large number of random numbers have to be generated, which is very expensive in computational cost. Based upon the first order Markov statistical chains, Beers[94] developed a general model framework to calculate monomer sequence length distributions for polymer melt blending and compared with experimental results in the literature. However, the calculation was mainly focused on the chain length distributions, sequence length averages and the simulation of sequence length distributions is not straightforward.

In a melt copolycondensation process, it is well known that transesterification and ester interchange reactions usually results in random copolymers. At high reaction temperatures large increase in entropy is believed to be the main driving force towards random polymer chains.[146] The sequence distributions of many condensation copolycarbonates via melt polymerization follow random distribution statistics as reported in the literature.[147,148] The model framework we have developed,

based on a probabilistic argument, presents a new simple approach in calculating both sequence length distributions and averages for random condensation terpolymers in melt copolycondensation processes. The copolycondensation occurs in three monomers: AR_1A, BR_2B, and BR_3B, in which both A and B end groups are reactive functional groups. The chain sequence length model we developed does not require the assumptions of equal reactivity and stoichiometric balance. The number- and weight-average sequence length distributions and sequence length averages can be calculated if the conversions of monomers and the initial monomer mole ratio of BR_3B to BR_2B are known. The model simulation results gave an excellent agreement with chain length averages calculated by the recursive method[92] and Flory's chain length distributions can be recovered when the conversion of third monomer is very small. The simulation of chain sequence length distributions and averages in the course of reaction is demonstrated through a melt copolycondensation in a semibatch reactor. To accurately account for the effect of diphenyl carbonate (DPC) loss, vapor-liquid equilibrium equations for a binary system of phenol and DPC are used in conjunction with the melt polymerization process. The effects of end group ratio, monomer ratio and reactivity have been studied. The model we developed not only can be used to describe the melt polymerization of copolycarbonates, but also can be applied for other random condensation terpolymers.

5.2 Model Development

5.2.1 Sequence Length Distribution

For a linear random copolymer derived from the system of AR_1A, BR_2B, and BR_3B monomers where only end group A reacts with end group B, the species of polymer chains can be defined as six types shown in Table 5.1 according the difference of end groups. In general, a linear polymer chain in this system can be expressed as $-R_1(R_2/R_3)R_1(R_2/R_3)R_1(R_2/R_3)-$. For the sequence length, we follow the definition given by Lopez-Serrano[92]: the sequence length of R_2 or R_3 is defined as the number of times of R_2 or R_3 repeated in a run. For example, for a polymer chain $-(R_2R_1R_2R_1R_2R_1)-$, the sequence length of R_2 is 3 and that of R_3 is 2 for a chain $-(R_3R_1R_3R_1)-$. It is obvious that in a polymer backbone a R_2 or R_3 unit is always next to a R_1 unit if any. Therefore, other than end groups a R_1 unit may be considered together with a R_2 unit or with a R_3 unit. If we assign "R_2" as a numeric number "0" and "R_3" as "1", the backbone of a polymer chain can be simplified as a combination of "0" and "1". In other words, if we know the type of a chain that defines the end groups in a chain and end units next to them, a certain combination of "0" and "1" stands for a unique chain. For instance, if we know a polymer chain is from the 3rd type shown in Table 5.1 (i.e. AR_1 and R_3B are present at the chain ends), a binary number of "0000011" corresponds to the unique chain:
$AR_1R_2R_1R_2R_1R_2R_1R_2R_1R_2R_1R_3R_1R_3B$, which has 1 count of sequence length of 5 for "R_2" and 1 count of sequence length of 2 for "R_3". If we switch the order of "0" and "1", the binary number "0000011" can vary into, for example, "0110011", which has 1 count of sequence length of 1 for "R_2", and 1 count of sequence length of 2 for "R_2"

Table 5.1 Chain types and number distributions

no.	molecular structure	number distribution
1	AR_1-----R_2-----R_1-----R_3-----R_1A i units n units n-1-i units	$\dfrac{C_i^{n-1}(1-p_1)^2 p_1^{n-1}\left(\dfrac{p_2^2}{p_2+\nu p_3}\right)^i\left(\dfrac{\nu p_3^2}{p_2+\nu p_3}\right)^{n-1-i}}{1-2p_1+p_1\dfrac{1+\nu}{p_2+\nu p_3}}$
2	AR_1-----R_2-----R_1-----R_3-----R_2B i+1 units n units n-1-i units	$\dfrac{2C_i^{n-1}(1-p_1)p_1^{n}\left(\dfrac{p_2^2}{p_2+\nu p_3}\right)^i\left(\dfrac{\nu p_3^2}{p_2+\nu p_3}\right)^{n-1-i}\dfrac{p_2(1-p_2)}{p_2+\nu p_3}}{1-2p_1+p_1\dfrac{1+\nu}{p_2+\nu p_3}}$
3	AR_1-----R_2-----R_1-----R_3-----R_3B i units n units n-i units	$\dfrac{2C_i^{n-1}(1-p_1)p_1^{n}\left(\dfrac{p_2^2}{p_2+\nu p_3}\right)^i\left(\dfrac{\nu p_3^2}{p_2+\nu p_3}\right)^{n-1-i}\dfrac{\nu p_3(1-p_3)}{p_2+\nu p_3}}{1-2p_1+p_1\dfrac{1+\nu}{p_2+\nu p_3}}$
4	BR_2-----R_2-----R_1-----R_3-----R_2B i+2 units n units n-1-i units	$\dfrac{C_i^{n-1}p_1^{n+1}\left(\dfrac{p_2^2}{p_2+\nu p_3}\right)^i\left(\dfrac{\nu p_3^2}{p_2+\nu p_3}\right)^{n-1-i}\dfrac{p_2^2(1-p_2)^2}{(p_2+\nu p_3)^2}}{1-2p_1+p_1\dfrac{1+\nu}{p_2+\nu p_3}}$
5	BR_3-----R_2-----R_1-----R_3-----R_3B i units n units n-i+1 units	$\dfrac{C_i^{n-1}p_1^{n+1}\left(\dfrac{p_2^2}{p_2+\nu p_3}\right)^i\left(\dfrac{\nu p_3^2}{p_2+\nu p_3}\right)^{n-1-i}\dfrac{(\nu p_3)^2(1-p_3)^2}{(p_2+\nu p_3)^2}}{1-2p_1+p_1\dfrac{1+\nu}{p_2+\nu p_3}}$
6	BR_2-----R_2-----R_1-----R_3-----R_3B i+1 units n units n-i units	$\dfrac{2C_i^{n-1}p_1^{n+1}\left(\dfrac{p_2^2}{p_2+\nu p_3}\right)^i\left(\dfrac{\nu p_3^2}{p_2+\nu p_3}\right)^{n-1-i}\dfrac{p_2(1-p_2)\nu p_3(1-p_3)}{(p_2+\nu p_3)^2}}{1-2p_1+p_1\dfrac{1+\nu}{p_2+\nu p_3}}$

Note: This work was done by Case.[91] $p1$, $p2$, and $p3$ stand for conversions with respect to each monomer, AR_1A, and BR_2B and BR_3B; ν means the initial mole ratio of the monomer BR_3B to the monomer BR_2B, and $C_i^{n-1}=\dfrac{(n-1)!}{i!(n-1-i)!}$ ($n\geq 2$ for type 1, and $n\geq 1$ for others; $0\leq i\leq n-1$). n means the total number of R_1 units, etc.

and 2 counts of sequence length of 2 for "R_3". If we vary the order of "0" and "1" to get all the possible combinations of the binary number "0000011" (i.e. "0000011", "0000101", "0001001", ···), the total counts for each sequence length can be obtained. If polymer chains follow the most probable distribution, the possibility for every single polymer chain should be same. Thus, the counts for a sequence length can be computed by adding all the contributions from all the possible combinations of binary numbers. Certainly, counting sequence length for each binary number may be obtained by using a computer program. But searching counts of sequence length for polymer chains one by one is very costly in computation. Therefore, generalized formulas would be more preferred.

The derivation begins with knowing the exact composition for a chain, i.e. the order of "0" and "1" inside of a chain is not considered. As mentioned before, a chain type, the total number of "0" (R_2) and "1" (R_3) units and the number of "0" (R_2) units are all the variables that need to be considered. Let m (m = 1-6) to stand for the chain type (see Table 5.1), k to stand for the total number of units of "0" and "1", and i to stand for the total number of number of units of "0". To visualize the simulation process, first chose an array (m, k, i), and then determine the probability of the array (m, k, i). This part of work has been done by Case[91] and is summarized in Table 5.1. The next step is to consider all the possible variations to get different sequence runs for the array (m, k, i) by switching the order of "0" and "1". Note that only units inside of a chain can be switched order since the end groups and end units are defined by the chain type m. Then we count the total number of each sequence and obtain a sequence distribution for the given n and i. Since the probability of the array (m, k, i),

$P(m, k, i)$, is known from Table 5.1, the contribution of the array (m, k, i) to a chain sequence length, j can be computed if we know generalized formulas to count chain sequence length. To count all the contributions from all the possible combinations for change sequence length, j, we need to vary i, k, m sequentially and sum up all of them.

Note that the total number of R_1, R_2, and R_3 units may be an odd number such as chain types 1, 4, 5, and 6. However, according to the definition of sequence length, each sequence length has an even number of combination of R_1, R_2, and R_3 units. Therefore, there is an extra unit at the end of chain shown in Table 5.2, which is dropped off and not counted in a sequence length. The number of counts for the sequence length, for example, of R_2, could vary from 0 to n-1 for the chain types of 1, 3, 5 and from 1 to n for the chain types of 2, 4, 6. From Table 5.1, we can see that a polymer chain could be ended up with either a R_1A, or a R_2B or a R_3B unit. As mentioned before, a chain end unit may be an extra unit that is not counted into the total sequence length, or it has to be counted. Therefore, we need to discuss them according to the different chain types. If a chain end unit is not counted, the binary digit next to it could be chosen either "0" or "1". Namely, this is a free end. If a R_1A unit is an end unit that has to be counted into the total sequence length, this end is also a free end because either a R_1 or R_2 unit can be linked next to it. However, if a R_2 or a R_3 unit is at a chain end, this is a fixed end because the binary digit is dependent of this end unit. For the fixed end, if a R_3B is at the end, the corresponding binary digit is "1", which has no contribution to the sequence length of "0". However, if a R_2B unit is at the end, it is a fixed end, and the distribution pattern of sequence length of "0" should differ from that of chains with free ends.

Table 5.2 Possible sequence length of R_2 units

no.	molecular structure	total number of units	range of R_2 sequence length
1	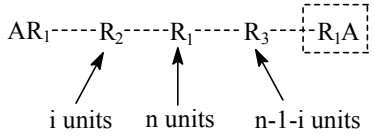	2n-1	$0 \sim n-1$
2	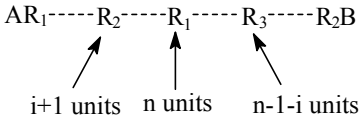	2n	$1 \sim n$
3	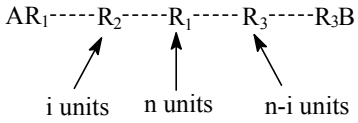	2n	$0 \sim n-1$
4	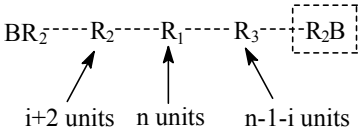	2n+1	$1 \sim n$
5	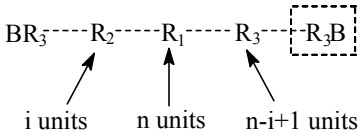	2n+1	$0 \sim n-1$
6	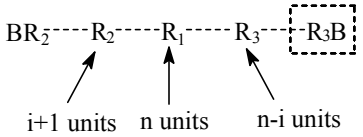	2n+1	$1 \sim n$

Note: The unit in the dotted frame is extra, which is not counted in a sequence length.

To implement this procedure, it is important to find out the distribution patterns for the number of counts of sequence length regarding different chain types. Notice that R_2 and R_3 units are interchangeable in this system. In the following, we only consider the sequence length of R_2 units (the sequence length of "0") and the sequence length of R_3 units (the sequence length of "1") can be found by simply swapping R_2 and R_3 position in formulas.

As mentioned before, an end unit is either a free or fixed end. Taken off extra end units shown in Table 5.2, all six chain types can be fitted into two categories: 1) free ends at both chain ends, and 2) one is free and the other is fixed. To derive the formulas for the distribution pattern of sequence length of R_2, we start with a simple case: both chain ends are free. First, assume the total number of "0" and "1" is *k*, and the number of "0" is 1. Then the possible chain combinations are "011···11", "101···11", ···, and "11···10". Obviously, the sequence length of "0" only can be 1 and the number of counts is *k*. Next we add one more "0", but keep the total number of "0" and "1" still as *k*. Thus we have two possible sequences of "R_2": "0" and "00". For the counts for the sequence of "00", if we simply treat the sequence "00" same as the sequence "0", the number of counts is related with the sequence length of "0" in the starting case. The difference is the total units because the total units should be reduced 1 as we view the sequence "00" as the sequence "0". Thus, the counts for "00" can be found by simply replace *k* with *k*-1 (see Figure 5.1a). For the counts of sequence of "0", we can obtain it by deducting the number of counts for the sequence "0"($i = 2$) from the total number of "0" for all the combinations ($2C_k^2$). Therefore, the number of counts for sequence "0" is $2C_k^2 - 2(k-1)$. Figure 5.1b shows the

(a)	$i=1$	$i=2$
$SL=1$	k	$2C_k^2-2(k-1)$
	$\searrow$	
$SL=2$		$k-1$(replace k with $k-1$)
Total number of "0"	$1C_k^1$	$2C_k^2$

(b)	$i=1$	$i=2$	$i=3$
$SL=1$	k	$2C_k^2-2(k-1)$ $=(k-1)(k-2)$	$3C_k^3-3(k-2)-2(k-2)(k-3)$
	$\searrow$		$\searrow$
$SL=2$		$k-1$	$(k-2)(k-3)$
			$\searrow$
$SL=3$			$(k-2)$
Total number of "0"	$1C_n^1$	$2C_n^2$	$3C_n^3$

Figure 5.1 A scheme to derive the number of counts of sequence length for simple cases: (a) i = 1, 2; (b) i = 1, 2, 3.

Note: SL = sequence length; the total number of "0" means the total counts of "0" in all possible combinations.

distribution pattern of number of counts when $i = 3$.

Repeating this above steps, we can obtain more general formulas for the number of counts of sequence length for the array (*m, k, i*) shown Figure 5.2.

As motioned above, the distribution pattern has to be modified for polymer chains that have a fixed end of R_2B, i.e. the chain types of 2, 4, 6. To find out the detailed general formulas for the chain types of 2, 4, 6, we also start with the simplest case i=0. Accordingly, the number of counts for the sequence of "0" is 1. For i=1, immediately we can find that the number of counts for the sequence of "0" is 1 and the number of counts for the sequence length of 1 is modified as $k + C_{k-1}^{1} - C_{k-2}^{0} = 2(k-2)$. Similarly, the number of counts for the case of i+1 can be derived from the case of i. A modified distribution pattern shown in Figure 5.3 also can be derived step by step.

From the distribution patterns for the number of counts of sequence length shown in Figure 5.2 and 5.3, we can calculate the number of counts of sequence length for any polymer chains in this linear copolymerization system. For each column in Figure 5.2 and 5.3, according to the number of counts we can obtain a normalized number distribution pattern S(*m, k, i, j*) by dividing every number of counts to the total number of counts in each column. Therefore, S(*m, k, i, j*) stands for the contribution of the array (*m, k, i*) to sequence length *j*. Thus, the number fraction of sequence length *j* can be expressed as follows.

$$SL_n(j) = \sum_{m=1}^{6} \sum_{k=1}^{\infty} \sum_{i=0}^{k-1} P(m,k,i) S(m,k,i,j) \tag{5.1}$$

where P is the number distribution of chain length shown in Table 5.1, and m, k, and i

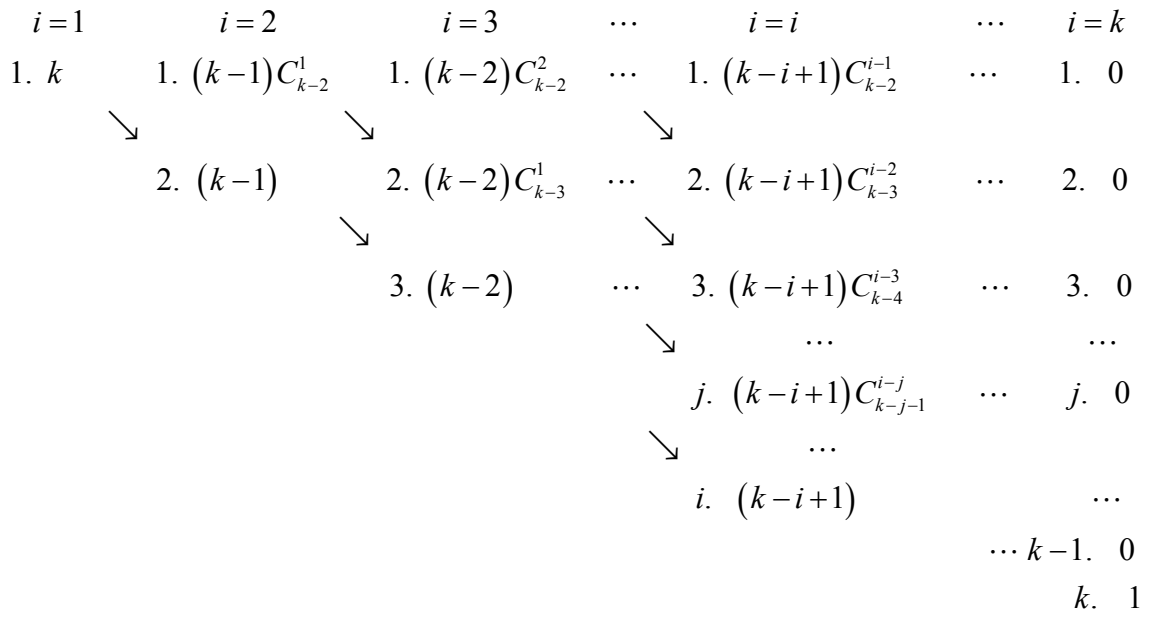

Figure 5.2 The number of counts of sequence length for the chain types of 1, 3, 5

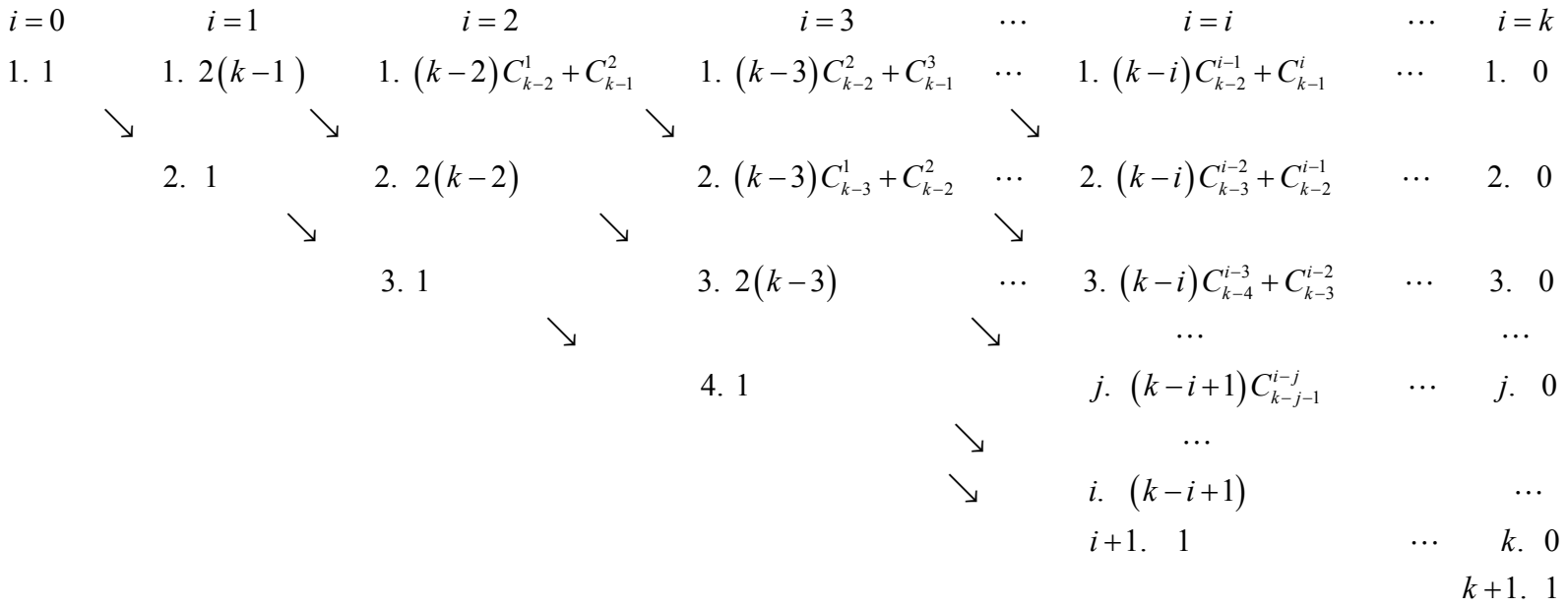

Figure 5.3 The number of counts of sequence length for the chain types of 2, 4, 6.

represent the chain type, the number of "R_1"units, and the number of "R_2" units inside of a chain, respectively. The weight-average distribution of sequence length can be calculated by the following equation.

$$SL_w(j) = \frac{j\left[SL_n(j)\right]}{\sum_{j=1}^{\infty} j\left[SL_n(j)\right]} \tag{5.2}$$

Thus, it is straightforward to get the number- and weight-average sequence lengths.

$$\overline{SL}_n(j) = \frac{\sum_{j=1}^{\infty} j\left[SL_n(j)\right]}{\sum_{j=1}^{\infty} SL_n(j)} \tag{5.3}$$

$$\overline{SL}_w(j) = \frac{\sum_{j=1}^{\infty} j^2\left[SL_n(j)\right]}{\sum_{j=1}^{\infty} j\left[SL_n(j)\right]} \tag{5.4}$$

From the above model equations, we can see that as long as the conversions of monomers and the initial monomer mole ratio of BR_3B to BR_2B are known, the number and weight average sequence length distributions and sequence length averages can be calculated.

5.2.2 Melt Copolycondensation in a Semibatch Reactor

To simulate chain sequence length distributions and sequence length averages in the course of reaction, as an example, we use the melt copolycondensation in a semibatch reactor with the following monomers: diphenyl carbonate (DPC, AR_1A), bisphenol A (BPA, BR_2B) and 3,3′,5,5′-tetramethylbisphenol A (TMBPA, BR_3B). The melt polymerization of BPA and DPC in a semibatch reactor given by Woo et

al.[98] is adopted in this simulation work. A simplified schematic diagram of semibatch reactor is shown in Figure 5.4. Same reaction conditions are applied in this study except that other than BPA and DPC monomers we assume there is a third monomer component of TMBPA present in the system and the vapor pressure of TMBPA is also negligible. Generally, a molecular species model[98] and an end group model[12] can be used to describe the melt polycondensation of BPA and DPC. To account for the loss of DPC, the molecular species model was developed by Woo et al.[98], which keeps tracking the amount of DPC and phenol in the system and accurately describes the melt polymerization process of BPA and DPC in the semibatch reactor. As a third monomer is added into the reaction system, which however makes the model equations very complicated if we keep tracking change of molecular species. In the following modeling, we are going to develop an end group model to simulate the melt copolycondensation process in a semibatch reactor and verify that the end group model we developed is equivalent to the molecular species model. It can also be used to calculate the volatile species of DPC and phenol in the reaction system.

The melt transesterifaction reactions occur between the diphenyl carbonate end group and the hydroxyl end group in the presence of $LiOH{\cdot}H_2O$ as a catalyst, and main polycondensation reactions take the following forms.

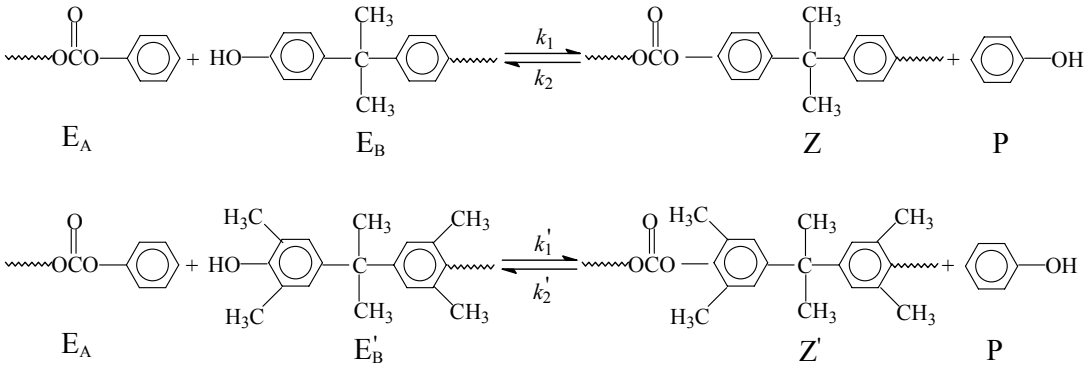

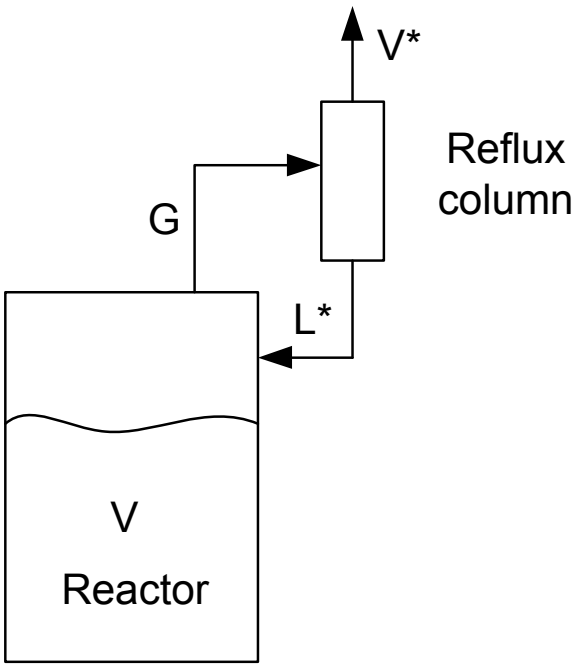

Figure 5.4 A schematic diagram of semibatch reactor.

(G: the total moles of the vapor phase after the flash separation; V^*: the molar flow rate of vapor leaving the reflux column; L^*: the molar flow rate of condensed liquid refluxing back to the reactor.).

where E_A = phenyl carbonate group, E_B = hydroxyl group from BPA, E_B' = hydroxyl group from TMBPA, Z, Z′ = polymer repeat units, and P = phenol.

Assuming that the reactivities of polymer chains are same regardless of polymer chain length, we can derive an end group model for the semibatch melt copolycondensation process as follows.

$$V\frac{dE_A}{dt} = -k_1E_AE_B + k_2P\left(E_{B,0} - E_B\right) - k_2'E_AE_B' + k_2'P\left(E_{B,0}' - E_B'\right) \tag{5.5}$$

$$V\frac{dE_B}{dt} = -k_1E_AE_B + k_2P\left(E_{B,0} - E_B\right) \tag{5.6}$$

$$V\frac{dE_B'}{dt} = -k_1E_AE_B' + k_2P\left(E_{B,0}' - E_B'\right) \tag{5.7}$$

$$V\frac{dP}{dt} = k_1E_AE_B - k_2P\left(E_{B,0} - E_B\right) + k_2'E_AE_B' - k_2'P\left(E_{B,0}' - E_B'\right) \tag{5.8}$$

where k_1 and k_2 represent the forward and backward reactions and E_A, E_B, E_B' and P are total moles of phenyl carbonate end group, hydroxyl end group from BPA, hydroxyl end group from TMBPA and phenol, respectively.

The vapor-liquid equilibrium equations used to calculate compositions in vapor and liquid phases were given by Woo et al.[98] Thus, it is necessary to know the amount of phenol and DPC produced in the semibatch reactor. The equation to calculate the amount of phenol is already given in the eq 5.8. To calculate the amount of DPC, we assume that polymer chains in the reactor follow the most probable distribution. Thus, the number fraction of DPC is given by[101]

$$\frac{\left(1-r_ap\right)^2/r_a}{1+1/r_a-2p}$$

The total number of chain ends can be expressed as,

$$\left(E_{A,0}+E_{B,0}+E_{B,0}^{'}\right)-2\left(E_{B,0}+E_{B,0}^{'}\right)p$$

and this should be equal to twice of the total number of molecules (polymer chains and monomers). Thus, the number of moles of DPC can be expressed as,

$$A_0=\frac{\left(1-r_a p\right)^2/r_a}{1+1/r_a-2p}\left[\frac{E_{A,0}+E_{B,0}+E_{B,0}^{'}}{2}-\left(E_{B,0}+E_{B,0}^{'}\right)p\right] \tag{5.9}$$

where A_0 is the moles of DPC; p is the conversion of hydroxyl end groups based on the total amount initially changed (i.e. BPA and TMBPA); r_a is the mole ratio of total hydroxyl end groups to phenyl end group (i.e. $\left(E_{B,0}+E_{B,0}^{'}\right)/E_{A,0}$).

The calculation procedure is summarized as follows: 1) Provide a small time step to integrate reaction eqs 5.5-5.8 and find out the number of moles of end groups and phenol; 2) Find the conversions of monomers; 3) Based on the assumption of most probable distribution, calculate the moles of monomers after reaction; 4) Follow the method given by Woo et al.[98], and use the vapor-liquid equilibrium equations together with the Flory-Huggins equation to compute the vapor- and liquid-phase compositions in the reactor, and calculate total moles of volatile species (i.e. phenol and DPC) entering into the reflux column; 5) Use the vapor-liquid equilibrium equations together with the Wilson equation to calculate the vapor flow rate leaving reflux column and liquid flow rate refluxing back to the reactor; 6) Update total volume and total moles of DPC (i.e. the moles of DPC initially charged – the moles of DPC loss during the reaction) in the reaction system, and recalculate the mole ratio of total hydroxyl end group to phenyl end group; 7) Repeat steps from 1 to 6 until the desired reaction time is reached.

5.3 Results and Discussion

5.3.1 Model Verification for Sequence Length Distributions

The first step is to verify the simulation results of sequence length averages by comparing calculation results with previous recursive method developed by Lopez-Serrano et al.[92] The number and weight average sequence lengths for R_2 units developed by Lopez-Serrano and coworkers[92] are given as follows.

$$\overline{SL}_n(j) = \frac{1}{1 - r_1 p_1^2} \tag{5.10}$$

$$\overline{SL}_w(j) = \frac{1 + r_1 p_1^2}{1 - r_1 p_1^2} \tag{5.11}$$

where r_1 is the initial mole ratio of BR_2B to AR_1A and it can be calculated by $\frac{p_1}{p_2 + \nu p_3}$, and p_1 is the conversion of BR_2B monomer.

In comparison with the results calculated by eqs 5.10 and 5.11, we first assume that BR_2B has a same reactivity as BR_3B and three monomers have same conversions. Figure 5.5 shows the comparison of number- and weight-average sequence lengths of R_2 units. It is seen that our simulation results are in good agreement with those calculated by eqs 5.10 and 5.11. For the case of unequal reactivity shown in Figure 5.6, we assume that BR_2B has same conversions as AR_1A, but the reactivity of BR_2B is different from that of BR_3B. Again, Figure 5.6 indicates our simulation results of the number- and weight-average sequence lengths are well matched with those calculated by the recursive method. Obviously, if the reactivity of BR_3B is much smaller than that of BR_2B, only small amount of third monomer is incorporated in the condensation terpolymer chains, which means that the number-

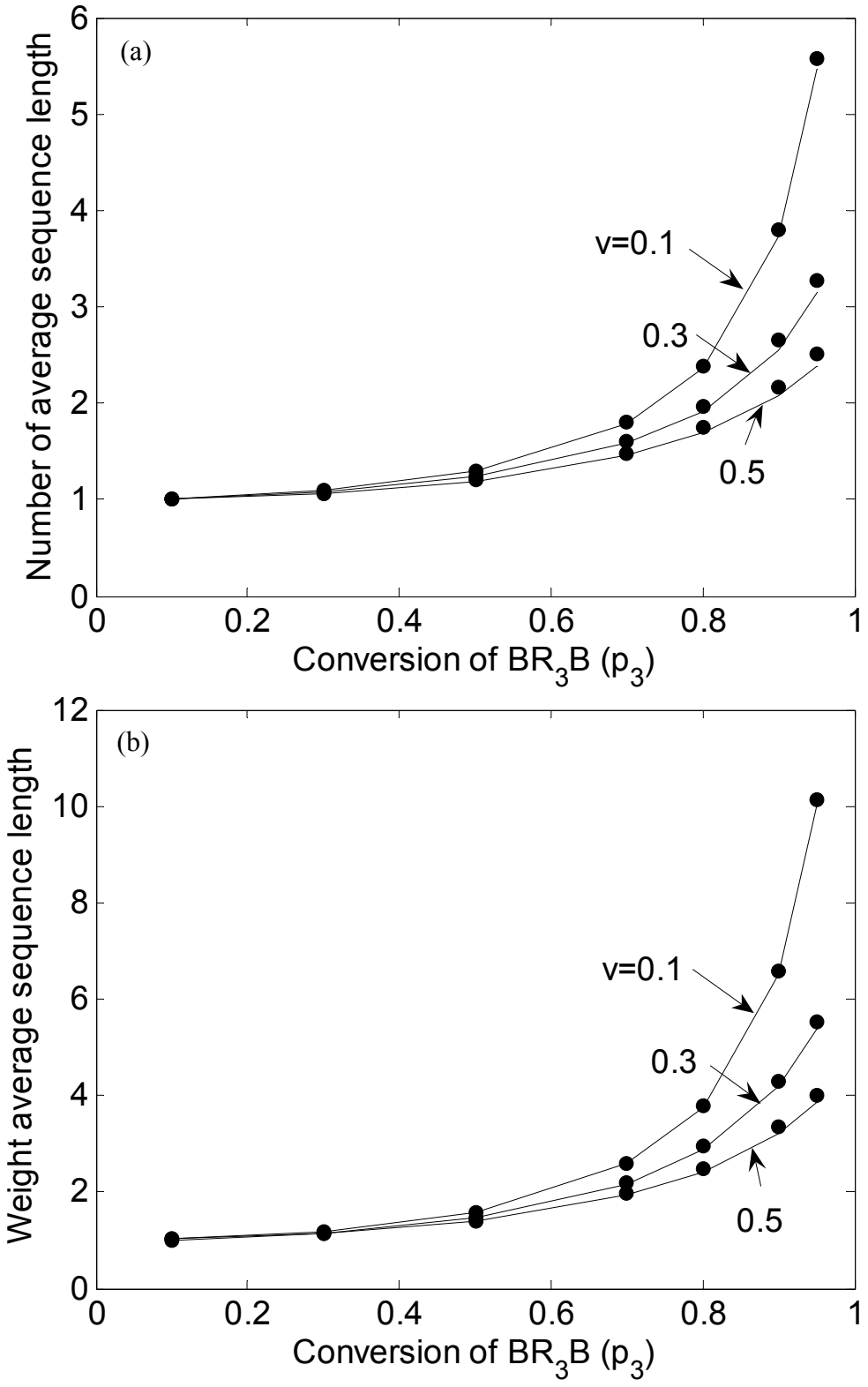

Figure 5.5 Comparison of number and weight average sequence length of R_2 units

($p_1 = p_2 = p_3$, "dot": eq 5.10 and eq 5.11; "line": this work).

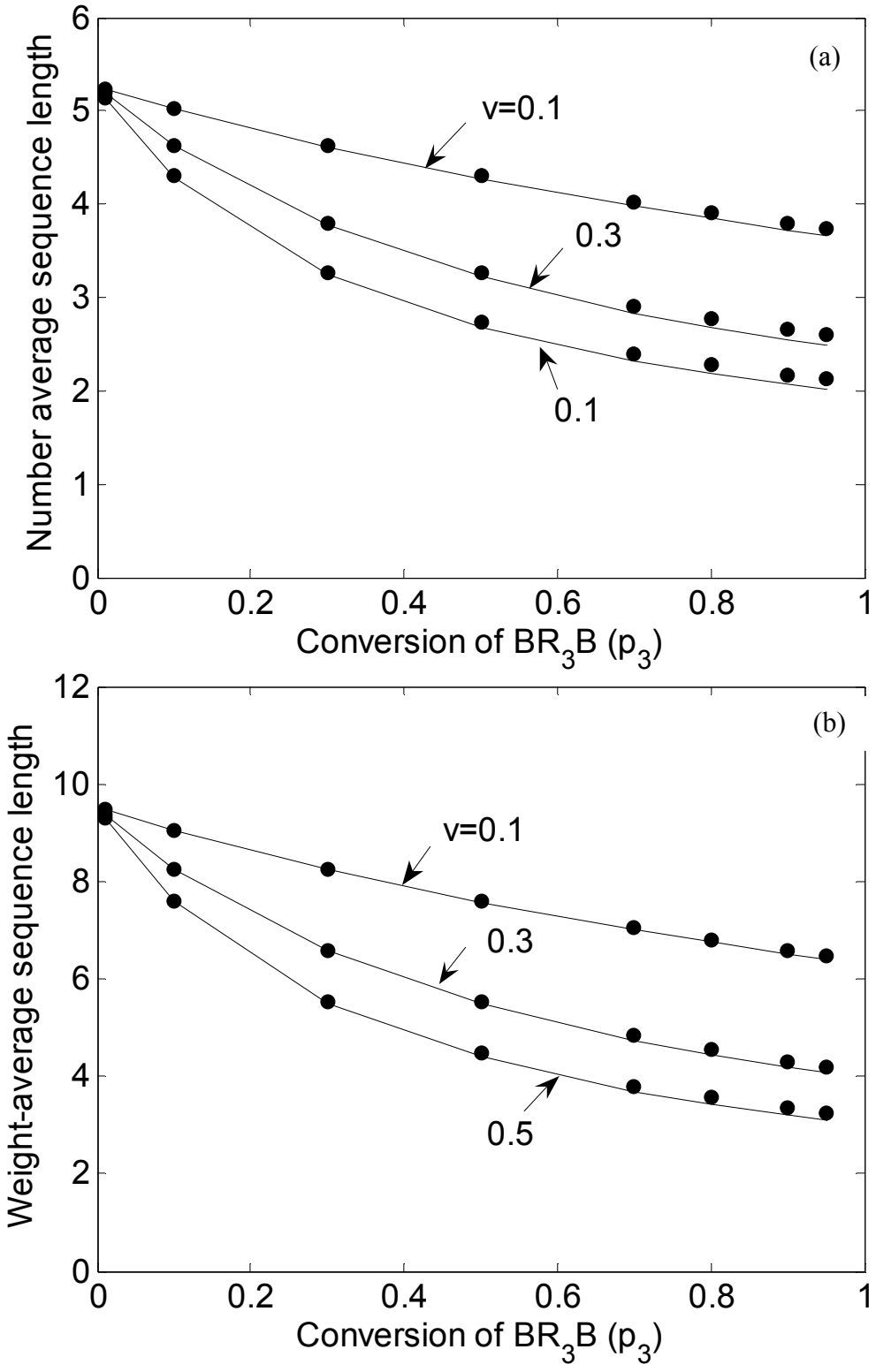

Figure 5.6 Comparison of number and weight average sequence length of R_2 units

($p_1 = p_2 \neq p_3$ $p_1 = p_2 = 0.9$,"dot": eq 5.10 and eq 5.11; "line": this work).

and weight-average sequence lengths with respect to BR_2B become fairly large. In particular, when the reactivity of BR_3B is close to zero ($p_3 = 0.01$, $p_1 = p_2 = 0.9$), according to the definition of sequence length, the sequence length of R_2 units will be close to the chain length of homopolymer -R_1R_2 R_1R_2 $R_1R_2R_1R_2R_1R_2$-. The ratio between weight- and number-average sequence lengths should be close to 2, which is shown in Figure 5.6 when $p_3 = 0.01$.

To verify the sequence distributions, we set the conversion of BR_3B as a very small value to compare with the most probable distribution.[101] Again, if conversion is very small, the sequence length distribution of R_2 units should be same as chain length distribution of homopolymer of BAPC. If a condensation homopolymer chains follows the most probable distribution, the number and weight chain length distributions can be approximated as[60],

$$P_n = \left(1 - r_a^{1/2} p\right)\left[\left(r_a^{1/2} p\right)^{2n-1} + \left(r_a^{1/2} p\right)^{2n}\right] \tag{5.12}$$

$$W_n = \left(1 - r_a^{1/2} p\right)^2\left[2n\left(r_a^{1/2} p\right)^{2n-1} + (2n+1)\left(r_a^{1/2} p\right)^{2n}\right] \tag{5.13}$$

where r_a is the mole ratio of end group at the beginning of melt prepolymerization, and p is the conversion of monomer. Figure 5.7 illustrates that the number and weight fractions of chain sequence length for B_2 units calculated in this work are in good agreement with Flory distributions when the conversion of third monomer takes a very small value ($p_3 = 0.01$, r_a=1). It means that sequence length distributions can be simplified as chain length distributions when the third monomer is not incorporated into polymer chains, and that the model equations we developed give good simulation results for sequence length distributions.

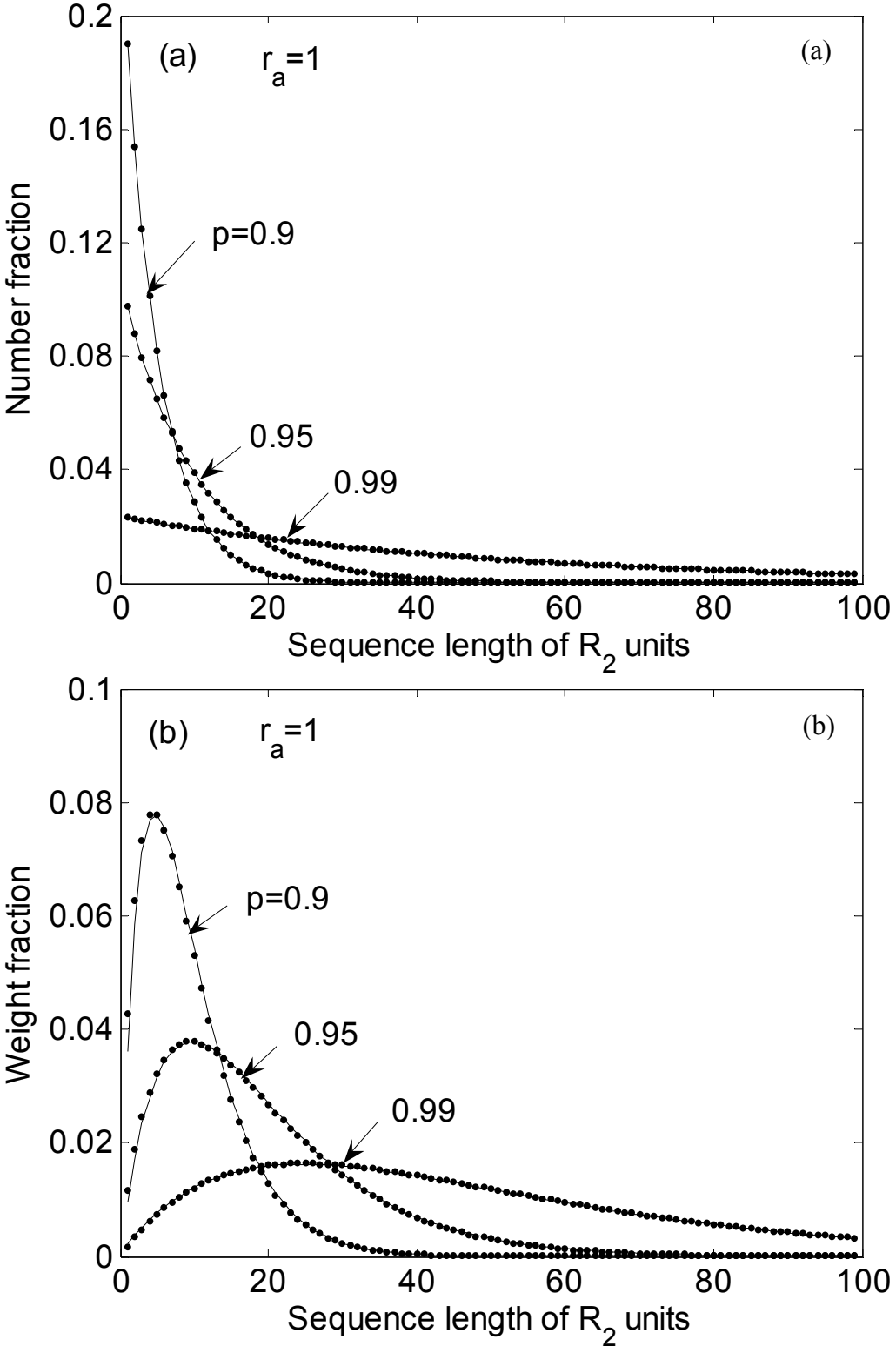

Figure 5.7 Comparison with Flory most probable distributions ((a). number distribution; (b). weight distribution; dot": eq 5.12 and eq 5.13; "line": this work).

5.3.2 Modeling of a Semibatch Melt Copolycondensation Process

The modeling of semibatch process is based on the melt polycondensation process of BPA and DPC given by Woo et al.[98] The reaction conditions are also taken from this paper as a reference and they are listed in Table 5.3. The initial mole ratio of BR_3B to BR_2B is assumed as 0.1 and the reactivity ratio of BR_3B to BR_2B, r_{re}, is treated as an adjustable parameter. Reaction constants and physical properties of DPC and phenol for the vapor-liquid equilibrium equations are given in Woo's paper.[98]

To verify the end group model developed above, we set the third monomer as BR_2B. Thus, the copolymerization is simplified as homopolymerization of DPC and BPA. In this way, results generated from the end group model can be verified against those calculated from the molecular species model that was used for modeling of the melt polymerization of BPA and DPC in a semibatch reactor. Figure 5.8 shows the comparison of number of moles of DPC and phenol calculated from the molecular species model and from the end group model. Figure 5.9 illustrates the comparison results of weight-average molecular weight in the course of reaction. It is seen that the simulation results from the end group model are in good agreement with those calculated from the molecular species model, meaning that the assumption of most probable distribution of polymer chains in the reactor is valid, and the amount of monomers in the reactor can be calculated from the number distribution of monomers.

Figure 5.10 shows the conversions of three monomers during the melt copolycondensation process in the semibatch reactor for the reference case. It is seen that conversions increase in a fast rate in the beginning and then quickly level off as they reach up to 95%. Here, the conversion of DPC (p_3) is not based on the total

Table 5.3 Standard reaction conditions used as a reference

reaction condition	value
reactor temperature	230 ºC
reflux column temperature	82 ºC
reaction pressure	5 mmHg
time to reach reaction pressure	2 mins
catalyst concentration	8×10^{-5} mol/L
initial mole ratio of phenyl group to hydroxyl group	1.05
initial mole ratio of BR_3B to BR_2B	0.1
reactivity ratio*	1

Note: "*", Regarding the forward and backward reaction rate constants for the reversible reaction between E_A and E_B', we don't have values available. Therefore, we estimate the values of k_2 and k_2' from the reactivity ratios, k_1'/k_1 and k_2'/k_2, and treat them as adjustable parameters. As the first approximation, the reaction equilibrium constants may be regarded as same, i.e. $k_1/k_2=k_1'/k_2'$. Thus, only one adjustable parameter is necessary.

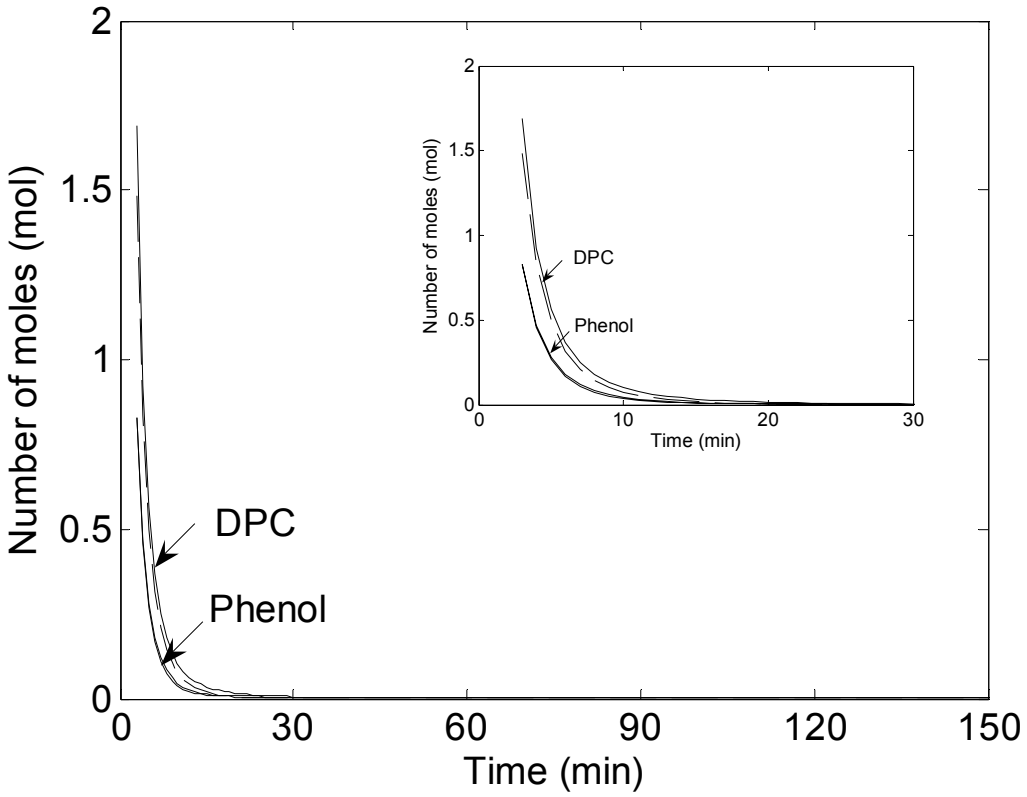

Figure 5.8 Comparison of phenol and DPC concentrations calculated from the end group model (solid line) and the molecular species model (dotted line).

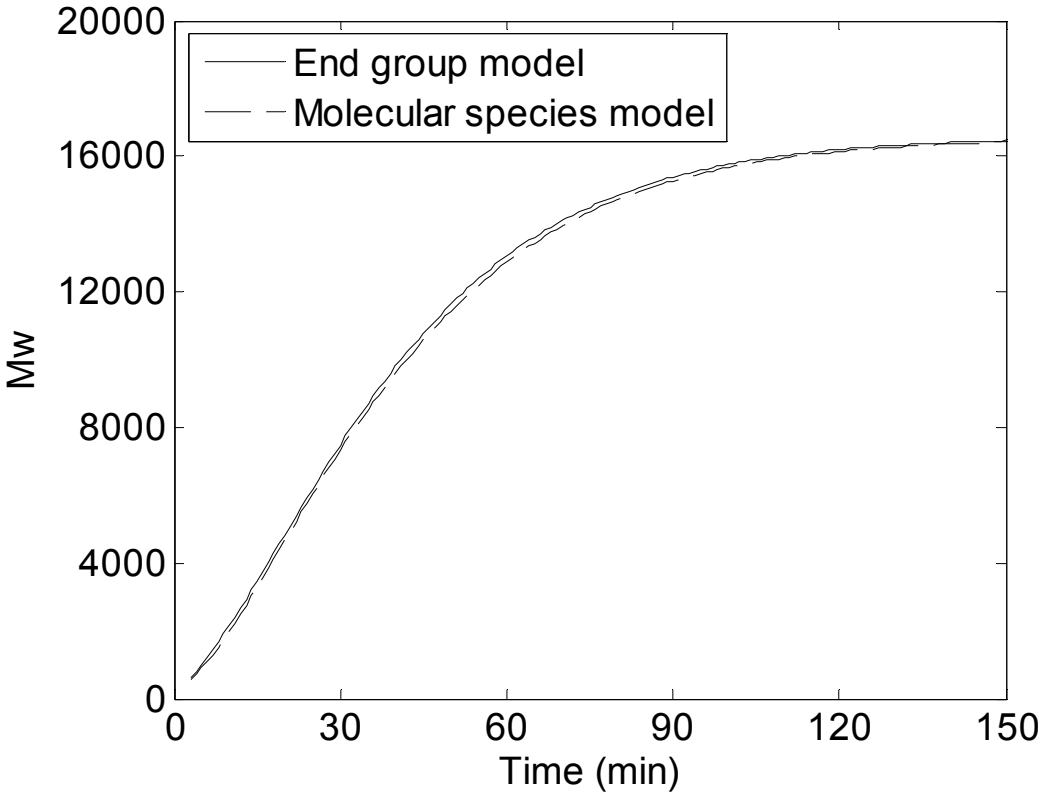

Figure 5.9 Comparison of weight-average molecular weight calculated from the end group model (solid line) and the molecular species model (dotted line).

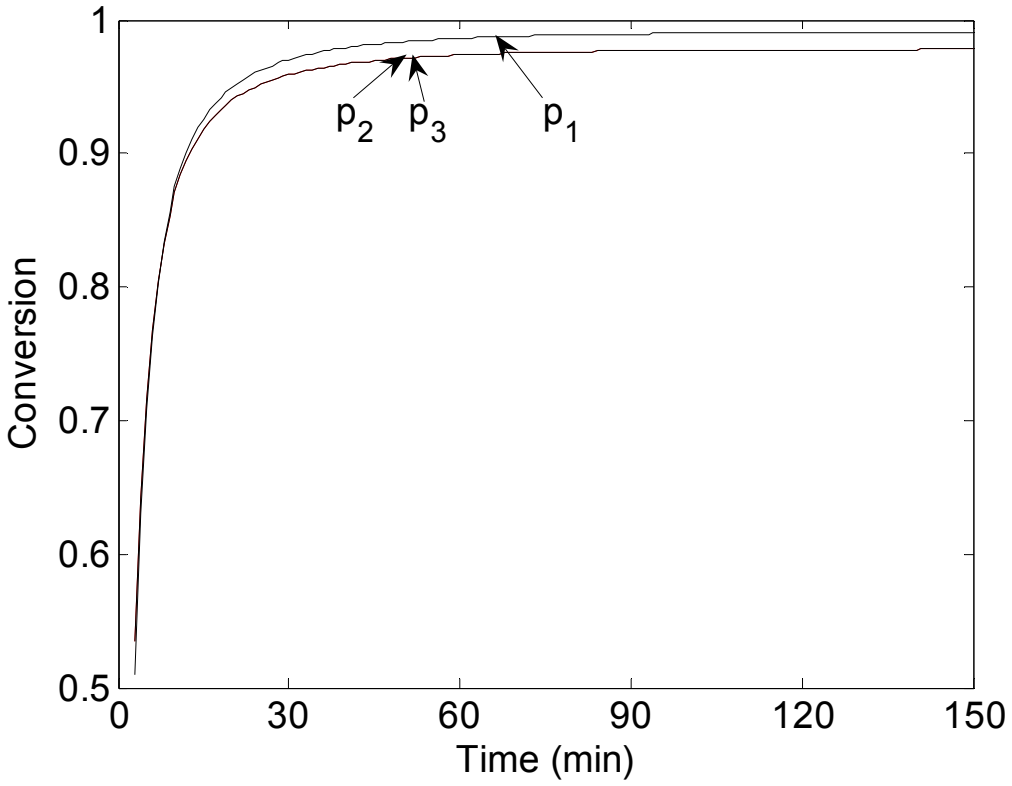

Figure 5.10 Conversions of monomers during the semibatch process.

amount that is initially charged, but based on the updated total amount (i.e. deduct DPC loss during the reaction from the DPC initially charged). Since the reactivity of hydroxyl group from TMBPA is assumed same as that from BPA, it is obvious that p_2 is equal to p_3. With the conversion values, based on the model of chain sequence length developed above we are able to calculate the chain sequence length distributions and averages in the course of reaction. Figure 5.11 shows number and weight fractions of sequence length of R_2 units under the standard reaction conditions. It is seen that the number fraction of sequence length of R_2 units decreases monotonously, meaning that longer polymer chains have lower number fraction. However, in contrast to the number fraction of sequence length, most weight fraction curves show a maximum value. As the conversion increases, the weight sequence length distribution of R_2 units shifts to a higher value, indicating that the sequence length of R_2 units is on the increase. Although both BR_2B and BR_3B have same conversions, more R_2 units are incorporated into polymer chains than R_3 units because of higher concentration of BR_2B present in the system. As conversion is getting close to a plateau value (t = 30 min), the further incorporation rate of R_2 units is very slow and the sequence length distributions stay almost same. The increase of sequence length of R_2 units also can be seen from those number- and weight-average sequence lengths shown in Figure 5.12. The increase trend is similar as conversion increase shown in Figure 5.10.

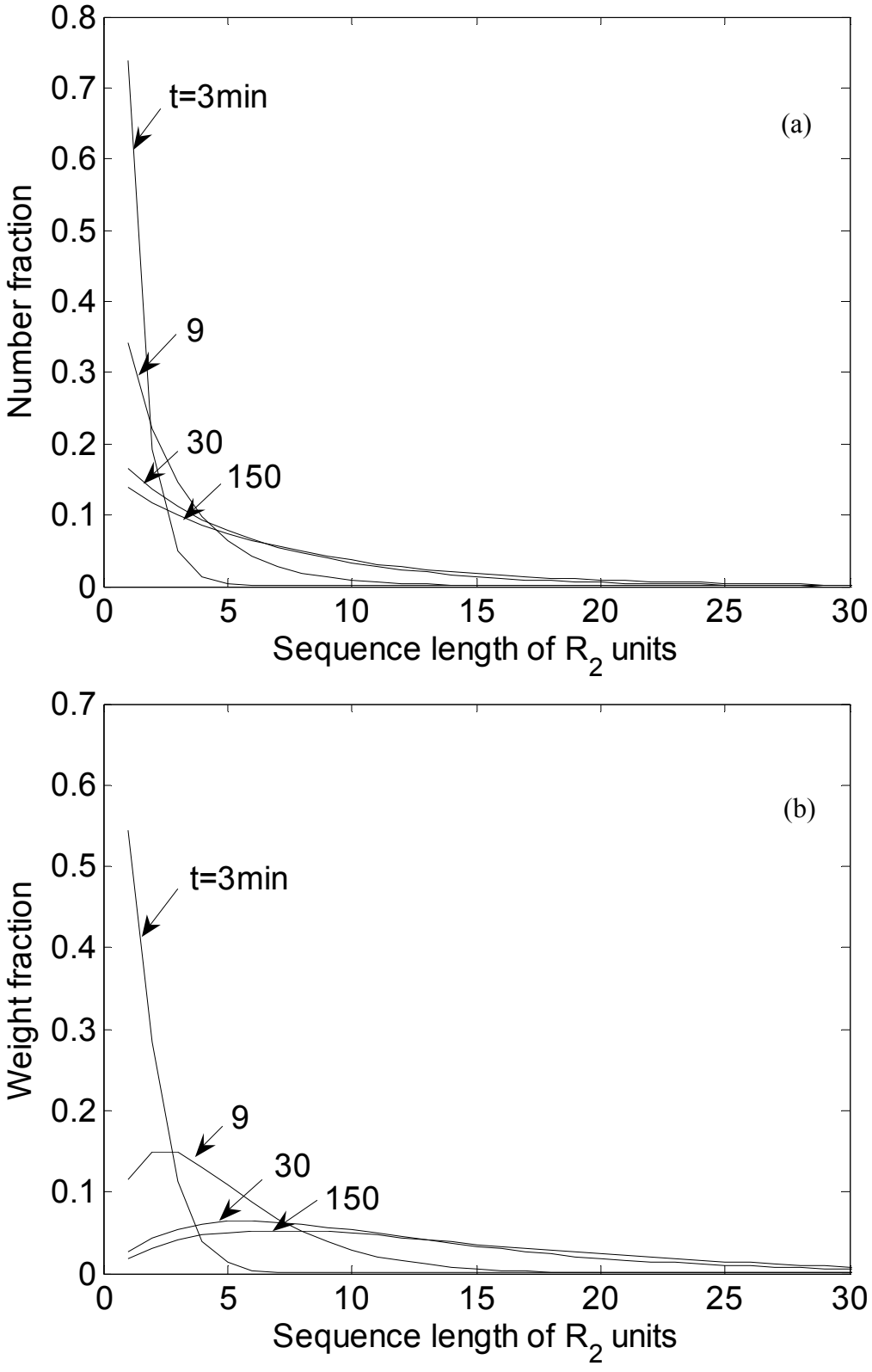

Figure 5.11 Sequence length distributions of R_2 units during the semibatch process.

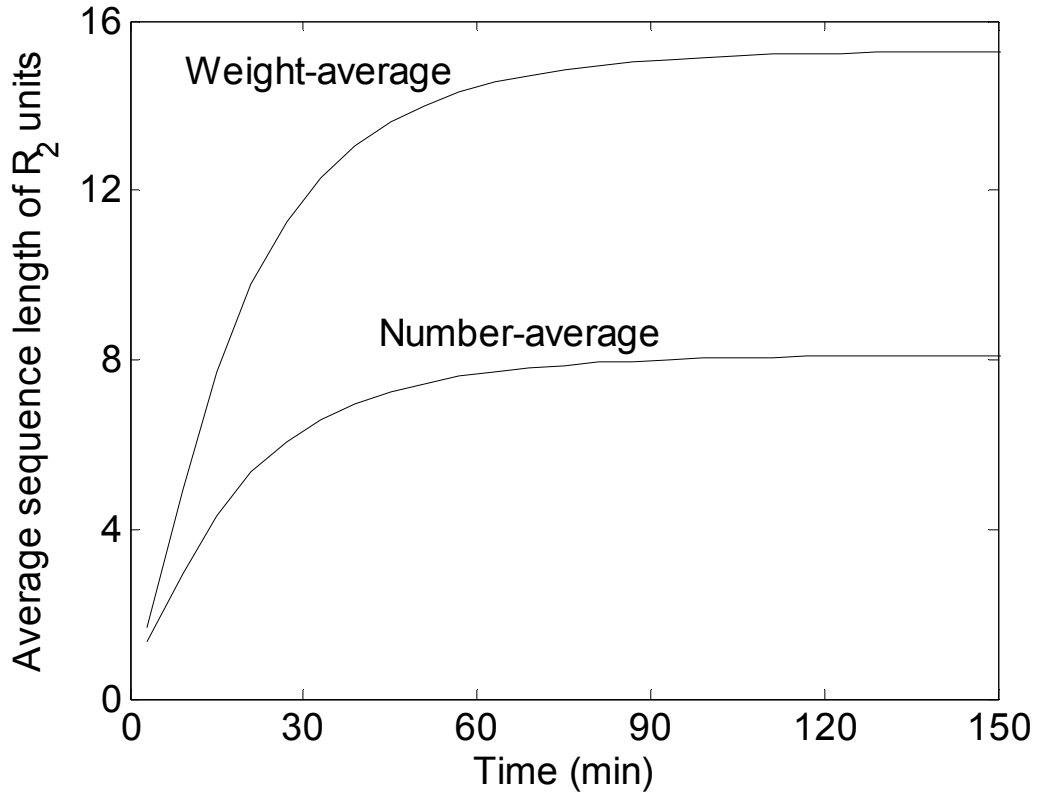

Figure 5.12 Average sequence length of R_2 units during the semibatch process.

1) Effect of End Group Ratio, r_a

It is well known that stoichiometric imbalance of end groups has a significant effect on the molecular weight increase during the melt polymerization. It was also pointed out that the end group mole ratio (i.e. the total amount of hydroxyl end group to the phenyl carbonate end group) is one of most important factors affecting the reaction kinetics, for example, in both melt polymerization[98] and further solid-state polymerization[60]. During the semibatch process, the loss of small amount of DPC is unavoidable since the vapor pressure of DPC is not negligible small as compared with phenol[98]. In practice, a slight excess of DPC is often used in the beginning of melt polymerization to compensate for the loss of DPC. Here, the end group ratio of 1.05 is used in the reference case. Therefore, it is important to understand how the stoichiometric imbalance of end groups affects the sequence length distributions during the preparation of condensation copolymers.

Figure 5.13 shows the effect of end group ratio r_a on the weight-average molecular weight at reaction t = 150 min. It is seen that the highest weight-average molecular weight at t = 150 min is obtained at the initial end group mole ratio about 1.07. The effect of end group ratio on the average sequence lengths is shown in Figure 5.14, which has similar trend as Figure 5.13. Figure 5.15 shows the effect of end group ratio on the monomer conversions. It indicates that as the amount of DPC increases, the conversion of DPC (p_1) itself drops, but the conversions of BPA and TMBPA (p_2, p_3) increase. As motioned before, since the reactivity of TMBPA is assumed same as that of BPA, both have same conversion values. Interestingly, the maximum values of molecular weight and sequence length averages appear around

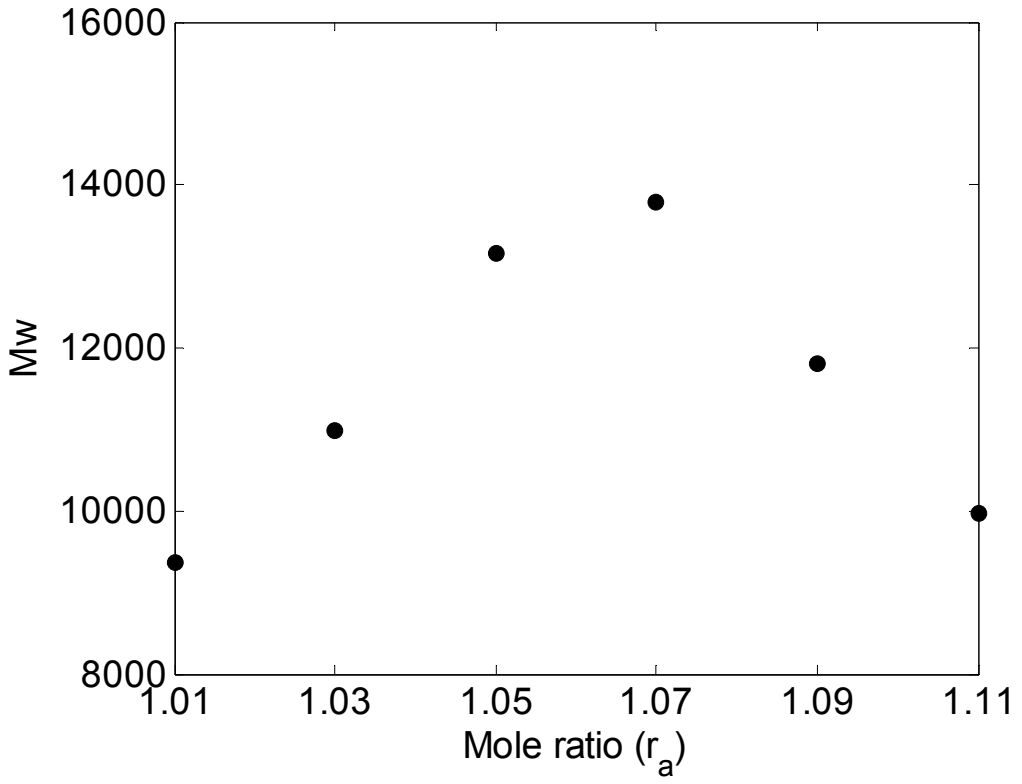

Figure 5.13 Effect of end group mole ratio on polymer molecular weight at t = 150 min.

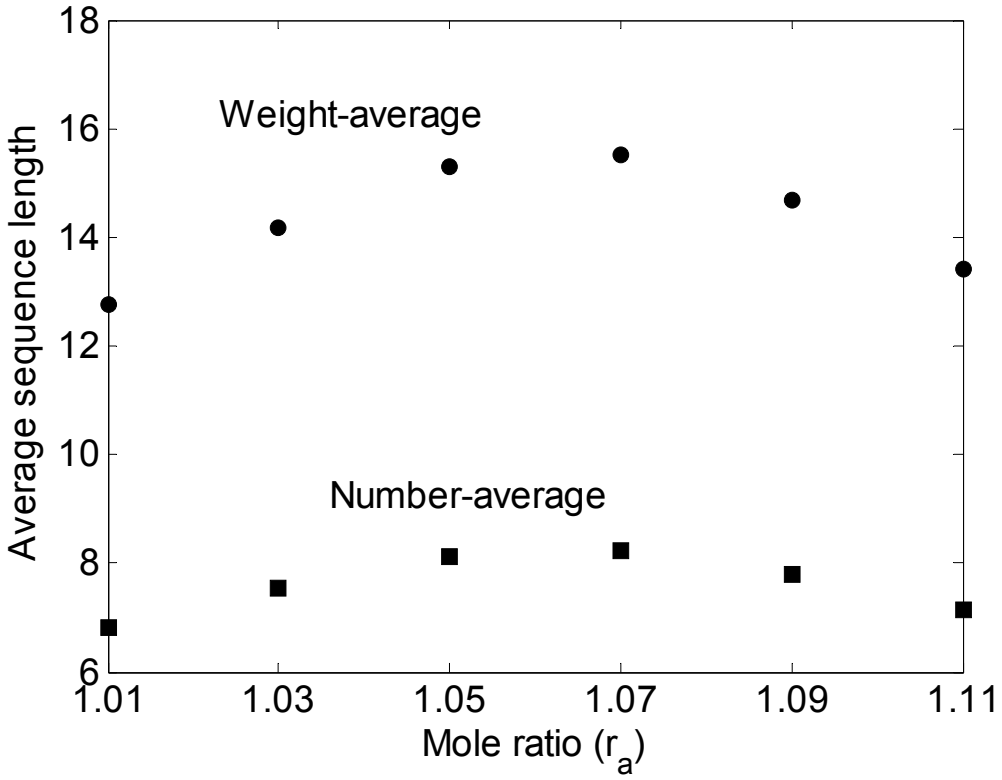

Figure 5.14 Effect of end group mole ratio on the average sequence length of R_2 units at t = 150 min.

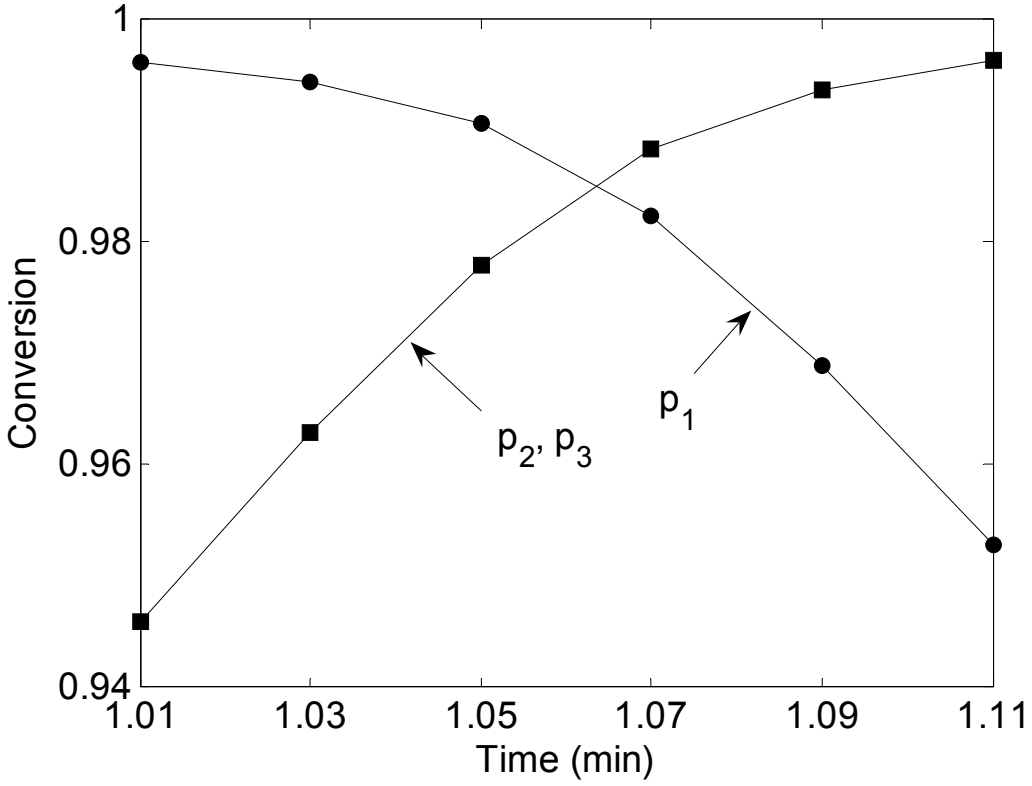

Figure 5.15 Effect of end group mole ratio on monomer conversions at t = 150 min.

the cross point where same conversion values meet. Again, note the conversion of DPC is not based on the total amount that was initially charged, but based on the updated value that excludes the loss of DPC during the melt polymerization, which is constantly changing and means that the cross point may not appear at same end group ratio for different reaction times. From Figure 5.13 and Figure 5.14, we can see that if third monomer has a same reactivity value as the second monomer, higher molecular weight is corresponding to larger sequence length. Therefore, average molecular weight may be used to qualitatively indicate whether average chain length is long or short, which may allow us to get around the measurement of chain sequence length.

2) Effect of Reactivity Ratio, r_{re}

The reactivity ratio r_{re}, defined by the ratio of rate constants, is an unknown variable. For the forward reaction and backward reaction, there are two reactivity ratios. To simplify the problem, we assume that both reactions have same equilibrium constants. Thus, only one adjustable parameter is necessary, i.e. $r_{re} = k_1'/k_1 = k_2'/k_2$) It is another important factor affecting polymer chain microstructures in the products. The difference of end group reactivity will result in different corporation rate of monomers, which will greatly affect the chain sequence length distributions and averages. Understanding the effect end group reactivity will help to determine and design chain microstructures. Figure 5.16 shows the effect of reactivity ratio on the conversions of monomers. Three reactivity ratios of 0.1, 1 and 10 have been investigated. Generally, higher reactivity of third monomer may result in higher conversion and larger amount of incorporation. However, Figure 5.16a and 5.16b

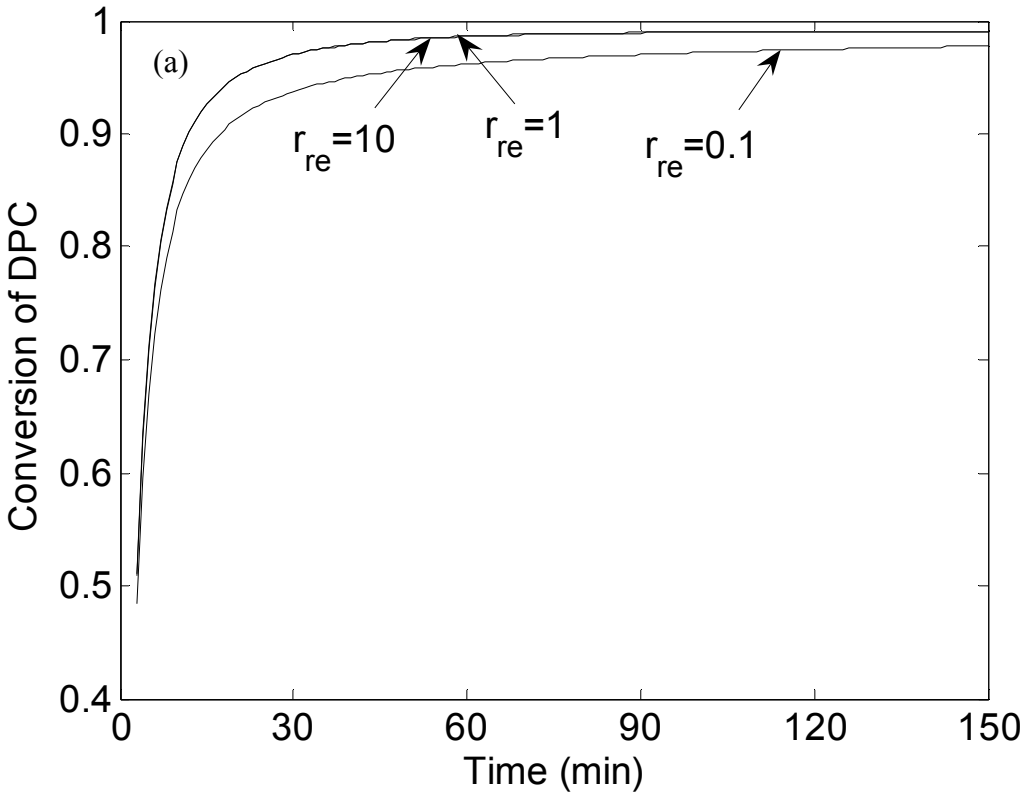
(a)
r_{re}=10
r_{re}=1
r_{re}=0.1
Conversion of DPC
Time (min)
1
0.9
0.8
0.7
0.6
0.5
0.4
0
30
60
90
120
150

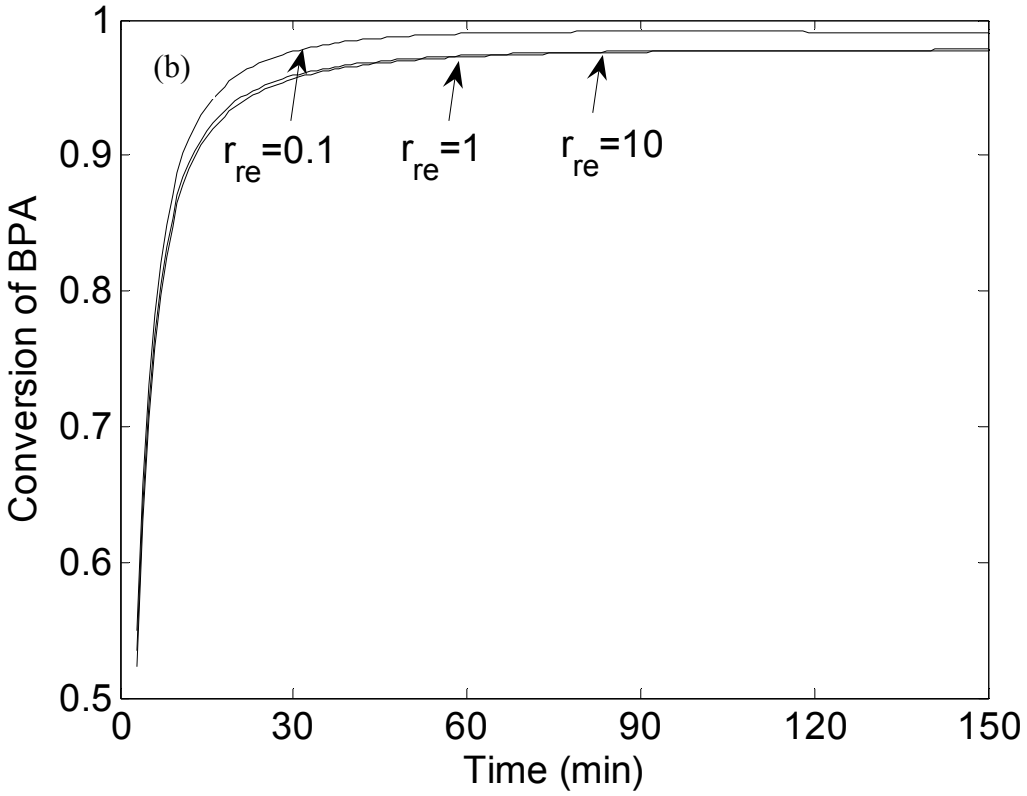
(b)
r_{re}=0.1
r_{re}=1
r_{re}=10
Conversion of BPA
Time (min)
1
0.9
0.8
0.7
0.6
0.5
0
30
60
90
120
150

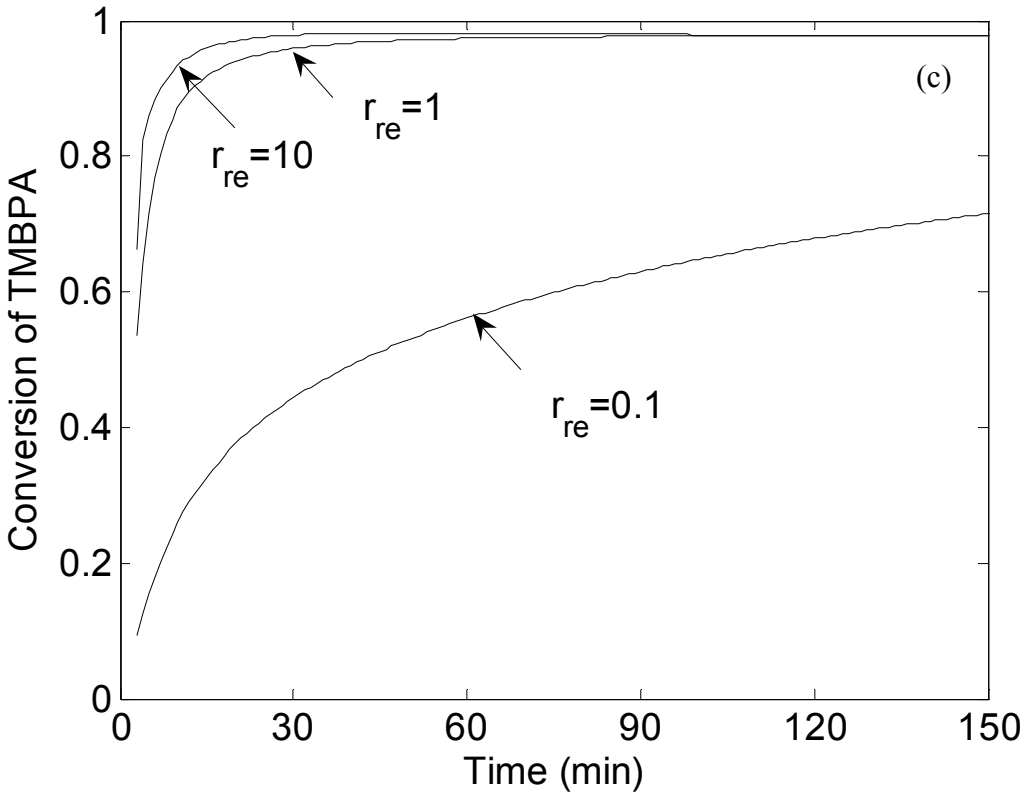

Figure 5.16 Effect of reactivity ratio on the conversion of monomers ((a): DPC; (b): BPA; (c): TMBPA).

show that there are negligible difference between the reactivity of 1 and that of 10 for the conversions of DPC and BPA, although Figure 5.16c shows some difference in the conversion of TMBPA. The reason is that the number of moles of BPA is much larger than that of TMBPA in the system ($v = 0.1$), and the reaction rate not only depends upon the reactivity, but also depends upon the concentration of monomers. Low reactivity combined with high concentration may still give significant reaction rate, while low reactivity combined with low concentration results in slow reaction rate and low conversion. Figure 5.16c shows that the third monomer of TMBPA has very low conversions if both amount ($v = 0.1$) and reactivity ($r_{re} = 0.1$) are small. Figure 5.17 shows the chain sequence length distributions at different reaction times. Again, we can see that as reaction time increases low reactivity of third monomer leads to large incorporation of R_2 units. Figure 5.18 presents the reactivity ratio effect on the chain sequence length averages. It is seen that if the reactivity of third monomer is low (e.g. $r_{re} = 0.1$), the average chain sequence length of R_2 units becomes quite large. In particular, if the reactivity of third monomer is extremely low, the sequence length distribution of R_2 units becomes chain length distribution of repeating units (i.e. homopolymer), and the average sequence length of R_2 units becomes average chain length of repeating units.

3) Effect of Monomer Ratio, *v*

Monomer ratio *v* is one of the key parameters that dominate the properties of modified polycarbonate polymer. If the reactivity of third monomer is not as high as the second monomer, excessive amount of third monomer has to be used in order to

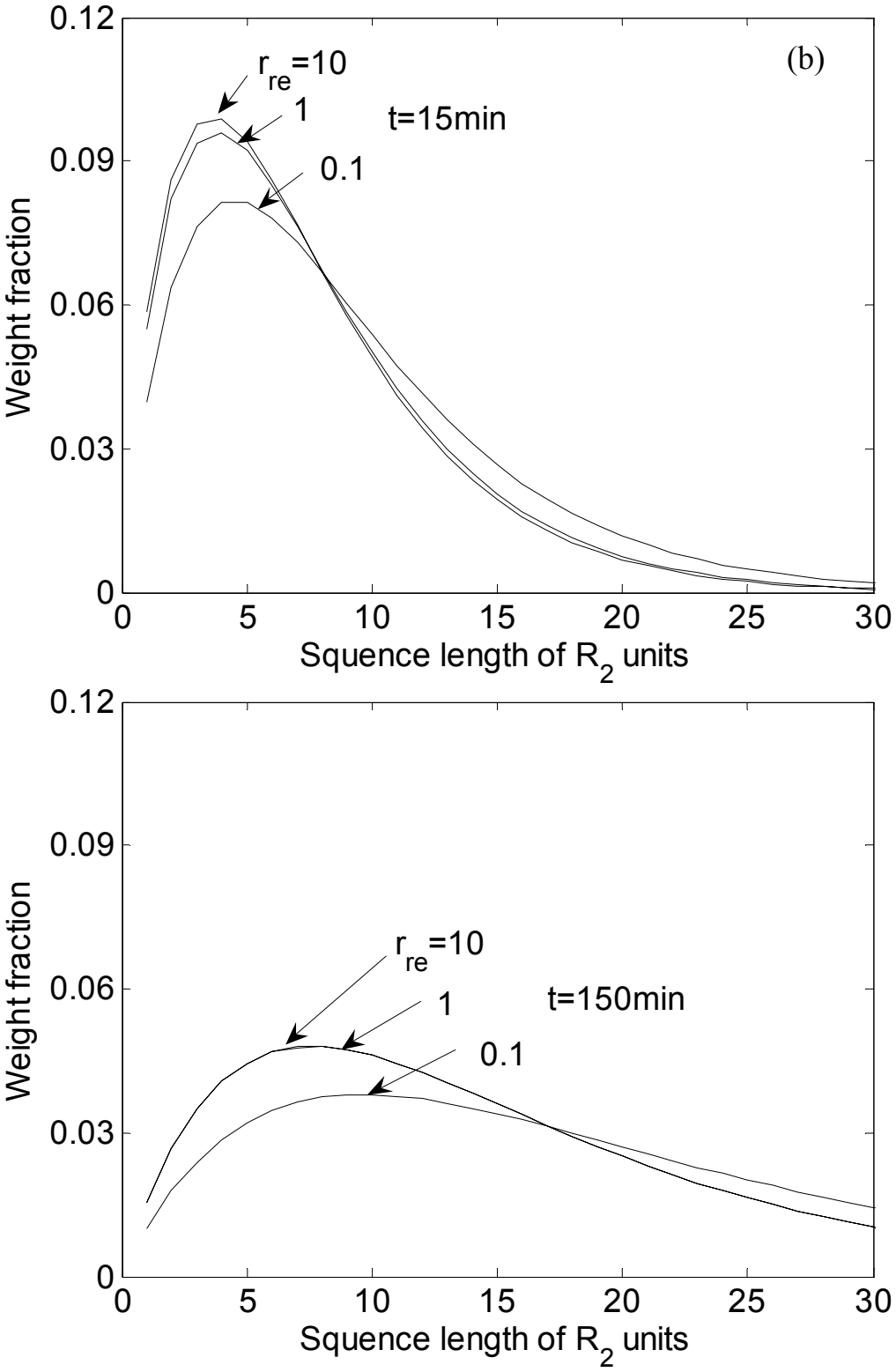

Figure 5.17 Effect of reactivity ratio on the sequence length distributions of R2 units ((a): t = 15 min; (b): t = 150 min).

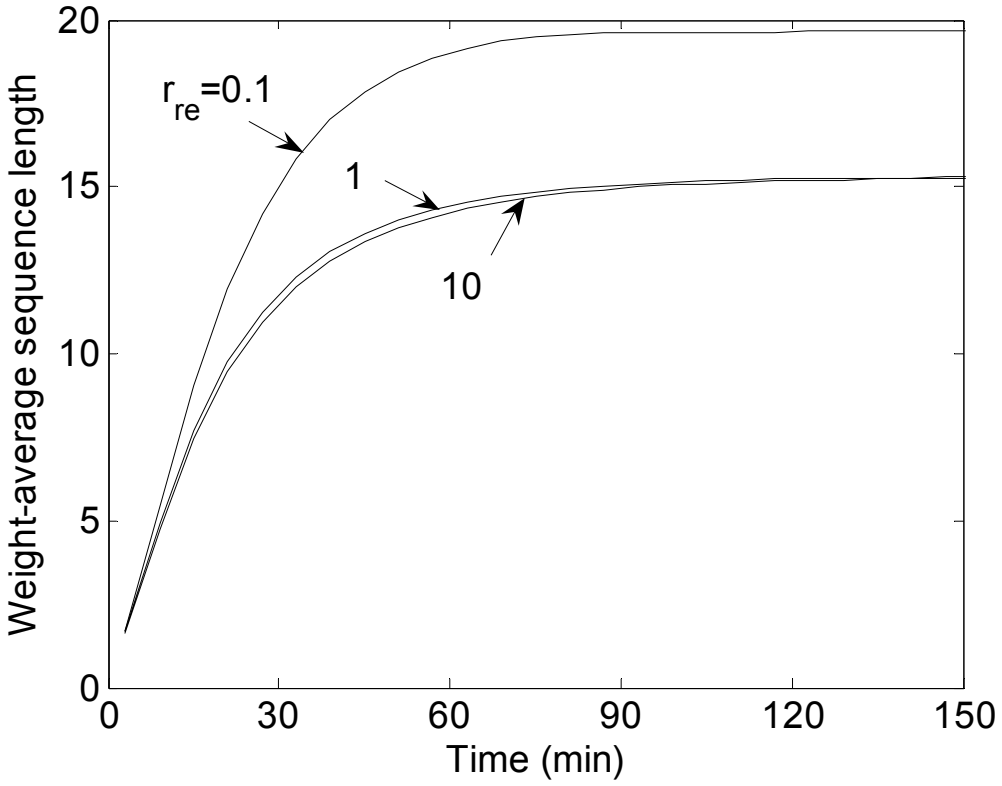

Figure 5.18 Effect of reactivity ratios on the weight-average chain sequence lengths of R_2 units.

reach desirable composition in the final products. However, the utilization of excessive amount of third monomer may give rise to large amount of oligomer derived from the third monomer, which may have a significant effect on the properties of final products. To investigate the effect of monomer ratio, *v* (i.e. the mole ratio of the third monomer to the second monomer), the value of *v* is varied from 0.1 to 0.5 while keeping other parameters same as the reference case. Figure 5.19 shows the effect of monomer ratio on the chain sequence length distributions. It is seen that the decrease of third monomer will significantly increase the incorporation of the second monomer and shift the distribution to a higher value of sequence length of R_2 units. Figure 5.20 shows there is a huge difference in average chain sequence length of R_2 units for different monomer ratio. It means that if there is little difference in monomer reactivity, the initial monomer ratio of BR_3B to BR_2B will dominate the chain compositions and sequence length distributions in the products. Therefore, in order to achieve desirable sequence length distributions, the first priority should be given to the initial monomer ratio that is going to be used in the reaction.

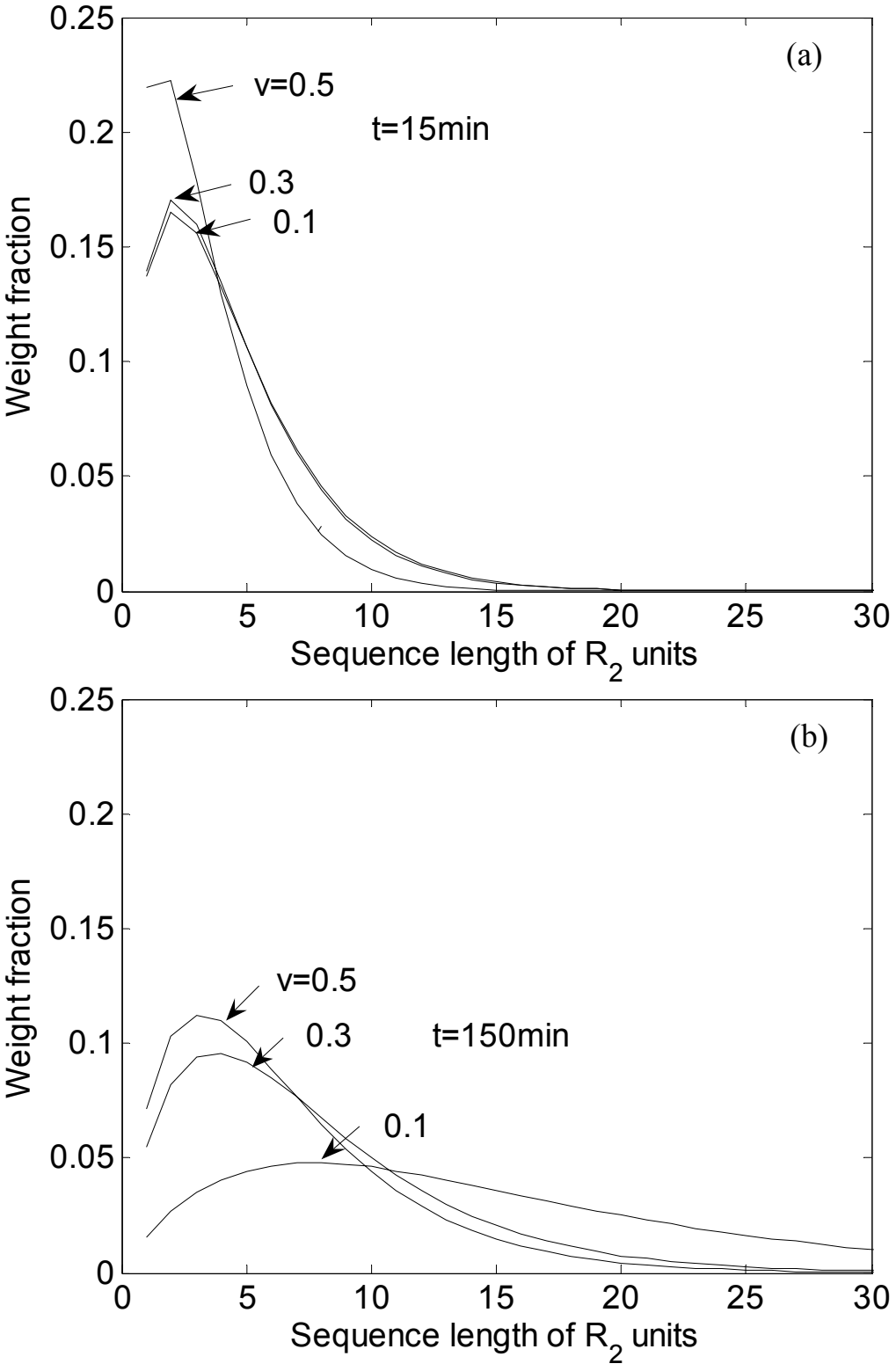

Figure 5.19 Effect of monomer ratio on the sequence length distributions of R_2 units ((a): t = 15 min; (b): t = 150 min).

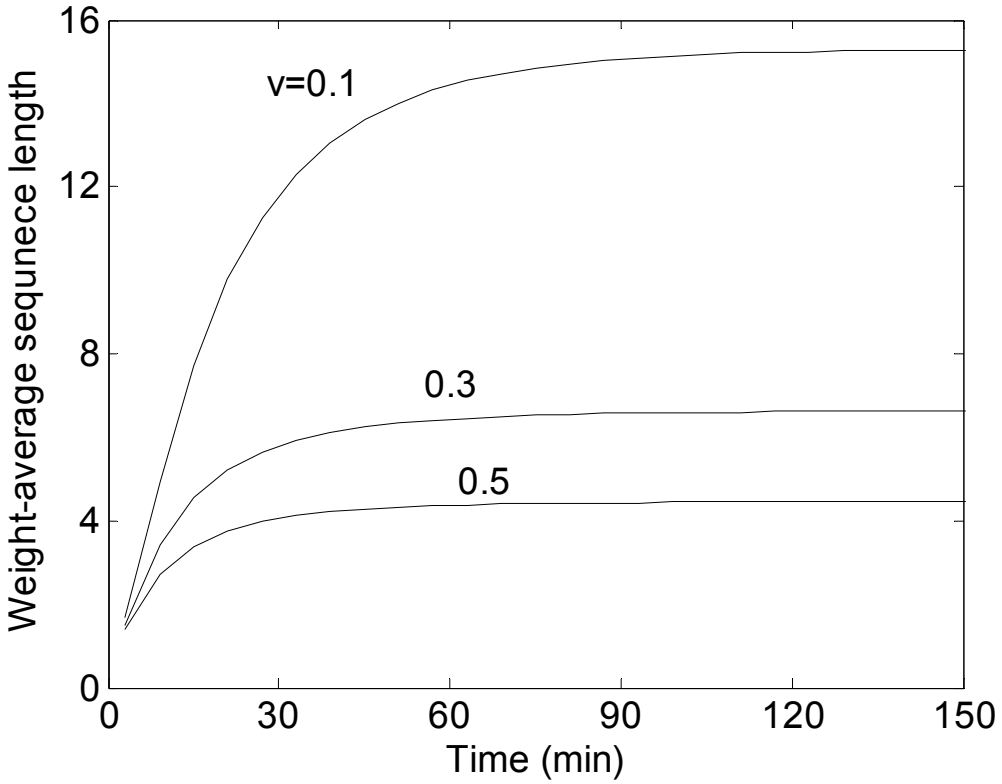

Figure 5.20 Effect of monomer ratio on the weight-average sequence length of R_2 units.

5.4 Conclusions

A new method, based on the probabilistic argument, has been developed to calculate the chain sequence length averages as well as sequence length distributions for condensation random copolymers. The procedure of this method is straightforward, and only a few parameters are involved. As long as we know the conversions of monomers and initial monomer ratios, chain sequence length distributions are readily obtained. Thus, this chain sequence length model can easily be incorporated with a melt polymerization. As an example, a semibatch process has been used to show the evolution of chain sequence length distributions and the change of average chain sequence lengths during the semibatch process. With the chain sequence length model and the end group model, important parameters that affecting chain microstructures such as end group ratio, reactivity ratio have been investigated. The chain sequence length model we developed provides a tool to estimate the chain microstructure for condensation terpolymers. With the relationship between physical properties and chain sequence length distributions available, it also allows us to design and optimize the chain microstructures.

5.5 Notation

A = functional end group A

A_0 = diphenol carbonate

B = functional end group B

B_0 = bisphenol A

E_A = moles of phenyl carbonate group at time *t*, mol

$E_{A,0}$ = initial moles of phenyl carbonate group, mol

E_B = moles of hydroxyl group from BR_2B at time *t*, mol

E_B' = moles of hydroxyl group from BR_3B at time *t*, mol

$E_{B,0}$ = initial moles of hydroxyl group from BR_2B, mol

$E_{B,0}'$ = initial moles of hydroxyl group from BR_3B, mol

i = number of R_2 units in a polymer chain

j = chain sequence length

K = equilibrium constant

k_1 = forward reaction rate, $L \cdot mol^{-1} \cdot min^{-1}$

k_2 = backward reaction rate, $L \cdot mol^{-1} \cdot min^{-1}$

m = chain type

$\bar{M}_n$ = number-average molecular weight

$\bar{M}_w$ = weight-average molecular weight

n = total number of units in a polymer chain

p = conversation of total hydroxyl end group

p_1 = conversation of monomer AR_1A

p_2 = conversation of monomer BR_2B

p_3 = conversation of monomer BR_3B

P = moles of phenol at time t, mol

r_1 = mole ratio of BR_2B to AR_1A

r_a = mole ratio of end group at the beginning of melt prepolymerization, $E_{A,0}/E_{B,0}$

r_{re} = reactivity ratio

SL_n = number-average chain sequence length

SL_w = weight-average chain sequence length

t = reaction time, min

V = volume of reaction system, cm^3

v = monomer ratio of BR_3B to BR_2B

Z = moles of polymer linage at time t, mol

Chapter 6

Crystallization of Bisphenol A Polycarbonate to Three-Dimensional Spherulites in Thin Films

6.1 Introduction

Chapter 2 and chapter 3 discussed the reaction kinetics of solid-state polymerization (SSP) of bisphenol A polycarbonate (BAPC) in a polymer particle. We have known that amorphous prepolymers produced from a melt transesterfication reaction process must be crystallized before the SSP. Otherwise, the SSP becomes impossible because amorphous BAPC prepolymer particles stick and fuse together at a temperature above T_g but below T_m, which significantly increases the diffusion path for phenol removal and hence reduces the reaction rate. Therefore, the crystallization of BAPC polymer is very essential and the crystalline part in a prepolymer particle serves the "scaffold" to maintain the thermal stability of a particle.

As we know, bisphenol A polycarbonate (BAPC) is a crystallizable polymer. However, it takes extremely long time, for example, hundreds of hours to achieve crystallization by thermal annealing at 170-205ºC[149] because the rigidity of polycarbonate chains prohibits the rearrangement of the polymer molecules to an ordered crystalline structure[150]. Therefore, when polycarbonate is melt-processed into disks, bottles, or films, the polymer essentially stays in the amorphous state.[26] To accelerate the crystallization rate, a number of techniques have been developed including treatments with plasticizers[151], nuclear agents[152], organic solvent liquids[153]

or vapors[154], super critical carbon dioxide[20], and even with mechanical means such as the processes of wet-drawn[155] and high-pressure molding[156]. Of all the available methods for the preparation of crystalline BAPC, the most facile technique is the method of solvent induced crystallization (SINC) in which polymer is exposed to either solvent vapor or liquid. The SINC proceeds first by the penetration of solvent molecules and then the swelling of the polymer matrix induced by the interaction between polymer chain segments. The molecular interaction reduces the glass transition temperature (T_g) of the polymer, greatly enhancing the chain mobility[157]. Then, the relaxation and rearrangement of polymer chains promoted by chemical environment lead to crystallization.

The studies of SINC of BAPC polymer have been carried over decades. It is well known that crystalline polycarbonate takes a spherulitic form.[150,158,159] However, the detailed morphological structures may vary from one to another depending a number of parameters, such as solvent, crystallization temperature, molecular weight of BAPC. Wilkes and Parlapiano[160] reported an interesting morphology of polycarbonate spherulites that have fibrils on the top surface of the spherulites. Zhao et al.[161] observed a spherulitic structure of polycarbonate with nano- and micro-sized protrusions. Although there are some reports available on the spherulitic structures of BAPC, most studies are focused on the process of VINC[153,154,157,162,163] but the morphology of BAPC polymer during the process of SINC is still not well understood. The studies of the morphological effect on the SSP are even fewer.

In this chapter, we will present the morphology of precipitated BAPC polymer particles and an interesting morphology of multi-layer stacked three-dimensional

BAPC spherulites formed by SINC in thin films. The melting temperature and crystallinity have been characterized by using DSC analysis. It is found that the newly discovered polycarbonate crystalline spherulites have much higher melting points and higher crystallinities than those precipitated crystalline particles from the bulk solution. The multi-layer stacked three-dimensional BAPC spherulites potentially can be used for many applications. For example, with higher melt temperature and a shorter diffusion path, the BAPC spherulites should be a good candidate for solid-state polymerization.

6.2 Experimental Section

6.2.1 Materials

BAPC samples in particle form prepared by the melt transesterification process were kindly supplied by LG Chemical (Daejon, Korea). A transparent BAPC film (Grade 8010MC, l = 635 μm) was provided by GE. Sample codes of 8k, 14k and 24k indicate the weight-average molecular weights are 8k, 14k and 24k, respectively. HPLC grade chloroform and acetone were used as received for the preparation of sample solutions and crystallization. Microscopic slide glasses and 2in x 2in x 1mm lime soda glasses were used as substrates for the preparation of BAPC thin films.

6.2.2 Preparation of Thin Films

BAPC polymers were dissolved in chloroform to give approximately 5-15% w/v solutions. Transparent amorphous thin BAPC films were prepared by the solution-casting method and the spinning-coating method. The film thickness can be

varied by changing the polymer concentrations. The film less than 1 μm in thickness was prepared by a P-6000 spin coater. The most important parameters affecting the film thickness are spinning speed and polymer concentration. After solution casting and spinning coating, polymer coated glasses were placed in the fume hood and vacuumed for further drying to remove solvent residue and moisture before crystallization. The films on the glasses were transparent after drying, indicating that no crystallization occurred. For those films made by solution-casting method, the thickness was measured by a Mitutoyo micrometer. For the films made by spinning-coating method, the thickness was measured by a Veeco Dektak 6M surface profilometer. To measure the thickness, a small spot of a thin film was dissolved by chloroform using a cotton swap. The height differences between the glass substrate and the film surface were averaged as the thickness of a thin film.

6.2.3 Crystallization and Characterization

The preparation of crystalline samples was done by immersing the films into an acetone bath at room temperature for 30 sec followed by air and vacuum drying. The morphological structures were investigated by an Amory 1820-D and a Hitachi S-4700 scanning electron microscopy (SEM) operating at 10-20kv and at 3-5kv, respectively. SEM samples were coated with Au-Pd in a Denton vacuum evaporator. Molecular weight was measured by GPC (gel permeation chromatography) equipped with Waters 410 differential refractometer operating at 30ºC. HPLC grade chloroform was used as a solvent carrier. The differential scanning calorimetry (DSC) analysis was used to measure melting temperature and crystallinity. The measurements were

carried out by a TA instruments Q100 in a temperature range from 40ºC to 300ºC with the heating rate at 10ºC/min.

6.3 Results and Discussions

6.3.1 Morphology of Spherulites

Precipitation from its bulk solution using an anti-solvent is a widely practiced method to prepare crystalline BAPC polymers for a SSP in industry.[130] BAPC crystalline particles also can be obtained by adding a poor solvent such as acetone into BAPC solution. Figure 6.1 shows the SEM photos of crystalline particles of 8k BAPC precipitated from its chloroform solution at room temperature. It is seen that the size of precipitated particle is in an order of hundred micrometers. Figure 6.1a shows that it is composed of a large number of highly aggregated spherulites. Because of local nonuniformity of crystallization rate, the size and uniformity of precipitated particles are poorly controlled in general. Figure 6.1b shows the size of spherulites is in the similar range as those reported before.[160]

To investigate the SINC of BAPC polymer in films, thin films (micrometer in thickness) and ultra-thin films (sub-micrometer in thickness) are prepared by the solution-casting method and the spinning-coating method, respectively. It is seen that as a thin BAPC film is immersed into the acetone bath, the transparent film quickly turns into opaque and then becomes whitish, indicating that the crystallization starts almost immediately when the film is in contract with acetone liquid. It is seen that both the diffusion of acetone liquid in polycarbonate matrix and crystallization are very fast. Figure 6.2 shows the SEM photos of spherulitic structure developed in the

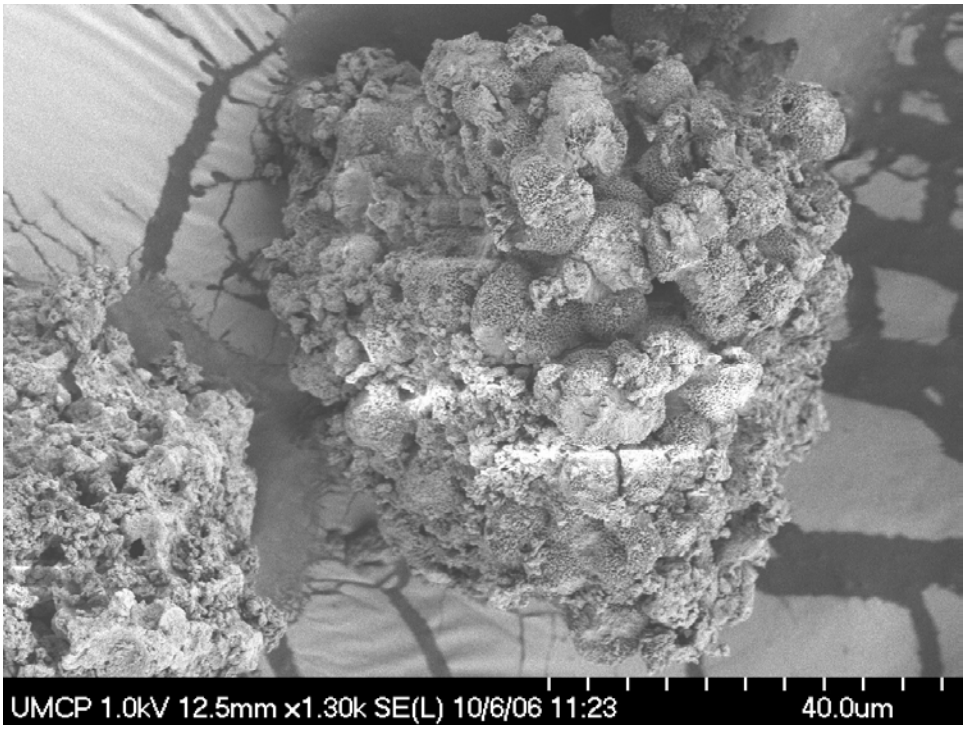

(a)

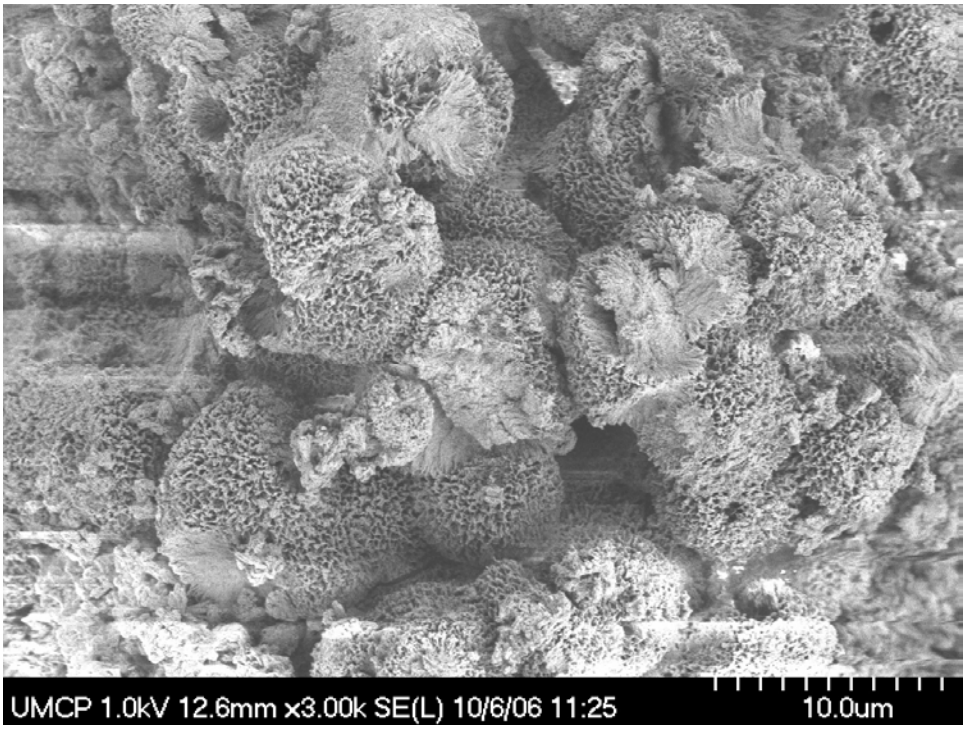

(b)

Figure 6.1 SEM photographs of the 8k BAPC particles precipitated from its chloroform solution by adding acetone (a) top view x1300; (b) top view x3000.

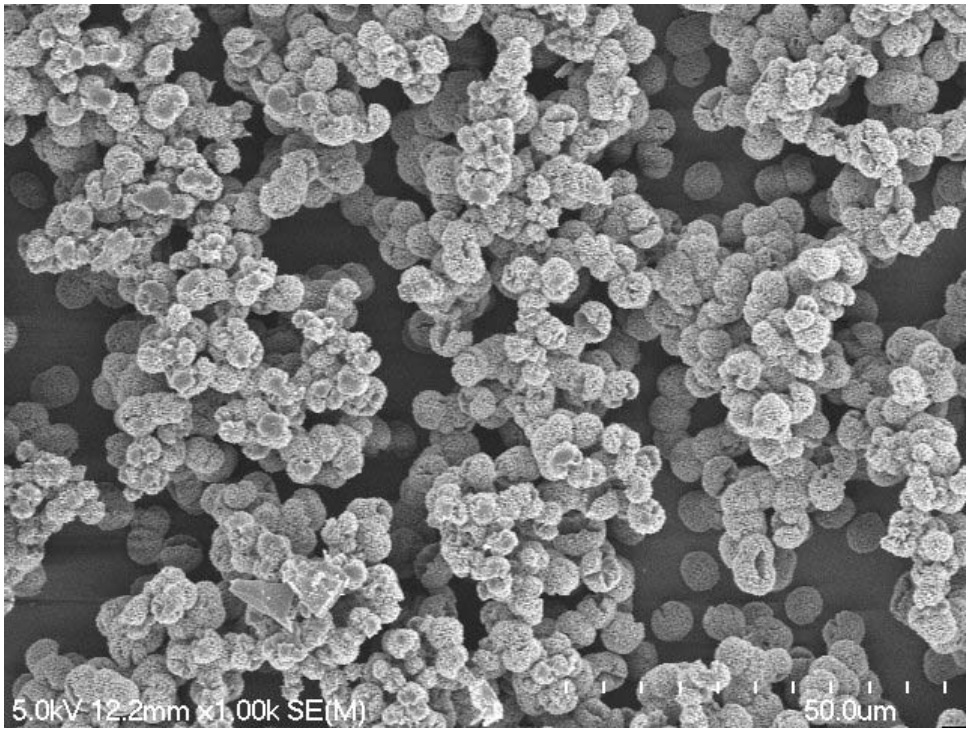

(a)

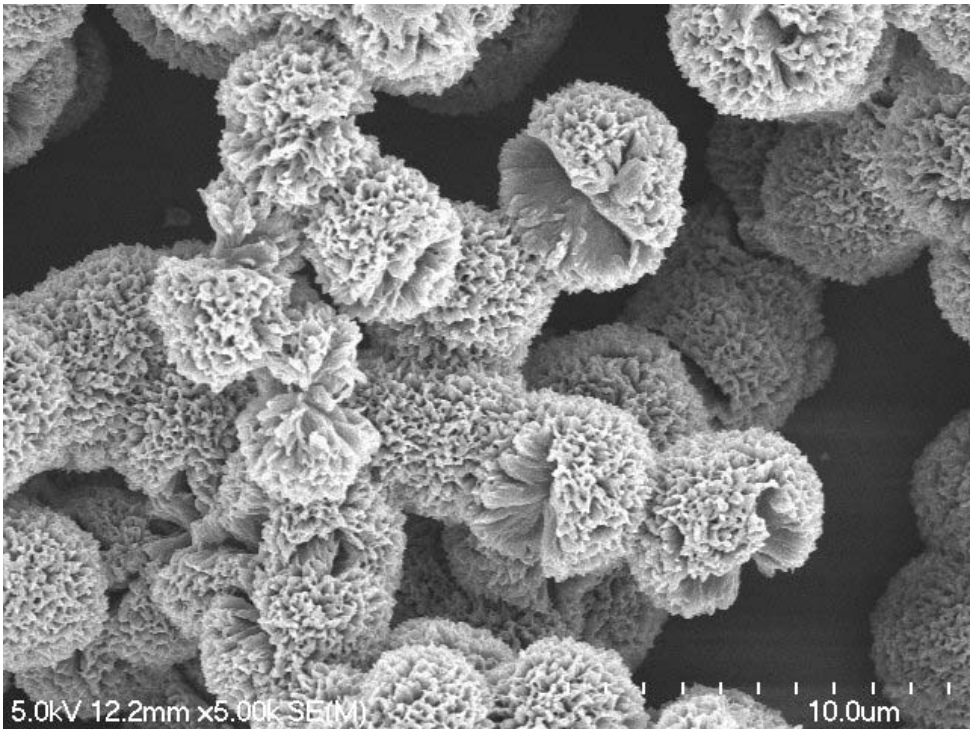

(b)

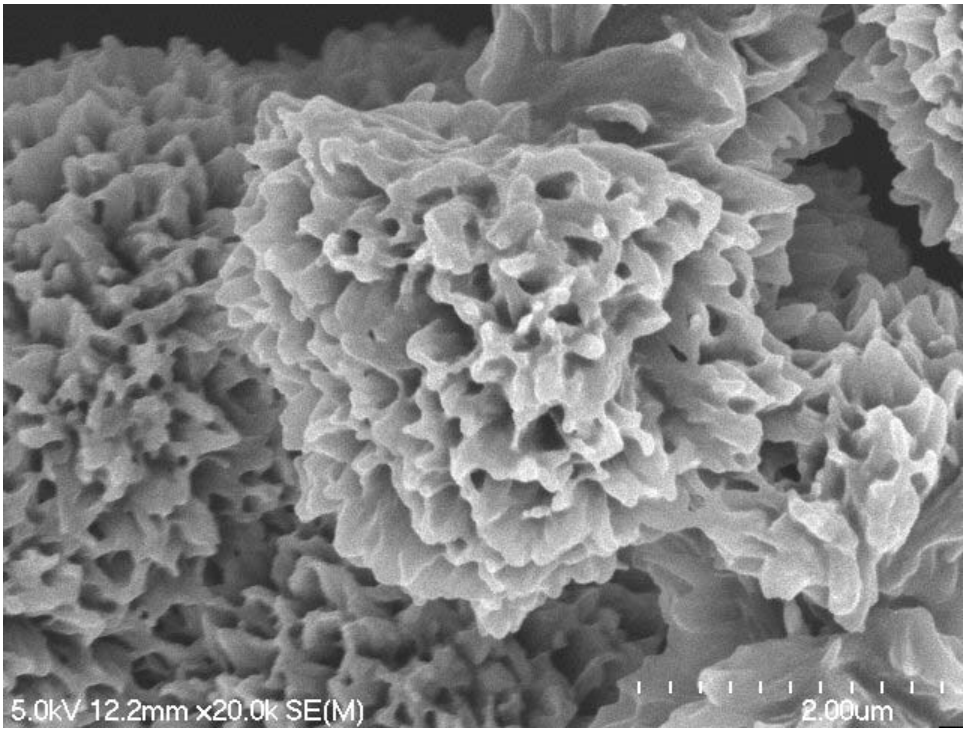

(c)

Figure 6.2 SEM photographs of the BAPC film of 8k crystallized by acetone at 25ºC:

(a) top view x 1 000; (b) top view x 5 000; (c) top view x 20 000 (l = 4.37 μm).

8k BAPC film after 30 sec's contact with acetone liquid. It indicates that acetone has a pronounced effect on the texture of BAPC thin films and the crystalline BAPC polymer shows spherulitic structures. The spherulites of BAPC polymer are in three-dimensional and formed as multiple layers as shown in Figure 6.2a. It also shows that some spherulites are separated from other neighbor particles, while most of others are in the aggregated form. Figure 6.2b is a close-up view of the spherulite particles. It is seen that they are about 2-5 μm in diameter and some spherulites have fully developed structure, while others have an opening filature where is not filled with BAPC polymer. Figure 6.2c shows more detailed nanoporous structures on the surface of spherulites. We can see that nanosized needlelike protrusions and porous holes are formed on the surface, which resembles a follower-like structure. Figure 6.3 shows the SEM photos for the BAPC film of 24k. Similar spherulitic structure with size about 3 μm in diameter is shown in Figure 6.3a. The cross sectional view of the crystallized polymer film is shown in Figure 6.3b. Note that the crystallization occurs from the film top to bottom and three-dimensional spherulites are indeed formed as multiple layers, indicating that acetone not only fully penetrates polymer thin films, but also crystallizes the whole film within 30 sec. Turska et al.[163] reported that acetone can penetrate BAPC films in 50 μm thickness less than 30 sec at 20ºC. Thus, in our experiments the 30 sec's immersion at room temperature is long enough to allow acetone molecules to fully penetrate into the BAPC thin films whose thickness is less than 10 μm. Interestingly, in contrast to what was reported by Wilkes and Parlapiano[159], no fibril structure is observed on the top of three-dimensional spherulitic bodies for the films that are less than 10 μm in thickness. It is also noted

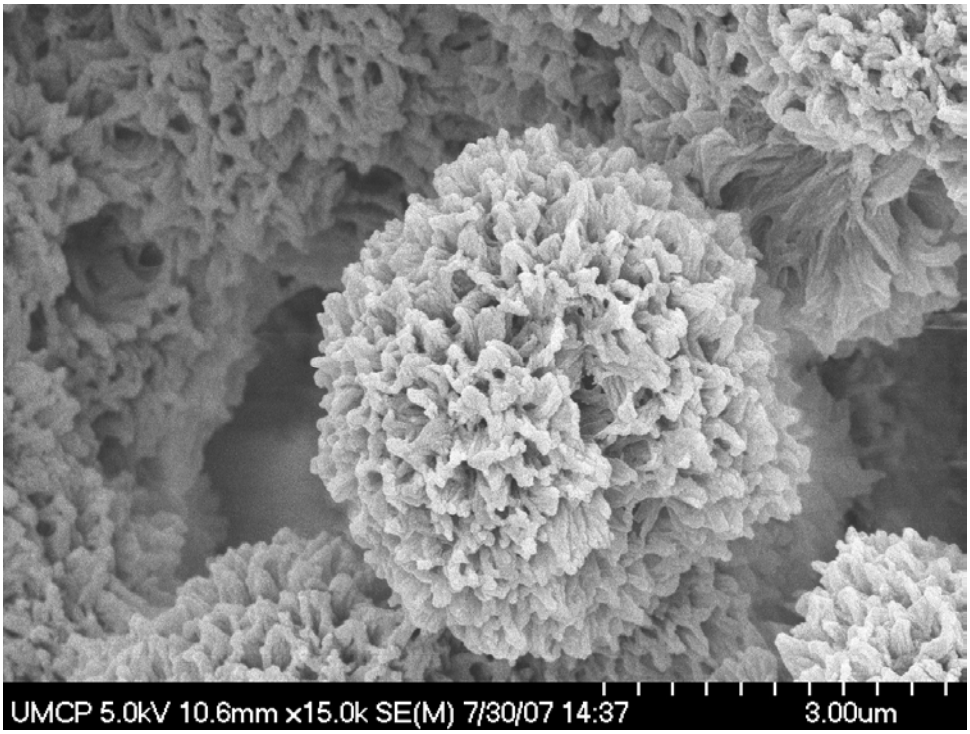

(a)

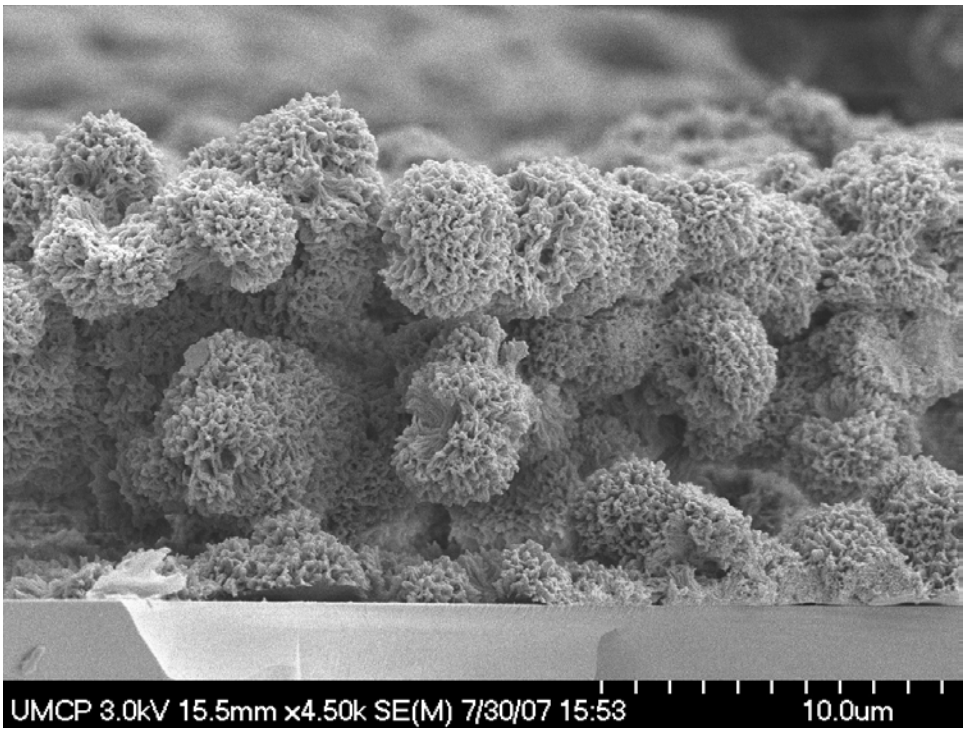

(b)

Figure 6.3 SEM photograph of the BAPC film of 24k crystallized by acetone at 25ºC:

(a) top view x 15 000; (b) cross sectional view x 4 500 (l = 4.80 μm).

that the three-dimensional BAPC spherulites formed as multiple layers throughout the film, to the author's best knowledge, has never been reported in the literature.

It is obvious that one of the important factors affecting the diffusion and crystallization rate is the film thickness, which may also have a significant impact on the structure of spherulites and the morphology of crystalline BAPC. As a comparison, we used two other films with the thickness varied by the order of magnitude. The transparent film with 0.84 μm in thickness was prepared by the spinning-coating method (8k BAPC), and the other one with thickness of 635 μm was kindly supplied by GE (8010MC). The same crystallization procedure was applied for both films. Figure 6.4 shows the SEM photos of the BAPC film provided by GE. It is seen that the surface crystallization does not occur everywhere after 30 sec as shown in Figure 6.4a. Figure 6.4b shows a closer view on the spherulites. They are connected each other and lack of voids between spherulite particles. The structure of these spherulitic bodies is of 3-D in nature, but the spherulite surface is not as porous as those shown in Figures 6.2 and 6.3. However, these spherulites are very similar with those shown in the paper by Wilkes and Parlapiano[159]: 3-D spherulites are mainly composed of fibril structure. Figure 6.4c shows that there is only a very shallow crystallized layer in the film, indicating that the main body of film remains unchanged.

For the ultra-thin film, i.e. sub-micrometers in thickness, the thickness is even less than the diameter of fully developed 3-D spherulites shown in Figures 6.2 and 6.3. Figure 6.5 shows the morphology of the ultra-thin film after immersion in the acetone bath. In contrast to the spherulites shown in Figures 6.1 and 6.2, spherulites are

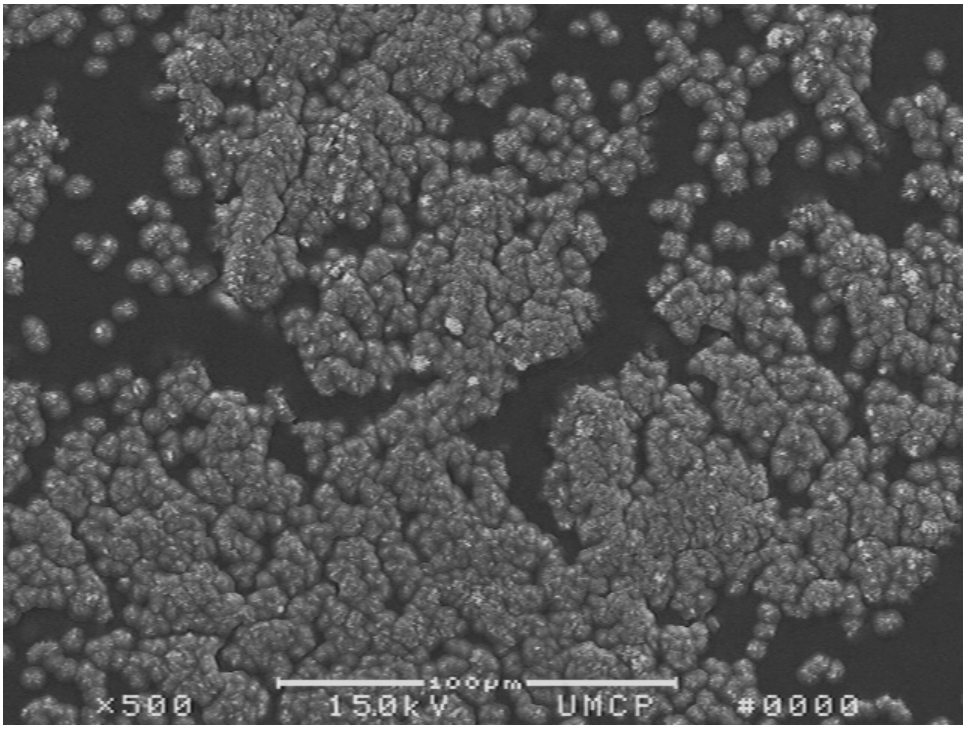

(a)

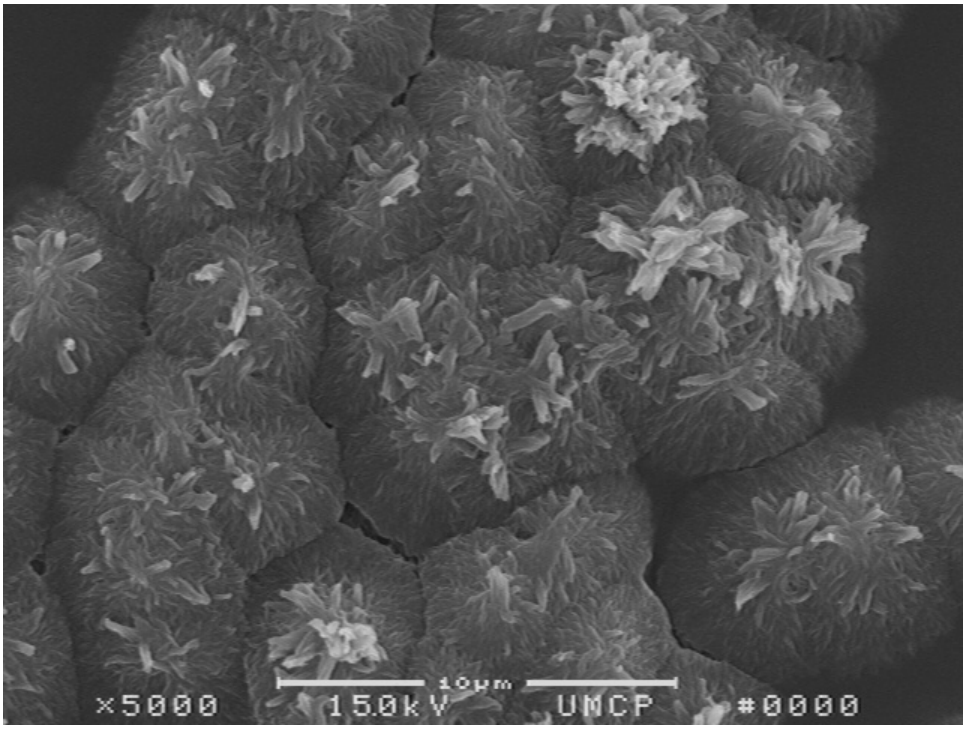

(b)

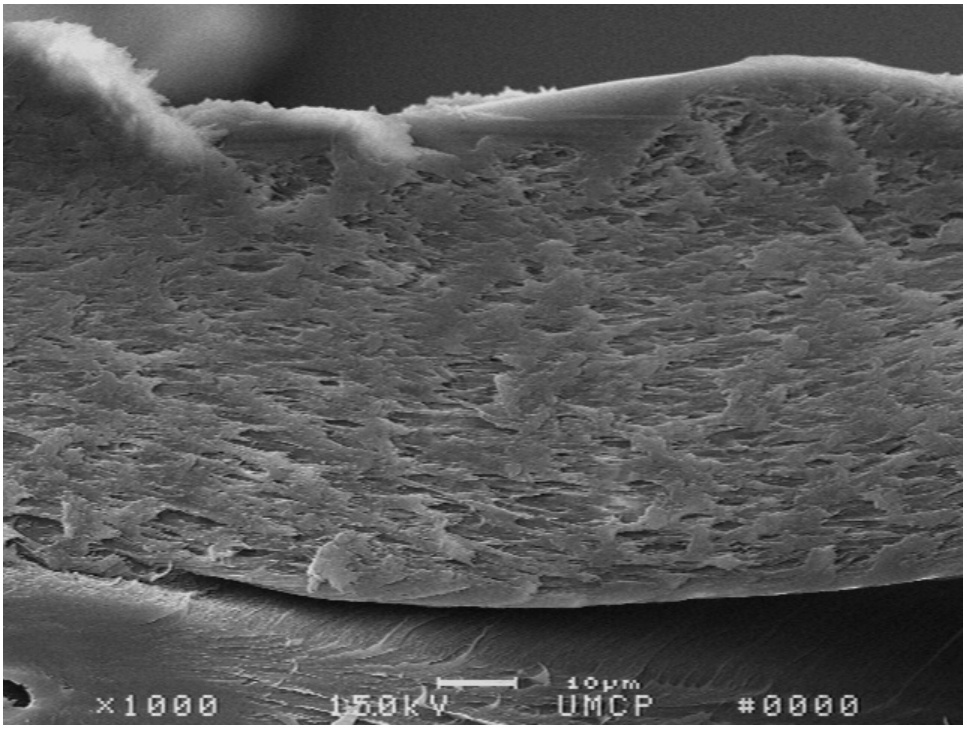

(c)

Figure 6.4 SEM photographs of the 8010MC BAPC film crystallized by acetone at 25ºC: (a) top view x 500; (b) top view x 5 000; (c) cross-sectional view x 1 000 (l = 635 μm).

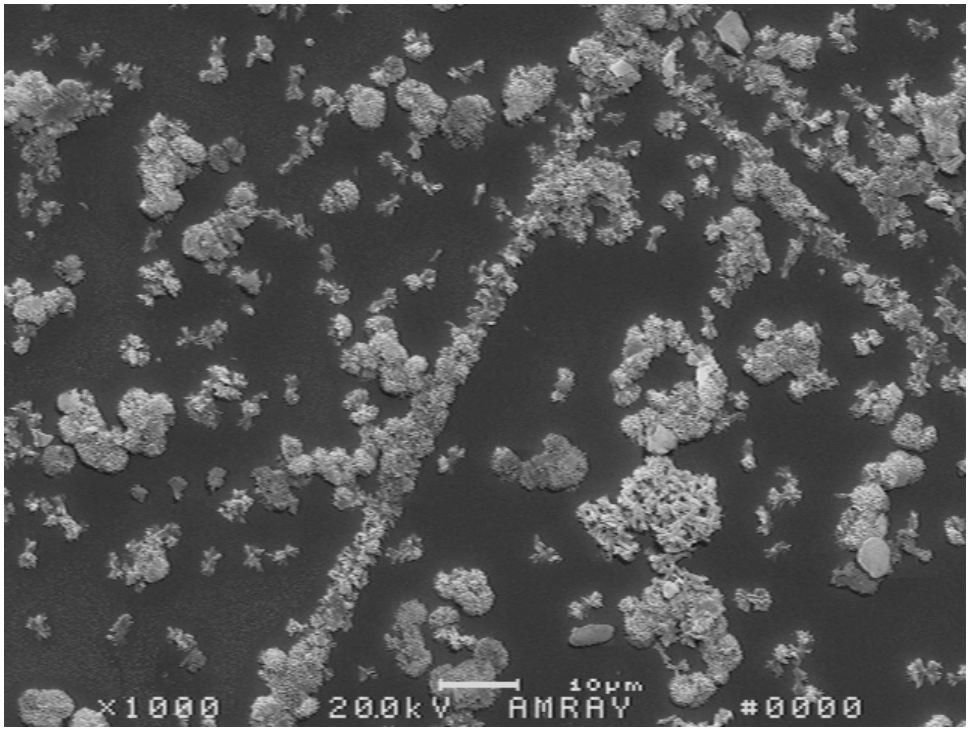

(a)

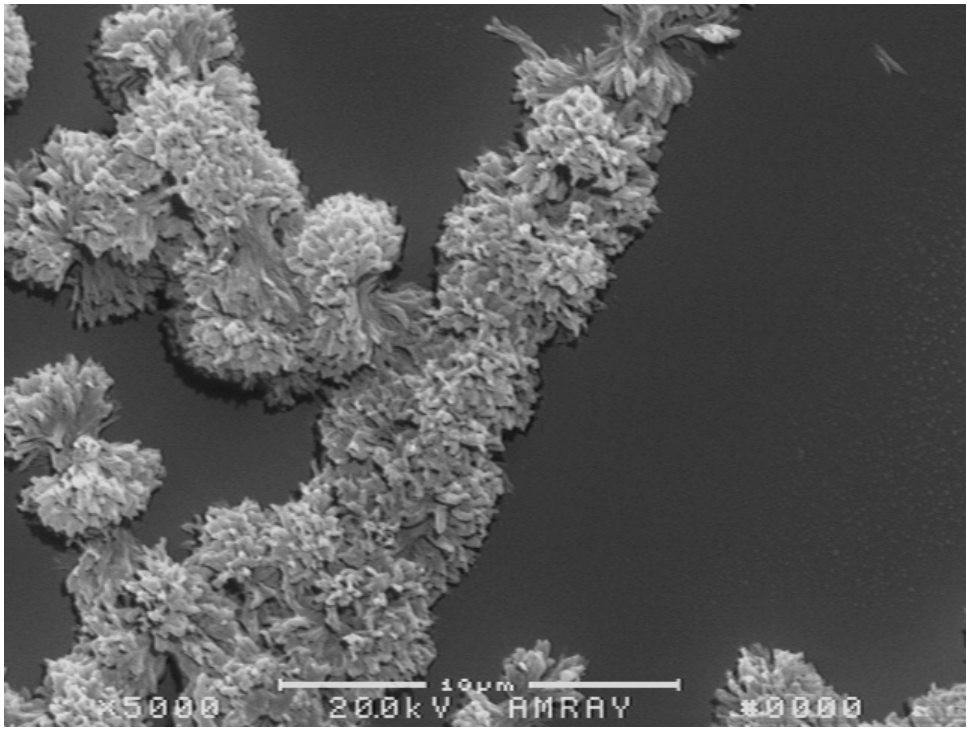

(b)

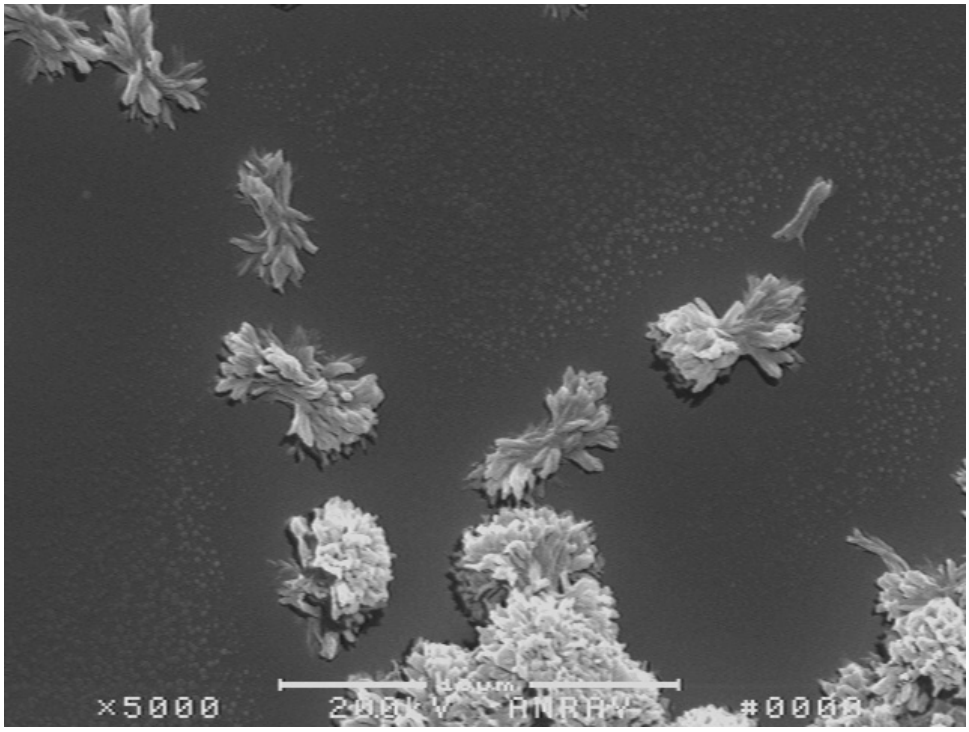

(c)

Figure 6.5 SEM photographs of the 8k BAPC ultra-thin film crystallized by acetone at 25ºC: (a) top view x 1 000; (b) top view x 5 000; (c) top view x 5 000 (l = 0.84 μm).

incomplete, more isolated, and no vertically stacked spherulites has been observed. Figure 6.5a shows that the shape and size of spherulites are not uniform. Some show the intermediate morphologies of spherulitic structure, meaning that they remain at an intermediate stage of crystallization, while others show the aggregated feature. A close-up image is shown in Figure 6.5b. It is seen that the size of spherulitic structure is even larger than the film thickness, which means that the molecular interaction between acetone and BAPC polymer is strong enough to drag polymer material towards the nuclei and cause the spherulitic particles continue to grow. However, due to the large difference between the film thickness and the diameter of fully developed spherulites, it is impossible for each one of nuclei to attract enough polymer material from its neighbor to form a full spherulite. Therefore, a great number of spherulitic particles only remain at a certain intermediate stage shown in Figure 6.5c. From the intermediate features such as anisotropic rod and sheaf-like structures, it may be not appropriate to visualize that the formation of spherulitic growth is nucleated in the center, followed by radiating growth simultaneously in all radial directions. One the contrary, Figure 6.5 suggests that the formation of BAPC spherulites undergoes in a stepwise manner similar as what Desai and Wilkes[164] proposed for the SINC of poly(ethylene terephthalate): nucleus → rod → sheaf → spherulite.

It is obvious that film thickness has a significant impact on the morphology of BAPC polymer. As the film thickness increases, the diffusion rate of acetone decreases. For a given immersion time, acetone may not be able to fully penetrate into the whole film. It is well known that as acetone molecules penetrate the polymer matrix, both melting and glass transition temperatures are depressed. It does so to a

certain extent, the interaction allows polymer chains to rearrange into the thermodynamically favored crystalline state, and then the crystallization occurs. Therefore, as film thickness decreases, the volume fraction of acetone increases, which significantly reduces T_g. The relaxation rate and mobility of polymer chains are greatly enhanced. As a result, the film thickness not only affects the crystallization temperature, but also the crystallization rate. Moreover, the large fraction of acetone in the film provides more physical interaction between acetone molecules and polymer chains. This allows polymer chains to relax in a great extent to drag towards nuclei, form a ball-like 3-D structure and create voids between spherulites. On the other hand, for a thick film, lower fraction of acetone may not be able to provide enough mobility for polymer chains to form distinctive spherulites and create voids. If the crystallization takes place under the acetone vapor environment, the interaction is further reduced and much longer time is required to reach crystallization. The weak drag force may not be able to drag local chains to form a 3-D spherulitic structure because the relaxation is only confined onto a two-dimensional space. Thus, the resulting morphology of SINC is also dependant upon the film thickness. In order to obtain the morphology shown in Figures 6.2 and 6.3, the film thickness has to be kept in a certain range, i.e. the same order of the diameter of spherulites.

In contrast, the spherulties in the precipitated BAPC particles are agglomerated together during the crystallization or further drying processes. It is seen that the morphology is poorly controlled for these precipitated particles and they have much less porous structures on the surface.

6.3.2 Differential Scanning Calorimetry (DSC)

The melting temperature and crystallinity are of interest for the spherulites obtained in the thin-film crystallization of BAPC. It is reported that the melting temperature (T_m) for the SINC of polycarbonate has a wide range, for example, 170-220ºC[100], or 220-230ºC[4]. Figure 6.6 shows the comparison of DSC curves of three BAPC spherulite samples collected from crystallized thin films and those samples precipitated from the bulk solution. More detailed results of melting temperatures are listed in Table 6.1. It is seen that the melting temperatures of spherulite samples obtained from thin-film crystallization have higher values than those precipitated particles, while the melting temperatures of precipitated particles fall in the range that was reported[4]. It suggests that these spherulites have a better ordered crystal structure compared to those precipitated particles.

The crystallinity, x_c, is calculated by the following equation[166].

$$x_c = \frac{\Delta H_m}{\Delta H_m^0} \tag{6.1}$$

where ΔH_m^0 is the heat of fusion of fully crystalline BAPC (109.6 J/g[3]), and ΔH_m is the heat of fusion of the sample measured. Table 6.1 shows the crystallinities for different BAPC samples. It is seen that the crystallinities of spherulites obtained from thin-film crystallization have higher value than those precipitated particles. However, the crystallinity values of spherulites are still about 30%, indicating that the major fraction in a spherulite is still amorphous portion.

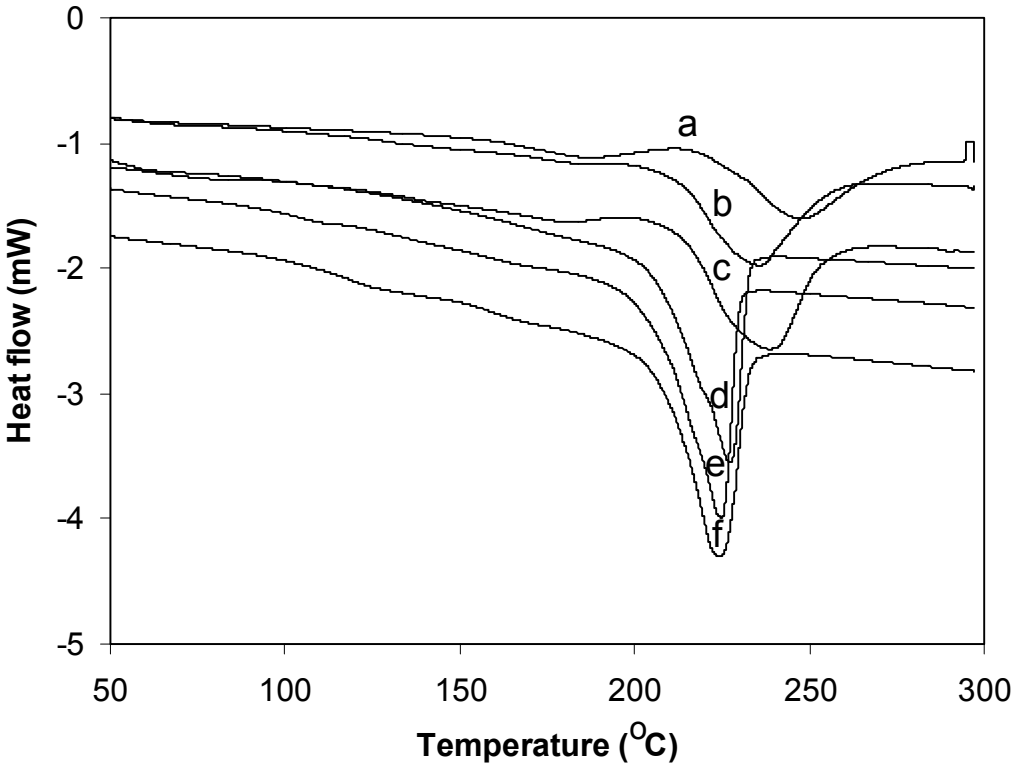

Figure 6.6 DSC curves of BAPC crystalline spherulites and precipitated particles: a.24k spherulites; b. 8k spherulites; c.14k spherulites; d.14k precipitated particles; e. 8k precipitated particles; f. 24k precipitated particles.

Table 6.1 Characterization of thermal properties by DSC analysis.

Samples	T_m (ºC)	$T_{m,o}$ (ºC)	ΔH_m (J/g)	x_c (%)
8k film	235.27	212.54	35.53	32.4
14k film	238.00	213.98	33.65	30.7
24k film	247.29	224.19	29.50	26.9
8k particle	224.86	206.66	30.21	27.5
14k particle	227.36	209.99	27.30	24.9
24k particle	224.17	208.58	23.50	21.4

Note: $T_{m,o}$ = onset melting temperature.

6.4 Conclusions

An interesting morphology of multi-layer stacked three-dimensional porous spherulites has been reported in the process of SINC of BAPC thin films. The morphology is different from what have been presented in the past literature. The film thickness is one of key parameters that determine the resulting morphology. In order to obtain the multi-layer stacked three-dimensional BAPC spherulites, film thickness has to be kept in a certain range, i.e. the same order of the diameter of spherulites. The crystalline particles precipitated from the bulk solution usually have much less porous structures on the surface. Higher melting temperatures and crystallinities of spherulites obtained by thin-film crystallization have been observed, suggesting that a better ordered crystal structures formed. The porous, multi-layer stacked three-dimensional BAPC spherulites potentially can be used for many applications. For example, they would be a good candidate for the SSP to accelerate the reaction rate and molecular weight increase.

6.5 Notation

l = film thickness, μm

T_g = glass transition temperature, °C

T_m = melting temperature, °C

$T_{m,0}$ = onset melting temperature, °C

x_c = crystallinity

ΔH_m = heat of fusion of the sample

ΔH_m^0 = heat of fusion of fully crystalline BAPC

Chapter 7

Conclusions and Recommendations

7.1 Conclusions

This study can be divided into the following four parts: 1) Particle modeling of solid-state polymerization of bisphenol A polycarbonate; 2) Reactor modeling of solid-state polymerization of bisphenol A polycarbonate in a moving packed bed; 3) Modeling of chain sequence length distributions; and 4) Solvent-induced crystallization of polycarbonate thin films.

In the part of particle modeling, an end group model and a molecular species model have been developed to study the reaction kinetics of solid-state polymerization of bisphenol A polycarbonate in a single polymer particle. A new back calculation method has been developed to determine the initial end group concentrations for the end group model. The calculation of initial conditions in a prepolymer for the molecular species model has been improved by using the back calculation method and the theory of Flory most probable distribution, which allows us to more accurately determine initial moments. With the solid-state polymerization models, the time evolution of complete polymer chain length distributions in a polymer particle at different radial positions under various reaction conditions can be calculated. Simulation results show that the end group mole ratio in a prepolymer has a significant effect on the molecular weight increase, and that large polymer particles exhibit strong intraparticle diffusion resistance to phenol removal and hence the chain length distribution varies significantly from position to position in the polymer

particle. It is also found that the reaction kinetics of solid-state polymerization is not dependent on the prepolymer molecular weight *per se*, but it depends strongly on the end group mole ratio in the starting prepolymer. To increase reaction rate and molecular weight of solid-state polymerization, a method has been proposed to adjust end group ratio for a prepolymer by blending with another prepolymer. With the molecular species model, weight-average molecular weight can be obtained in case of blending prepolymers, which is, however, incapable for the end group model. The redistribution of end groups in a particle by remelting and recrystallization has been reinvestigated. Both number- and weight-average molecular weights have been studied during the remelting and secondary solid-state polyemrization, which provides a deeper understanding in the mechanism of remelting and its effect on the further solid-state polymerization.

In the part of reactor modeling, a dynamic continuous process model has been developed for the solid-state polymerization of bisphenol A polycarbonate in a moving packed bed reactor. The process model consists of a macroscopic reactor model and a microscopic polymer particle model to calculate the reactor temperature profiles and the polymer properties. Here, a new approach is used to treat heat transfer in reactor scale and mass transfer in particle scale separately. The effects of various reactor design and operation parameters on the performance of the solid-state polymerization reactor have been analyzed and evaluated through modeling studies. Simulation results show that a large scale moving packed bed reactor can have significant nonuniformities of temperature and molecular weight, e.g. in a dynamic state such as a startup process. This new approach not only allows us to account for

the nonuniformities in the reactor scale, but also to consider the nonuniformities in the particle scale, which helps us to have a better understanding of the performance of solid-state polymerization in a moving packed reactor.

In the part of copolycondensation modeling, a new method, based on the probabilistic argument, has been developed to calculate not only the chain sequence length averages but also the chain sequence length distributions for condensation terpolymers. The chain sequence length model has been verified by comparing chain sequence length averages with the recursive method, and by comparing with Flory most probable distributions. This model has been coupled with a melt copolycondensation process in a semibath reactor to show the evolution of chain sequence length distributions and the change of chain sequence length averages. To simplify the model complexity, a new end group model has been developed to replace the molecular species model for the description of a melt polymerization process. With the chain sequence length model and the end group model, important parameters that affect chain microstructures such as end group ratio, reactivity ratio and monomer ratio have been investigated in the copolycondensation process. The chain sequence length model we developed provides a tool to estimate the chain microstructure. With the relationship between physical properties and chain sequence length distributions available, it also allows us to design and optimize physical properties for the condensation terpolymers by manipulating chain microstructures.

In the part of thin-film crystallization, an interesting morphology of crystalline bisphenol A polycarbonate has been reported: multi-layer stacked three-dimensional porous spherulites. The morphology is different from what have been presented in the

past for the solvent-induced crystallization of bisphenol A polycarbonate polymer. Generally, the crystalline particles precipitated from the bulk solution usually have much less porous structures on the surface. It was found that the film thickness is one of the key parameters that dominate the resulting morphology. Higher melting temperatures and crystallinities of spherulites obtained by thin-film crystallization have been observed, suggesting that a better ordered crystal structures formed.

7.2 Recommendations

In the particle modeling, simulation results show that the particle size of a prepolymer has a significant effect on the reaction rate and molecular weight increase. The diffusion of phenol condensate is a rate-controlling step for such relative big particles. It is of interest to understand in what conditions the translational diffusion of end groups would come to play in an important role, and how it would affect the reaction rate, and molecular weight increase, etc.

In the reactor modeling of solid-state polymerization in a moving packed bed, plug flows were assumed for both gas and solid phases. For a more complicated reactor system such as side feed of purge gas or agitation involved, the assumption of plug flows may not be good enough. A more detailed analysis of momentum transfer and heat transfer might be required to know the velocity field and the temperature field. For example, using computational fluid dynamics (CFD) would be a good method to try.

For the modeling of chain sequence length distributions, it is important to apply this method to other step-growth polymerization processes such as solid-state

polymerization. It would be interesting to see how the particle size affects the chain sequence length distributions at different particle radial positions.

The solvent-induced crystallization of polycarbonate thin films results in interesting multi-layer stacked three-dimensional spherulites. It would be of interest to investigate other solvents and other polymers such as poly(ethylene terephthalate) and nylon.

Appendix A Analysis of Heat Transfer in a Polymer Particle

In our modeling, it is assumed that there is no temperature gradient inside the particles. Let us consider the following energy balance equation for a nonisothermal particle:

$$\rho_s C_{p,s} \frac{\partial T_s}{\partial t} = k_s \nabla^2 T_s + r_p \left(-\Delta H_r\right), \quad \text{at } t = 0,\ T_s = T_{s,0} \tag{A.1}$$

where ρ_s is the polymer density, $C_{p,s}$ is the heat capacity, k_s is the thermal conductivity, r_p is the reaction rate, and ΔH_r is the reaction heat. The polymerization rate is given by

$$r_p = \frac{k_1}{\left(1-x_c\right)}\left[\frac{[P]}{K}\left([E_A]_0 - [E_A] + [Z]_0\right) - [E_A]\left([E_A] - [E_A]_0 + [E_B]_0\right)\right] \tag{A.2}$$

The boundary conditions for eq (A.1) are:

$$\frac{\partial T_s}{\partial t} = 0 \text{ at } r = 0 \tag{A.3}$$

$$-k_s \frac{\partial T_s}{\partial r} = h\left(T_s - T_b\right) \text{ at } r = R \tag{A.4}$$

where T_b is the temperature of the bulk gas phase.

The heat transfer coefficient from the bulk gas phase to the particle surface is estimated from the following correlation:

$$Nu = 2 + 0.6\,\mathrm{Re}^{1/2}\,\mathrm{Pr}^{1/3} \tag{A.5}$$

where *Nu* is the Nusselt number defined as $Nu = \frac{hd}{k}$. If $Nu = 2$ is used, the heat transfer coefficient will have a minimum value and the particle temperature nonuniformity will be the most significant. Figure A.1 shows the radial temperature

profiles in a spherical particle of radius 0.15 cm. It is observed that this relatively large polymer particle reach a temperature uniformity in about 12 sec, which is extremely short compared to the particle residence time in the reactor (10 hr).

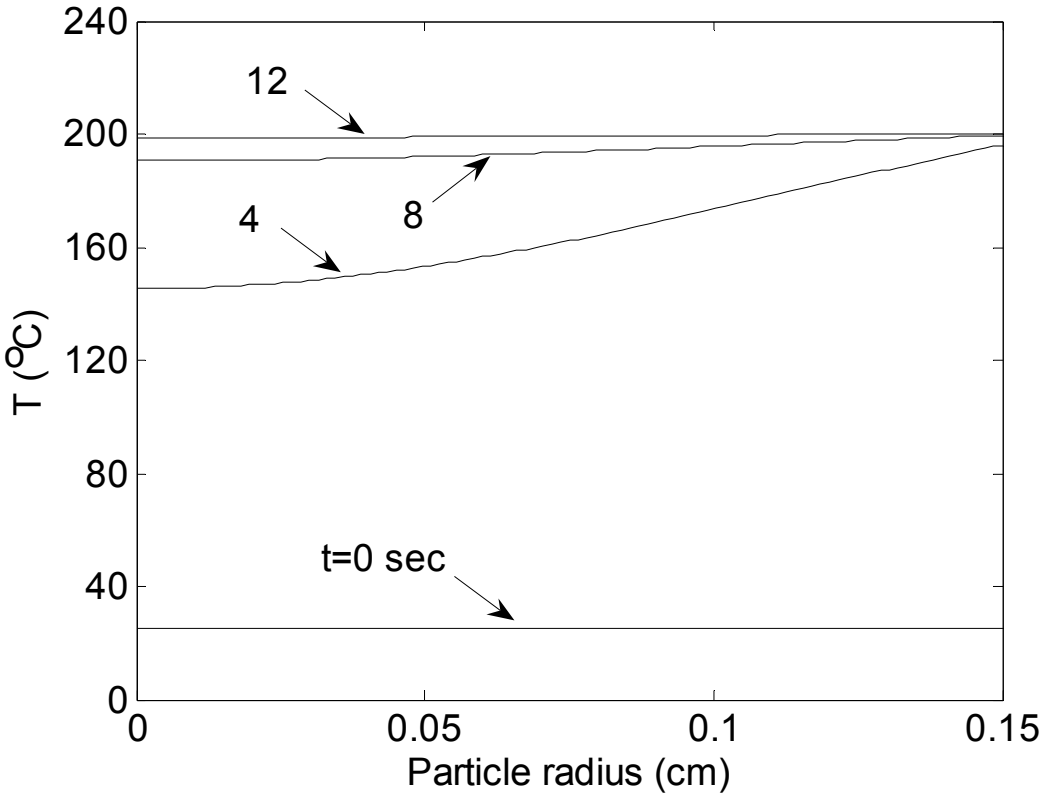

Figure A.1 Dynamic simulation of radial temperature profiles in a polymer particle of radius 0.15 cm: Initial temperature = 25ºC, the purge gas temperature = 200ºC, $\left(-\Delta H_r\right) = 6.8$ kcal/mol, $C_{p,s} = \left(0.559T + 249.17\right)/254.3$ (J·g^{-1}·K^{-1}), k_s =0.156 J·cm^{-1} ·K^{-1}·min^{-1}.

Appendix B Pressure Profile in the Reactor

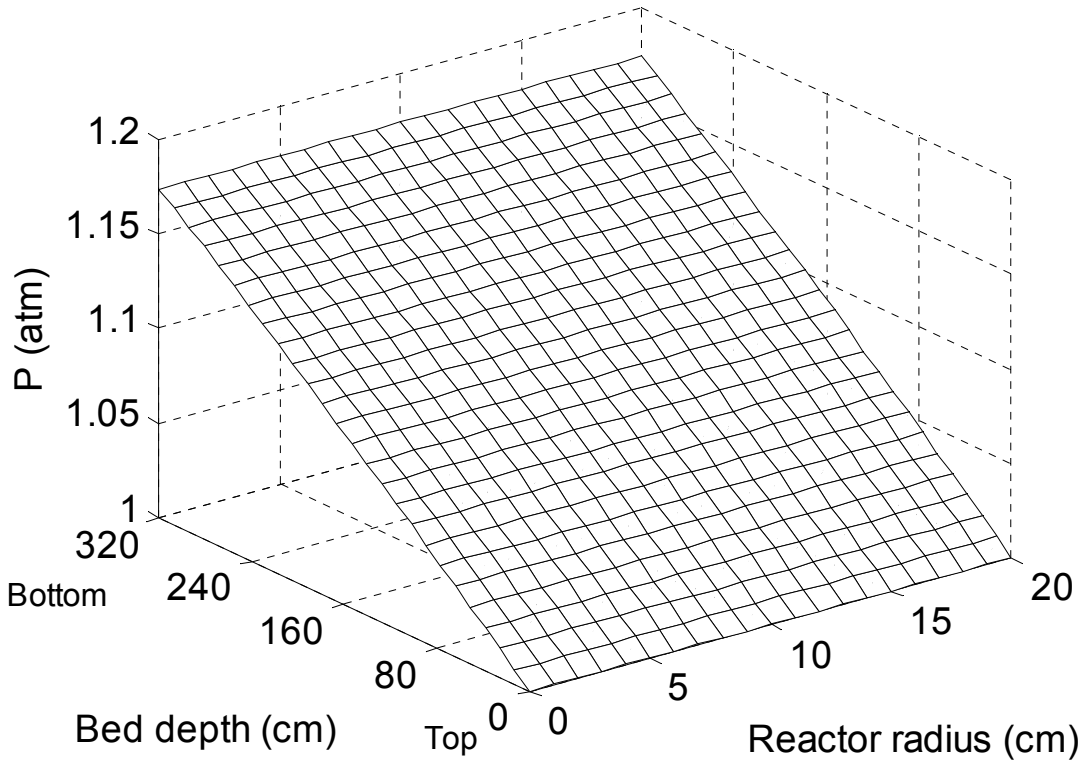

Figure B.1. Steady state pressure profiles in the reactor (standard operating conditions).

Bibliography

1 Fukuoka, S.; Tojo, M.; Hachiy, H.; Aminaka, M.; Hasegawa K. Green and Sustainable Chemistry in Practice: Development and Industrialization of a Novel Process for Polycarbonate Production from CO_2 without Using Phosgene. *Polymer J*. **2007**, *39*, 91-114.

2 Brunelle, D. J.; Korn, M. R. *Advances in Polycarbonates*; ACS symposium series, 898: Washington D.C., 2005.

3 Schnell, H. *Chemistry and Physics of Polycarbonates*; Wiley: New York, 1964.

4 Sohn, S. Crystallization Behavior of Bisphenol-A Polycarbonate: Effects of Crystallization Time, Temperature, and Molar Mass. Ph.D. Dissertation, Virginia Polytechnic Institute and State University, **2000**.

5 Brandrup J.; Immergut, E. H.; Grulke, E. A. *Polymer Handbook*; 4th Ed., Wiley: New York, 1999.

6 Babad, H; Zeiler, A. G. Chemistry of Phosgene. *Chem. Rev.*, **1973**, *73*, 75-91.

7 King, J. A. Jr. Synthesis of Polycarbonates. In: Legrand, D. G.; Bendler, J. T. *Handbook of Polycarbonate Science and Technology*; Marcel Dekker: New York, **2000**.

8 Kim, Y. S. Modeling of A Melt Polymerization Process for the Synthesis of Bisphenol A Polycarbonate. Ph.D. Dissertation, University of Maryland at College Park, **1992**.

9 Fukawa, I.; Fukuoka, S.; Komiya, K.; Sasaki, K. Porous, Crystallized, Aromatic Polycarbonate Prepolymer, A Porous, Crystallized Aromatic Polycarbonate, and Production Methos. U.S. Pat. 5,204,377, **1993**.

10 Fox, D. W. Polycarbonate Polymerization Process. U.S. Pat. 3,144,432, **1964**.

11 Kim, Y. S.; Choi, K. Y. Multistage Melt Polycondensation of Bisphenol-A and Diphenyl Carbonate to Polycarbonate. *J. Appl. Polym. Sci*. **1993**, *49*, 747-764.

12 Woo, B. G.; Choi, K. Y.; Song, K. H. Melt Polycondensation of Bisphenol A Polycarbonate by a Forced Gas Sweeping Process. *Ind. Eng. Chem. Res*. **2001**, *40*, 1312-1319.

13 Komiya, K.; Kawakami, Y.; Okamoto, H. Wire-Wetting Fall Polymonization

Process for the Production of Polycarbonates. U.S. Pat., 5,589,564, **1996**.

14 Fox, D. W. Aromatic Carbonate Resins and Preparation thereof. U.S. Pat. 3,153,008, **1964**.

15 Schulz, J. M.; Fakirov, S. *Solid State Behavior of Linear Polyesters and Polyamides*; Prentice Hall: Englewood Cliffs, NJ, 1990.

16 Inata, H.; Morinaga, T.; Kuratsuji, T.; Urasaki, T.; Kawase, S. Aromatic Polyester Carbonate and Method for Producing the Same. U.S. Pat. 4,107,143, **1978**.

17 Fukuoka, S.; Watanabe, T.; Dozono, T. Method for Producing a Crystallized Aromatic Polycarbonate, and a Crystallized Aromatic Polycarbonate Obtained thereby. U.S. Pat. 4,948,871, **1990**.

18 Iyer, V. S.; Sehra, J. C.; Ravindranath, K.; Sivaram, S. Ind. Pat. Appl. 1236, **1991**.

19 Sivaram, S.; Sehra, J. C.; Iyer, V. S.; Ravindranath, K. Solid State Process for the Preparation of High Molecular Weight Poly(arylcarbonate)s from Amorphous Oligomer. U.S. Pat. 5,266,659, **1993**.

20 Beckman, E.; Porter R. S. Crystallization of Bisphenol-A Polycarbonate Induced by Supercritical Carbon Dioxide. *J. Polym. Sci.: Part B: Polym. Phycs.* 1987, *25*, 1511-1517.

21 Goodner, M. D.; Gross, S. M.; DeSimone, J. M.; Roberts, G. W.; Kiserow, D. J. Modeling and Experimental Studies of the Solid State Polymerization of Polycarbonate Facilitated by Supercritical Carbon Dioxide. *Polym. Prep.* **1999**, *40*, 97-98.

22 Gross, S. M.; Flowers, D.; Roberts, G. W.; Kiserow, D. J.; DeSimone, J. M. Solid-State Polymerization of Polycarbonates Using Supercritical CO_2, *Macromolecules* **1999**, *32*, 3167-3169.

23 Shi, C.; Roberts, G. W.; Kiserow, D. J. The Effect of Supercritical Carbon Dioxide on the Diffusion Coefficient of Phenol in Poly(bisphenol A carbonate). *J. Poly. Sci. Part: B. Poly. Phys.* **2003**, *41*, 1143-1156.

24 Shi, C.; Gross, S. M.; DeSimone, J. M.; Kiserow, D. J.; Roberts, G. W. Reaction Kinetics of the Solid State Polymerization of Poly(bisphenol A

carbonate). *Macromolecules* **2001**, *34*, 2060-2064.

25 Kim, J. H.; Woo, B. G.; Park, E. D.; Hong, M. J. Method for Preparing High Molecular Weight Polycarbonate. U.S. Pat., 7,084,232, **2006**.

26 Garbauskas M. F. Polycarbonate Crystallinity. In: D. G.; Bendler, J. T. *Handbook of Polycarbonate Science and Technology*; Marcel Dekker: New York, 2000.

27 Schnell, H.; Botttenbruch, L. Über Cyclische Carbonate Aromatischer Dihydroxyverbindungen. *Makromol. Chem.* **1962**, *57*, 1-11.

28 Brunelle, D. J.; Shannon, T. G. Preparation and Polymerization of Bisphenol A Cyclic Oligomeric Carbonates. *Macromolecules* **1991**, *24*, 3035-3044.

29 Chalk, A. J. Catalytic Aromatic Carbonate Process. U.S. Pat., 4,187,242, **1980**.

30 Hallgren; J. E. Catalytic Aromatic Carbonate Process. U.S. Pat., 4,201,721, **1980**.

31 Schmidhauser, J.; Sybert, P. D. Nonbisphenol A Polycarbonates. *J. Macromol. Sci. Polym. Rev.* **2001**, *C41*, 325-367.

32 Vaughn H. A.. The Synthesis and Properties of Alternating Block Polymers of Dimethylsiloxane and Bisphenol-A Carbonate. *J. Polym. Sci. Part B: Polym. Phys.* **1969**, *7*, 569-572.

33 Wambach; A. D. Flame Retardant Foamed Polyester Compositions. U.S. Pat. 3,936,400, **1976**.

34 Schmidhauser, J. C.; Longley K. L. The Effect of Bisphenol Monomer Structure on the Gas Permeability of Aromatic Polycarbonates. *J. Appl. Polym. Sci.* **1990**, *39*, 2083-2096.

35 Schmidt, L. R.; Caraher, J. M.; Maxam, J. L. Method for Extruder Devolatilation of Spiro(bis)indane Polycarbonate. U.S. Pat., 4,980,105, **1990**.

36 Fontana, L. P.; Buckley, P. W. Preparation of Polyestercarbonate from Aliphatic Dicarboxylic Acid. U.S. Pat. 5,025,081, **1991**.

37 Factor, A.; Engen, P. T. The Synthesis, Characterization, and Weathering Behavior of Polycarbonates Derived from Bis(p-hydroxyphenyl)dimethylsilane (BPSi). *J. Polym. Sci. Part A: Polym. Chem.* **1993**, *31*, 2231-2236.

38 Kratschmer, S; Horn, K.; Konig, A.; Wehrmann, R.; Kuhling, S. Use of

Copolycarbonates. U.S. Pat. 6,646,101, **2003**.

39 Kratschmer, S.; Bunzel, L.; Alewelt, W.; Wilms, R. Production and use of polyester carbonates U.S. Pat. 6,646,099, **2003**.

40 Pilati, F. Solid-State Polymerization. In: *Comprehensive Polymer Science*; v5, Pergamon: New York, 1989.

41 Gantillon, B.; Spitz, R.; Mckenna, T. F. The Solid State Postcondensation of PET, 1: A Review of the Physical and Chemcial Processes Taking Place in the Solid State. *Macromol. Mater. Eng.* **2004**, *289*, 88-105.

42 Vouyiouka, S. N.; Karakatsani, E. K.; Papaspyrides, C. D. Solid State Polymerization. *Prog. Polym. Sci.* **2005**, *30*, 10-37.

43 Kaushik, A.; Gupta, S. K. A Molecular Model for Solid-State Polymerization of Nylon 6. *J. Appl. Polym. Sci.* **1992**, *45*, 507-520.

44 Wu, D.; Chen, F.; Li, R.; Shi, Y. Reaction Kinetics and Simulation for Solid-State Polymerization of Poly(ethylene terephthalate). *Macromolecules* **1997**, *30*, 6737-6742.

45 Chen, F. C.; Griskey, R. G.; Beyer G. H. Thermally Induced Solid State Polycondensation of Nylon 6, 6, Nylon 6-10 and Polyethylene Terephthalate. *AIChE J.* **1969**, *15*, 680-685.

46 Chang, T. M. Kinetics of Thermally Induced Solid State Polycondensation of Poly(ethylene terephthalate). *Polym. Eng. Sci.* **1970**, *10*, 364-368.

47 Ravindranath, K.; Mashelkar, R. A. Modeling of Poly(ethylene terephthalate) Reactors. IX. Solid State Polycondensation Process. *J. Appl. Polym. Sci.* **1990**, *39*, 1325-1345.

48 Jabarin S. A.; Lofgren, E. A. Solid State Polymerization of Poly(ethylene terephthlate): Kinetic and Property Parameters. *J. Appl. Polym. Sci.* **1986**, *32*, 5315-5335.

49 Karayannidisa, G.; Sideridoua, I.; Zamboulisa, D.; Stalidisa, G.; Bikiarisa, D.; Lazaridisa, N.; Wilmesb, A. Solid-State Polycondensation of Poly(ethy1ene terephthalate) Films. *Angew. Makromol. Chem.* **1991**, *192*, 155-168.

50 Duh, B. Reaction Kinetics for Solid-State Polymerization of Poly(ethylene terephthalate). *J. Appl. Polym. Sci.* **2001**, *81*, 1748-1761.

51 Duh, B. Semiempirical Rate Equation for Solid State Polymerization of Poly(ethylene terephthalate). *J. Appl. Polym. Sci.* **2002**, *84*, 857-870.

52 Gao, Q.; Huang, N.; Gerking, L. Modelling of Solid State Polycondensation of Poly(ethylene terephthalate). *Chem. Eng. Sci.* **1997**, *52*, 371-376.

53 Huang, B.; Walsh, J. J. Solid-Phase Polymerization Mechanism of Poly(ethylene terephthalate) Affected by Gas Flow Velocity and Particle Size. *J. Polym.* **1998**, *39*, 6991-6999.

54 Ma, Y.; Agarwal, U. S.; Sikkema D. J.; Lemstra P. J. Solid-State Polymerization of PET: Influence of Nitrogen Sweep and High Vacuum. *Polymer* **2003**, *44*, 4085-4096.

55 Griskey, R.; Lee, B. Thermally Induced Solid-State Polymerization in Nylon 6,6. *J. Appl. Polym. Sci.* **1966**, *10*, 105-111.

56 Mallon, F. K.; Ray, W. H. Modeling of Solid-State Polycondensation. I. Particle Models. *J. Appl. Polym. Sci*. **1998**, *69*, 1233-1250.

57 Goodner, M. D.; Gross, S. M.; DeSimone, J. M.; Roberts, G. W.; Kiserow, D. J. Broadening of Molecular-Weight Distribution in Solid-State Polymerization Resulting from Condensate Diffusion. *J. Appl. Polym. Sci*. **2001**, *79,* 928-943.

58 Kim, T. Y.; Lofgren E. A.; Jabarin S. A. Solid-State Polymerization of Poly(ethylene terephthalate). II. Modeling Study of the Reaction Kinetics and Properties. *J. Appl. Polym. Sci.* **2003**, *89*, 213-227.

59 Lee, E. H.; Yeo, Y. K.; Choi, K. Y.; Kim, H. Y. Modeling of A Solid-State Polycondensation Process for the Production of PET. *J. Chem. Eng. JP.* **2003**, *36*, 912-925.

60 Ye, Y.; Machado, B.; Choi, K. Y.; Kim, J. H.; Woo, B. G. Modeling of Solid-State Polymerization of Bisphenol A Polycarbonate. *Ind. Eng. Chem. Res.* **2005**, *44*, 2494-2505.

61 Zhao, J.; Xiao, H.; Qiu, G.; Zhang, Y.; Huang, N.; Tang, Z. Solid-State Polycondensation of Poly(ethylene terephthalate) Modified with Isophthalic Acid: Kinetics and Simulation. *Polymer* **2005**, *46*, 7309-7316.

62 Goodner, M. D.; DeSimone, J. M.; Kiserow, D. J.; Roberts, G. W. An Equilibrium Model for Diffusion-Limited Solid State Polycondensation. *Ind.*

Eng. Chem. Res. **2000**, *39*, 2797-2806.

63 Kumar, A.; Saksena, K. Effect of Segmental Diffusion on Irreversible, Step Growth Polymerizations of ARB Monomers. *Polym. Eng. Sci.* **1987**, *27*, 753-763.

64 Kulkarni, M. R.; Gupta, S. K. Molecular Model for Solid-State Polymerization of Nylon 6. II. An Improved Model. *J. Appl. Polym. Sci.* **1994**, *53*, 85-103.

65 Chiu, W. Y.; Carratt G. M.; Soong, D. S. A Computer Model for the Gel Effect in Free Radical Polymerization *Macromolecules* **1983**, *16*, 348-357.

66 Li, L.; Chan, C.; Yeung, K. L. ; Li, J.; Ng, K; Lei, Y. Direct Observation of Growth of Lamellae and Spherulites of a Semicrystalline Polymer by AFM. *Macromolecules* **2001**, *34*, 316-352.

67 Zimmerman, J. Equilibria in Solid Phase Polymerization. *J. Polym. Sci.*, *Polym. Lett. Ed.* **1964**, *2*, 955-963.

68 Gostoli, C.; Pilati, F.; Sarti G. C; Digiacomo, B. Chemical-Kinetics and Diffusion in Poly(butylene terephthalate) Solid-State Polycondensation: Experiments and Theory. *J. Appl. Polym. Sci.* **1984**, *29*, 2873-2887.

69 Li, L.; Ng, K. M.; Chan, C. M.; Feng, J. Y.; Zeng, X. M.; Weng, L. T. Surface Studies of the Rearrangement of End Groups of a Polymer by ToF-SIMS and AFM. *Macromolecules* **2000**, *33*, 5588-5592.

70 Gross, S. M.; Roberts, G. W.; Kiserow, D. J.; DeSimone, J. M. Crystallization and Solid-State Polymerization of Poly(bisphenol A carbonate) Facilitated by Supercritical CO_2. *Macromolecules* **2000**, *33*, 40-45.

71 Lu, W.; Debelak, K. A.; Witt, A. R.; Yang, C.; Collins, W. E.; Lott, C. Structural Features of Crystallized Poly(ethylene terephthalate) Polymers. *J. Polym. Sci. Part B: Polym. Phys.* **2002**, *40*, 245-254.

72 Medellin-Rodriguez, F. J.; Lopez-Guillen, R.; Waldo-Mendoza, M. A. Solid-State Polymerization and Bulk Crystallization Behavior of Poly(ethylene terephthalate) (PET). *J Appl. Polym. Sci.* **2000**, *75*, 78-86.

73 Weger, F.; Hagen; R. Method and Apparatus for the Production of Polyamides. U.S. Pat., 5,773,555, **1998**.

74 Day, J.; Hait; S. B. Branched Polycarbonate and Method. U.S. Pat., 6,365,703,

2002.

75 Duh, B. Solid State Polymerization. U.S. Pat. 5,408,035, **1995**.

76 Beaton, D. H. Continuous Solid-Phase Polymerization of Polyamide Granules. U.S. Pat. 3,821,171, **1974**.

77 Halek, G. W.; Freed, W. T.; Schaul, J. S.; Rupp, R. W.; Pauls, S. L. Process for Preparing Polyethylene Terephthalate Useful for Beverage Containers. U.S. Pat. 4,223,128, **1980**.

78 Chen, C.; Yuan; L. Apparatus and Process for Continuous Solid-State Polycondensation in A Fluidized Reactor with Multiple Stages. U.S. Pat., 7,098,300, **2006**.

79 Gerking, L; Taurat, D. O. Process for the Crystallizing, Drying, and aftercondensation of Polycondensates. U.S. Pat. 4,584,366, **1986**.

80 Mallon, F. K.; Ray, W. H. Modeling of Solid-state Polycondensation. II. Reactor Design Issues. *J Appl. Polym. Sci*. **1998**, *69*, 1775-1788.

81 Yao Z.; Ray W. H. Modeling and Analysis of New Processes for Polyester and Nylon Production. *AIChE J.* **2001**, *47*, 401-412.

82 Yao, K. Z.; McAuley, K. B.; Berg, D.; Marchildon E. K. A Dynamic Mathematical Model for Continuous Solid-Phase Polymerization of Nylon 6, 6. *Chem. Eng. Sic.* **2001**, *56*, 4801-4814.

83 Yao, K. Z.; McAuley, K. B. Simulation of Continuous Solid-Phase Polymerization of Nylon 6,6 (II): Processes with Moving Bed Level and Changing Particle Properties. *Chem. Eng. Sic.* **2001**, *56*, 5327-5342.

84 Yao, K. Z.; McAuley K. B.; Marchildon, E. K. Simulation of Continuous Solid-Phase Polymerization of Nylon 6,6 (III): Simplified Model. *J. Appl. Polym. Sci*. **2003**, *89*, 3701-3712.

85 Algeri, C; Rovaglio, M. Dynamic Modeling of a Poly(ethylene terephthalate) Solid-State Polymerization Reactor I: Detailed Model Development. *Ind. Eng. Chem. Res.* **2004**, *43*, 4253-4266.

86 Rovaglio, M.; Algeri, C.; Manca D. Dynamic Modeling of a Poly(ethylene terephthalate) Solid-State Polymerization Reactor II: Model Predictive Control. *Ind. Eng. Chem. Res.* **2004**, *43*, 4267-4277.

87 Lucas, B.; Seavey, K. C.; Liu, Y. A. Steady-State and Dynamic Modeling for New Product Design for the Solid-State Polymerization of Poly(ethylene terephthalate). *Ind. Eng. Chem. Res.* **2007,** *46,* 190-202.

88 Dias, R. C. S.; Costa, M. R. N. A General Kinetic Method to Predict Sequence Length Distributions for Non-linear Irreversible Multicomponent Polymerizations. *Polymer* **2006**, *47*, 6895-6913.

89 Flory P J. Fundamental Principles of Condensation Polymerization. *Chem. Rev.* **1946**, *39*, 137–97.

90 Stockmayer, W. H. Distribution of Chain Lengths and Compositions in Copolymers. *J. Chem. Phys.* **1945**, *13*, 199-207.

91 Case L. C. Molecular Weight Distribution in Polycondensation Involving Unlike Reactions. 2. Linear Distributions. *J. Polym. Sci*. **1958**, *29*, 455-495.

92 Lopez-Serrano, F.; Castro, J. M.; Macosko, C. W.; Tirrell, M. Recursive Approach to Copolymerization Statistics. *Polymer* **1980**, *21*, 263-273.

93 Johnson, A. F.; O'driscoll, K. F. Monte-Carlo Simulation of Sequence Distributions in Step Growth Copolymerization. *Euro. Polym. J.* **1984**, *20*, 979-983.

94 Beers, K. J.; Ray, W. H. A Linkage Moment Approach to Modeling Condensation Polymerization with Multiple Monomers. I. Linear Polymers. *J. Appl. Polym. Sci.* **2001**, *79*, 246–265.

95 Shi, C.; Gross, S. M.; DeSimone, J. M.; Kiserow, D. J.; Roberts, G. W. Reaction Kinetics of the Solid State Polymerization of Poly(bisphenol A carbonate) Facilitated by Supercritical Carbon Dioxide. *Macromolecules* **2001**, *34*, 7744-7750.

96 Iyer, V. S.; Sehra, J. C.; Ravindranath, K.; Sivaram, S. Solid-State Polymerization of Poly(aryl carbonate)s: A Facile Route to High Molecular Weight Polycarbonates. *Macromolecules* **1993**, *26*, 1186-1187.

97 Gross, S. M.; Roberts, G. W.; Kiserow, D. J.; DeSimone, J. M. Synthesis of High Molecular Weight Polycarbonate by Solid-State Polymerization. *Macromolecules* **2001**, *34*, 3916-3920.

98 Woo, B. G.; Choi, K. Y.; Song, K. H.; Lee, S. H. Melt Polymerization of

Bisphenol A and Diphenyl Carbonate in a Semibatch Reactor. *J. Appl. Polym. Sci*. **2001**, *80*, 1253-1266.

99 Schilling, F. C.; Ringo, Jr., W. M.; Sloane, N. J. A.; Bovey, F. A. Carbon-13 Nuclear Magnetic Resonance Study of the Hydrolysis of Bisphenol A Polycarbonate. *Macromolecules* **1981**, *14*, 532-537.

100 Jonza, J. M.; Porter, R. S. High-Melting Bisphenol-A Polycarbonate from Annealing of Vapor-Induced Crystals. *J. Polym. Sci.:Part B: Polym. Phys*. **1986**, *24*, 2459-2472.

101 Flory, P. J. Molecular Size Distribution in Linear Condensation Polymers. *J. Amer. Chem. Soc*. **1936**, *58*, 1877-1885.

102 Gaymans, R. J.; Amirtharaj, J.; Kamp, H. Nylon 6 Polymerization in the Solid State. *J. Appl. Polym. Sci*. **1982**, *27*, 2513-2526.

103 Gross, S. M.; Bunyard W. C.; Erford K.; Roberts, G. W.; Kiserow, D. J.; DeSimone, J. M. Determination of the Equilibrium Constant for the Reaction between Bisphenol A and Diphenyl Carbonate. . *J. Polym. Sci*. *Part A: Polym. Chem*. **2002**, *40,* 171-178.

104 Hersh, S. N.; Choi, K. Y. Melt Transesterification of Diphenyl Carbonate with Bisphenol A in a Batch Reactor. *J Appl. Poly. Sci.* **1990**, *41*, 1033-1046.

105 Kim, Y. S.; Choi, K. Y.; Chamberlin, T. A. Kinetics of Melt Transesterification of Diphenyl Carbonate and Bisphenol-A to Polycarbonate with Li·OH Catalyst. *Ind. Eng. Chem. Res.* **1992**, *31*, 2118-2127.

106 Li, L. F.; Huang, N. X.; Tang, Z. L.; Hagen, R. Reaction Kinetics and Simulation for the Solid-State Polycondensation of Nylon 6. *Macromol. Theory Simul.* **2001**, *10*, 507-517.

107 Hagenarrs, A. C.; Goddrie, W. J.; Bailly. C. Thermally Induced Redistribution and Degradation of Bisphenol-A Polycarbonate Fractions in Open and Closed Systems. *Polymer* **2002**, *43*, 5043-5049.

108 Russemeyer, H.; Kerl, M.; Schmidt, H. J.; Hani, B.; Kagi, W. Method and Apparatus for Continuously Crystallizing Polyester Material. U.S. Pat. 5,090,134, **1992**.

109 Duh, B.; Corey, A. M. High Temperature Solid State Polymerization of Poly

(trimethylene terephthalate). U.S. Pat. 6,441,129, **2002**.

110 Kerscher, F. C.; Nowacki, J. J. Polymerization Apparatus and Process. U.S. Pat. 4,276,261, **1981**.

111 Duh, B. Process for the Production of High Molecular Weight Polyester. U.S. Pat. 4,374,975, **1983**.

112 Alsop, A. W.; Blanchard, E. N.; Cohen, J. D.; Iwasyk, J. M.; Lin, C. Y.; Marks, D. N.; Stouffer, J. M. Process for Preparing Polyamides. U.S. Pat. 6,069,228, **2000**.

113 Gey, W.; Langhauser, W.; Heinze, H.; Rothe, H.; Freund, P. Process for the Solid State Polycondensation of Linear Polyesters. U.S. Pat., 4,069,194, **1978**.

114 Parisi, D. R.; Laborde, M. A. Modeling of Counter Current Moving Bed Gas-Solid Reactor Used in Direct Reduction of Iron Ore. *Chem. Eng. J.* 2004, *104*, 35-43.

115 Lee, H. H. *Heterogeneous Reactor Design*; Butterworth: Stoneham MA, 1985.

116 Ergun, S. Fluid Flow Through Packed Columns. *Chem. Eng. Prog.* **1952**, *48*, 89-94.

117 Span, R.; Lemmon, E. W.; Jacobsen, R. T.; Wagner, W.; Yokozeki, A. A Reference Equation of State for the Thermodynamic Properties of Nitrogen for Temperatures from 63.151 to 1000 K and Pressures to 2200 Mpa. *J. Phys. Chem. Ref. Data* **2000**, *29*, 1361-1433.

118 Lemmon, E. W.; Jacobsen, R. T. Viscosity and Thermal Conductivity Equations for Nitrogen, Oxygen, Argon, and Air. *Int. J. thermophys.* **2004**, *25*, 21-69.

119 Zoller, P. A Study of the Pressure-Volume-Temperature Relationships of Four Related Amorphous Polymers: Polycarbonate, Polyarylate, Phenoxy, and Polysulfone. *J. Polym. Sci. Part B: Polym. Phys.* **1982**, *20*, 1453-1464.

120 Cheng, S. Z. D.; Wunderlich, B. Heat Capacities and Entropies of Liquid, High-Melting-Point Polymers Containing Phenylene Groups (PEEK, PC, and PET). *J. Polym. Sic.: Part B: Polym. Phys.* **1986**, *24*, 1755-1765.

121 Kazeminejad H. Thin Copper Foil Heater for Measuring the Thermal Conductivity of Polymers. *J. Appl. Polym. Sci.* **2003**, *88*, 2823–2827.

122 Yoshida, F.; Ramaswami, D.; Hougen, O. A. Temperature and Partial Pressures at the Surfaces of Catalyst Particles, *AIChE J.* **1962**, *8*, 5-11.

123 Hanrattry, T. J. Nature of Wall Heat Transfer Coefficient in Packed Beds, *Chem. Eng. Sci.* **1954**, *3*, 209-214.

124 Dixon, A. G.; Cresswell, D. L. Theoretical Prediction of Effective Heat Transfer Parameters in Packed Beds. *AIChE J.* **1979**, *25*, 663-676.

125 Alizadeh, A.; Sohn, A.; Quinn, J.; Marand, H. Influence of Structural and Topological Constraints on the Crystallization and Melting Behavior of Polymers: 3. Bisphenol A Polycarbonate. *Macromolecules* **2001**, *34*, 4066-4078.

126 Giordano, D.; Bianchi, R. Process for the Solid State Polycondensation of Polyamide Resins. U.S. Pat. 5,859,180, **1999**.

127 Halek, G. W.; Freed, W. T.; Schaul, J. S.; Rupp, R. W.; Pauls, S. L. Process for Preparing Polyethylene Terephthalate Useful for Beverage Containers. U.S. Pat. 4,223,128, **1980**.

128 Yau, C. C.; Cherry, C. Production of Branched Polyesters. U.S. Pat. 5,393,863, **1995**.

129 Kunii, D.; Levenspiel, O. *Fluidization Engineering*; 2nd Ed., Butterworth-Heinemann: Stoneheim, MA, 1991.

130 Kim, J. H.; Woo, B. G.; Park, E. D.; Hong, M. J. Preparation Method of High Molecular Weight Polycarbonate Resin. U.S. Pat. 7,148,312, **2006**.

131 Day, J.; Hait, S. B. Method of Crystallizing Polycarbonate Prepolymer. U.S. Pat. 6,222,001, **2001**.

132 Weger, F. Process and Apparatus for Continuous Crystallization of Plastic Granules. U.S. Pat. 5,558,678, **1996**.

133 Master K. *Spray Drying Handbook*, 5th Ed., Longman Group UK Ltd., 1991, p79.

134 Hait, S. B. Preparation of Copolycarbonates via Solid State Polymerization. U.S. Pat. 6433126, **2002**.

135 Rosenquist, N. R. Copolyester-Carbonates Containing Aliphatic Diol Co-monomers. U.S. Pat., 4,381,358, **1983**.

136 Barreiro, M. F.; Disa, R. C. S.; Costa, M. R. N. Experimental Determination of Sequence Length Distribution of Hard Segments in Polyester-Polyurethanes. *Macromolecules*, **1994**, *27*, 7650-7653.

137 Sung, P. C. S.; Hu, C. B.; Wu, C. S. Properties of Segmented Poly(urethaneureas) Based on 2,4-Toluene Diisocyanate. 1. Thermal Transitions, X-ray Studies, and Comparison with Segmented Poly(urethanes). *Macromolecules* **1980**, *13*, 111-116.

138 Mayo, F. R.; Lewis, F. M. J. Copolymerization. I. A Basis for Comparing the Behavior of Monomers in Copolymerization; the Copolymerization of Styrene and Methyl Methacrylate. *Am. Chem. Soc.* **1944**, *66*, 1594-1601.

139 Debling, J. A.; Teymour F. A New Arithmetic for Linear Free Radical Copolymerization. *Macromol. Symp.* **2002**, *182*, 195-207.

140 Peebles, L. H. Jr. Sequence Length Distribution in Segmented Block Copolymers. *Macromolecules* **1974**, *7*, 872-882.

141 Peebles, L. H. Jr. Hard Block Length Distribution in Segmented Block Copolymer. *Macromolecules* **1976**, *9*, 58-61.

142 Speckhard, T. A.; Miller, J. A.; Cooper S. L. Monte Carlo Simulation Study of the Polymerization of Polyurethane Block Copolymers. 1. Natural Compositional Heterogeneity under Ideal Polymerization Conditions. *Macromolecules* **1986**, *19*, 1558-1567.

143 Speckhard, T. A.; Homan, J. G.; Miller, J. A; Cooper, S. L. Monte-Carlo Simulation Study of the Polymerization of Polyurethane Block Copolymers. 4. Modeling of Experimental Data. *Polymer* **1987**, *28*, 768-776.

144 Miller, J. A.; Speckhard, T. A.; Cooper S. L. Monte Carlo Simulation Study of the Polymerization of Polyurethane Block Copolymers. 2. Modeling of Premature Phase Separation during Reaction Using the Two-Phase Ideal Reaction Model. *Macromolecules* **1986**, *19*, 1568-1574.

145 Miller, J. A.; Speckhard, T. A.; Homan, J. G.; Cooper, S. L. Monte-Carlo Simulation Study of the Polymerization of Polyurethane Block Copolymers .3. Modeling of Premature Phase-Separation During Reaction and Differing Reactivities of the Chain Extender and Polyol Using the Simple Sinking Pool

Model. *Polymer* **1987**, *28*, 758-767.

146 Fakirov, S.; Sarkissova M.; Denchev. Sequential Reordering in Condensation Copolymers. 1. Melting- and Crystallization-Induced Sequential Reordering in Immiscible Blends of Poly(ethylene terephthalate) with Polycarbonate or Polyarylate. Z. *Macromol. Chem. Phys.* **1996**, *197*, 2837-2867.

147 Matsuda, H.; Nagasaka, B.; Asakura, T. Sequence Analysis of Polyarylate (U-Polymer) and its Polyestercarbonate Using ^{1}H and ^{13}C NMR. *Polymer J.* 2003, *35*,740-747.

148 Yokoe, M.; Okada, M.; Keigo, A. O. I. Biodegradable Polymers Based on Renewable Resources. VII. Novel Random and Alternating Copolycarbonates from 1,4:3,6-Dianhydrohexitols and Aliphatic Diols. *J. Polym. Sci. Part A: Polym. Chem.* **2003**, *41*, 2312-2321.

149 Falkai, B. V.; Rellensmann, W. Kristallisation von Polycarbonaten. II. Dilatometrische Untersuchungen an Poly-4,4'-dihydroxidiphenyl-2,2-propan-carbonat. *Makromol. Chem.* **1965**, *88*, 38-53.

150 Siegmann, A.; Geil, P. H. Crystallization of Polycarbonate from the Glassy State Part I. Thin Films Cast from Solution. *J. Macromol. Sci. Part B: Phys*., **1970**, *4*, 239-271.

151 Gallez, F.; Legras R.; Mercier, J. P. Crystallization of Bisphenol-A Polycarbonate. I. Influence of Trimellitic Acid Tridecyloctyl Ester on the Kinetics of Crystallization. *J. Polym. Sci.: Part B: Polym. Phycs.* **1976**, *14*, 1367-1377.

152 Bailly, C. H.; Daumerie, M.; Legras R.; Mercier, J. P. Crystallization of Bisphenol-A Polycarbonate Induced by Organic Salts. Physical Aspects I. Crystallization Rate, Melting Behavior, and Morphology. *J. Polym. Sci. Part B: Polym. Phycs.* 1985, 23, 751-770.

153 Mercier, J. P.; Groeninckx, C.; Lesne, M. Some Aspects of Vapor-Induced Crystallization of Polycarbonate of Bisphenol A. *J. Polym. Sci.: Polym. Symp.* **1967**, *16*, 2059-2067.

154 Fan, Z.; Shu, C.; Yu, Y.; Zaporojtchenko, V.; Faupel, F. Vapor-Induced Crystallization Behavior of Bisphenol-A Polycarbonate. *Polym. Eng. Sci.* **2006**,

46, 729-734.

155 Falkai, B.; Hinrichsen, G. Drawing Behavior and Mechanical Properties of Highly Oriented Polycarbonate Fibers. *J. Polym. Sci.: Polym. Symp.* **1977**, *58*, 225-235.

156 Djurner, K.; Manson, J-A.; Rigdahl, M. Crystallization of Polycarbonates during Injection Molding at High Pressures. *J. Polym. Sci.: Polym. Lett. Ed.* **1978**, *16*, 419-424.

157 Harron, H. R.; Pritchard, R. G.; Cope, B. C.; Goddard, D. T. An Atomic Force Microscope (AFM) and Tapping Mode AFM Study of the Solvent-Induced Crystallization of Polycarbonate Thin Films. *J. Polym. Sci. Part B: Polym. Phycs.* **1996**, *34*, 173-180.

158 McNulty, B. J. The Structure of Polycarbonate Spherulites. *Polymer* **1968**, *9*, 41-44.

159 Fryer, R. E. J. Spherulite Crystallization in Bisphenol-A-Polycarbonate of Varying Molecular Weight Distribution. *J. Appl. Polym. Sci.* **1974**, *18*, 2261-2267.

160 Wilkes, G. L.; Parlapiano J. Solvent and Vapor Induced Crystallization of Bisphenol A Polycarbonate. *Polymer Preprints*. **1976**, *17*, 937-942.

161 Zhao, N.; Weng, L.; Zhang, X.; Xie, Q.; Zhang, X.; Xu, J. A Lotus-Leaf-Like Superhydrophobic Surface Preparedby Solvent-Induced Crystallization. ChemPhysChem. **2006**, *7*, 824-827.

162 Daniewska, I.; Dobkowski, Z.; Czlonkowska-Kohutnicka, Z. Solvent-Vapor-Induced Crystallization of Branched Polydisperse Polycarbonate. *J. Appl. Polym. Sci.* **1986**, *31*, 2401-2405.

163 Mochizuki, H.; Mizokuro, T.; Tanigaki, N.; Ueno, I.; Hiraga, T. Crystallization Behavior of Bisphenol A Polycarbonate with a Simple Vacuum Process. *J. Polym. Sci. Part B: Polym. Phycs.* **2005**, *43*, 2307-2313.

164 Turska, E.; Benecki, W. Studies of Liquid-Induced Crystallization of Bisphenol A Polycarbonate. *J. Appl. Polym. Sci.* **1979**, *23*, 3489-3500.

165 Desai, A. B.; Wilkes, G L. Solvent-Induced Crystallization of Polyethylene terephthalate. *J. Polym. Sci. Part C: Symp. 1974*, **46**, 291-319.

166 Eisele U. *Introduction to Polymer Physics*; Springer-Verlag: New York, 1990.